A finite element strategy applied to intramedullary nailing of the proximal femur.

David John Simpson

A Thesis submitted for the degree of Doctor of Philosophy at Brunel University.

July 2005.

In loving memory of my Nan, Berol Davies.

ABSTRACT

An intramedullary nail is a trauma treatment device used for fracture fixation of long bones. These devices are subject to failure, including lag screw cut-out and failure at the lag screw insertion hole from high stress concentrations in that region.

Clinical developments for such devices are frequently based on a trial and error method, which often results in failure before improvement. However, the finite element method can be used for the development of trauma treatment devices, and their interaction with bone, by providing a large data set at a relatively low cost. Also, parameters can be changed to assess the relative benefits of one device to another.

A novel finite element model has been developed that can be used for the analysis of intramedullary nails inserted into long bones. A commercially available finite element package, ANSYS, has been used to implement the modelling strategy. The finite element modelling technique has been applied to fractures of the proximal femur, but the model is generic, and can be developed to deal with any form of intramedullary device where contact between the bone and implant is important.

The finite element strategy can be used in pre-clinical trials to test a new device, or for the design optimisation of existing devices. The finite element model consists of the device surrounded by a thin layer of bone, which forms a 'base' model component that is re-usable. This 'base' component can be mathematically connected to any long bone model, forming an integrated implant and bone construct. The construct can be used to assess which device is best suited to a particular fracture, for example.

Contact elements have been used to allow stresses to develop as contact is achieved within the implant and bone construct. Pre-assignment of contact points is not required.

Verification of the finite element model is achieved by comparison to available data from experiments carried out on constructs of bone and device that use intramedullary femoral nails.

In this thesis the finite element model has been applied to two areas of proximal femoral nailing.

The finite element model is used to analyse the distal end of a Gamma nail, and shows that analyses that do not consider contact may not lead to accurate predictions of stresses.

The model has been developed for using configurations with one and two distal locking screws. The most distal locking screw is more critical under axial loading, and the more proximal screw is more important for bending loads. The use of 'softer' screws distributes the load more evenly between them.

The finite element model has been used to investigate the mechanical environment of a fracture callus for a femoral neck fracture, and a subtrochanteric fracture. The use of one and two lag screws, fracture gap size and material properties of the nail have been investigated for a stiffening callus.

Results show that the use of two lag screws for a neck fracture provides a more rigid support at the early stages of fracture healing, and minimises stress-shielding once the callus has healed. For subtrochanteric fractures there is a critical point at which the fracture callus is able to carry any load.

A Titanium nail significantly reduces the peak stress at the lag screw insertion hole, and titanium lag screws share the load more evenly between them. Each two-lag- screw configuration used transfers a similar load into the fracture callus. A configuration using a larger lag screw above a smaller has a significantly higher stress at the upper lag screw insertion hole.

Critically, the load shared between two lag screws changes as the fracture callus stiffens and an assessment should be made at different stages of fracture healing to optimise the use of a device.

ACKNOWLEDGMENTS

I would like to express my indebted gratitude to the following people, without which this research would not have been possible:

- C. J. Brown and Prof. A. L. Yettram for their invaluable guidance, supervision and advice throughout the duration of this research.
- Brunel University for sponsoring the research and providing the necessary resources.
- My wife, who has believed in me from the beginning, and has grown with me throughout this research.
- My family and friends, who have patiently awaited the completion of this work and provided encouragement throughout.

CONTENTS

CHAPTER 4 – SIMPLIFIED CONTACT MODEL

LIST OF FIGURES

CHAPTER 2 – STRUCTURE OF THE FEMUR, FINITE ELEMENTS AND INTRAMEDULLARY NAILS – A REVIEW

CHAPTER 3 – A NOVEL MODELLING TECHNIQUE

CHAPTER 5 - EXPERIMENTATION

CHAPTER 6 - VERIFICATION

CHAPTER 7 – SENSITIVITY STUDY

CHAPTER 8 – DISTAL SCREW CONFIGURATION ANALYSIS

CHAPTER 9 – FRACTURE HEALING

LIST OF TABLES

CHAPTER 9 – FRACTURE HEALING

1.0 Introduction

1.1 Orthopaedics and trauma treatment

The fracturing of a bone in the human skeleton is unfortunately a common occurrence in the present day, and has been throughout history. Approximately 660 000 bone fractures will occur per year in the United Kingdom, out of a population of 60 million, and 21% of these fractures will occur in the femur (Eveleigh, 1997). Fractures of the femur, the largest long bone in the human body, are a common occurrence and incidence reports of these fractures are on the increase, as reported in a National Report by the Audit Commission (1995). The number of hip fractures world-wide has been estimated to increase from 1.2 million in 1990 to 7.3-21.3 million by 2050 (Gullberg *et al.*, 1997). A major cause of the increase in hip fractures is the increasing population and life expectancy. The occurrence of injury to the human femur over the years has led to a need for the increased development of fracture fixation techniques.

Fixation of fractures depends on the type of fracture and bone, and it is the orthopaedic surgeon who has the responsibility to repair broken bones. Orthopaedic surgeons deal with diseases to bone and joints, deformities and injuries to the musculo-skeletal system. The word orthopaedic derives from the Greek 'orthos pais', meaning 'straight child', and the word orthopaedic was first introduced from the title of a book published by a French physician, Nicolas Andry, in 1741 entitled 'Orthopaedia': 'or the Art of Correcting and Preventing Deformities in Children: by such means, as may easily be put in Practice by Parents themselves, and all such as are Employed in Educating Children'. Trauma is a particular segment of orthopaedics and can be considered as high-energy injuries, or one such injury that will cause considerable damage and shock to the patient. The fracturing of a bone falls under the fold of trauma treatment and there are a variety of means to repair a broken bone, including: traction, external splints and braces, plaster casts, slings, external and internal fixation.

When a long bone is broken internal fixation may be the optimum choice for fracture repair. Internal fixation can utilise plates and screws, wires, nail-plates

and intramedullary nails. Intramedullary nails have some distinct advantages over other devices, as will be highlighted in later sections, and an intramedullary nail comprises of a nail or rod being inserted into the medullary canal. The use of cross-screws holds the bone in position and minimises shortening or rotation at the fracture site. Dynamisation may also be incorporated to allow compression at the fracture plane encouraging effective fracture healing.

1.2 Evaluation of Intramedullary nails

The use of intramedullary nails is a common surgical technique that is well established for fractures of the proximal femur (McRae, 1996). This technique has some documented advantages such as less intra-operative blood loss with smaller skin incisions (Leung *et al.*, 1992; Radford *et al.*, 1993), reduced incidence of screw cut-out (Haynes *et al.*, 1997), and a shorter time to full weight bearing (Leung *et al.*, 1992; Schick *et al.*, 1996).

There is incidence of failure of such fixation devices, including cut-out of the lag screw (Dubbeld and Den Outer, 2000) and failure of the nail at the lag screw insertion hole due to the large stress concentration in this region (Randle *et al.*, 1999). Coupled with the failure of intramedullary devices there is also the question of nail configuration, for example the number and size of lag screws and distal locking screws. Many intramedullary devices use one lag screw, especially in poor quality bone. It has been reported however, that two screws are a more viable option, especially when the surrounding bone is of good quality. (Brown *et al.*, 2004).

There is therefore a need for continued assessment and evaluation of intramedullary techniques. Evaluation can be from a number of sources. Clinical trials provide an empirical basis, and there are also some theoretical approaches available (Lin *et al.*, 2001, Genda *et al.*, 2001). Theoretical approaches however tend to be very specific to certain areas of intramedullary nailing, as well as fairly time consuming and quite often patient specific. Clinical assessments are based on a trial and error method, which inevitably leads to failure before improvement and these studies are also time consuming and costly.

Another approach used for the evaluation of intramedullary nailing is in numerical methods, and more specifically finite element analysis. With the use of finite elements, results can be obtained relatively quickly, and there is the possibility of varying parameters and geometries used, leading to a large data set at relatively low cost. In literature the use of finite element analysis tends to constrict itself to patient or case specific studies (Sitthiseripratip *et al.*, 2002; Seral *et al.*, 2003; Cheung *et al.*, 2004). These studies also limit the capabilities of finite element analysis by making certain assumptions within the intramedullary nailing system, such as pre-assigned contact points and the merging of certain components. Other authors reporting on finite element methods have gained an evaluation of a case specific model, but have highlighted the need for parameter identification and limitations on the modelling technique, with regards to the solution accuracy (Bernakiewicz, 2002; Viceconti *et al.*, 2000).

Some works have assessed the interaction between implant and bone by using a generic model that focuses on the general case, and is not patient specific but system interaction dependent (Brown *et al.*, 2004; Wang *et al.*, 2003). Results from such a study give the relative benefits of any particular configuration.

This thesis presents a finite element technique that can be used to assess the interaction between implant and bone without having to pre-assign contact points by the use of a generic model that can be used in a multitude of applications with respect to fracture fixation of the proximal femur. The method can be extended to any trauma treatment of long bones in the human body by use of an intramedullary nail.

Such a strategy can only be implemented with numerical techniques. Kinematic constraints imposed on contact mechanics render the problem statically indeterminate unless pre-determined contact is employed, or an iterative approach is adopted through, for example, finite elements. Experimental techniques can be awkward to undertake, costly and time-consuming. There is also uncertainty over the repeatability of experiments as individual specimens vary considerably and cadaveric specimens vary in their material properties over time.

Furthermore it is almost impossible to quantify some contact parameters experimentally. Contact stiffness is a theoretical phenomenon and cannot be measured directly, contact pressure is measurable with photosensitive film but is very difficult to quantify. There are also the logistics of measuring strain at various points on the intramedullary system, whether in *in-vitro* or *in-vivo*.

Also, a numerical approach allows an assessment of implant-bone interaction, and stress and strain in the construct at any region.

This thesis will: model a proximal femur instrumented with an intramedullary device using a novel finite element technique; validate by means of experimentation the novel modelling concept; and investigate certain aspect of an intramedullary nail, extending the analysis to investigate fracture healing of two types of proximal femoral fractures.

1.3 Contribution to the body of knowledge

A novel finite element modelling technique is presented to describe the interaction between bone and implant concerning any long bone instrumented with an intramedullary device. The model is used to investigate fractures of the proximal femur in this thesis.

Verification of the finite element model is provided by comparison with experimental data.

The finite element model is used to investigate fracture healing of a femoral subtrochanteric and femoral neck fracture. Lag screw configuration, fracture gap size and material properties are assessed.

The finite element model is used to investigate different distal screw configurations for the fixation of intramedullary nails into cortical bone.

1.4 Thesis outline

In chapter 2 the skeletal system is introduced, highlighting the structure of bone and a brief description of bone fracture and repair is given. A history of analysis of the human femur is given, along with its structure and loading. Fractures of

the femur and an overview of intramedullary nailing are discussed, along with the use of finite elements in intramedullary design.

Chapter 3 presents the novel finite element model and boundary conditions.

A simple contact model is used in Chapter 4 to investigate certain contact parameters and to verify the novel modelling technique.

An experiment used to compare to the finite element model is presented in chapter 5, and results reported.

Chapter 6 compares the results from the finite element model to those obtained from the experiment described in chapter 5, to validate the finite element technique.

A sensitivity study is presented in chapter 7 with comparison to experimental data. This study investigates the importance of each parameter used in the finite element model.

Chapter 8 uses the model to investigate variations in the distal locking screw configurations, comparing one and two screws with slotted and non-slotted distal screw insertion holes.

The effect of lag screw configuration, material properties and fracture callus size on fracture healing of a femoral subtrochanteric and femoral neck fracture is given in Chapter 9.

Chapter 10 draws together the findings of previous chapters and reviews the outcomes of the work. Recommendations for further work are presented.

2.0 The skeletal system

The skeletal system provides an internal support system in all higher vertebrates, and bone provides a highly specialised form of connective tissue, adding marked rigidity and strength while still maintaining a degree of elasticity. Bones account for one sixth of the body weight, and muscles make up two fifths.

The skeletal system provides structural support for the body and attachments for soft tissues and organs. The skeleton is responsible for the storage of minerals and lipids. Minerals are inorganic ions that contribute to the osmotic concentration of bodily fluids. Concentrations of calcium and phosphate ions in bodily fluids are maintained by the important mineral reserves found in the skeletal system. The bones of the skeleton store energy as lipids in areas filled with yellow marrow. Blood cell production is a function of the skeleton, with red marrow filling the internal cavity of many bones where red and white blood cells are produced. The skeleton also protects many delicate organs and provides leverage in the body, with many bones acting as levers that can change the magnitude and direction of the forces generated by the skeletal muscles.

Every adult skeleton consists of 206 major bones. These may be classified into six broad categories.

1. Long bones are relatively long and slender and are located in the arm and forearm, thigh and leg, palms, soles, fingers and toes. The long bone in the thigh, the femur is the largest bone in the body.

2. Short bones or boxy bones can be found in the wrist and ankles, named carpal and tarsal respectively.

3. Flat bones are thin and have roughly parallel surfaces. These bones provide an extensive surface area for the attachment of muscles and provide a protective layer for underlying organs. Examples of flat bones are the scapula, sternum and ribs.

4. Irregular bones have complex shapes with short, flat, notched or rigid surfaces. An example of irregular bones is the vertebrae in the spinal column.

5. Sesamoid bones are generally flat and small and cause the discrepancy in the total number of bones accounted for in the human body. They form inside tendons and are predominantly located at joints such as the knees, hand and feet. All of us possess a sesamoid patellae or kneecap.

6. Sutural bones or wormian bones are small and flat irregular shaped bones that exist between the flat bones of the skull.

2.1 The structure of bone

Each bone in the human skeleton contains two types of osseous tissue, or bone tissue: compact bone and spongy bone. Compact bone or cortical bone is very dense and solid, whereas spongy bone or cancellous bone is more porous, forming an open network of struts and plates. Cortical bone is located on the surface of bones where it forms a rigid protective layer. Cancellous bone however is found on the inside of bones. Cortical bone provides the mechanical and protective functions and cancellous bone provides the metabolic functions. The relationship of cortical to cancellous bone is dependent on the bone shape and size.

The anatomy of the femur is introduced in figure 2.1. There is a long tubular shaft known as the diaphysis that expands at each end to the epiphysis. The diaphysis is connected to the epiphysis by the metaphysis. The wall of the diaphysis consists of cortical bone that surrounds the marrow cavity of medullary canal. This is the weakest part of the bone, indeed if buckling were to occur than it would be here and thus there are large amounts of cortical bone present. The epiphysis consists largely of cancellous bone with a thin covering or cortex of cortical bone.

The marrow cavity of the diaphysis and the spaces in the cancellous bone of the epiphyses contain bone marrow, a loose connective tissue. Red bone marrow consists mostly of white and red blood cells, and the stem cells that produce them. Yellow bone marrow is dominated by fat cells or lipids and provides an important energy reserve.

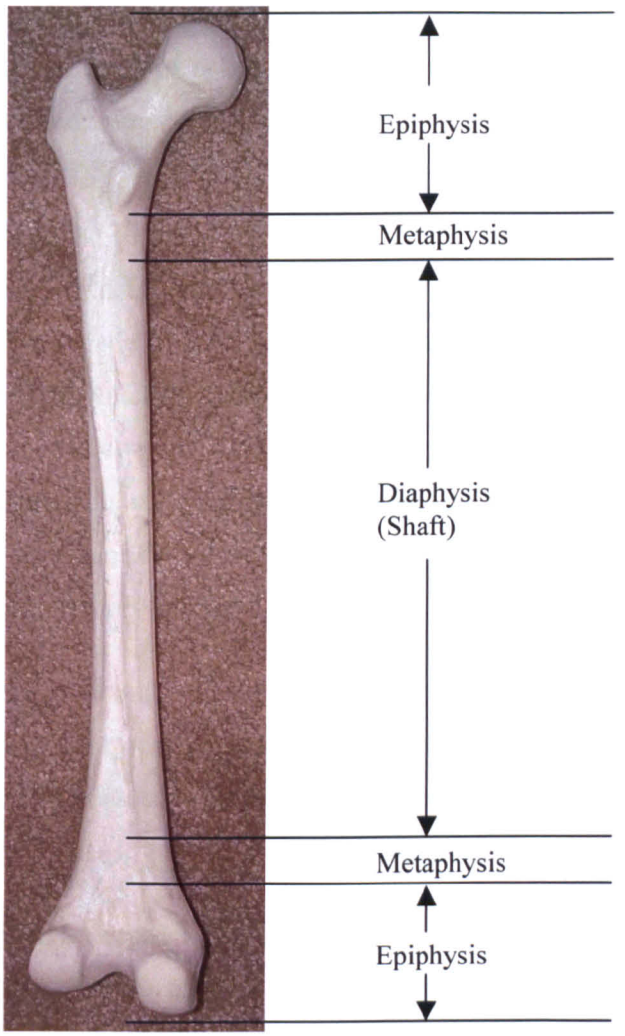

Figure 2.1 – The human femur.

The matrix of bone owes its rigidity to the calcium salt deposition about protein fibres. There are four main characteristics of bone that add to its uniqueness and strength:

1. Bone matrix is very dense and contains deposits of calcium salts.

2. This matrix contains bone cells or osteocytes that exist within pockets called lacunae. These lacunae are typically organised about blood vessels that branch through the bone matrix.

3. Narrow passageways through the matrix called canaliculi extend between the lacunae and blood vessels providing transportation for nutrients and waste.

4. Except at joints, the outer surfaces of bones are covered by the periosteum, consisting of outer fibrous and inner cellular layers.

2.2 The matrix of bone

The matrix of bone consists of calcium salts and protein fibres. Approximately two thirds of a bone's weight is made up of calcium phosphate, $Ca_3(PO_4)_2$. The calcium phosphate combines with calcium hydroxide $Ca(OH)_2$ to form the main ingredient of bone, hydoxyapatite crystals, $Ca_{10}(PO_4)_6(OH)_2$. As these crystals form they include other calcium salts such as calcium carbonate $CaCO_3$ and ions such as sodium magnesium and fluoride. About one third of a bone's weight is from collagen fibres and approximately 2% from cells.

Calcium phosphate is extremely strong but not very flexible and quite brittle. These salts are very resistant to compressive loads but are likely to shatter under bending and torsion conditions or sudden impact. Collagen fibres are remarkably strong in tension and are very flexible.

In bone collagen fibres provide an organic framework on which hydroxyapatite crystals can form. The hydroxyapatite crystals form rods and plates that are locked into the framework of collagen fibres forming a very strong protein crystal matrix. The properties of which are intermediate between the pure collagen fibres and the mineral crystals. Bone is thus very strong and somewhat flexible.

2.3 Bone Cells

The most abundant cells found in bone are osteocytes. There are three other types of cell found in bone, these are osteoblasts, osteoprogenitor cells and osteoclasts.

Osteocytes are mature bone cells that cannot divide. They each occupy a lacuna; a pocket sandwiched between layers of the matrix. Only one osteocyte occupies a lacuna and the layers of the matrix are known as lamellae. Canaliculi connect the lacuna with one another through the matrix, providing nutrient sources. The

function of the osteocyte is two fold: firstly to maintain and monitor the protein and mineral concentrations in the surrounding matrix, and secondly to aid in the repair of a damaged bone.

Osteoblasts are responsible for the creation of new bone matrix, known as osteogenesis. These cells produce and release proteins and other organic compounds for the bone matrix. Before calcium salts have deposited the matrix is known as an oseteoid. Osteoblasts raise levels of calcium phosphate and promote the deposition of calcium salts, thus converting osteoid to bone. Oseocytes are formed from osteoblasts that are completely surrounded by bone matrix.

Small numbers of mesenchymal cells or osteoprogenitor cells occupy the inner cellular layer of the periosteum. These cells divide to produce daughter cells that differentiate into osteoblasts. Osteoprogenitor cells maintain levels of osteoblasts and are essential in the repair of fractures.

Osteoclasts are huge cells that are not related to osteoprogenitor cells or their descendants. They are responsible for the dissolving of bone matrix and the release of stored minerals. This process, known as osteolysis or resorption is important in the regulation of calcium and phosphate concentrations in bodily fluids. Osteoclasts are continually dissolving bone matrix and osteoblasts are continually adding to it. It is the balance of this process that determines the strength of a bone.

2.4 Cortical and Cancellous bone

The composition of the matrix in both these types of bone is identical. It is the arrangement of osteocytes, canaliculi and lamellae that give them remarkably differing properties.

In compact bone a Haversian system or osteon provides the base functional unit. In an osteon, osteocytes form concentric layers around a central canal or Haversian canal. Such a canal contains blood vessels that provide transportation of blood to and from the osteon. Other canals known as perforating canals extend roughly to the surface perpendicular to the orientation of the central canal. Blood

vessels in these canals supply blood to the marrow cavity. Concentric lamellae are aligned parallel to the long axis of the central canal, interstitial lamellae fill spaces between the osteons and circumferential lamellae are covered by the periosteum or endosteum.

All osteons in cortical bone are arranged in the same orientation making bones very strong when stressed along the axis of alignment. Cortical bone is thus at its thickest where stresses arrive at a limited range of directions. The osteons in the diaphysis are parallel to the long axis of the shaft and thus the shaft is extremely strong in compression and tension. The femur can withstand ten to fifteen times that of the bodies' weight without breaking for example. However a much smaller force applied to the side of the femoral shaft can cause a fracture.

The matrix of cancellous bone forms struts and plates known as trabeculae. The lamellae are not arranged into osteons as with cortical bone. The thin trabeculae of cancellous bone branch out, creating an open network. An example of cancellous and cortical bone is shown in the proximal femur, in figure 2.2. The individual struts of the cancellous bone are clearly visible in the femoral head and trochanter, cortical bone can be seen on the underside of the femoral head and leading into the femoral shaft. Figure 2.3 demonstrates the amount of cortical bone present in the femoral shaft, or diaphysis.

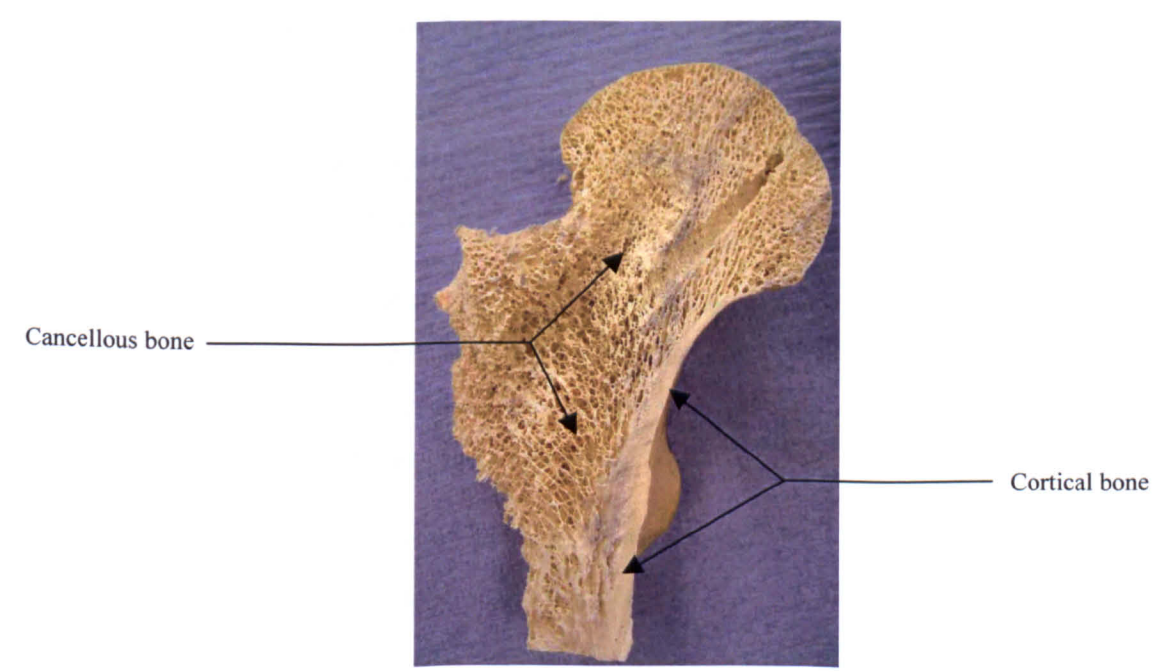

Figure 2.2 – Cancellous and cortical bone in the proximal femur.

Figure 2.3 – Cancellous and cortical bone in the femur shaft.

Cancellous bone can be found at places where bone is not heavily stressed and where stress arises in many directions. Trabeculae are orientated along stress lines but there is a great deal of cross bracing. At the proximal end of the femur trabeculae transfer load through the epiphysis to the compact bone of the diaphysis. At the distal end of the femur trabeculae transfer weight from the shaft to the leg, across the knee joint. Cancellous bone is lighter than cortical bone, thus reducing the overall weight of the skeleton. Finally trabeculae support and protect the cells of the bone marrow. The red bone marrow within the cancellous bone of the femoral epiphysis is a key site of blood cell formation.

2.5 Vascular and Nerve supplies to bone

Osseous tissue is very vascular and the bones of the skeletal system have an extensive blood supply. In a typical bone such as the femur, three main sets of blood vessels are present.

1. The nutrient artery and vein. Most bones only have one nutrient artery and one nutrient vein, however a few, such as the femur have more. The vessels enter the bone through the diaphysis and extend along the length of the shaft into the osteons of the surrounding cortex.

2. Metaphyseal Vessels. These vessels supply blood to the inner surface of epiphyseal cartilage where that cartilage is being turned into bone.

3. Periosteal Vessels. Blood vessels from the periosteum are incorporated into any developing bone surfaces. These vessels provide blood to the superficial osteons of the shaft.

All three sets of these vessels become extensively connected in mature bone. The periosteum contains an extensive network of lymphatic vessels and sensory nerves. The lymphatics are responsible for collecting lymph from branches that enter the bone and to reach osteons via perforating canals. Sensory nerves penetrate the cortex with the nutrient artery to innervate the endosteum, marrow cavity and epiphyses. It is because of the abundant sensory supply to bones that injuries to them are usually very painful.

2.6 Fracture Repair and Classification

The repair of a fracture can be placed into four distinct stages.

1. Firstly a blood clot or haematoma is formed around the break, which acts to close off surrounding blood vessels, and leaves a fibrous meshwork in the damaged area.

2. In adults the cells of the periosteum and endosteum are relatively inactive. After a fracture the cells of the intact endosteum and periosteum undergo mitosis (cell division) and the daughter cells migrate into the fracture zone. An internal and external callus is formed about the fracture site. At the centre of the external callus cartilage is formed, at the internal callus cells differentiate into osteoblasts and the fracture ends are slowly knitted together.

3. As the repair continues osteoblasts replace the cartilage with cancellous bone. As the process is completed the internal and external callus form a solid bridge at the fracture site. Struts of the cancellous bone now bind the fracture ends together.

4. Osteoclasts and osteoblasts continue to remodel the fracture site for a period ranging from 4 months to over a year. When the process is complete, the callus is gone and only cortical bone remains.

Fractures are classified according to their external appearance, location and the nature of the break or crack in the bone. The broadest classification of fractures is that of open and closed. An open fracture involves a break in the skin whereas a closed fracture is completely internal. Four main fracture modes are highlighted below. Other fracture modes will be discussed in later sections when dealing specifically with the femur.

- Transverse fractures are the result of a direct blow or a pure angular force applied to the bone. The shape of the bone ends helps the fracture site to remain together.

- Oblique or spiral fractures are quite common in long bones from twisting about the long axis of the shaft. The fragments of a spiral fracture are more difficult to align than the square ends of a transverse fracture and are very unstable.

- Comminuted fractures are fractures where the bone is broken into more than two fragments. These fractures are very difficult to repair in an exact anatomical sense.

- Crush fractures occur where cancellous bone is crushed in on itself. These fractures can be particularly difficult to detect and are awkward to repair, as there are no fragments left to manipulate into position.

2.7 The aged skeleton

As bones increase in age they become thinner and weaker as a normal part of the ageing process. Reduction in bone mass begins between the ages of 30 and 40 and it is oseoblast activity that begins to decline. Osteoclast activity continues however at the same rate as previous. The term given to inadequate ossification is known as osteopenia and every person becomes slightly osteopenic as they age. Once the reduction in bone mass begins, women lose approximately 8 percent of their skeletal mass every decade whereas men decline at approximately 3 percent each decade. The loss of bone mass is not even throughout the body. The epiphyses, vertebrae and jaws are the worst effected areas resulting in a loss of height and teeth and fragile limbs.

When this reduction in bone mass suffices to compromise normal functioning, the condition is known as osteoporosis. The resultant fragile bones are much more likely to break in these cases; for example an old lady may break her femur merely by standing up. Over the age of 45 an estimated 29 percent of women and 18 percent of men have osteoporosis (Martini *et al.*, 2001).

2.8 A Brief History of Bone analysis – The Femur

The occurrence of injury and deformities to the human femur encountered over the years has led to a requirement to obtain an understanding of the femur and its internal architecture. The femur has been studied in more detail than any other bone in the human body, owing to its largeness and uniqueness of structure. Despite the wide variety of literature there still remains many discrepancies on the theory of remodelling, techniques for fracture fixation and the internal architecture of the femur. The following section provides a brief explanation considering the femur as a load carrying structure. An exhaustive account has not been recorded due to the large amount of work that is available to peruse.

The earliest mention of bone architecture is accredited to Galileo (1638) who made important discoveries in applied mechanics of beams and the comparison to bones. He also recognised the possible significance of trabeculation and concluded that hollow cylinders are stronger than solid rods in certain applications.

It was not until 1832 that the issue of inner architecture and mechanics of bone begun to be understood more clearly. Bourgery (1832) published an anatomy atlas that was intended to tackle the problem of bone inner architecture. Jacobs illustrated the work whereby the inner structure of the femur and tibia were accurately portrayed (Koch, 1917). Understanding and explanations of the inner workings were alas erroneous, the illustrations however were almost as accurate as photographs.

Jefferies Wyman (1857) advanced the theory of inner bone architecture by analysing the femur and grouping the trabeculae of cancellous bone into three groups. The first was a tensile group, moving from the lateral part of the diaphysis and crossing into curves at the femoral head. The second was a

compressive group rising from the medial portion of the diaphysis, traversing radially as straight lines upwards to reach either the articular surface of the femoral head or meeting lines in the first group. The third group considered many struts merging the other two groups together. This last group was quite inaccurate however the first two were not.

Humphry (1858) published his findings on inner bone architecture and made two major contributions to the inner surface of the femoral head. Firstly, in the frontal section trabeculae from the articular surface of the head are perpendicular to the surface at all points. Secondly, that there are two principal groups of trabeculae that intersect at right angles to each other (Koch, 1917).

Hermann von Meyer (1867) demonstrated a collection of human bones and discussed the arrangement of trabeculae of cancellous bone. By chance the great mathematician Culmann attended and noticed that the trabeculae of many bones arranged themselves in forms similar to those he had calculated as the lines of maximum internal stress in similar structures. This in turn led to his calculations of lines of maximum internal stress in a Fairbairn crane having a form which was approximately that of the upper fourth of the femur. The conclusion was that trabeculae lie along the paths of maximum internal stress within the bone and transmit a maximum load with minimum material usage (Von Meyer 1867).

Then in 1892 Wolff's classic paper on the law of bone transformation was published and Culmann's theory of lines of maximum stress was cited. Wolff used the citation as mathematical proof that inner bone architecture follows exact mathematical laws and that the form and inner structure of bone is determined by static conditions present in normal cases.

There were many more publications after this time expanding upon the work of Wollf and Culmann. Zschokke (1892) for example insisted that inner architecture of bone is designed only for compressive loading, a theory that is utilised to some degree today.

To discuss all theories of interest concerning bone architecture and leading to the mechanical properties of bone would be an exhaustive task. The main early

theories have been presented to give the reader an understanding of the history of bone architecture and mechanical understanding.

2.9 The mechanical properties of bone

A large amount of material has been gathered over the years concerning the mechanical properties and architecture of bone and to summarise them all would be futile. Most of the data is in agreement and the work presented here is, in general, consistent. There are inherent problems with classifying the mechanical properties of bone. A large variance in data occurs from sex of specimen, age and the use of cadaver test specimens. Also, bone is a complex material being non-homogeneous and anisotropic. As such, material properties are very difficult to measure and quantify.

Form of specimen tested also has an influence, whether whole or blocks of cortical or trabecular bone are tested, or indeed a combination of the two. Bones from cadavers can yield misleading results, especially with regards to plastic deformation (Reilly & Burstein 1974). Sampling from a bone also presents problems due to varying trabeculae systems.

In addition, strain rate has a pronounced effect on many of the properties under investigation and for practical reasons many tests are carried out at lower strain rates than occurs in reality. For this reason actual values are often higher than those measured.

The mechanical properties that will be dealt with in this section are elastic properties of bone, particularly Young's modulus, and the strength of bone (compressive and tensile).

There are two main ways in which the elastic modulus of a bone specimen can be ascertained. The first is by mechanical methods, by applying a load to the specimen and measuring the resultant deformation within it, and the second is by ultrasonic methods. The elastic modulus can be gained from measuring the speed of sound in the specimen.

Early testing of bone was of the mechanical method and Rauber (1876) measured the modulus of elasticity of the femur in a 46-year-old man to be between 19.4 and 20.5GPa. He also measured the modulus of bone from a human tibia to be between 18.3 and 20GPa.

Later testing from Reilly, Burstein and Frankel (1974) and Reilly and Burstein (1975) gave mechanical testing of 17GPa axially, and 11.5GPa in the radial and tangential directions for cortical bone in long bones.

Ultrasonic testing yielded a value between 18.4 and 27.4GPa axially, 8.5-18.8GPa tangentially and between 6.9 and 18.8GPa in the radial direction for cortical bone. This testing was carried out by; Knets *et al.,* (1975) Van Buskirk *et al.,* (1981) and Yoon *et al.,* (1976b).

Van der Sloten and Van der Perre (1989) divided the femur into four areas for their finite element analysis, a cortex zone, femoral head, femoral neck and intertrochanter zone. In the cortex region 17GPa is used, 0.9GPa for the cancellous bone in the femoral head, 0.6GPa for the femoral neck and 0.26GPa for the intertrochanter zone. Taylor *et al* (1996) divided the cancellous bone into five groups with the modulus varying from 0.25 to 1.25GPa in increments of 0.25GPa. 17GPa were used for the cortical bone.

There is a greater variation in the data presented for cancellous bone due to the architecture of it, and cancellous bone density varies greatly due to the orientation and structure of the trabeculae. Indeed, Keaveny and Hayes (1993) reported that a variation in cancellous moduli of up to 60% could be caused by a change in density alone. Cancellous bone is a complex three-dimensional porous structure, with an open cellular matrix at low densities and a closed network of plates at higher densities. The density of cancellous bone seems to be dependent on the magnitude and direction of any applied loads (Cowin, 1989). The structure of cancellous bone is dependent on the direction of the applied load. If the load is multi-directional as in the acetabular cup (socket in pelvic girdle mating with femoral head), there is no preferred orientation (Dalstra *et al.,* 1993). Lisbeth *et al.,* (1991) reported no systematic variation between the Young's modulus of cancellous bone under tensile and compressive conditions, measuring the mean

value for Young's modulus under compression as 0.485GPa and in tension 0.483GPa. Carter *et al.*, (1980) measured an elastic modulus of between 0.5 and 3GPa for the proximal and distal femur, whereas Martens *et al* (1983) measured 0.9GPa (± 0.7GPa) for the femoral head and 0.6GPa (±0.7) for the femoral neck. The compressive modulus of cancellous bone has been measured to be as low as 4MPa (Goldstein, 1983) and as high as 3.4GPa (Ashman *et al.*, 1989), with a mean modulus typically being in the range of 200-600MPa.

Another possible method used to determine the elastic constants of bone is modal analysis. This technique uses frequency of vibration on a bone specimen with its mass and density values to determine the modulus of elasticity. The advantage of modal analysis is that it offers the possibility of measuring the elastic constants at all portions of a bone. W.R. Taylor *et al* (2002) used such a method, both experimentally and with finite element analysis. Modal analysis produced an axial elastic modulus of 22.9 GPa, a radial value of 13.4 GPa, and a tangential modulus of 14.1 GPa. The limitation of this work is that no account was taken for the function of the cancellous architecture, only the orientation of the bone material.

Tables 2.1 and 2.2 show a selection of values for the elastic moduli for cortical and cancellous bone.

In many respects the strength of a specimen is much easier to measure, as the specimen can be loaded until it breaks and the strength is calculated directly. It has been proposed quite reasonably that the tensile strength of bone is not a useful parameter as there is no clear indication to the sensitivity bone has to cracks and flaws in it, which are inevitable through the life of any bone. Fracture mechanics has been proposed as a better indication of how bone really behaves. Bonfield, (1981) was a supporter of this proposal. Relatively simple strength tests do have several advantages however, one such being simplicity as fracture mechanics requires large specimens with pre-cut notches.

Author	Method	Modulus (GPa)
Rauber (1876)	Mechanical	E_{11} = 19.4 - 20.5
Reilly *et al* (1974,75)	Mechanical	E_{11} = 17
		E_{22} = 11.5
		E_{33} = 11.5
Knets *et al* (1975)	Ultrasonic	E_{11} = 18.4
		E_{22} = 8.5
		E_{33} = 6.9
Yoon *et al* (1976)	Ultrasonic	E_{11} = 27.4
		E_{22} = 18.8
		E_{33} = 18.8
Van Buskirk *et al* (1981)	Ultrasonic	E_{11} = 21.5
		E_{22} = 14.4
		E_{33} = 13.0
Carter *et al* (1981a)	Mechanical	E_{11} = 17.5
Taylor *et al* (2002)	Modal	E_{11} = 22.9
		E_{22} = 14.1
		E_{33} = 13.4

Table 2.1 – The elastic modulus of human cortical bone. E_{11} – along the axis of the femur, E_{22} – radial direction, E_{33} – circumferential direction.

Author	Location of specimen	Youngs Modulus (MPa)
Carter *et al.*, 1980	Proximal and distal femur	500-3000
Rohlman *et al.*, 1980	Proximal and distal femur	389(43-1531)
Martens *et al.*, 1983	Proximal femoral head	900±710
	Proximal femoral neck	616±700
Tanner *et al.*, 1988	Proximal femoral head	110(50-200)
Lisbeth *et al.*, 1991	Proximal and distal femur	485

Table 2.2 – The elastic modulus of human cancellous bone.

The values presented from strength tests are from two papers, Reilly, Burnstein and Frankel (1974), and Reilly and Burnstein (1975). These two tests used comparable methods in tension and compression from the same shaped specimens, loaded at the same strain rate.

Parallel to the long axis tensile strength is given as 148MPa and compressive as 193MPa.

Shear modulus is reported as 3.3 from Reilly *et al* (1974) and 4.9 by ultrasonic methods from Knet *et al* (1975). Reilly *et al* (1974) also stated a Poisson's ratio of 0.41 and Knet *et al* as 0.32. However W.C. Van Buskirk and R.B. Ashman (1981) stated that the value of Poisson's ratio from Reilly *et al* was too high and confirmed from Bernstein (1974) that their method for measuring this value was not accurate. W.R. Taylor *et al* (2002) found Poisson's ratio to be between 0.31 and 0.37.

Bone has a number of design features that reduce the likelihood of fracture. Bone is stronger in compression than in tension, Stone *et al* (1983), and as such the skeleton is designed to avoid tensile loading and to be stressed predominantly in compression. It has been shown by Duda *et al* (1997), that the anatomy and function of the system comprising of the femur, pelvis and acting muscles is optimised in a way that limits the highest bending stresses in the femoral shaft. However bending stress will cause part of a bone to be placed in tension and so the design of the skeleton along with muscles, tendons and ligaments all account for reducing the bending moments within bones.

Another aspect of bone is in its microscopic structure reducing stress concentration effects. Bone has a microscopic structure equivalent to that of a fibrous composite with a high volume fraction of fibres. Cement layers around Haversian systems and blood channel networks in laminar bone act as interfaces that can stop crack propagation, divert the route of the crack and generally increase the amount of energy required to keep the crack travelling through the bone. Haversian systems also have a vigorous blood and nerve supply and can repair micro-cracks. It is however very difficult to evaluate this and little work has been carried out on micro-cracks in bone.

2.10 Structure of the Human Femur

The femur is the longest and heaviest bone in the body and serves primarily as a lever providing attachments for muscles that propel the body forward. It also serves many important metabolic functions and is a key resource for energy

supplies in the storage of lipids in yellow bone marrow. In the proximal end there is the greater trochanter, lesser trochanter, femoral neck and femoral head (see figure 2.4). The neck is obliquely placed and limited laterally by the greater trochanter. The femoral head forms two thirds of a sphere and is directed medially upwards and forwards. The shaft of the femur is slightly bowed forward with its middle two quarters approximately circular in cross-section.

The femur articulates with the os coxae at the hip joint and with the tibia of the leg at the knee joint. The rounded epiphysis, or femoral head, articulates with the pelvis at the acetabulum. The acetabulum is attached to the femur by a ligament at the fovea capitis, a small pit in the centre of the femoral head. The neck of the femur joins the shaft at an angle of about 125°.

The greater and lesser trochanters are large, rough projections that extend laterally from the junction of the neck and shaft. Both trochanters develop where large tendons attach to the femur. On the anterior surface of the femur, the raised intertrochanteric line marks the edge of the articular capsule. This line continues around to the posterior surface as the intertrochanteric crest.

The linea aspera is a prominent elevation that runs along the centre of the posterior surface, marking the attachment site of powerful hip muscles.

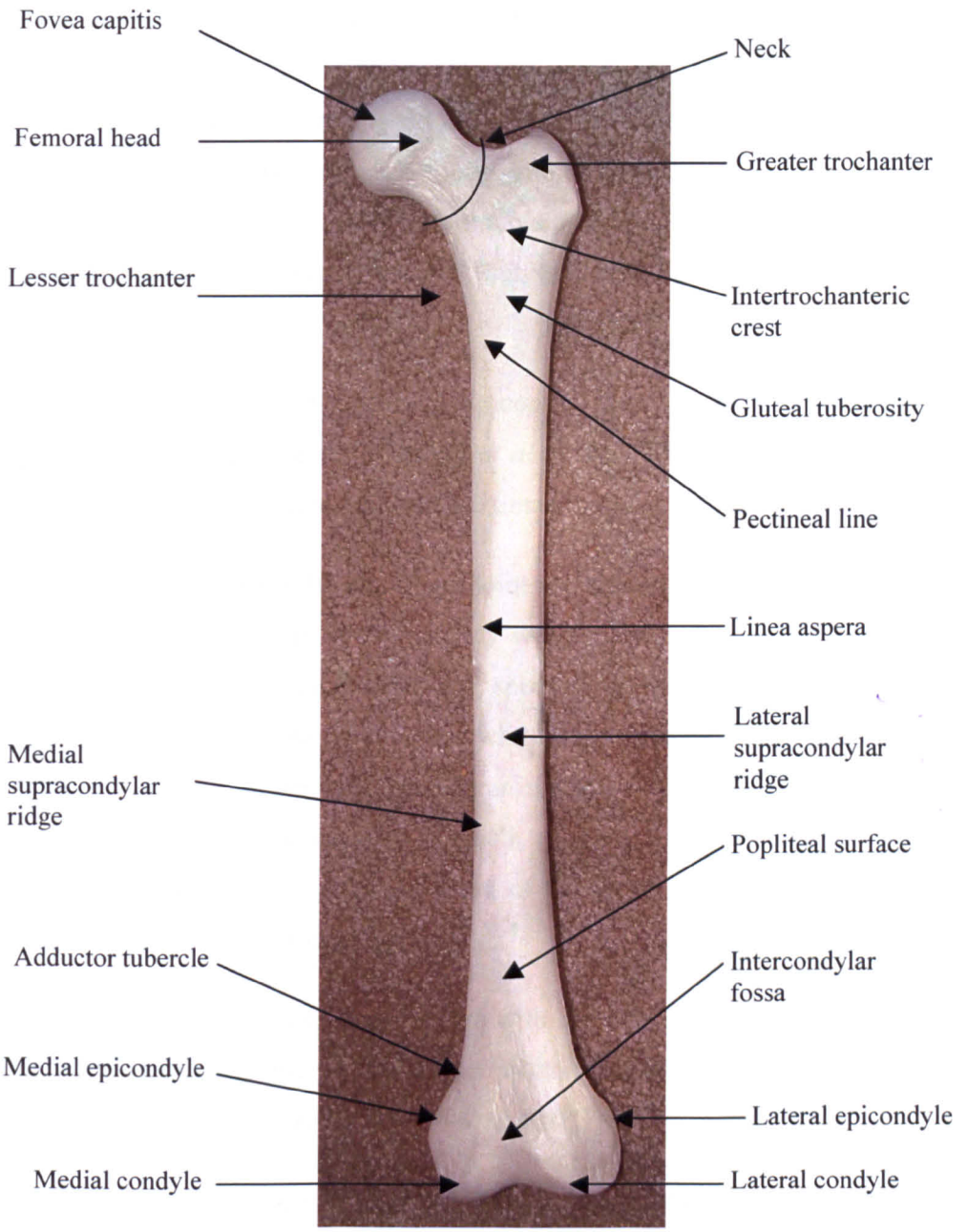

Figure 2.4 – Structure of the human femur.

2.11 Loading of the Femur

The femur is subject to many types of loading, from static loading when standing, to varying degrees of dynamic loading when walking, running or climbing stairs. The femur itself does not withstand the entire load but surrounding muscles and ligaments aid in the support of the body and propulsion of it. The hip joint is a ball and socket joint, and as such cannot withstand a net moment. Muscular forces are required to maintain an upright posture. Values for the muscle loading have been calculated, but vary with change in posture and activity.

English and Kilvington (1979) obtained hip contact forces measured *in-vivo* and more data became available from Kotzar *et al* (1991). These studies measured the total hip force to be between 2.3 and 3.6 times the body weight.

At a slow pace of walking the maximum joint force when the leg is supporting weight has been reported as 300% of body weight at 4km/h, and this rises to 400% or 450% of body weight when the speed is at 5km/h (Bergmann *et al* 1994). A smaller average maximum force when slow walking, of 238% of body weight, has also been shown by Bergmann *et al* (2001). Whilst the leg is in the swinging phase of walking the load is small, typically 100% of body weight. Bergmann has also reported on the loading of the femur at low speeds taking place predominantly in the frontal plane.

During jogging the joint loads increase less with speed than they do in walking. About 500% of body weight is a typical maximum for jogging at speeds between 4.2 and 7km/h (Bergmann *et al* 1993, 1994, and 2001).

Stumbling and falling cause a dramatic rise in the average maximum force applied to the hip joint. Stumbling whilst walking causes an increase to 620% and 870% of body weight (Bergmann *et al* 1994).

Walking upstairs increases the load on the hip by 20-35% of normal walking. The increase is more pronounced when walking downstairs rather than up (Bergmann *et al* 1994). High torsional loading is created when walking upstairs, and greater torsional loads have been measured *in-vivo* than can be withstood in

laboratory testing. Torsional loads can lead to micromotion between implant and bone and certainly lead to high bone stresses. Davy *et al* (1988) measured the stair climbing loads and found that the anterior-posterior component of the force in the joint reaction force is 41.3% of the total resultant of the joint reaction force. Harrigan and Harris (1991) carried out similar experiments and derived the anterior posterior component to be 45.1% of the resultant force.

Whilst standing on two legs the joint forces are typically between 60-100% of body weight (Bergmann *et al* 1994). In theory only about 33% is required for this position and the discrepancy is accounted for by the muscle activity required to stabilise the position. Standing on one leg causes almost the same joint forces and load directions as slow walking. Van der Stolen and Van der Perre (1989) carried out simple calculations on a simplified model for a one legged stance and proposed that the resultant force on the femoral head amounts to 1711N and the traction of the abductor muscles amounting to 1270N. Harrigan and Harris (1991) and Prendergast and Taylor (1990) also used this type of bending load.

The designation of forces applied to the human femur in both experimental and finite element studies has been somewhat arbitrary. The majority of studies consider the femur model to be simplistically loaded. Usually only a joint reaction force is applied to the femoral head, and sometimes this is coupled with an additional abductor muscle force. Fagan and Lee (1986) used a force and moment analysis to calculate the load applied to the proximal femur for a one legged stance. The actions of the muscles around the trochanter were simplified into three groups; the abductor muscles, the ilio-tibial band and the ilio-psoas muscle.

Taylor *et al.*, (1996) concluded that the femur is loaded predominantly in compression in the one-legged stance and recommended that the compressive loading consists of a 3kN load applied to the femoral head, a 1.25kN abductor load, a 1.2kN ilio-tibial tract load and a 0.8kN ilio-psoas load. This loading condition produced a predominantly bending load in the femur.

In summary there has been a varied amount of data available for the loads acting on the human femur. However, few studies incorporate a large population and

thus trends and maximum average loads observed could easily become more varied if a greater number of patients were to be included (Bergmann *et al.*, 2001).

2.12 Fractures of the Femur

Fractures of the proximal femur are seen in young patients from high-energy injuries or from elderly patients with weakened bones. These fractures are more common in women because women live longer than men, and the hormonal changes experienced through the menopause make them more likely to get osteoporosis. Fractures of the femur are becoming more common as the population of the world increases coupled with the average life expectancy increasing.

2.12.1 Fractures of the femoral neck

These types of fracture are caused from trivial injury or without any injury at all. An old lady standing up from a chair can break the femoral neck if the bone is very brittle. Clinical indication tends to show the broken leg as shorter and rotated externally because the fracture allows the femoral shaft to act independently of the hip joint.

There are two types of fracture that occur to the femoral neck; intracapsular and extracapsular. Intracapsular fractures occur from a high transcervical fracture and interrupt the blood supply to the femoral head. In severe cases these fractures can cut off the blood supply completely to the femoral head and in turn cause aseptic necrosis, non-union of the fracture ends or both. The fracture line is inside the capsule and as a result the intracapsular pressure rises, causing further damage to the femoral head. Visible bruising is not present, as the blood cannot reach the subcutaneous level. Furthermore intracapsular fractures leave the femoral head very mobile in the capsule, which makes accurate reduction extremely difficult. Extracapsular fractures are notorious for their high complication rate.

Extracapsular fractures occur outside the capsule of the hip and are less serious for three main reasons. Firstly the blood supply to the bone is not as restricted as in intracapsular fractures, second the fracture area available for union is larger

and thirdly the femoral head is less mobile within the capsule. Undisplaced and impacted fractures comprise of the bone ends being crushed together meaning that the fracture may go undiagnosed for some time. Some patients are able to still bear weight on their leg even after fracture, and the bone ends may become displaced weeks after the fracture actually occurred.

Treatment of femoral neck fractures is usually from internal fixation, by means of a screw and plate, a pair of cross screws or an intramedullary nail.

2.12.2 Trochanteric fractures

There are four types of trochanteric fractures. These are pertrochanteric, intertrochanteric, subtrochanteric and avulsion of the trochanters. Figure 2.5 demonstrates these fracture types.

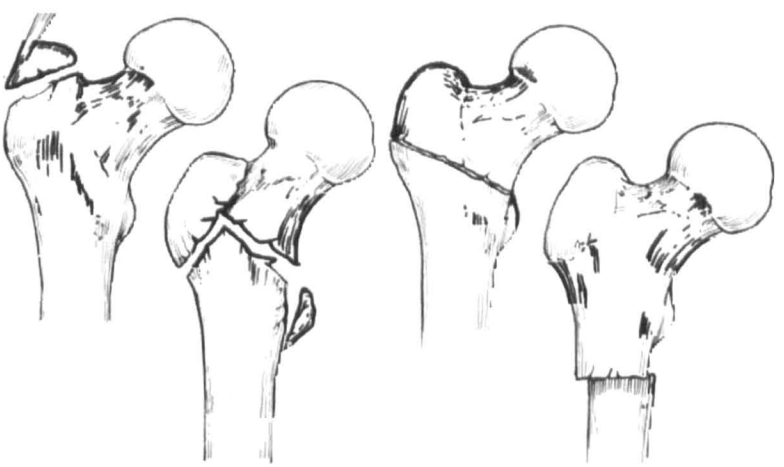

Figure 2.5 - Types of femoral trochanteric fractures, from left to right; avulsion of the greater tuberosity, pertrochanteric fracture, intertrochanteric fracture, subtrochanteric fracture.

Unlike fractures to the femoral neck, trochanteric fractures usually involve a history of trauma. Different fractures of the trochanter pose different problems from those of the femoral neck. Due to the fact that these fractures occur through cancellous bone and are surrounded by muscle they almost always unite but are highly unstable and mal-union can easily occur.

Avulsion of the greater trochanter can occur through violent adduction strain and is usually very painful to the patient.

Trochanteric fractures may be treated with a dynamic compression screw or an intramedullary nail. Both have their advantages as is discussed later in section 2.14. As a general rule if the fracture is considered clinically unstable whereby there are many fracture fragments, such as the pertrochanteric fracture in figure 2.5, an intramedullary nail is favoured. However if the fracture is in only two pieces and thus considered stable, a dynamic hip screw is favoured as the bone is able to support itself in the trochanteric region. At present, approximately 20% of stable fractures are treated with an intramedullary nail.

2.13 Fracture fixation

The three principles of fracture management are as follows:

1. Reduction of the fracture
2. Immobilisation / fixation of the fracture fragments long enough to allow union
3. Rehabilitation of the soft tissues and joints

There are four ways to reduce a fracture site; traction, external splints, external fixation and internal fixation. Some fractures may not be displaced and thus do not require traction, others do however to maintain correct bone positioning.

Traction involves pulling on a broken limb to draw the ends of the fractured bone into alignment for healing of the fracture site. Traction can be applied to the skeleton or to the skin. Skeletal traction is often less painful to the patient and presents less practical problems.

Any device that holds a fracture steady is known as a splint. Splints do not provide rigid fixation and often can become loose as swelling about the fracture site occurs.

Fractures that cannot be reduced by traction or the use of a splint can either be held by internal or external fixation. Internal fixation should not be used when severe contamination of the wound is present because of the risk of infection.

Two advantages of external fixation are that it can be used in patients with skin loss or infection and the position of fragments can be easily adjusted.

Internal fixation can provide exacting anatomical alignment of fracture sites. There are four types of internal fixation in common use: screws, plates, nails and wires.

Screws are used to compress plates against bone or to compress bone fragments together. There are two main types of bone screw in operation today. These are cortical screws, which can be self-tapping, and cancellous screws that have a wide thread to grip the soft more porous bone.

Plates serve to hold bone fragments together and to apply compression to the fracture site. Fixation by use of a plate has some disadvantages. Firstly, wide exposure of the fracture is needed to allow access. It may also be difficult to close the skin over a fracture depending on the size of the plate. The plate may be so rigid that it acts as a stress raiser at either end where further fractures may occur, and also from the occurrence of disuse, osteoporosis of the underlying bone.

Wires can be used to fix fractures in two ways. Firstly, a tension band wire can be applied as a loop to the outer side of the fracture so that it comes under tension when the joint is flexed. This method is particularly useful for the patella. Secondly a cerclage wire can be used in spiral fractures with minimal displacement. Wire fixation has the problems of slipping, and rigid support is not provided.

Nails are devices that are inserted into the centre of the medullary canal and are fixed with screws to hold fracture fragments together. One common nail in use today is the Gamma nail. Nailing offers several advantages such as less operative exposure as the technique is minimally invasive and also early weight bearing at the fracture site. The following section provides a discussion on nailing techniques used.

2.14 Intramedullary nailing – Overview

2.14.1 A brief history of femoral fracture fixation

2.14.2 Femoral neck fractures

Nailing can be traced as far back as 1858, when two surgeons, Johann Friedrich Dieffenbach and Bernhard Rudolf von Langenbeck, nailed a femoral neck fracture (Brunn, 1929; Gluck, 1930). At the time however non-surgical methods were preferred, and with a healing rate of 60%-80%, surgical procedures were pushed into the background. In 1925 Smith-Petersen introduced a three-blade nail that shortened fixation and immobilisation times and thus brought surgical treatment to the fore (Lentz, 1990). In 1934 Palmer showed that foreign body reactions with negative effects to fracture healing did not occur, and in 1951 extra-articular nailing was declared the method of choice for treating medial femoral neck fractures (Hohle, 1952; Koslowski, 1960). Over the next few years the surgical procedure became the method of choice due to the lower mortality rates, reduced hospitalisation times and favourable economic benefits.

ancellous trabeculae are 'bent' in an elastic manner when an intramedullary nail is used, and elastic forces from the trabeculae help keep the nail in place.

However, Kuntscher made the point that elastic jamming would become ineffective during healing as a result of resorption of the trabecular bone, thus loosening the implant (Kuntscher, 1972). Furthermore the viscoelastic nature of the trabeculae might lead to a loosening of the fit. Kuntscher did however develop the Steep nail based on this principle for the treatment of pertrochanteric fractures. Indeed, dislocation of the Smith-Petersen nail was shown from X-rays, and attributed to femoral necrosis and misalignment of the nail. In 1952 Ernst Pohl developed the double screw to prevent nail migration, whereby the lower screw was the supporting screw, connected to a slightly smaller lag screw (Marwege, 1957). In 1955 Wassner summarised guidelines for the treatment of medial femoral neck fractures which are valid today, they included: Fracture surfaces should interlock where possible; true immobilisation of all movements in the fracture region is desirable, stable internal fixation should be the aim (Wassner, 1955).

The 'sliding plate' developed by Pohl met these conditions, and from then on the plates and screws for the fixation of femoral neck fractures to bring the fracture line into compression were continually used and developed (Ungern-Sternberg, 1966).

2.14.3 Pertrochanteric fractures

Since the beginning of surgical fracture treatment various implants have been developed and used to stabilise pertrochanteric fractures. They fall into two distinct classes: extramedullary and intramedullary. The Smith-Petersen three-blade nail developed for femoral neck fractures in 1925 was the first implant to be used for the treatment of pertrochanteric fractures. The nail was only used with the extra-articular technique and there were restraints on its use for pertrochanteric fractures, such as requiring the fracture fragments to be sufficiently large to hold the nail. To remove the constraints on the Smith-Petersen nail the Johansson nail was developed. Made from vitallium and featuring a stem this nail was used in America from 1939-1941. A German team named Rehbein developed the three-blade nail and plate into a two-blade V profiled nail and plate, which was possible as rotation of the nail was prevented from fixation with the femur.

In 1939 Kuntscher pointed out that his Steep nail could also be used to fix pertrochanteric fractures, however if there were parts of the lesser trochanter broken off, then this nail was no longer suitable as the bone could not support itself. He thus designed in 1940 the double nail or Y nail, the first intramedullary nail. In 1964 Kuntscher presented a long slightly bent trochanteric nail for pertrochanteric fractures, which had the advantages of smaller surgical incisions away from the fracture and early weight bearing (Kuntscher, 1970). In 1952 Ernst Pohl developed the non-locking Pohl plate system from the Kuntscher Y nail, which consisted of a hip screw that fixed firmly in the femoral head and allowed dynamisation with a plate fixed to the femoral shaft, allowing compression at the fracture surface. In the following decades all implant manufacturers developed this type of fixation with various modifications. Based on the Pohl plate the AO/ASIF developed the Dynamic Hip Screw, which was indicated for the treatment of all pertrochanteric hip fractures. This device

secured itself as the most commonly used device in German speaking countries for the stabilisation of pertrochanteric femoral fractures.

The stability of a fracture is a good indication of the usefulness of an implant, and from synopsis of the results from the Dynamic Hip Screw, coupled with years of experience, intramedullary devices are beginning to be favoured over extramedullary ones. In 1988 the Gamma nail was introduced with favourable advantages over compression hip screws. The Gamma nail utilises a smaller lever arm, and thus is capable of carrying a higher load, and is therefore better suited to unstable or comminuted fractures where the bone fragments cannot support themselves. A comparison of the two devices is given in the following section.

2.14.4 Intramedulary or extramedullary

Intramedullary nailing of the proximal femur involves the insertion of a nail into the medullary canal, and securing it in place at the proximal and distal ends, more often than not with the use of locking screws. A lag screw is often used to stabilise and reduce fractures, especially in the pertrochanteric region. A lag screw inserted into a human femur is shown in figure 2.6. Intramedullary nailing offers some distinct advantages over other fracture fixation devices, which has led it to become, in many cases, the preferred treatment in adult subjects. Surgical exposure is low, with minimally invasive techniques being used; preservation of periosteal vascularity is also achieved. Predictable restoration of length and alignment coupled with early mobilisation and weight bearing also adds to the preference of intramedullary nailing.

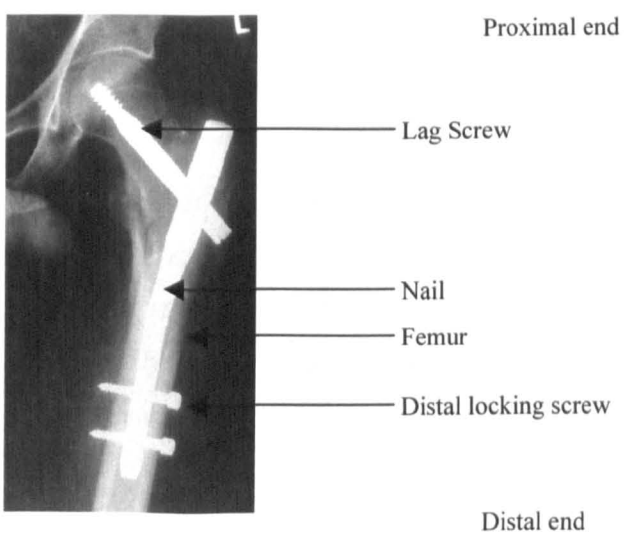

Figure 2.6 – An intramedullary nail inserted into a human femur.

Prior to the use of intramedullary nailing, rigid combinations of a femoral head nail with a lateral plate or angled blade plates were used. These devices were subject to failure however, including nail cut-out, secondary fracture displacement and metal failure, (Chinoy *et al* 1999). As a result dynamic fixation methods such as the compression hip screw or dynamic hip screw were introduced. Pohl introduced the first of such in 1952. These consist of a lag screw passed up the femoral neck to the femoral head. This lag screw is then attached to a plate on the side of the femur. These devices are considered dynamic as they have the capacity for sliding at the plate/screw junction to allow for collapse of the fracture site. Surgeons commonly use the dynamic hip screw as a preferred method of internal fixation and its use can be considered the standard implant for stable intertrochanteric fractures (Brandt *et al.*, 2002; Bridle *et al.*, 1991; Leung *et al.*, 1992; Haynes *et al.*, 1997; Radford *et al.*, 1993; Zafiropoulos *et al.*, 1994). The reason for the preferred use of the compression hip screw could be accounted for by the fact that other nailing devices such as the Gamma nail are relatively new devices and as such surgical procedures require a learning curve for efficient fitting, causing a surgical bias towards the compression hip screw (Goldhagen 1994; Guyer 1991; Hoffman 1996).

It is also reported that dynamic hip screws are more suitable for stable subtrochanteric fractures, (Kulkarni *et al.*, 2003), even in older patients with osteoporotic bone so long as early weight bearing is minimised. In the case where the fracture may extend to the greater trochanter the use of intramedullary devices may become contraindicated (Guyton 1998). Subtrochanteric fractures have a high complication and non-union rate with operative measures (Schatzker *et al* 1980). The reason for this is that the majority of the bone in this region is cortical, which has less vascularity and is often comminuted. Also, the biomechanical stresses here lead to implant failure before fracture union.

There have been a number of studies that have reported failures of the compression hip screw. Between 10% and 25% failure rates have commonly been reported (Simpson *et al.*, 1989; Davis *et al.*, 1988; Brandt *et al.*, 2002; KulKarni *et al.*, 2002). The dynamic hip screw failure mechanisms are from lag screw cut-out of the femoral head (Bridle *et al.*, 1991), bending of the lag screw

itself or the cortical screws pulling out of the lateral side of the femur causing loosening of the plate (Haynes *et al.*, 1997). Haynes reported of the high bending moments being placed upon the laterally positioned cortical screws. This resulted in the screws being pulled out at relatively low failure loads.

An alternative to the compression plates is an intramedullary nail, and one such device is the Gamma nail. There is still much debate as to which device is best suited to a particular fracture, but in general it is considered that the Gamma nail is more suited to unstable proximal femoral fractures due to the shorter lever arm.

Biomechanical studies have shown that intramedullary nailing of most subtrochanteric fractures, particularly those with unstable fracture patterns are significantly stronger and more rigid than compression hip screws (Curtis *et al.*, 1994; Mahomed *et al.*, 1994). The Gamma nail has been shown to have a 30% greater load to failure than the dynammic hip screw (Mahomed *et al.*, 1994), and this increased strength has been attributed to many factors. One such factor is the fact that the proximal end of the Gamma nail is larger than the hip screw, which makes it more resistant to bending. Also the lag screw is larger than with the hip screw, and the increased cross-section dimensions of the gamma nail give it a six-fold increase in moment of area. As the maximum deflection of the tip of the screw is inversely proportional to its second moment of area and directly proportional to its length, the Gamma nail can show significantly less deflection than the sliding hip screw (Rosenblum *et al.*, 1992). Haynes *et al.*, (1997), who showed that Gamma nail fails at greater loads than the dynamic hip screws, also cited this fact.

Aside from increased load capacity of the Gamma nail, intramedullary nails are positioned nearer to the axis of weight bearing and thus the lever arm is reduced. There is thus a more medial transmission of the load from the femoral head to the diaphysis. The use of an intramedullary nail is a closed procedure having less soft tissue damage, less surgical trauma and a smaller operating time (Davis *et al.*, 1991; Halder 1992; Goldhagen *et al.*, 1994; Bellabarba *et al.*, 2000; Ahrengart *et al.*, 2002).

Intramedulalry nailing is also associated with less intraoperative blood loss and with smaller skin incisions (Leung *et al.*, 1992; Radford *et al.*, 1993; Ahrengart *et al.*, 2002), coupled with a lower rate of wound complications (Radford *et al.*, 1993).

Ahrengart *et al.*, (2002) reported a greater fracture reduction when using intramedullary nails and Bellabarba *et al.*, (2000) found a 98% union rate when using Gamma nailing for femoral fractures.

Other promising results from Gamma nail trials include reduced cut-out in osteoporotic bone (Haynes *et al.*, 1997), and a shorter time to full weight bearing (Leung *et al.*, 1992; Schick *et al.*, 1996). The possibility of still being able to manipulate fracture fragments with the nail during operation is also a possibility not available to the dynamic hip screw (Brandt *et al.*, 2002).

There are reports of failures to the Gamma nail, along with contradicting studies of certain findings. Bridle *et al.*, (1991) compared the fixation of 100 intertrochanteric fractures of the proximal femur in elderly patients and found no difference between operating times and intraoperative blood loss. Indeed, a study by Ahengart *et al.*, (2002) studied 426 fractures fixed with a compression hip screw or Gamma nail and showed that operating times for Gamma nails took longer than dynamic hip screws. Also the intraoperative bleeding was shown to be less in most fracture types with use of the compression hip screw. It must be noted however that the difference in operating time was not highly significant, and that the surgical procedure for the Gamma nail is still relatively new.

As with the compression hip screws, cut out of the lag screw also occurs with the Gamma nail (Bridle *et al.*, 1991; Haynes *et al.*, 1997). The cut-out of the lag screw can be reduced by central positioning of the lag screw in the femoral head. Ballabarba *et al.*, (2000) achieved this and the resultant cut-out failure was 1 in 100.

One of the greatest problems that arises from the use of intramedullary fixation is that of femoral shaft fractures whilst inserting the nail. There is a high incidence of femoral shaft fractures (Radford *et al.*, 1993; Parker *et al.*, 1996), which can be very damaging and painful to the patient, requiring further, and often more

complicated surgery. Reasons for the secondary fracturing of the femur are due to the increased stiffness of the nail and the curvature and size of it that leads to three point loading of the femur (Bellabarba, *et al* 2000).

Along with the problems cited here for intramedullary nailing, there is also the question of the configuration of the nail and its components. For example one or two lag screws can be used in the nail configuration, Tornetta *et al.,* (2002) found that two medium sized lag screws increase the rotational stability of the femoral head and neck fracture components.

The use of one, two or no distal screws has also come into question in the past. Ahengart *et al.,* (2002) reported greater fracture healing with two distal locking screws (93%) to those with no distal screws (81%). Bridle *et al.,* (1991) initially used no distal locking screws in any of the trials and later complications of rotational stability were incurred. The conclusion was that distal screws are essential for subtrochanteric fractures but not required as routine for intertrochanteric fractures, and this is consistent with findings from Rosenblum *et al.,* (1992). Radford *et al.,* (1993) also cited the non-importance of using distal screws for unstable fractures. It has also been suggested that distal screws can lead to spiral fractures in the femoral shaft (Lacroix *et al.,* 1995) from the addition of the stress raiser in the bone caused by the screw hole. Jinn *et al* (2001), carried out a stress analysis of distal locking screws in femoral locked nails with relation to nail-cortical contact. This work showed that the stress present in the screws was substantially affected by the amount of cortical bone contact, the distance from the fracture site to the locking screws and the number of locking screws. An optimised design for the distal end was for an increased distance between the distal locking screws, a smaller clearance between the screw and the screw holes and possibly the use of a smaller elastic modulus for the main nail, when compared to the locking screws.

Due to the problems associated with both the gamma nail and the dynamic hip screw, other intramedullary nails have been introduced. One such nail is the Proximal Femoral Nail. This device utilises a second lag screw placed above the first, smaller in dimensions to the other, for the purpose of preventing rotation of the device. Ramakrishnan *et al* (2004), carried out 49 long proximal femoral nail

operations for subtrochanteric fractures and had no mechanical failures of the implant. Union rates were relatively high with low complications and full bony union in all traumatic fractures. They concluded that using this device was a reliable choice for subtrochanteric femoral fractures. A further study carried out by Al-yassari *et al.,* (2002) used an AO/ASIF proximal femoral nail for the fixation of unstable femoral fractures in 76 patients. There was an 8% failure rate of the device due to screw cut-out within the femoral head, however fractures united in all patients and a 94% success rate was reported. Immediate weight bearing was achieved in 75% of the patients and all femurs had to be reamed before insertion of the device. The conclusion here was also that the proximal femoral nail is a useful device for the treatment of unstable trochanteric fractures. It is also stated that the use of fixation devices for unstable trochanteric fractures is controversial, and that comparison between the gamma nail and proximal femoral nail is required.

Finally the Gamma nail is a more expensive implant than the dynamic hip screw and this could be an issue when considering which device to use (Brandt *et al.,* 2002). Figure 2.7 shows radiographs of a dynamic hip screw and intramedullary nail.

There is a requirement for progressive research to understand failure mechanisms of intramedullary devices and to improve their design. Finite element analysis is one method that can be employed to analyse implant and bone constructs.

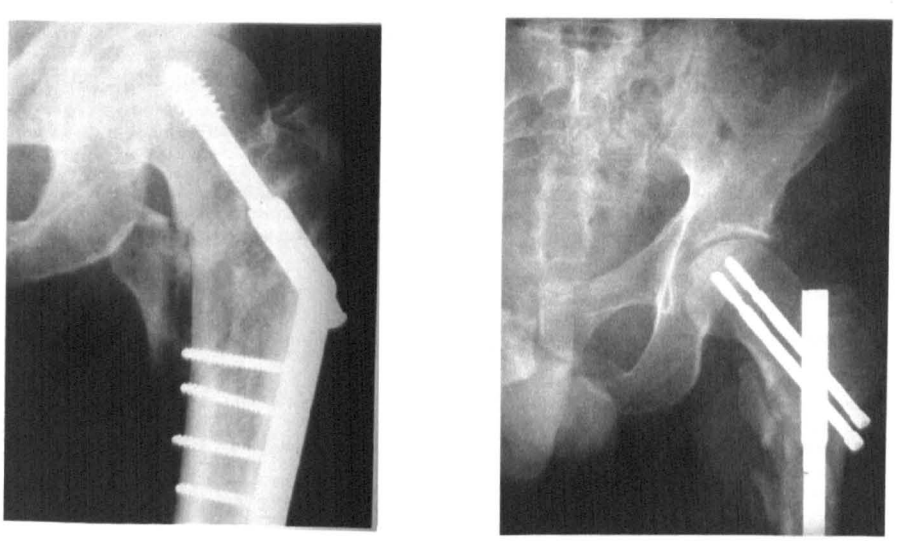

Figure 2.7 – Radiograph of dynamic hip screw and intramedullary nail used to stabilise subtrochanteric fractures.

2.15 Finite Elements and Intramedullary nailing

Finite element analysis can indicate potential failure points and can be of particular use in determining stress distributions throughout an entire intramedullary construct (Stolk *et al.*, 2002). Added benefits of finite element analysis of intramedullary constructs are that they do not require physical copies of the implant. Therefore parametric testing can proceed directly from design specifications without having to produce expensive prototypes. Finite element analyses have been used for the evaluation of intramedullary nailing and can provide a large data set at relatively low cost. Simplifications of finite element models concerning implant and bone interaction include merging together certain 'disconnected' components. A more detailed analysis incorporates contact mechanics between the implant and bone surfaces.

When dealing with contact between two bodies a variety of modelling approaches can be used. Many studies use node-to-node contact elements (Couteau *et al.*, 1998; Ramaniraka *et al.*, 1996). However these elements are not accurate when used with contact involving large sliding, a phenomenon frequently observed in bone-implant contact. Therefore other studies have used more accurate elements known as node-to-surface or surface-to-surface (Hefzy *et al.*, 1997; Mann *et al.*, 1995). When using finite element techniques with contact there are many numerical parameters that need to be defined, such as contact stiffness and convergence norm. Many studies do not pay attention to the problem of parameter identification. Vicenconti *et al.*, (2000), were the first group to attempt to systematically validate finite element models used in predicting bone-implant micromotion. They found that surface-to-surface contact, when simulating bone / implant friction, was far more accurate in predicting micromovement than node-to-surface contact and that such contact elements are much more accurate and flexible in terms of modelling and simulation. It was also stipulated that node-to-node contact models were almost insensitive to this friction. However, Vicenconti *et al.*, (2000), reported that caution should be exercised when analysing finite element models without the comparison to in-vitro measurements.

Finite element models using contact employ parameters that are difficult to evaluate, and the accuracy of such a model should be measured by some external reference. Bernakiewicz *et al.,* (2002) carried out a numerical-only study concerning micro-movements of a hip stem and stated that any numerical-only study involving contact non-linearity, without careful qualification of the models limits, should be rejected from any peer-reviewed journal.

The study by Bernakiewicz *et al.,* (2002), investigates the role of parameter identification on the accuracy of results produced by finite element models. The result of the study was that contact penetration and convergence tolerance play a crucial role in establishing the accuracy of the finite element results. Other studies investigating parameter investigation are presented in table 2.0, reproduced from Bernakiewicz *et al.,* (2002). The finite element model used was able to accurately predict the micro-movements measured experimentally when the appropriate parameters were used.

The paper produced accurate finite element results when compared to experimental data, however the fact of potential error sources and their unpredictable impact upon the model are cited as an essential consideration on any numerical study where experimental data is not available. Reference results for the study were taken from a synthetic femur with an implanted cementless prosthesis. The finite element model was adopted from a previous study (Viceconti *et al.,* 2000). Surface-to-surface elements were used with two contact groups being defined: stem-spongy bone and stem-cortical bone. Poisson's ratio was taken as 0.3 for all materials and the Young's modulus of cortical bone was taken to be 14.2GPa and that of cancellous bone 0.07GPa.

The usefulness of a numerical-only study can be considerable when a comparative study is undertaken. One such numerical-only study was presented by Sitthiseripratip *et al.,* (2003), who investigated the influence that material properties had on a trochanteric gamma nail. This study found that the use of a titanium nail resulted in a maximum von Mises stress below the yield stress, whereas that in the steel nail was above the yield stress. They also cited that there was a 30%-50% reduction in the stress magnitude when using the titanium nail, however there were greater deflections. This study analysed a one-legged stance

configuration. The material model assumes all properties are linear and isotropic and uses four different regions of the femur: cortical bone, 17GPa; femoral head (trabeculae), 0.9GPa; femoral neck (trabeculae), 0.62GPa, and an intertrochanteric region of 0.26GPa. The model constructed in this work used 10-noded hexahedral elements throughout and did not analyse contact between the nail and the bone and fixed the distal locking screws into the surrounding cortical bone.

With reference to fracture healing, Sitthiseripratip *et al.*, (2003), concluded that for both material implants used the stress distribution after fracture healing is similar in magnitude to that beforehand, leading to the assertion that the nail should be removed after full union of the bone. Wang *et al.*, (1999) stated that although the modulus of elasticity affects the pressures across the fracture site, more information is required concerning effects of contact pressure at the fracture plane to improve the design of the implant.

Seral *et al.*, (2003) presented a comparison between a Proximal Femoral Nail and a Gamma nail, again without any empirical data for verification, but a numerical-only study. They stated only slight differences between the two constructs when used to fix a pertrochanteric fracture. The Gamma nail produced a decrease in stress along the axis of the femur, not present with the Proximal femoral nail, and showed a stress concentration at the distal end with or without locking screws. They used this to explain instances of patients feeling pain with the Gamma nail. It was also showed that the Gamma nail had the higher von Mises stress, although both implants had stress values below there yield strength. Their material model was linear elastic, with values of cortical and cancellous bone of 14217MPa and 100MPa being used respectively. A Poisson's ratio of 0.3 was used throughout.

Detailed finite element analysis has been performed by Wang *et al.*, (1998, 2000) and Brown *et al.*, (2004) concerning a Gamma nail inserted into fractured proximal femur models, under hip reaction and abductor force loads. The results were not experimentally verified, but were numerical based with extensive parametric investigation. They were able to show that small changes in the lag screw configuration and dimensions can lead to large changes in the behaviour of

the biomedical device. It is stipulated that for subtrochanteric fractures, the most critical stress areas of the system occur at the most proximal distal screw and in the lag screw. Furthermore to reduce stresses in the system a slightly larger lag screw should be placed above a slightly smaller screw, contrary to that predicted by clinical studies carried out for a proximal femoral nail. It is also stated however that such a configuration can lead to large stresses at the fracture plane and therefore may not be reasonable for subtrochanteric fractures. This in turn can lead to screw cut-out, especially in osteoporotic bone, which is in agreement with the findings from Al-yassari *et al.*, (2002). With reference to the design features of the Gamma nail, reducing the modulus of elasticity reduces the contact stress present in the distal end but can significantly increase the contact pressure across the fracture site. Also a change in nail length can lead to a change in contact at the proximal end. The material model in this study is linear elastic and isotropic. There is a cortical region of the femoral shaft and part of the trochanter, (17GPa), a cancellous region about the femoral head, (1.3GPa), and a cancellous region in the trochanter, (0.32GPa). Three different load conditions are normally used: tension, torsional and compression loading.

Rohlmann *et al.*, (1983) performed an experimental and finite element test on an intact human femur, and on the same femur instrumented with a hip endoprosthesis. The femur was instrumented with strain gauges and tested in the two-legged stance position. The prosthesis was then instrumented with strain gauges and inserted into the femur. For the finite element model the femur was transsected into 38 sections and radiographs were then taken at each section. A perfect bond was assumed between the prosthesis and the bone, all materials were assumed linear and isotropic and the value of cortical bone was set to 18GPa. A minimum value of 40MPa and maximum of 1800MPa was used for the properties of cancellous bone. The paper showed an average difference between experimental and theoretical results of 8.5% and 12.7%, however they did point out that at some points on the finite element model the stress values were wholly inaccurate and attributed this to irregular elements at these points. It was also pointed out that at the middle of the element sides the stresses must be extrapolated from the Gauss points, which in itself incorporates numerical inaccuracies. They therefore stipulated that it is not useful to look at single stress

components, and that even principal stresses were very inaccurate at certain points. Other errors in the procedure were highlighted, including deviation of the locations of the strain gauges from the points for which values were calculated, and also in the fact that the finite element model was loaded from an undeformed state (geometrically and materially linear), whereas due to the bending load in the experiment it became geometrically non-linear. It was concluded that as there was a reasonable agreement between the experimental and theoretical work, that further results from the finite element model would be valid. The results of this investigation provided good indication for finite element modelling, as there was good qualitative conformity of results from experimental and finite element calculations.

A study by Cheung *et al.*, (2004), used finite elements to analyse a femoral nail subject to gait loading. Experimental verification is also given from the nail being inserted into a synthetic bone, subjected to a compressive load at different points of the gait cycle with surface strains being measured. Differing material properties of the nail were used, and linear elastic isotropic material properties of 206MPa for cancellous bone and 10GPa for cortical bone were used to model the femur. It is reported that the omission of the cancellous bone for their model resulted in strains that varied by 1% leading to the removal of this bone. Contact between the implant and bone is not modelled, but they do state that a detailed examination of the stresses in the system while the bone heals does require contact mechanics between the medullary canal and nail. It is reported that for the statically locked nail with no fracture, the non-coupling of the nail and bone is a valid assumption, as shown from their agreement with experimental data. The paper stated that the use of a steel nail significantly reduced the overall stress in the bone when compared to a titanium nail, and that the screw configuration was essential to the stresses within the nail. It is also suggested that due to the nail being a 'true' load-sharing device, it may be left in patients not participating in high-risk activities after the fracture has healed.

Joyce *et al.*, (2000), examined the performance of stress and strain failure theories of bone by use of experimental methods and finite element methods performed on femoral fractures. Single stance phase of gait and impact from a

fall were simulated in the study, and the measured and finite element fracture loads were correlated for both load conditions. There is little knowledge provided on the modelling method and material properties used, however good correlation between measured and finite element results is reported and use of finite elements with varying failure theories are recommended for future work.

Keyak, (2001), studied fracture loads of the proximal femur with the use of non-linear finite element analysis. The models used were found to predict fracture load within $\pm$2kN, sufficient to identify lower than average femora fracture loads with 97.5% reliability. The computed results were correlated to measured data and the finite element method proved to be highly predictive with a 95% confidence interval. Young's modulus ranged from 5 to 22GPa and a Poisson's ratio of 0.4 was assumed throughout. The study showed that the non-linear finite element model used could provide precise estimates for proximal femoral fracture loads in the single legged stance configuration.

A study by Schmitt *et al.*, (2001), used a hybrid finite element model for patient specific pre-operative simulation of intertrochanteric osteotomies of the femur. Cubic elements were used to construct the femur initially with a smoothing algorithm to follow the geometry of the femur more precisely. The results were not accurate enough due to the roughness of the femoral head. The femoral head was constructed by approximating it to a sphere. Cancellous bone modulus of elasticity was taken between 1.5GPa and 5.5GPa and that of cortical bone between 5.5GPa and 15GPa. This study stated the need for further experimental studies to be carried out for the validation of the finite element results.

Finite elements can play a useful role in the evaluation of biomechanical devices, in particular intramedullary devices. There are many limitations on these models to date, such as patient specific modelling or the assumption of contact at certain points in the construct. Results gained from a finite element model can be very useful when compared on a relative basis, and as such numerical only-studies using comparative methods can be very useful. However, careful consideration of the modelling technique and parameters in a contact analysis must be given. If the finite element model can be experimentally verified than its significance in

the biomedical field is greatly enhanced, however not all models can be validated in such a way.

Author	Contact Element	Constraint approach	Contact Stiffness	Contact Traction	Conv. Tolerance	Conv. Norm
Biegler *et al.*, 1995	3D, point to face				1%	
Hefzy and Singh, 1997	3D, point to face	Penalty	2.0E+72	Gauss		
Kang *et al.*, 1993	3D, point to point	Penalty	4.0E+07			
Mann *et al.*, 1991	2D, point to point		1.0E+02			
Mann *et al.*, 1995				Gauss		
Mann *et al.*, 1997	2D, point to point		2.0E+03			
Mottershead *et al.*, 1996		Lagrangian	N/A	Gauss		
Rakotomana *et al.*, 1992		Augm, Langrangian				
Rohlmann *et al.*, 1988				Nodes		
Rubin *et al.*, 1993		Augm, Langrangian				
Sathasivam *et al.*, 1999	3D, point to face		1.0E+01			
Sharma *et al.*, 1998	3D, point to point				1%	
Skinner *et al.*, 1994	3D, point to point				0.01%	
Tissakht *et al.*, 1995		Penalty				
Viceconti *et al.*, 2000	3D, face to face		6.0E+03	Gauss	0.50%	
Weinans *et al.*, 1990	2D, point to point	Augm, Langrangian	1.0E+07		5%	
Wheeler *et al.*, 1997	2S, point to line		2.0E+04		0.50%	L2

Table 2.3 – Parameter identification using finite element contact analysis.

3.0 Introduction

This chapter presents a novel finite element modelling technique for the analysis of intramedullary trauma treatment devices used for the stabilisation of fractures in long bones in the human body. Application of the finite element modelling technique is described for the use of intramedullary nails used to stabilise fractures of the proximal femur. A commercially available software package, ANSYS, is used in the creation of the finite element model.

The key features of the modelling technique are:

- No pre-assignment of contact.
- Generic, modular construct.
- Versatility to input a multitude of implant-bone constructs.
- Nail model is surrounded by a thin layer of bone which enables:
    - A defined group of constructs to be inserted into a femur model, and the construct of nail and bone layer to be re-usable.

3.1 Modelling Technique

The analysis of intramedullary devices poses particular problems for finite element analysis. Some problems are familiar - the materials involved are non-linear, and the geometry is difficult to define because of anatomical differences. However, one of the other major problems is the definition of contact. It was shown in section 2.15 that all researchers have allowed the pre-assignment of areas of contact, but this can be both difficult to predict and misleading.

The novel modelling strategy adopted here enables multiple nail and screw configurations to be rapidly generated. A thin layer of bone surrounds the nail construct forming a base component. This layer of bone is an integrated part of the bone being instrumented with a nail and does not affect the stiffness of the construct. A modular approach is used, allowing versatility of configurations required. The model allows for contact to occur anywhere on the interface

between the device and bone, eliminating pre-assigned contact. The nail and bone layer component allow for the creation of an envelope of plausible cases of intramedullary nails that can be re-used in any femoral model, providing an evaluation technique for investigating implant / bone interaction.

The finite element modelling procedure can be used for any intramedullary nail inserted into a long bone in the human body. It is used in this thesis for the evaluation of an intramedullary device inserted into the human femur for fixation of trochanteric fractures. Material models can be changed as can the contact state at any point in the model. The assertion is that for detailed evaluation of an intramedullary nail construct, contact mechanics should be employed, and that there is no pre-assignment of the contact points.

3.2 Description of modelling technique - overview

The modelling technique uses a modular approach for the construction of multiple nail designs, and a generic concept that models 'bone contact volumes' surrounding the nail and screw configuration and modelling the interaction between the implant and bone. The nail and surrounding 'bone contact volumes' have the advantage of being re-used in any femur geometry, providing a general model to evaluate an intramedullary device and being able to be used for patient specific analysis. The modelling concept is shown in figure 3.1.

Any number of nail configurations can be represented from the generic modelling technique and inserted into different bone geometries iteratively to find the best arrangement for particular fracture cases. The modelling technique also allows for the analysis of individual cases where required. Figure 3.2a shows some possible variations for the distal end of an intramedullary nail, and Figure 3.2b shows some possible variation for the proximal and distal end.

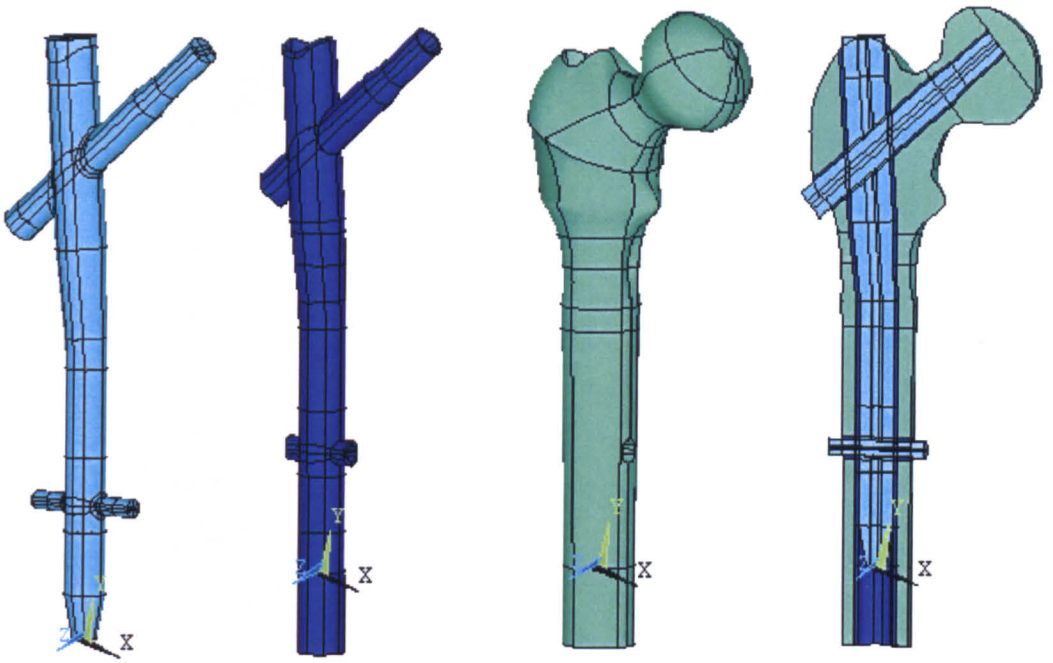

Figure 3.1 – From left to right: the nail; bone contact volumes; femur; cross-section of complete construct.

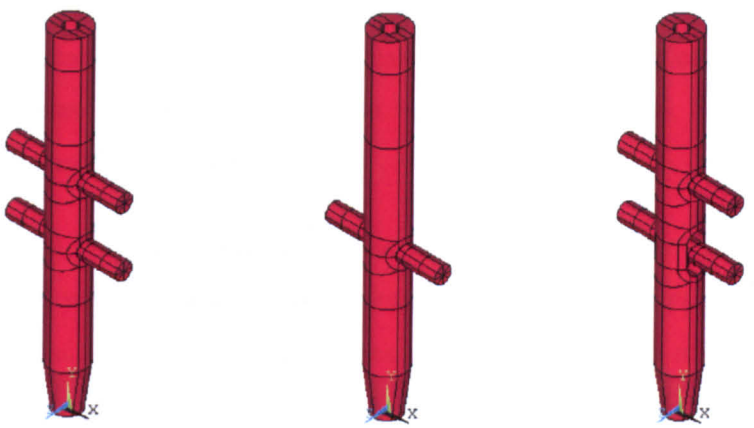

Figure 3.2a – Some possible variants for the distal and proximal regions of the nail.

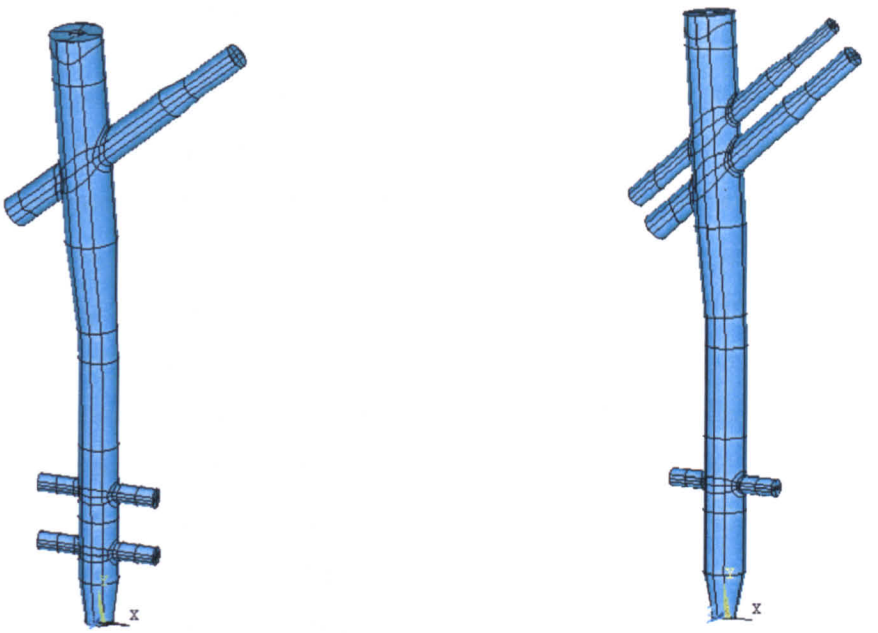

Figure 3.2b – Some possible variants for the distal and proximal regions of the nail.

No pre-assumption of contact is used in the model; in effect the nail 'floats' inside the 'bone contact volumes'. Contact points however can be assumed where known for definite, or eliminated altogether if required. Separate contact pairs are used for the interaction between different implant components and the bone contact volumes. Contact parameters can be easily varied on each contact pair, and the contact model itself can also be altered if required. Surface-to-surface contact is used in this thesis.

This contact model is suitably sensitive to the coefficient of friction between the implant and bone, whereas node-to-node contact is not (Viceconti *et al.*, 2000). Furthermore, surface-to-surface contact does not rely heavily on matching of nodes between the contact surfaces, so long as the mesh is sufficiently dense.

The modular nail and bone contact volume construct is meshed with hexahedral elements. This allows for easier alignment of nodes on the contacting bodies. The femur geometry is modelled with tetrahedral elements, as their quadratic displacement functions make them well suited to this type of topology. Viceconti *et al.*, (1998), have also reported this.

3.3 The nail and screws

The nail is constructed from a series of volumes, and is split into two main regions: proximal and distal. Both the proximal end and distal end utilise a 'function' volume, where any changes to the screw configuration can be made. The function volume is a generic component of the model that is used to make specific changes, such as number and size of the locking screws. The rest of the nail can remain unchanged, providing a quick and effective means of updating or changing any model. Creating the model in this way enables specific parts of the nail to be altered without having to change existing parts. The model can therefore be optimised relatively quickly. The nail is cannulated and meshed with 20-noded hexahedral elements. The main parts of the nail model are shown in figure 3.3. Figure 3.4 shows the parameters used in the construction of the nail and screws. Table 3.1 defines these parameters.

Any distal locking screw is modelled as a cylinder of an appropriate diameter. The screw thread detail is not modelled.

The lag screw(s) is modelled as a cylinder, with a cone and smaller cylinder being used as the screw thread portion. The screw thread region is merged with the surrounding bone to model the screw fixation at this point. Both the lag screw and distal locking screw are meshed with 20 node hexahedral elements. Any reasonable gap size can be entered between the nail and screws.

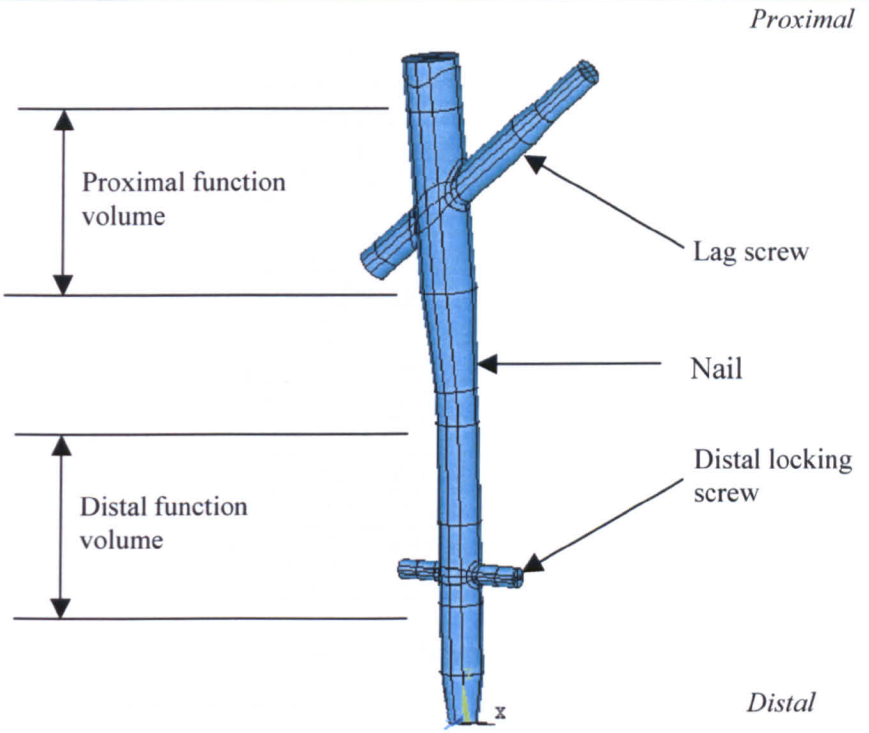

Figure 3.3 – The nail, lag screw and distal locking screw construct.

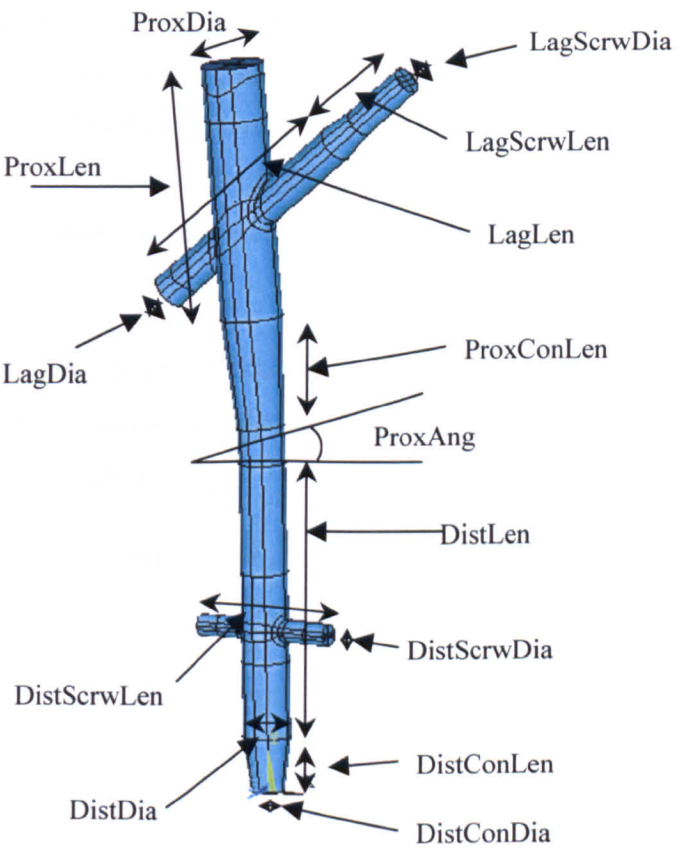

Figure 3.4 – Parameters used in modelling the nail and screws.

Parameter	Definition
ProxDia	Diameter of the proximal nail
ProxLen	Length of the proximal function volume
ProxConLen	Length of the cone leading to the proximal function volume
ProxAng	Angle between the proximal and distal parts of the model
LagDia	Diameter of the lag screw
LagScrwDia	Diameter of the lag screw thread portion
LagScrwLen	Length of the lag screw thread
LagLen	Length of the lag screw not including thread
DistLen	Length of the distal function volume
DistScrwDia	Diameter of the distal locking screw
DistConLen	Length of the cone leading to the distal function volume
DistConDia	Diameter of the ditsal cone leading to the distal function volume
DistDia	Diameter of the diatal nail
DistScrwLen	Length of the distal locking screw

Table 3.1 – Parameter identification.

3.4 Bone contact volumes

A thin bone layer surrounds the nail, distal locking screw(s) and lag screw. The volumes that make up this layer are designated the 'bone contact volumes' and model the contact between the implant and the bone. The bone contact volumes are meshed with 20 node hexahedral elements so that mesh matching is easily achieved on the contacting surfaces. The combined entity of nail and bone layer forms a base component that can be re-used in any femur geometry to assess fracture fixation.

The parameters for the bone contact volumes are assigned from those used in the modelling of the nail and screws. An appropriate gap is entered to model any gaps between the implant and bone.

Figure 3.5 shows the bone layer surrounding the nail and lag screw.

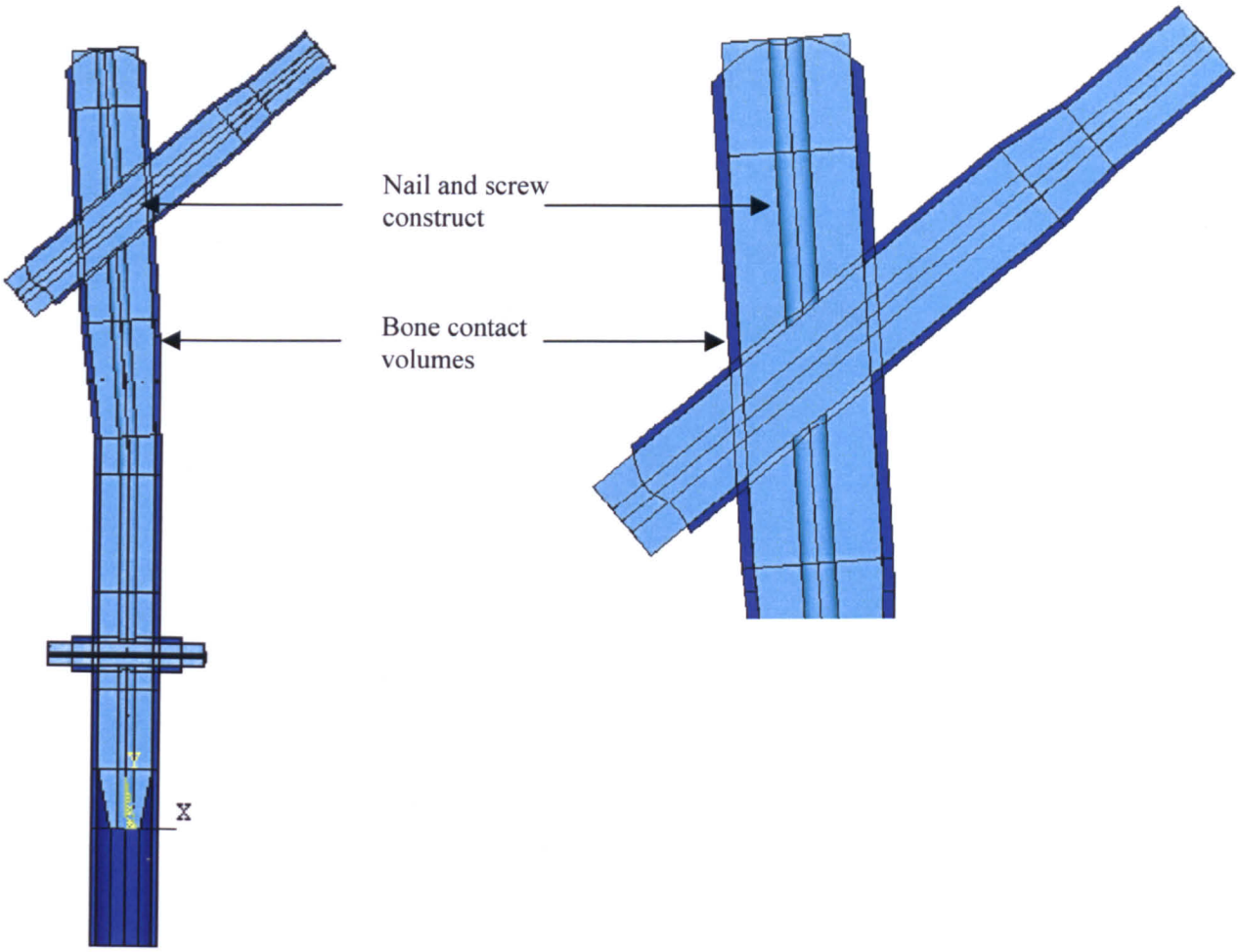

Figure 3.5 – The nail surrounded by a thin layer of bone form a base component for insertion into the femoral model.

3.5 Femur geometry

In figure 3.6 point 1 is the centre of the 'sphere' of the femoral head, points 2 and 3 are the widest parts of the femoral neck and points 4 and 5 are the narrowest. Point 9 is the most proximal part of the trochanter. Point 6 is the bisect of line 4-5. Line 1-6 is drawn and extended to points 8 and 7 at the lateral and medial cortex. Lines L_1, L_2 L_3 and L_4 are construction lines along the length of the femoral shaft. A line c-c is drawn through the centre points of the construction lines on the femoral shaft. Point B and point 7 are joined, and intersects line 7-8 at point A. Angle C-B-9 is the mediolateral angle, and angle 1-0-B is the neck shaft angle.

Leung *et al.*, (1996) used a similar method in the 3-D reconstruction of 28 pairs of Chinese femora, as did Wang at al, (1999) in their finite element study of a Gamma nail.

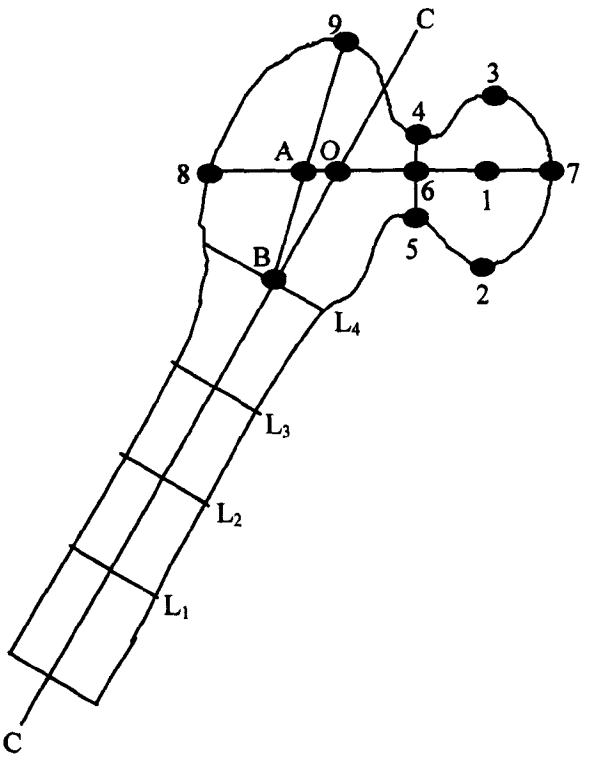

Figure 3.6 – Femur geometry.

The femur is constructed from a series of reference lines, and a skinning operation is performed to create the desired areas and volumes. The geometry is represented with this method for simplicity. There is increasing advancement in technology available in the representation of femur geometries, such as computerised topography methods. However the visual similarity obtained by accurate geometric representation is no guarantee of providing a model that can be interpreted in good faith, as demonstrated by Viceconti *et al.*, (1996). They suggest that an over emphasis on visual similarity of the model and reality has occurred because clinicians are trained to rely on 'observation' rather than 'modelling' as the critical task of the scientific process. Prendergast (1997) mentioned such a point, and included a prudent quote from the field of computer-based analysis of orthopaedic implants: "the successful design of real things in a

contingent world will always be based more on art than on science" (Fergusen, 1992). The aim therefore, is to represent the global stiffness of the construct without creating an exact anatomical model of the femur.

Figure 3.7 shows the complete femur model and a cross section. The volumes in blue are designed such that they can be meshed with higher order hexahedral elements. This is to enable modelling of the interaction between the implant and the bone. These bone volumes have been designated the 'bone contact volumes'. The volumes shown in green are meshed with higher order tetrahedral elements, and the two volumes have connectivity and continuity at their interface.

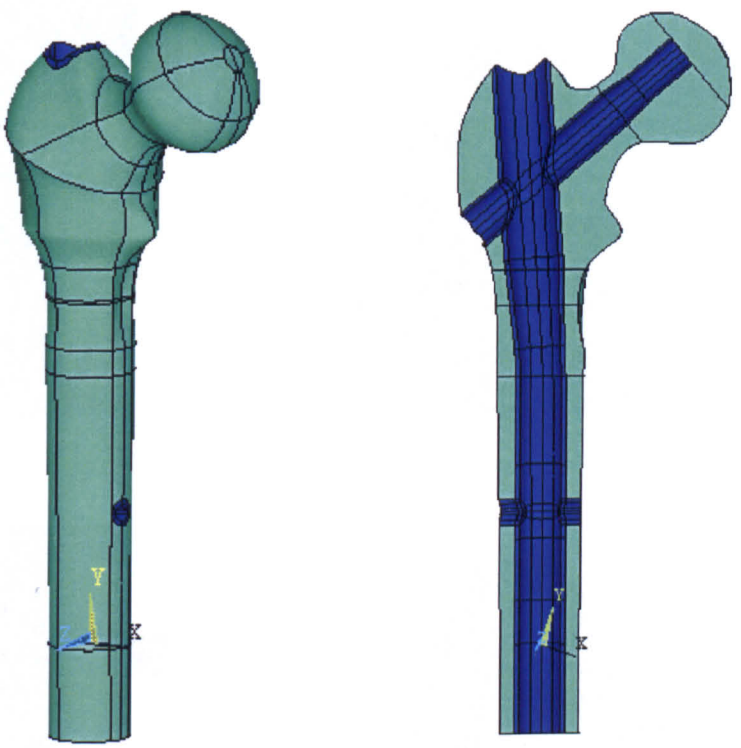

Figure 3.7 – The femur model. The bone contact volumes are shown in blue.

3.6 Conforming surfaces

Node-to-node matching is desirable for increased accuracy of the contact solution, faster solution times and is more significant when contact is not pre-assumed. Surface-to-surface contact elements alleviate the need somewhat for precise node-to-node matching, so long as the mesh is of adequate density. By having an adequately dense mesh, a node on the contact surface is 'near' to other nodes on the target surface. The surfaces that may come into contact throughout the model in this thesis have an equal mesh density on each face. Mesh matching is shown in figure 3.8.

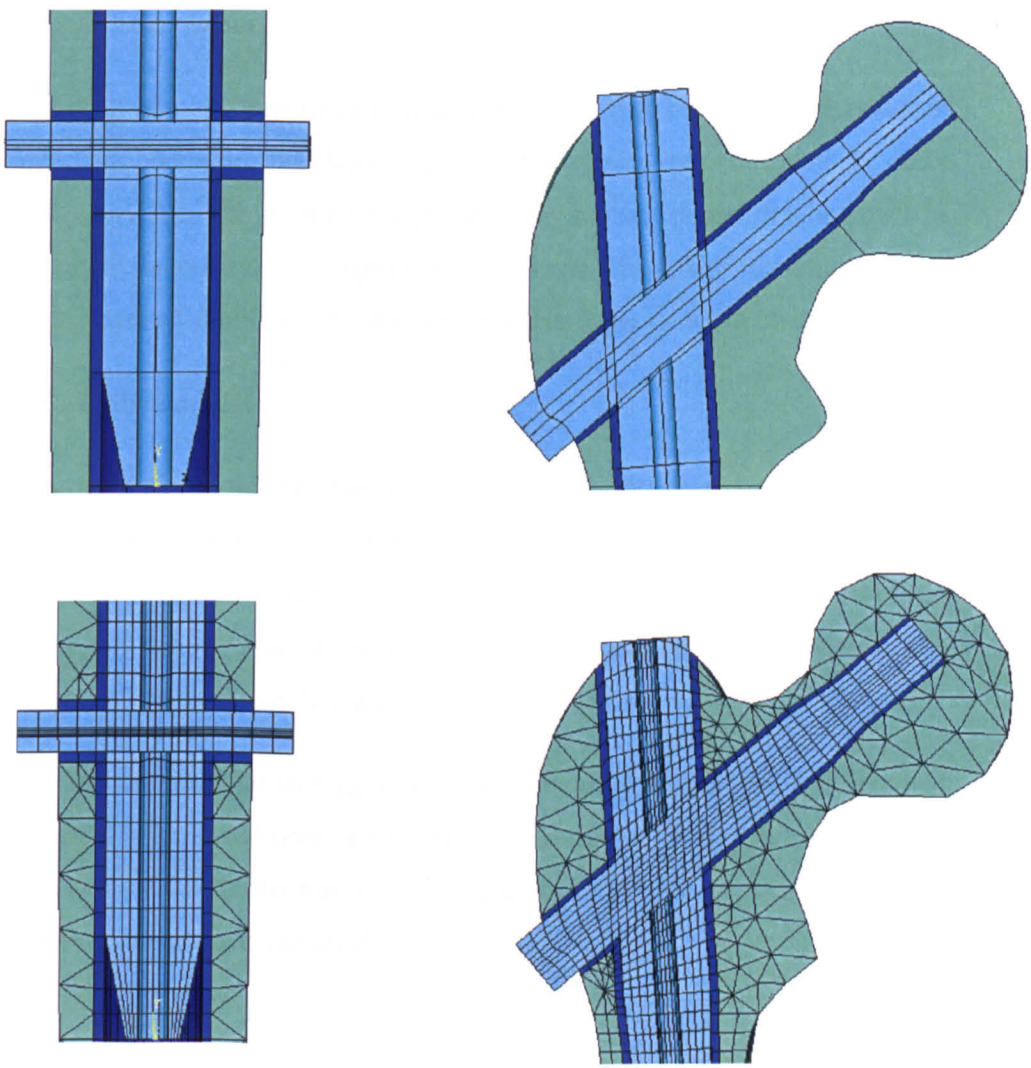

Figure 3.8 – Conforming surfaces and node-to-node matching, as demonstrated at the distal and proximal end of the construct.

3.7 Contact

Surface-to-surface contact elements are employed wherever contact may be achieved throughout the construct. The nail, lag screw and distal locking screws are defined as contact bodies, and thus 8-noded quadrilateral contact elements overlay the solid hexahedral elements on all surfaces. The lag screw thread detail is not modelled and is merged into the surrounding bone; contact elements are not used here.

The thin bone layer surrounding the nail and screws is designated as the target body, and thus target elements overlay the hexahedral elements on all surfaces where contact may occur.

A standard, frictional contact model is used in ANSYS to model the behaviour of the contacting bodies in this thesis, whereby the system can continuously make and break contact as the solution progresses. Any contact model can however be applied where necessary. An Augmented Lagrange Multiplier algorithm is used to solve the contact problem, which is described in more detail in chapter 4.

3.8 Complete model

To create the full model the thin layer of bone is subtracted from the femoral volumes and left in place. The volume left behind after this operation is deleted, enabling the nail to be inserted. It is therefore possible to re-use the nail and bone layer construct for any fracture type or femur geometry. A cross-section of the complete construct is shown in figure 3.9.

The nail, lag screw, distal locking screw and bone contact volumes are designed to be meshed with hexahedral elements and the femur model is meshed with tetrahedral elements. In this thesis higher order twenty-node hexahedral and ten-node tetrahedral elements are used.

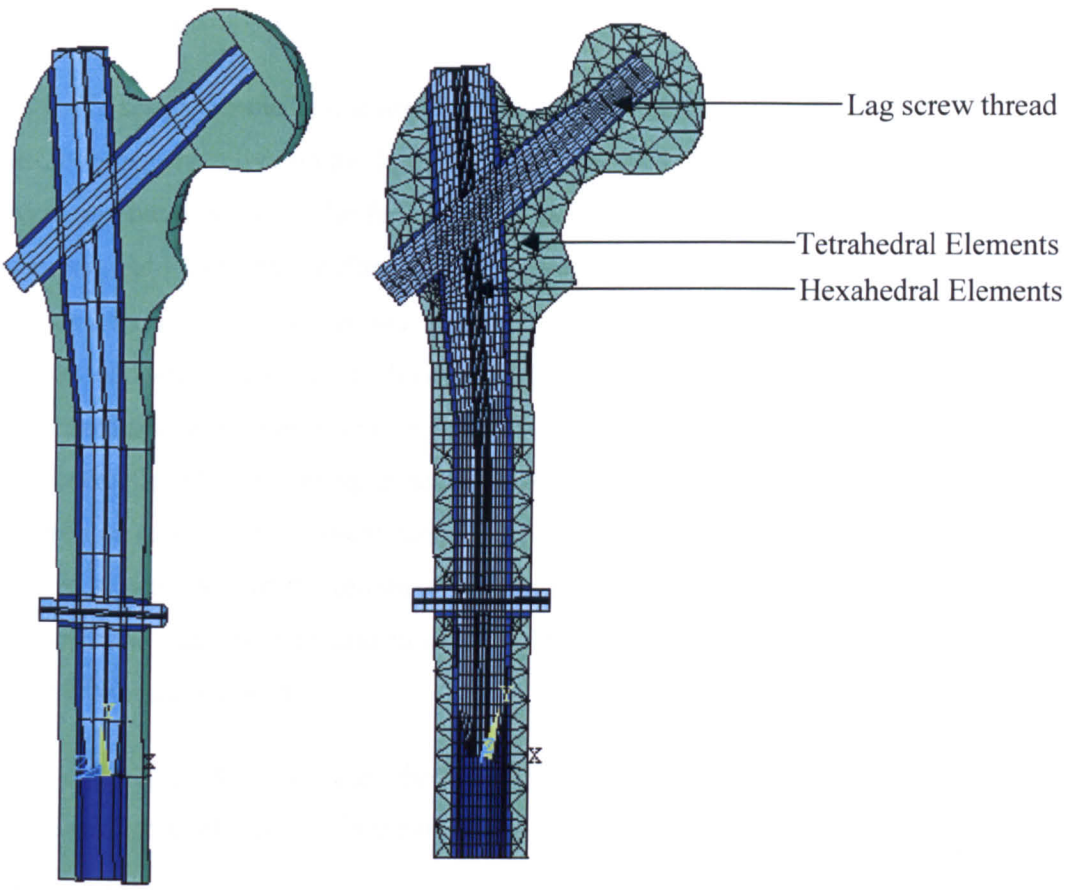

Figure 3.9 – A cross-section of the whole model volumes and elements.

Gaps are included in the model, and can be varied to suit any particular situation. Gaps between metal and bone are assumed and gaps between nail and screws are measured. Unless otherwise stated the construct used in this thesis has the following features:

- There is a radial gap between the nail and bone of 0.05mm.
- There is a radial gap between the lag screw and bone of 0.05mm.
- There is a radial gap between the lag screw and nail of 0.01mm.
- There is a radial gap between the distal locking screw and nail of 0.01mm.
- There is no gap between the distal locking screw and surrounding bone.
- The lag screw threaded portion is merged into the surrounding bone.

3.9 Loading

The loads acting on the femur are not simple. There is uncertainty as to which muscle forces are active on the femur and the magnitude of force that they apply. Seventeen muscles act on the femur to produce locomotion and the majority of these originate from the surface of the pelvis and insert into the femur. The muscles can be grouped together according to the principal motion that they provide: abduction, adduction, flexion, extension and internal/external rotation. When performing an analysis of the femur it is important to represent the muscle force correctly when requiring exact simulation of the *in-vivo* situation. For the purposes of some finite element models, particularly where comparative studies are used to provide information on a relative basis, it is more important to define the dominant load regimes, and in this case many of the muscle forces may be omitted from the analysis.

Fagan and Lee (1986) calculated the loading applied to the proximal femur from a force and moment analysis in the one-legged stance, and this is demonstrated in figure 3.10.

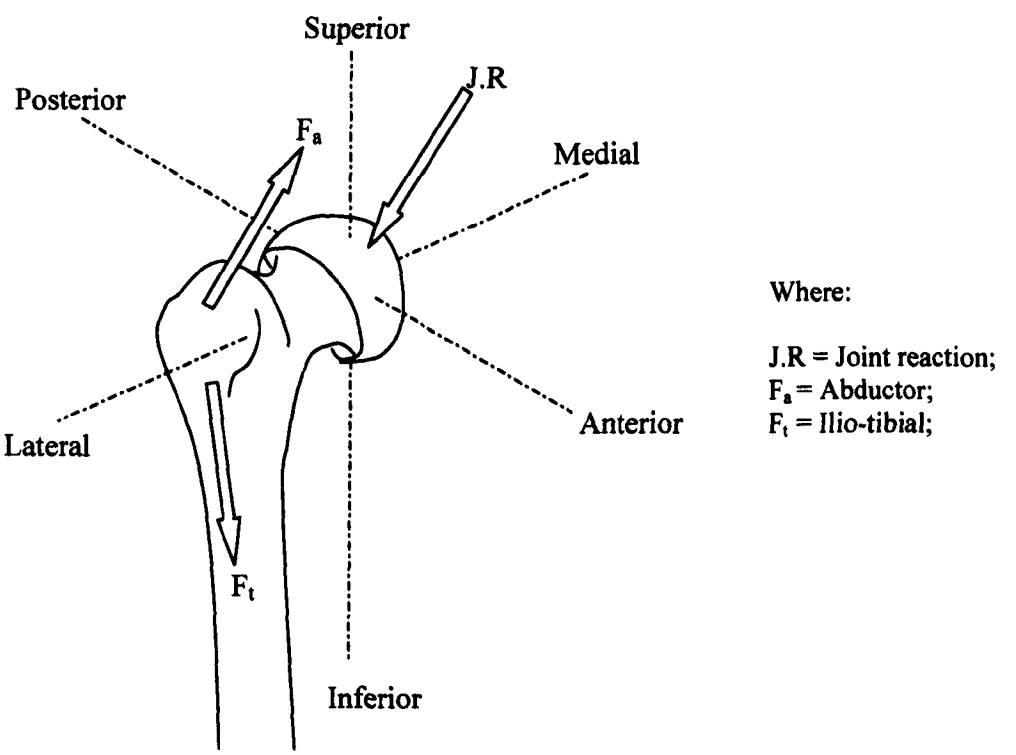

Figure 3.10 - Anatomical schematic diagram of the left femur showing muscle forces and joint reaction force for standing on one leg.

It is generally accepted that there are three predominant load conditions that can be used to analyse the femoral structural behaviour; bending, compression and torsion (Wang 1999, Taylor 1997). The bending condition has been well documented (Huiskes, 1990; Prendergast and Taylor 1990), with and without an abductor force. Taylor (1997) performed a finite element analysis on the femur under a bending load condition using the joint reaction force and abductor muscles. The study also varied values for the ilio-psoas muscle and stated that the femur was predominantly under compression from this load regime. It was also reported that predominantly bending loads do not accurately represent the true *in-vivo* conditions, and that care should be taken when assessing the muscle forces of the femur.

The ilio-tibial muscle force shown in figure 3.10 does not attach to the femur, but to the pelvis (ileum) and the tibia. This muscle provides flexion and medial rotation of the hip by tensing the fascia lata, a muscle attached to the iliac crest. This action is particularity important when balancing on one foot, and is included in the femoral loading as a simplification of the actual loading.

Various finite element models have used similar loading techniques to analyse the femur, and these are mainly bending loads. Seral *et al* (2003) examined a proximal femoral nail and Gamma nail for the bend load case only, applying 2460N as the joint reaction force, 1700N for the abducter load and 771N for the ilio-psoas muscle. Sitthiseripratip *et al* (2003) again only used the bending load condition applying 2800N, 616N and 171N in the S-I, M-L and A-P directions respectively for the joint reaction force and 430N and 1160N in the M-L and S-I directions respectively for the abductor force. A study by Rohlmann *et al* (1983) used a loading regime for a single legged stance, and used a joint reaction force with various abductor magnitudes. They reported that the simple load regime of joint reaction and abductor muscle is appropriate for qualitative experimental investigations, and that the use of just the joint reaction force is inappropriate.

A study by Brown *et al* (2004) used two load conditions, bending and torsion, as it was stated that the torsion load case is the dominant design case for intramedullary nails (Wang *et al.*, 2003).

		Applied force (kN)		
		Anterior-Posterior (A-P)	Medial-Lateral (M-L)	Superior-Inferior (S-I)
Bend Load	**Joint Reaction Force**	0.171	0.616	2.8
	Abductors		0.430	1.16
Torsion Load	**Joint Reaction Force**	1.195	0.616	2.54
	Abductors		0.430	1.16

Table 3.2 – Loading applied to the femur.

The use of finite elements in the analysis of the proximal femur often requires simplification of the actual loading, and furthermore should assess the construct under the governing design case. In such a simplification, the loads applied may not necessarily be self-equibrilating so long as there is global equilibrium maintained from reactions at the restraints (Wang *et al.*, 2004). Indeed, this allows for models of the proximal or distal femur only.

When analysing an intramedullary construct in the human femur, it is prudent to look at the governing design case or cases, and these are bend and torsion. The definition of different muscle forces is arbitrary in many cases, and it would be beneficial to produce a standard set of forces for analysis of the human femur. Bergmann *et al* (2001) is a possible source for such data.

It is thus the task of the analyst to model the complicated loading of the femur with muscle loads that represent the dominant design case. For comparative studies these loads can be somewhat arbitrary, and the exclusion of certain muscle forces, eliminating self-equilibrium of the femur, is appropriate provided global equilibrium is achieved through restraints imposed upon the model.

The loading used in this thesis is described in each section for the different models. Where the global femur construct is used two load conditions are considered: bending and torsion. The values of the forces acting on the femur are given in Table 3.2. These are taken from Wang *et al.*, (2003) who in turn took the loading from Taylor *et al*, (1997).

When analysing an intramedullary nailing system with finite elements, it would be of benefit for a standard load or set of loads to be applied to the femur. This would enable cross-institutional comparison and provide a benchmark for the analysis of intramedullary systems in general. The process of simplifying and approximating load regimes on a subjective basis would be avoided.

3.10 Material properties

There is a great deal of information available concerning the material properties of cancellous and cortical bone. Reported values are given in chapter 2, (section 2.9 and 2.15). Average values for the elastic modulus of cancellous bone are in the range of 200 to 600MPa, and that of cortical bone between 15 and 20GPa.

It is in the inter-subject variability together with the anisotropic nature and non-homogeneity of bone that makes its description difficult in a numerical simulation. Many numerical models have assessed biomechanical implants with varying degrees of success without incorporating anisotropy. Huiskes *et al.*, (1983) stated that the majority of finite element models used in orthopaedic biomechanics are those concerned with artificial joint design and fixation, and that in the majority of these cases linear elasticity, isotropy and homogeneity of cortical and trabecular bone were assumed, and that any interfaces were modelled as rigidly bonded. Wang *et al.*, (1998, 2003, 2004) used linear-elastic material properties and reported that elasto-plastic models are more difficult to interpret and that the requisite parameters can lead to a greater uncertainty in the results gained. Many other authors also use linear isotropic material properties in the evaluation of an implant-femur construct (Rohlmann *et al.*, 1983; Viceconti *et al.*, 2000; Stolk *et al.*, 2002; Wang *et al.*, 1998, 2000, 2003;; Sitthiseripratip *et al.*, 2003; Seral *et al.*, 2003). This is often a successful approach because the aim is to represent a heterogeneous material by a homogeneous continuum (Prendergast *et al.*, 1997; Huiskes *et al.*, 1983). Indeed, some finite element models with homogeneous material properties have shown an overestimation of 30% with non-homogeneous 'realistic' properties, (Dalstra *et al*; 1993).

It has been demonstrated that the stress distribution of trabecular bone is hardly affected by anisotropy so long as the nonhomogeneity is correctly accounted for

(Huiskes *et al* 1983). Askew and Lewis (1981) performed an extensive parametric analysis, including anisotropy and nonhomogeneity of trabecular bone, and found that if the nonhomogeneity is taken into account, the effect of anisotropy is only minor, an effect also reported by Hayes *et al* (1982). Taylor, (1997) conducted a study into the effects of isotropic and anisotropic cancellous bone models for the fixation of a full hip prosthesis and its migration within the proximal femur. It was concluded that the degree of anisotropy on the model had an insignificant effect on the cancellous bone stress within a certain range, a finding also reported by Brown *et al.,* (1980). Where the anisotropy did have an influence on the cancellous bone stress, the effect was always less than 15%, and this is also dependent upon the type of fixation used for the prosthesis. The same study by Taylor also investigated the effect of homogeneity in the model, and reported that there is the potential for a 35% difference when using a homogeneous proximal femur instead of accounting for heterogeneity. This is however dependent upon the fixation method used for the device, with a press-fit prosthesis having no difference in the cancellous bone stress when either a heterogeneous or homogeneous model is used.

There is certainly an argument for the correct modelling of trabecular bone when investigating cancellous bone stress and implant failure via migration. However the above studies were not concerned with the overall stiffness of the proximal femur, and in the case of assessing the stiffness of a bone-implant construct there is indeed an argument for not modelling the trabecular bone at all. This argument has been reported by a variety of studies. McNamara *et al.,* (1994), evaluated an experimental and finite element model by use of a four point bending technique on cadaveric and synthetic specimens. They stated that because of its small contribution to the bending stiffness of the overall bone the spongy bone in the medullary canal was not modelled. The cortical bone was modelled as a linear elastic continuum with isotropic properties. A similar assumption was made by Cheung *et al.,* (2004), who used the same material property assumption for cortical bone, and reported that by omitting the cancellous bone in the model there was a 1% difference in the strain values calculated. This model was concerning a femoral nail, and both of these models did not involve the fixation of a screw into cancellous bone, and were not considering screw cut-out. Martens

et al., (1983) investigated the mechanical properties of the proximal femur and showed that there was a significant decrease in strength for the specimens that had the central part of the cancellous bone removed. They also reported that the stiffness and failure mode were not affected by the removal of the central trabecular bone.

The incorporation of cancellous bone into models of the femur may be considered unnecessary when assessing the stiffness of the bone, however it is the structural integrity of trabecular bone that is critical for fixation devices for the treatment of proximal femoral fractures. To some extent therefore, the ultimate properties of the cancellous bone and not of the foreign material are the limiting factors for the strength of internal fixation of femoral neck fractures (Martens *et al.*, 1983). It is in the incorporation of the cancellous bone into finite element models that can lead to further assessments of the bone-implant interaction, such as the potential for screw cut-out, or the migration of an implant, as is reported by Wang *et al.*, (2000).

In the human femur, the femoral shaft consists of cortical bone and the trochanter consists mainly of cancellous bone by volume. There is a thin layer of cortical bone surrounding the femoral head. The proximal femur is often considered as three distinct sections; the trochanter, femoral neck and femoral head, with the femoral head having the greatest modulus of elasticity (similar to that of the femoral neck) and the trochanter having the lowest modulus, with a considerable variance between the material properties of each section (Martens *et al.*, 1983). The finite element model used in this thesis is split into three separate regions; the femoral shaft, trochanter and femoral head, as described by Wang, *et al* (1998, 2000), an approach also used by other authors, (Seral, *et al.*, (2003); Sitthiseripratip, *et al.*, 2003). This segmentation is shown in figure 3.11.

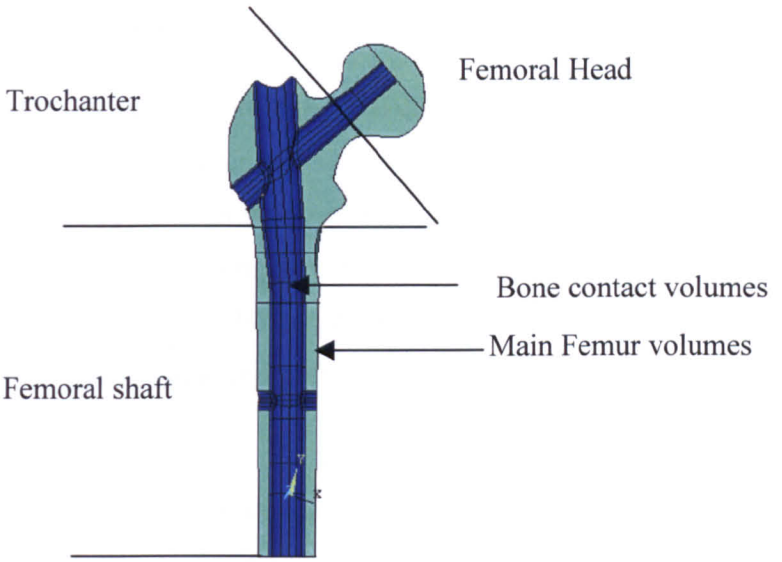

Figure 3.11 – Cross-section of femoral material properties.

3.11 Summary

This chapter has presented a novel finite element technique that can be used to model an intramedullary nail inserted into a long bone, for the stabilisation of fractures. The model is applied to fractures of the proximal femur in this thesis.

A key feature of the model is that the nail is constructed using a generic, modular approach and is surrounded by a thin layer of bone. The combined construct allows for an envelope of plausible nail and screw configurations to be created and inserted into any femur model to analyse a multitude of fractures.

No pre-assumption of contact is used in the construct and the assembly of nail and bone layer can be used as an effective tool in the analysis of implant and bone interaction.

The loading of the femur has been simplified with assumed values, however the load regime can be changed depending on the analysis performed.

The representation of the geometry does not use precise anatomical data for simplicity.

4.0 Introduction

A simplified finite element model is used in this chapter to verify the novel modelling technique described in chapter 3. The construction of the finite element model using conforming surfaces and a combination of element types is verified by solving a simple contact model. Parameters considered to be important to the contact solution are investigated to provide information that will be used for implementation of the novel finite element modelling technique in later chapters.

An overview of contact mechanics and some solution techniques is provided to give the reader basic information of how the finite element modelling technique will be implemented.

4.1 Contact Overview

The importance of contact mechanics in engineering design has long been recognised and began in 1882 when Heinrich Hertz published his classic paper "On the contact of elastic solids". Hertz made the hypothesis that the contact area is in general, elliptical, and introduced the assumption that, for the purpose of local deformations each body may be treated as an elastic half-space loaded over a small elliptical region of its plane surface. Hertz theory can only be applied to frictionless surfaces of perfectly elastic solids, and progress in contact mechanics over the years has concentrated on removing these restrictions. Slipping and rolling contact can now be modelled in a realistic way.

The actual contact area between bodies is seldom known intuitively, and if friction is present the behaviour may be dependent on load history. Contact problems must be solved using an iterative technique with the use of small load increments.

Contact problems can be considered inherently non-linear for two main reasons:

1. Prior to contact, boundary conditions are given by traction conditions between the two interfering bodies, which are often zero at the start of a problem.

2. During contact kinematic constraints (gap conditions) between the bodies must be considered to prevent one boundary penetrating into the other.

Figure 4.1 shows a situation where one body is coming into contact with another. In figure 4.1 the bodies are not in contact with each other and the boundary conditions are specified by zero traction conditions for both bodies. In figure 4.2 the bodies are in contact along a part of the boundary segment and conditions must be inserted to ensure that penetration does not occur.

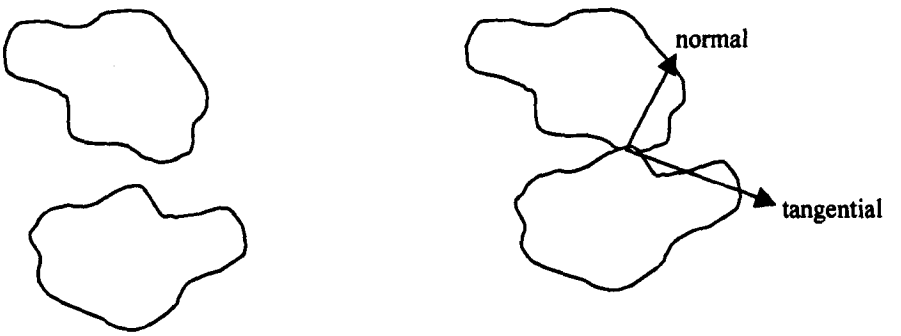

Figure 4.1 – Two bodies coming into contact.

Along the boundary different types of contact can be modelled, the simplest being frictionless contact where the only non-zero traction is normal to the surface. A more complex condition occurs in which traction tangential to the surface is generated by frictional conditions. The simplest model for a frictional condition is the Coulomb friction where:

$$|t_s| \leq \mu |t_n| \qquad 4.1$$

Where μ is a positive frictional parameter.

t_n represents the magnitude of the normal traction.

t_s represents the magnitude of the tangential traction.

If the magnitude of the tangential traction is less than the limit condition, the points on the contacting surfaces will stick. If however this value is on or above

the limit, than sliding will occur and a tractive force opposite to the direction of slip with the magnitude of $\mu|t_n|$ will be opposed on each surface.

In modelling contact problems there are two immediate difficulties involved. Firstly, it is not possible to represent the contacting boundaries continuously. This is due to the fact that finite element analysis utilises the approximation of a boundary. Secondly the finite element model often represents element 'normals' in a manner that is discontinuous between nodes. When node-to-node matching is present the normals may start coincidence, however after deformation of the surfaces they may well be non-coincidence.

4.2 Penetration Prevention

Evaluation of the contact between contacting surfaces is possible by use of nodes upon the surface. The nodes on one surface must coincide with the location of the nodes on the other surface for node-node contact, within conditions acceptable for small deformation analysis. One such problem is the simple case of Hertzian contact between two semicircular discs. Node-to-node matching occurs when the traction conditions are zero however once the discs are brought into contact the deformation of the surfaces results in a slight node-to-node mismatch. This mismatch is usually not severe and usable results can be drawn from the analysis. Figure 4.2 shows the contact problem.

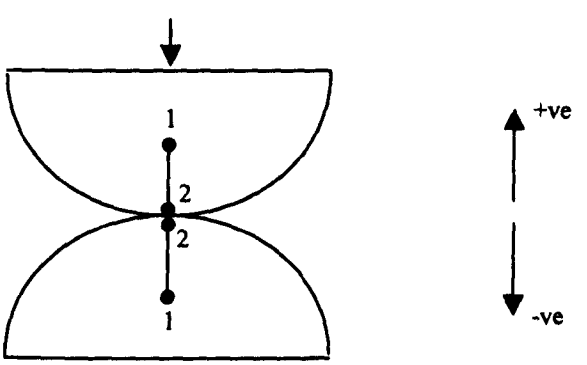

Figure 4.2 – Contact between two hemispheres.

Nodes that come into contact can be monitored by comparing the vertical displacement of each node pair (kinematic condition), which can be treated as a

two-node element in the example given. If the surface of the hemisphere moving toward the other (upper hemisphere) is designated the contact surface, and the stationary hemisphere (lower hemisphere) the target surface, than the gap condition can be monitored by:

$$g = x_2^{\,c} - x_2^{\,t} \qquad 4.2$$

If this gap is greater than zero no contact occurs, whereas for g less than or equal to zero contact is achieved and penetration is realised. Penetration is a measure of the displacement of one node onto another. It is desirable to maintain very small penetrations, as this is a numerical term and not a physical entity. To control penetration some form of constraint condition must be used for any nodal pair that will form contact. Three commonly used methods are described below.

4.2.1 Lagrange multiplier

This approach multiplies the gap condition given in equation 4.2 by the multiplier (or interface traction), λ. Thus it can be written for each nodal pair for which contact has been assigned a variational term:

$$\Pi = \lambda g \qquad 4.3$$

The first variational term of equation 4.2 is added to the variational equations being used to solve the problem. The first variation of equation 4.2 is given by:

$$\partial\Pi = \partial\lambda g + \left[\partial x_2^{\,c} - \partial x_2^{\,t}\right]\lambda \qquad 4.4$$

λ is the 'force' applied to each node to prevent penetration. Linearisation of equation 4.3 leads to a tangent matrix term for use in a Newton-Raphson solution process. The final tangent and residual for the nodal contact element is written thus:

$$\begin{vmatrix} 0 & 0 & 1 \\ 0 & 0 & -1 \\ 1 & -1 & 0 \end{vmatrix} \begin{vmatrix} \partial x_2^{c} \\ \partial x_2^{t} \\ \partial\lambda \end{vmatrix} = \begin{vmatrix} -\lambda \\ \lambda \\ -g \end{vmatrix} \qquad 4.5$$

This tangent matrix is then added into the equations as in any element assembly process. This method introduces another unknown into the system; also, as is the case for all Lagrange multiplier approaches, the equations are not positive definitive and have a zero diagonal for each multiplier term. Therefore care is needed during the solution process to avoid division by the zero diagonal.

4.2.2 Penalty Function

This approach avoids solution difficulties experienced with the Lagrange multiplier. In this case the contact term is given by:

$$\Pi = kg^2 \qquad 4.6$$

Where k is known as a penalty parameter and the matrix equation for each nodal pair is given by:

$$\begin{vmatrix} k & -k \\ -k & k \end{vmatrix} \begin{Vmatrix} x_2^c \\ x_2^t \end{vmatrix} = \begin{vmatrix} -kg \\ kg \end{vmatrix} \qquad 4.7$$

In this approach the gap condition will never be zero but is dependent on the value of k that is selected. Therefore the advantages of this method are compromised by the need to identify an adequate value for the parameter k, which is the contact stiffness between the contacting bodies.

4.2.3 Augmented Lagrangian method

By updating the multiplier at every iteration, combined with a penalty form, the Augmented Lagrangian method strikes a useful compromise between the two methods described above. The augmented matrix is written thus:

$$\begin{vmatrix} k & -k \\ -k & k \end{vmatrix} \begin{Vmatrix} x_2^c \\ x_2^t \end{vmatrix} = \begin{vmatrix} -\lambda_k - kg \\ \lambda_g + kg \end{vmatrix} \qquad 4.8$$

This method is effectively an iterative series of penalty updates to find the exact Lagrange multipliers or traction conditions. Compared to the penalty method the Augmented Lagrangian method usually leads to better conditioning and is less sensitive to the magnitude of the contact stiffness parameter.

Node to surface and surface-to-surface contact models can also be employed and in these models it is not critical to match nodes in a contact pair because a node can contact a surface segment. An interpolation along the edge facets of elements or an interpolation that smooths the slope discontinuity between adjacent element surface facets can be made. The determination of contact requires a search to find which target facet is a potential contact surface and computation of the associated gap for each one. To determine the gap it is necessary to find the point on the target facet that is closest to the contact node.

The implementation of a computer-based analysis is used in this thesis, using a surface-to-surface contact analysis. This strategy is implemented so that the contact area of each body is taken as the boundary of elements so that node matching is not critical but important. Furthermore, surface-to-surface contact analysis minimises small discontinuities between the contact and target surface that can occur with a node-to-node contact.

4.3 Contact Classification

In general contact problems can be placed into two different categories: rigid-to-flexible and flexible-to-flexible. The latter concerns contacting bodies that are both deformable. The former allows analysis of contacting bodies where one can be considered perfectly rigid, and does not deform in space. All entities in this project are deformable and a flexible-to-flexible contact analysis is used.

A common numerical representation of contact is based on the node-to-node contact model (Rubin *et al.*, 1993; Van Rietbergen *et al.*, 1993; Verdonschot *et al.*, 1993). However more advanced models known as node-to-surface and surface-to-surface are available. Surface-to-surface elements have several advantages over the other elements due to the fact that they:

- Support lower and higher order elements on the surface
- Support large deformations, with a significant amount of sliding and friction, efficiently.
- Have no restrictions on the shape of the target surface.

- Require fewer contact elements than the node-to-surface elements, resulting in less disk space and computer processing usage.

For flexible-to-flexible contact the choice of target and contact surfaces is dependent upon the amount of penetration that will occur within the system not the stiffness of the associated surfaces. The following guidelines are used in ANSYS to establish surface designation:

- If a convex surface is expected to come into contact with a flat or concave surface, the flat/concave surface should be the target surface,
- The surface with the finer mesh should be the target surface,
- If one surface has underlying lower order elements, than it is designated the target surface,
- When one surface is markedly larger than the other such as where one surface surrounds the other, than it is the larger surface that is designated the target surface.

4.4 Contact Stiffness

Contact stiffness is a parameter that controls the amount of penetration that occurs between interfering bodies. To reduce the penetration between interfering bodies a suitable value of contact stiffness must be assigned. In theory, if the stiffness between two contact surfaces were infinite, than the penetration would be zero. Alternatively, if the contact stiffness is zero than the two bodies are able to pass through each other.

A high value of contact stiffness may cause ill-conditioning of the global stiffness matrix, which in turn leads to convergence difficulties. Decreasing the contact stiffness too far will result in too much penetration.

The value of the contact stiffness is derived from the material properties of the underlying deformable elements. Both surfaces are considered in the derivation of contact stiffness.

In ANSYS, a contact stiffness factor can be entered from 0 to 10.

4.5 Summary

- Contact problems are highly non-linear and inherently difficult to solve. Modelling considerations such as node-to-node matching along with solution routine and penetration prevention are essential considerations in any contact problem.
- A flexible-to-flexible contact model will be used in this thesis using a deformable-deformable contact pair.
- Surface-to-surface contact elements are used.
- Contact and target surface designation is independent of the stiffness of the bodies involved.

4.6 Element Continuity

A simplified finite element model is created to validate the novel modelling technique approach presented in chapter 3. The objective is to show element continuity at the hexahedral / tetrahedral interface and to investigate certain parameters that will be used in the model. The model consists of a hollow cylinder (annulus) attached to an arbitrary block. A second solid cylinder is inserted into this construct. A diagram of the model and mesh is shown in figure 4.3.

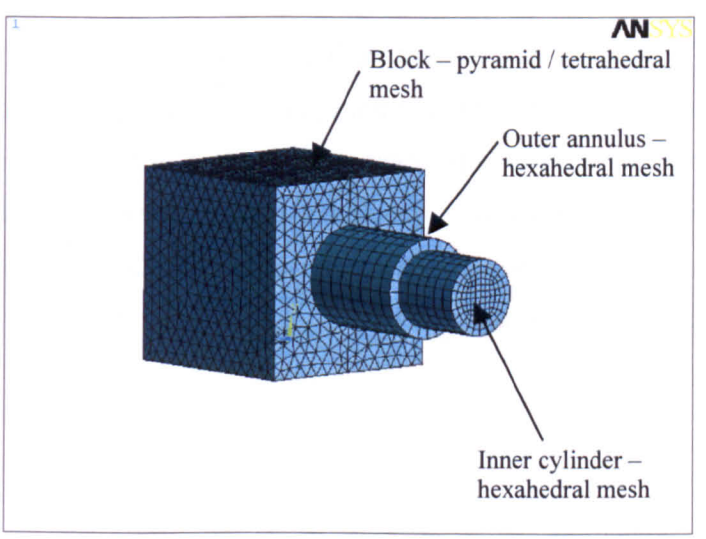

Figure 4.3 – The model and mesh.

When constructing the above geometry, Boolean operations are used to subtract a cylindrical volume from a complete block, and the hollow cylinder is then inserted. The same technique is used for the novel finite element technique. To achieve element continuity between the block and annulus, pyramid elements are used. The use of pyramid elements allows coincident nodes at the hexahedral / tetrahedral interface. The use of pyramid transitioning requires the surfaces of these components to conform. This is illustrated in figure 4.4. The rest of the block is meshed with tetrahedral elements.

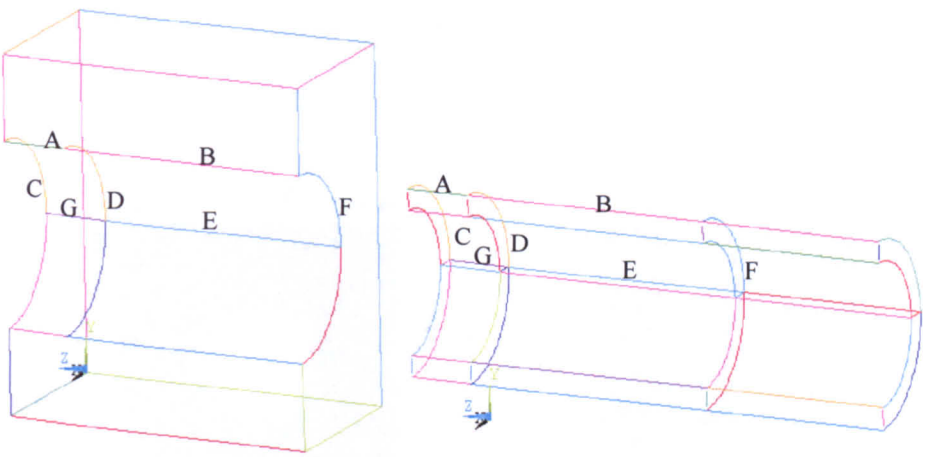

Figure 4.4 – Construction line matching for surface conformity.

Lines A through to G are illustrated in one quadrant of the model. This surface conformity enables the required transitioning between hexahedral and tetrahedral elements. It is noted that the tetrahedral element consists of ten nodes, whereas the hexahedral element has twenty. To realise the pyramid transition the outer annulus must be meshed first. The transitioning is demonstrated in figure 4.5. Figures 4.6 and 4.7 demonstrate the geometric model under investigation:

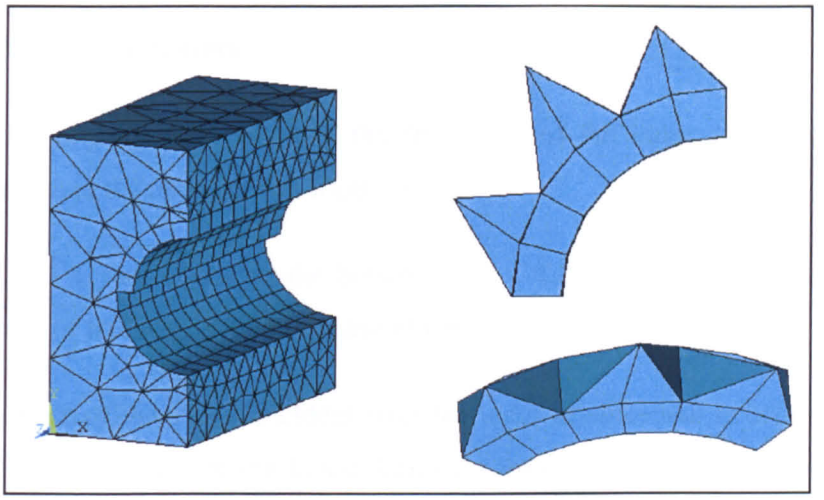

Figure 4.5 – Element continuity at hexahedral / tetrahedral interface.

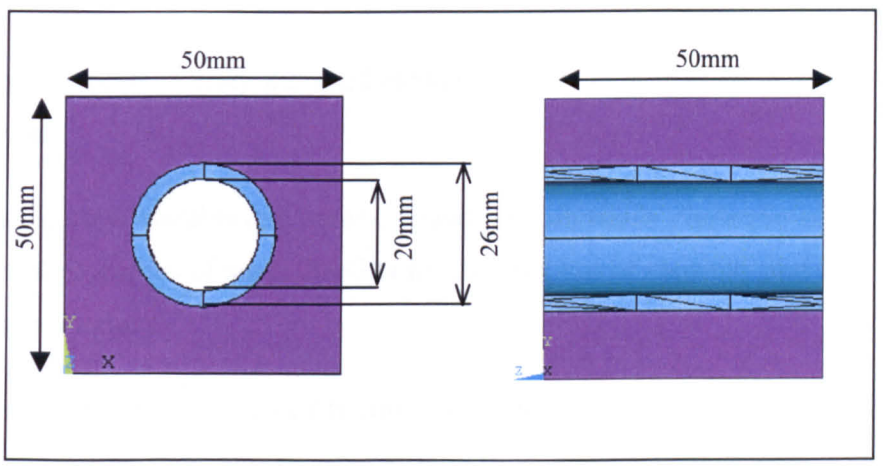

Figure 4.6 - Block and annulus dimensions.

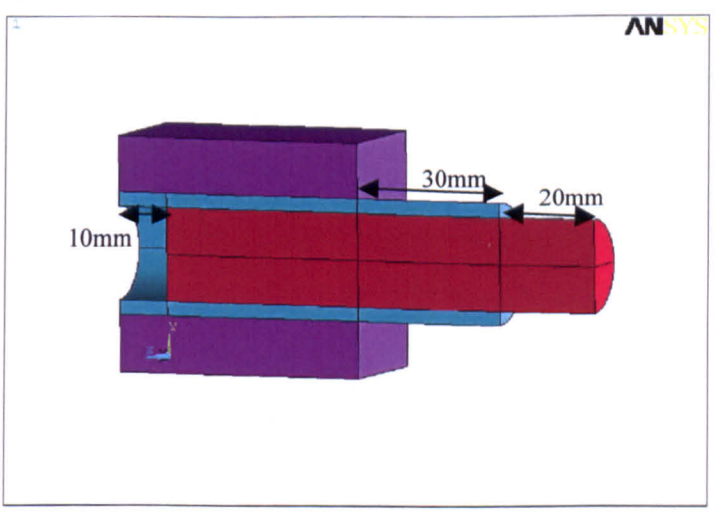

Figure 4.7 - Dissection of whole model.

4.7 Model Parameters

- A load of 100N is applied to the front face of the inner cylinder, spread evenly over the nodes at this location.
- The four corner nodes on the bottom face of the block are restrained in all degrees of freedom, fixing the base of the block.
- The inner cylinder is coincident with the outer annulus and is offset 10mm from the back face of the block. Utilising zero gap conditions between the discontinuous entities aids in the contact solution.
- Contact elements overlay the solid elements on the outer surface of the inner cylinder.
- Target elements overlay the solid elements on the inner surface of the outer annulus.
- Both the outer annulus and inner cylinder, are arbitrarily chosen to have the material properties of steel: 200GPa for the modulus of elasticity and 0.33 as Poisson's ratio.
- There are two main forms of friction, which will be applicable to the finite element model: static and sliding. A static friction coefficient between a steel bolt and surface is in the region of 0.1 to 0.18 for dry conditions. Sliding friction between two hardened steel surfaces can be as high as 0.6. An arbitrary coefficient of friction of 0.1 is assigned to the contact pair to induce frictional contact.

4.8 Contact Results

The diagram in figure 4.8 indicates the main contact areas in the system.

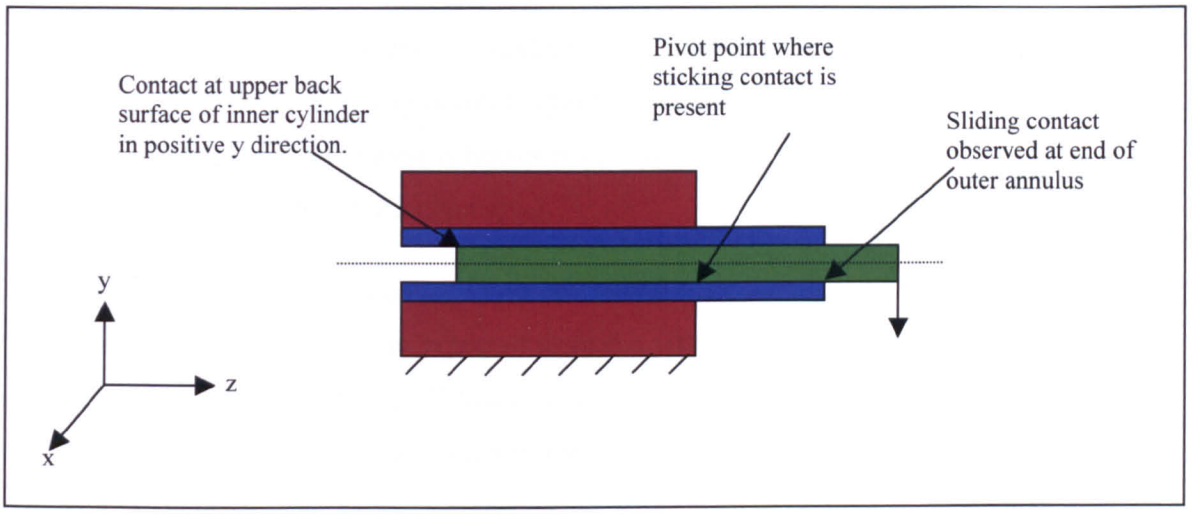

Figure 4.8 – Main contact areas.

In ANSYS contact status indicates whether there is closed and sticking contact (value of 3), closed and sliding contact (value of 2), open and near contact (value of 1) or open and far contact (value of 0). Contact status results in Figure 4.7 show that for a contact stiffness factor of 1, the contact status varies from 1 to 2.75. Closed and sticking contact is demonstrated at the top surface of the inner cylinder where the bending moment displaces the back end of it in the positive y-direction due to the pivot point at the front of the block. This pivot point also realises closed and sticking contact at the bottom surface where there is a displacement in the negative y-direction. It is at these two points that the inner cylinder is expected to stick to the outer annulus. Sliding contact is expected at the front of the outer annulus, as the force applied will promote sliding of the inner cylinder from out of the block. The outer annulus protruding from the block has a relatively small amount of material and its deformation will promote sliding at this point. This sliding is prevented by the coefficient of friction multiplied by the normal tractive force as described in section 4.0. Other areas of the inner cylinder are in open and near contact where the displacement of the inner cylinder has caused some separation with the outer annulus.

The most significant areas of contact penetration are where there is the greatest closed sticking and sliding contact status, or a combination of both. These regions are at the top back surface of the inner cylinder and the bottom front surface where contact with the block and outer annulus is present (each corresponding to the influence of loading). The greatest penetration occurs where the negative y-direction displacement into the outer annulus and block is greatest, as expected. This penetration is however very small (magnitude of $1x10^{-6}$) and is not of concern for this particular case.

Contact pressure and frictional stress are realised predominantly at the areas of interest described above, as expected from the influence of the bending moment on the system. The sliding distance is small and effective at the front bottom surface of the inner cylinder. Figure 4.9 demonstrates the contact status of the inner cylinder

The nodal displacements for each coincidental position at the hexahedral and tetrahedral interface are identical, and the contour plot shown in figure 4.10 depicts this. This proves continuity between the pyramid and hexahedral elements.

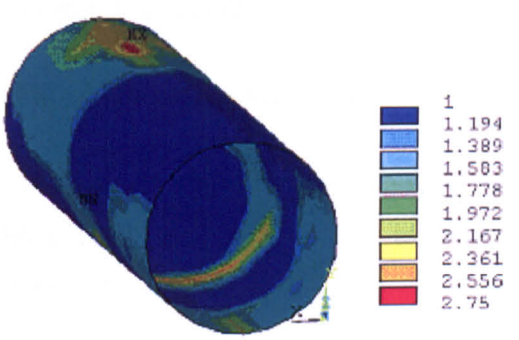

Figure 4.9 – Contact status on inner cylinder.

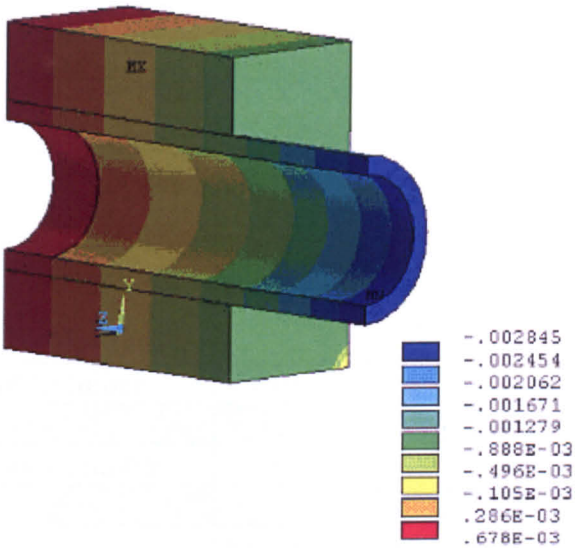

Figure 4.10 – Cross section view of hollow cylinder and block.
Displacement in the y-direction is continuous between the two.

4.9 Summary

- A simplified finite element model has been used successfully to achieve element continuity between hexahedral and tetrahedral elements.
- The contact results obtained using a contact stiffness coefficient of 1 provide:
  - Appropriate contact status results for the boundary conditions specified.
  - Penetration values of an acceptable magnitude.
- The solution process and contact algorithm used coupled with the modelling technique adopted have been used successfully to generate a simplified working model of contact.

4.10 Parameter Investigation

4.10.1 Element thickness

An investigation into the number of underlying elements on the target surface is carried out. Three tests were completed, using one, two and three solid elements in the outer annulus. The outer annulus has a thickness of 1.5mm.

Maximum deflection and von Mises stress data for the solid and hollow cylinder are given in table 4.1. Table 4.2 presents contact data for the inner cylinder.

	Elements in target volume		
	1	2	3
	Maximum deflection in y-direction (mm)		
Solid Cylinder	2.60E-04	2.60E-04	2.60E-04
Hollow Cylinder	5.10E-04	5.10E-04	5.10E-04
	Maximum von Mises stress (MPa)		
Solid Cylinder	1.76	1.77	1.77
Hollow Cylinder	2.01	2.10	2.13

Table 4.1 – Deflection and peak stress data in the solid and hollow cylinder whilst varying the number of elements in the hollow cylinder (annulus).

	Elements in target volume		
	1	2	3
Maximum contact status	2.8	3.0	3.0
Maximum penetration (mm)	3.11E-07	3.07E-07	3.03E-07
Total Stress (MPa)	0.81	0.78	0.77
Number of iterations to	81	121	94

Table 4.2 – Contact results gained from varying the thickness in the hollow cylinder (annulus).

4.10.2 Element thickness summary

- A negligible difference in the displacements of the system is observed – less than 1% difference.
- A negligible difference in the maximum von Mises stress for the inner cylinder is observed – under 1%.

- A small increase in the maximum von Mises stress for the outer annulus is recorded – 6% increase from one to 3 elements thick.
- Contact status displayed a small increase in the amount of sticking contact as the element thickness is increased.
- Penetration of the contact surface into the contact showed a negligible decrease – 1%.
- Contact total stress has a small decrease in value as the element thickness was increased – 4% decrease.
- The number and thickness of elements present underlying the target surface has a negligible effect on the displacement, peak stress and contact data.

4.10.3 Contact Stiffness Investigation

An understanding of the influence that the contact stiffness parameter has on the maximum displacement and von Mises stress, as well as contact data and convergence criteria is obtained. Contact stiffness is evaluated by the use of a scaling factor between 0 and 10. For a value of 2, the solution did not converge. The range arbitrarily chosen for investigation is from 0.2 to 1 in increments of 0.2. A value of 0.01 is also used.

The contact stiffness has a marked effect on the penetration of the system and on the amount of substeps taken to reach convergence. However the penetration is considered negligible for a contact stiffness of between 0.1 and 1. The data is presented in table 4.3 and 4.4.

	Contact Stiffness factor					
	1	**0.8**	**0.6**	**0.4**	**0.2**	**0.01**
Maximum contact status	2.75	3	3	3	3	3
Maximum Penetration (mm)	3.11E-07	3.85E-07	5.11E-07	7.58E-07	1.47E-06	2.41E-05
Total contact stress (MPa)	0.81	0.79	0.79	0.78	0.76	0.67

Table 4.3 – Deflection and von Mises data for varying contact stiffness.

	Contact Stiffness factor					
	1	**0.8**	**0.6**	**0.4**	**0.2**	**0.01**
	Maximum deflection in the y-direction (mm)					
Solid cylinder	2.62E-04	2.62E-04	2.62E-04	2.62E-04	2.62E-04	2.64E-04
Hollow cylinder	5.08E-04	5.08E-04	5.08E-04	5.08E-04	5.08E-04	5.09E-04
	Maximum von Mises stress (MPa)					
Solid cylinder	1.8	1.8	1.8	1.8	1.8	1.8
Hollow cylinder	2.0	2.0	2.0	2.0	2.0	2.1

Table 4.4 – Contact data gained for inner cylinder as a result of varying the contact stiffness value.

	Contact stiffness					
	1	**0.8**	**0.6**	**0.4**	**0.2**	**0.01**
Substeps	**Equilibrium Iterations**					
1	23	19	18	17	14	6
2	35	28	27	24	20	9
3	40	35	33	28	23	11
4	46	42	38	31	26	13
5	51	45	42	34	28	15
6	56	49	46	38	31	17
7	60	53	49	41	33	18
8	64	57	52	45	35	20
9	68	59	54	48	37	21
10	71	62	56	50	39	23
11	74	64	58	52	40	24
12	77	66	60	54	42	25
13	81					
Total	81	66	60	54	42	25

Table 4.5 – Convergence of solution with different contact stiffness.

4.10.4 Contact stiffness summary

By varying the contact stiffness, the following is observed:

- A negligible (<1%) increase in the maximum von Mises stress of the inner cylinder.
- A negligible (<1%) increase in the maximum von Mises stress of the outer annulus.

- Negligible variance on the limit of contact status for up to $1/5^{th}$ of the default value. The effect is noticed by the distribution of the status about the contact surface. $1/100^{th}$ of the default value has a marked effect upon the amount of closed and sticking contact involved.

- There is a significant increase in the penetration of the system (factor of 10).

- A substantial difference to the convergence of the solution is realised with a decreased contact stiffness value. A value of 1 requires 81 substeps for convergence completion where a value of 0.01 requires only 25. Contact stiffness therefore will have a significant effect on the time taken to gain solution convergence and the computational resources.

4.10.5 Load Dependency

The contact solution is non-linear, and an increase of loading on the system may produce a significant difference in the overall solution data. The problem is solved with ten times the amount of load (1kN) acting on the inner cylinder.

Results are given in table 4.6 and 4.7.

	Load (kN)	
	100N	**1000N**
	Maximum deflection in y-direction (mm)	
Solid Cylinder	2.62E-04	2.62E-03
Hollow Cylinder	5.08E-04	5.08E-03
	Maximum von Mises stress (MPa)	
Solid Cylinder	1.76	17.63
Hollow Cylinder	2.01	20.05

Table 4.6 – Displacement and peak von Mises stress data for solid and hollow cylinder for varying the applied load.

	Load (kN)	
	100N	1000N
Maximum contact status	2.75	2.75
Maximum penetration (mm)	3.11E-07	3.11E-06
Total Contact Stress (MPa)	0.81	7.96

Table 4.7 – contact data for the solid cylinder and varying the applied load.

4.10.6 Load dependency summary

By increasing the load ten fold the following is observed:

- All displacements increase by ten times.
- The maximum von Mises stress increases by a factor of nearly ten.
- Contact status regions remain constant, but more closed and sticking contact is observed with a higher load.

The problem being described is not linear in the mathematical sense, as the two different load regimes cannot be superimposed. Rather for a given load distribution shape the outcome is proportional to the load magnitude.

This situation arises due to the contact area being reduced from an increase in load. Contact is observed all around the inner cylinder and once the load has been applied this contact area is reduced as the ends of the inner cylinder are pulled away from and towards the outer annulus. Once the same loading pattern is doubled the contact region changes and the resultant stress and strain and displacements are doubled. Thus the load distribution shape remains the same however the response is proportional to the magnitude of the load.

4.11 Bone – Steel construct

The material properties of the outer annulus and block are changed to be markedly different to that of the inner steel cylinder, and are assigned an elastic modulus of 20GPa. This is representative on an implant and bone construct.

The results of the two material property models are given in tables 4.8 and 4.9.

	Steel - steel model	**Steel - bone model**
	Maximum deflection in y-direction (mm)	
Solid Cylinder	2.62E-04	2.79E-03
Hollow Cylinder	5.08E-04	5.14E-03
	Maximum von Mises stress (MPa)	
Solid Cylinder	1.76	3.11
Hollow Cylinder	2.01	0.67

Table 4.8 – Displacement and peak von Mises stress data for the solid and hollow cylinder.

	Steel - steel model	**Steel - bone model**
Maximum contact status	2.75	3
Maximum penetration (mm)	3.11E-07	2.13E-06
Total Contact Stress (MPa)	0.81	0.56

Table 4.9 – Contact data for inner cylinder.

4.11.1 Bone-Steel Summary

- The deformation of all parts of the system is greater in the bone – steel model.
- The inner cylinder has a greater deformation due to the fact that the softer outer annulus and block are unable to resist the bending moment applied in the same manner as the rigid steel-steel construct.
- This greater deformation of the steel inner cylinder results in a higher von Mises stress value.
- An increase in contact status and penetration is observed due to the increased deformation of the contact and target surfaces and the smaller contact stiffness.

- Normal traction and total contact stress have decreased, as the softer target surface is now not as capable of resisting the bending moment applied to the system.

4.12 Target surface inversion

An investigation is given for reversing the target and contact surfaces to assess the importance of the definition of these surfaces. Figure 4.11 shows the contact status for the inner cylinder with the surfaces reversed.

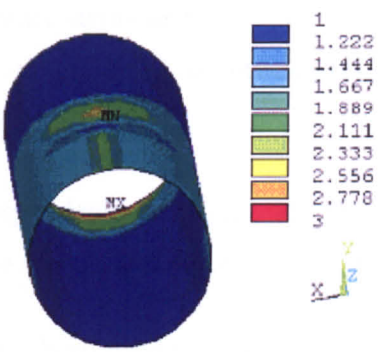

Figure 4.11 – contact status on solid inner cylinder.

4.12.1 Target surface inversion summary

- The displacement of the system shows a negligible difference – max difference is 1%
- Contact status is identical but reversed in position.
- The penetration is increased by 50%.
- Contact gap remains the same however reversed.
- Total contact stress is increased by 25% with a reverse in trend.

The results obtained from reversing the contact and target surfaces have provided similar results in magnitude relative to the stiffness of the surfaces. Intuitively the results given from reversing the surfaces are non-sensible, with contact being

achieved at regions in the system that is not consistent with the displacement of it.

4.13 Summary

- The number of elements underlying the target surface has a negligible effect on the contact results or global stress and strain data.
- Contact stiffness is an essential real constant value in contact problems and has a significant effect on the penetration observed between the target and contact surface, the contact status and the amount of substeps required for solution convergence. Using a value of between 0.1 and 1 has a negligible effect on the results.
- The system is load dependent, with an increased load resulting in an increased response of the system and overall von Mises stress criterion.
- A bone-steel construct has been used to compare this simplified model to the actual differing materials used in an intramedullary fixation. The results are, in general, comparable to the all-steel construct with differing magnitudes.
- There is a greater amount of sticking contact in the bone-steel construct, and the regions of such contact are reduced in size. This is due to the fact that there is more deformation in the softer outer entities.
- The correct designation of contact and target surfaces is essential to the problem under investigation.

4.14 Conclusion

A simple finite element model has been used to investigate conforming surfaces, element continuity and contact parameters. This model has verified the novel modelling technique described in chapter 3.

The bone contact volumes will require conforming surfaces in the model described in chapter 3 to establish element continuity at their interface. Element continuity is achieved by the use of pyramid elements.

The number of elements underlying the target surface is not an issue for the contact solution, deflection data and von Mises stress.

A contact stiffness of between 0.1 and 1 has a negligible effect on the deflection and stress data. There is a significant effect on the number of iterations required to gain solution convergence. A small value of contact stiffness is recommended for computational efficiency.

The correct designation of the contact and target surfaces is essential to providing accurate results.

5.0 Introduction

This chapter presents an experimental procedure that will be used for the verification of the finite element modelling technique presented in chapter 3. In subsequent chapters a finite element model will be generated and a comparison made between the finite element and experimental data.

Sections 5.1 to 5.3 give details of finite element models used in biomedical device design, and refer to the use of experimental validation. The use of numerical-only studies has been included, but the reader should refer to chapter 2 for a more thorough review of finite element techniques used with and without experimental validation. Subsequent sections introduce the experimental technique used.

5.1 Verification of finite element models

When using the finite element method, a distinction must be made between a specific analysis that requires critical accuracy of results, and an analysis that is indicating a trend. How validation of a finite element model is used depends on this distinction. Either way, a finite element model should be verified.

Comparative studies including parametric data can be used for the design optimisation of a system. Accuracy of results may not be required, but the effect of relative change in data can lead to relative benefits in device design. The use of comparative studies may not therefore require validation.

The finite element modelling technique presented in chapter 3 may be used, in the longer term, to provide accurate, clinically relevant information. Validation by comparison to experimental data for this first generation model is therefore presented in chapter 6. A comparison with experimental data serves to verify the finite element modelling technique, so that comparative studies can be used in later chapters.

5.2 Experimental validation

When properly interpreted and experimentally verified, the finite element method can provide valuable insight into the stress distribution of a trauma treatment

device and its interaction with the human skeleton. Few finite element studies involving intramedullary nails implanted in femurs exist, and fewer still are experimentally verified (Huiskes *et al.*, 1983; Prendergast, 1997; Cheung *et al.*, 2004). Sanchez Gimeno *et al.*, (1997) performed an analysis on a Gross-Kempf femoral nail, but the analysis did not consider the presence of the bone or locking screws and furthermore no experimental validation was given.

Finite element models of intramedullary nailing systems can be validated by various experimental methods. A comparison relative to bone surface strains is one such method (Rohlmann *et al.*, 1983; McNamara *et al.*, 1997; Viceconti *et al.*, 1998; Stolk *et al.*, 2002). Cadaveric testing may be employed, a synthetic femur may be used and *in-vivo* data can also be compared to a finite element model.

5.2.1 Cadaver testing

There is a great deal of literature available concerning cadaveric testing. Eveleigh (1995) carried out a review of intramedullary devices and the testing methods used, reporting that there is a wealth of cadaveric test methods available. Steinberg *et al.*, (1998), investigated the biomechanical properties of a new proximal femoral nail, by carrying out mechanical and cadaveric tests. The cadaver specimen comprised only of the femoral head, and was submerged in epoxy resin before pull-out and torsional tests performed. Haynes *et al.*, (1997) also performed cadaveric experiments in the comparison of a dynamic hip screw and a gamma nail. Twelve pairs of human femora kept in frozen storage and defrosted were used in their study. Rohlmann *et al.*, (1983), compared a finite element model with an experimental investigation in a cadaver femur with hip endoprosthesis. There are disadvantages with using cadaver specimens, in that they vary greatly in their inter-femur strains and a sample of several hundred may be required for a 95% confidence interval (Crowninshield *et al.*, 1980; Shybut *et al.*, 1980). There is also the problem of availability, handling and preservation.

5.2.2 Synthetic femur tests

In the search to eliminate the inherent difficulties of cadaver specimens a number of standardised synthetic femurs have been proposed. The only commercially available composite prototype has been proposed by Pacific Research labs (Vashon Island, WA), and is modelled with carbon-fibre reinforced epoxy to represent the cortical bone, and polyurethane foam to represent the cancellous bone (Cristofolini *et al.*, 1996). The same manufacturers also have a second and third generation composite femur, all being designed to mimic as closely as possible the mechanical behaviour of human bone. There is much ambiguity in literature as to the viability of the use of a synthetic standard femur. Szivek *et al.* (1990) observed highly variable torsional and bending responses in the first generation composite femurs. Szivek and Gealer (1991) measured the strains in six second generation composites and found a great deal of variability in their deformation response to axial loads, and noted that their stiffness was generally low in comparison to cadaveric specimens. Harmen *et al.* (1995) showed, however, that composite femur models were advantageous when trying to define a reproducible protocol to measure the implant stability. Cristofolini *et al.* (1996) demonstrated that from a geometric point of view the similarity between cadaveric and composite femurs was satisfactory, except that the synthetics have a reduced diaphyseal antero-posterior bowing. They suggested allowing 4 minutes between tests to eliminate any time-dependant behaviour. It was stated that the measurement of femoral head deflection under axial loading for the synthetic femur was far more repeatable than the cadaver specimens, and that the composite femurs fell well within the range observed from human femurs. Heiner *et al.* (2001), also found similar results when testing a new composite femur. Cheung *et al.*, (2004), used a finite element model of a femoral retrograde intramedullary nail and compared to experimental data using a third generation synthetic femur. This analysis did not consider the interaction between the implant and the bone along the shaft, did not use contact elements and was not concerned with a fractured bone.

5.2.3 In-vivo testing

The ultimate test of a model's ability to replicate reality is comparison with *in-vivo* data. *In-vivo* testing may be of particular interest. However, such experiments are rare, and require patient cooperation. There are only a few studies available that present *in-vivo* data and they concentrate on implant loading. Data gathered from an implant that is *in-situ* may be used to test wear, strength, fixation stability and for optimising implant design and materials by computer simulation (Bergmann *et al.*, 2001). *In-vivo* testing allows for more advanced models of the load acting on the femur to be considered and justified. There have been very few finite element models of intramedullary nails implanted in a femur, and verified with *in-vivo* measurements (Cheung *et al.*, 2004). *In-vivo* testing is expensive to carry out and patient specific.

5.2.4 Standard testing

Some literature has suggested that a standardised femur could be used in the scientific community for the testing and evaluation of implants (Viceconti *et al.*, 1996a; Cristofolini *et al.*, 1996; Eveleigh, 1997) and in the validation and/or calibration of finite element methods (Viceconti *et al.*, 1996). Given the variability in femur size and shape, requiring a large data set to have a high confidence rating, it would seem prudent to introduce, and use if available, a standardised femur model. This would allow repeatability of experiments and the validation of finite element models as far as the same reference geometry is concerned. As well as considering the use of standard reference geometry, a standard test method could also be introduced. Eveleigh (1995) reported a review of intramedullary devices and cited many cadaveric testing methods, highlighting the vast differences in these methods and calling for a standardised test procedure.

In addition to a standard test method there may need to be a standard load, or set of loads, that will be applied to the femur model. Loading conditions are often oversimplified by displaying only the hip contact force acting on the femoral head, which tends to leave the impression that the forces are transmitted through the bone and leave at the distal end, a concept that is widely used in experimental

procedures and numerical analysis. However, studies have shown the load to be modified along the length of the bone through the actions of the muscles and any study should consider the close relationship between joint contact forces and muscle action (Heller *et al.*, 2001). It would seem appropriate to agree upon a standard set of forces that should be applied to the femur when examining implant devices. A standard set of forces would provide a platform from which different finite element models could be compared. Emphasis on producing a model with an accurate stiffness rather than anatomical detail could then be advanced. A standard test method with the use of standard loading would enable different finite element and experimental tests to be rigorously compared across institutions, without perhaps requiring a standard geometry which is by its very nature impossible to measure. Designs often use ranges that include 90% of the mature population of working age, and define what can be termed the Standard Person. However, consider the story of a man who invented a shaving machine for the Standard Person. It is clamped to the face and from the press of a button the machine shaved. When asked what happens if the person didn't have a standard face, the inventor replied that they would after using the machine (Ashby, 2002).

To date there is no recognised 'standard' femur, loading or test method used in the scientific community. Furthermore there is little agreement in literature as to whether the available composite models are equivalent substitutes for cadaveric specimens. It is recognised that for validation of a finite element model, a synthetic, dried, frozen or wet femur could have been used, so long as the finite element model represents the test specimen. The longer-term issue of repeatability and facilitation of comparison between different modelling approaches is still a concern in the use of a 'non-standard' procedure.

5.3 Verification using parametric analysis

Finite element analysis can be validated by comparison with some reference data, but numerical-only studies can also provide useful results where information is attained on a relative basis. In their survey of finite elements in biomechanics, Huiskes *et al.*, (1983) and Prendergast *et al.*, (1997) stated that the validity of a finite element model must be regarded in the light of the analysis objectives, and

that the question is whether the results, given the model assumptions, justify the conclusions reached. Huiskes *et al.*, (1983) stated that a finite element model could be validated by way of in-depth investigation of the structure under investigation from parametric analysis. It is further recommended that such parametric studies need not be carried out with expensive 'anatomic' models but can often be limited to simplified, general representations (Huiskes, 1979). It would seem beneficial to validate any numerical studies with experimental data where possible. The use of numerical only studies can play an important part in biomechanics when considering the large variability in fracture types and surgical techniques. An aim for general information on a relative basis from parametric studies would provide useful information.

5.4 Experimental procedure and methodology

The experiments carried out for this study follow on from previous work set out in an internal Brunel University report. Because this report is not in the public domain an outline of the technique is repeated here. Dr P. Hillard and Mr C. J. Brown originally devised the experiment. The author, using the same constructs, has carried out all tests reported in this thesis independently.

5.4.1 Femur construct used

Two cadaveric femora are used in the experiment, and have been supplied by Sawbones Europe AB (Limhamm, Sweden), and selected from a batch of six. They are numbered femur 2, and femur 6. Prior to dispatch the femora had been macerated, heat treated and bleached. No age and sex data were provided with the femora. However the femora are relatively small and slender and are likely to have come from young adults. Femur 2 may well be female and femur 6 male, because femur 6 is slightly larger. Dried femora have the advantage of easy handling and storage. Figures 5.1a and 5.1b show both instrumented femora.

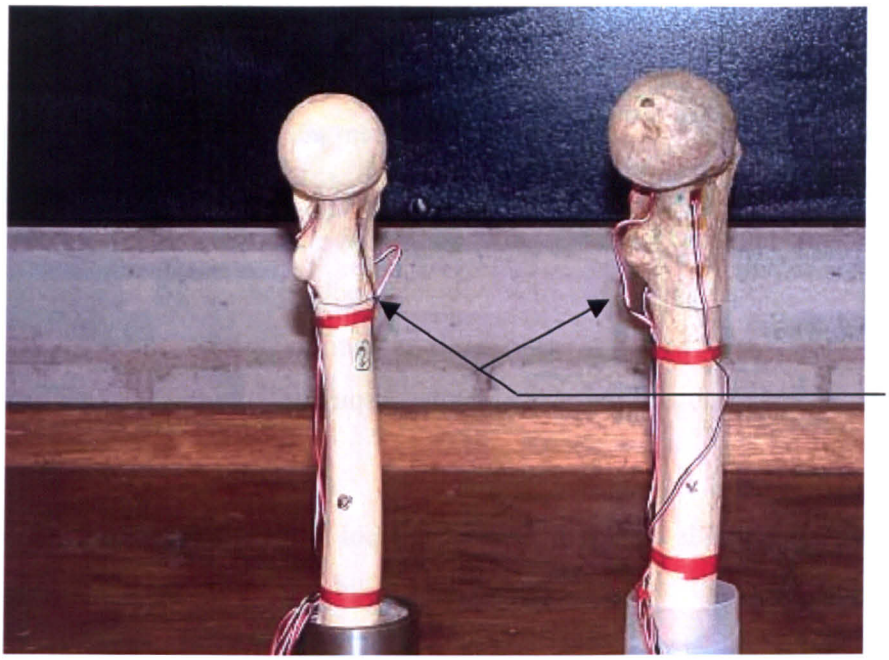

Figure 5.1a - The instrumented femora. Femur 2 is on the left.

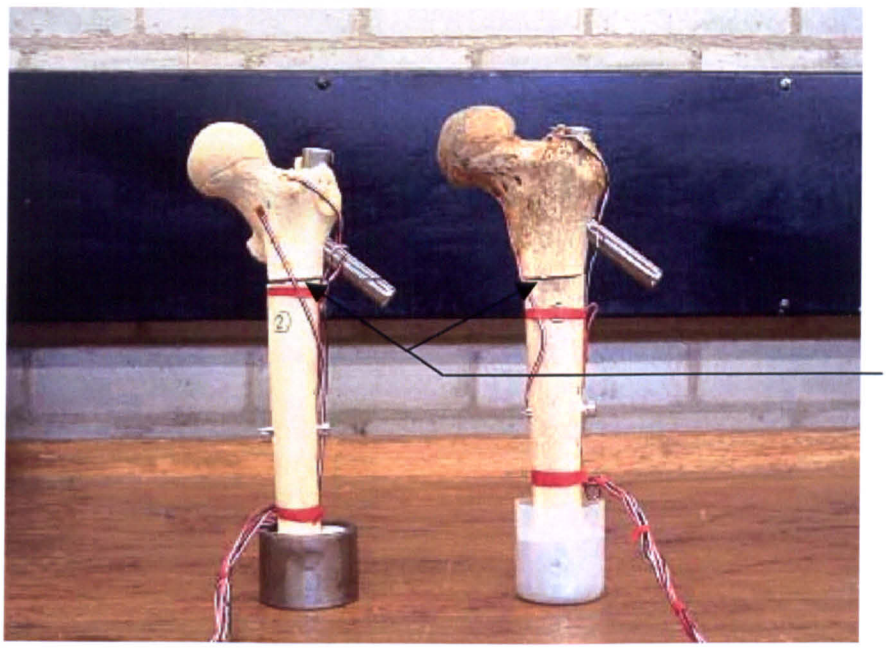

Figure 5.1b - The instrumented femora. Femur 2 is on the left.

The condyles and distal part of the diaphysis of each femur have been removed, so that each femur has an overall length of 300mm, taken from the most distal part of the femoral shaft to the most proximal part of the upper trochanter on a line parallel to the axis of the femoral shaft. Subtrochanteric fractures or osteotomies were created in the femora by a consultant orthopaedic surgeon, Mr G. J. Andrew, at Manchester Hope Hospital who then implanted the nails. The standard procedure for implanting the device was followed (Standard Gamma Locking Nail Operating Technique, Howmedica International Ltd., London, 1993).

Standard stainless steel Gamma locking nails with one distal locking screw and one lag screw were used to stabilise the fractured femora. Dimensions for the gamma nail used are shown in figure 5.2.

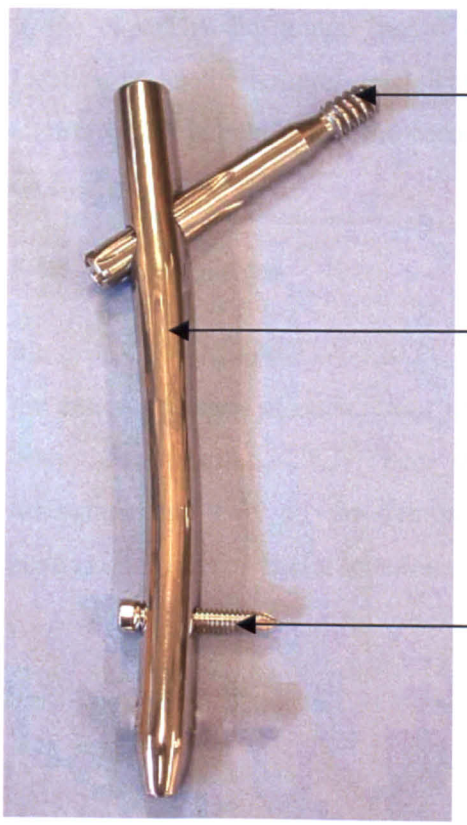

Figure 5.2 – The Gamma nail used.

5.4.2 Apparatus

Each femur is mounted in an Instron material testing machine using a special jig. Their principal axis will be inclined at 21° to the vertical in the coronal plane and 10° to the vertical in the sagittal plane. This orientation represents the first maximum resultant peak load during a walking phase, in a machine capable of vertical loading. The same load condition and experimental set-up is used by Haynes *et al.*, (1997a), who investigated lag screw cut-out with a gamma nail in cadaveric specimens. The loading used in this work is deemed appropriate for qualitative experimental investigations that may be compared to finite element data.

Diagrams of the jig components are given in Appendix I, with a picture of the experimental set-up. The material used for each component is mild steel. A Cerrobend (Hoyt-Darchem, UK) potting compound is used to align the distal end in the cup. The dial gauge shown schematically in figure 5.3 demonstrates its location under the femoral head. The dial gauge is held in position by a magna-clamp, which is held below the coronal block. The complete testing rig is shown on figure 5.3.

5.4.3 Strain gauges

Six type CEA-XX-062UW-120/P2 uni-axial strain gauges have been bonded to the exterior surface of each femur using M-Bond 200 (both from Measurements Group, Basingstoke, UK). There are four on the femoral neck, four on the trochanter and two on the femoral shaft. Photographs of the strain gauge positions and their general location are shown in figures 5.4 and 5.5.

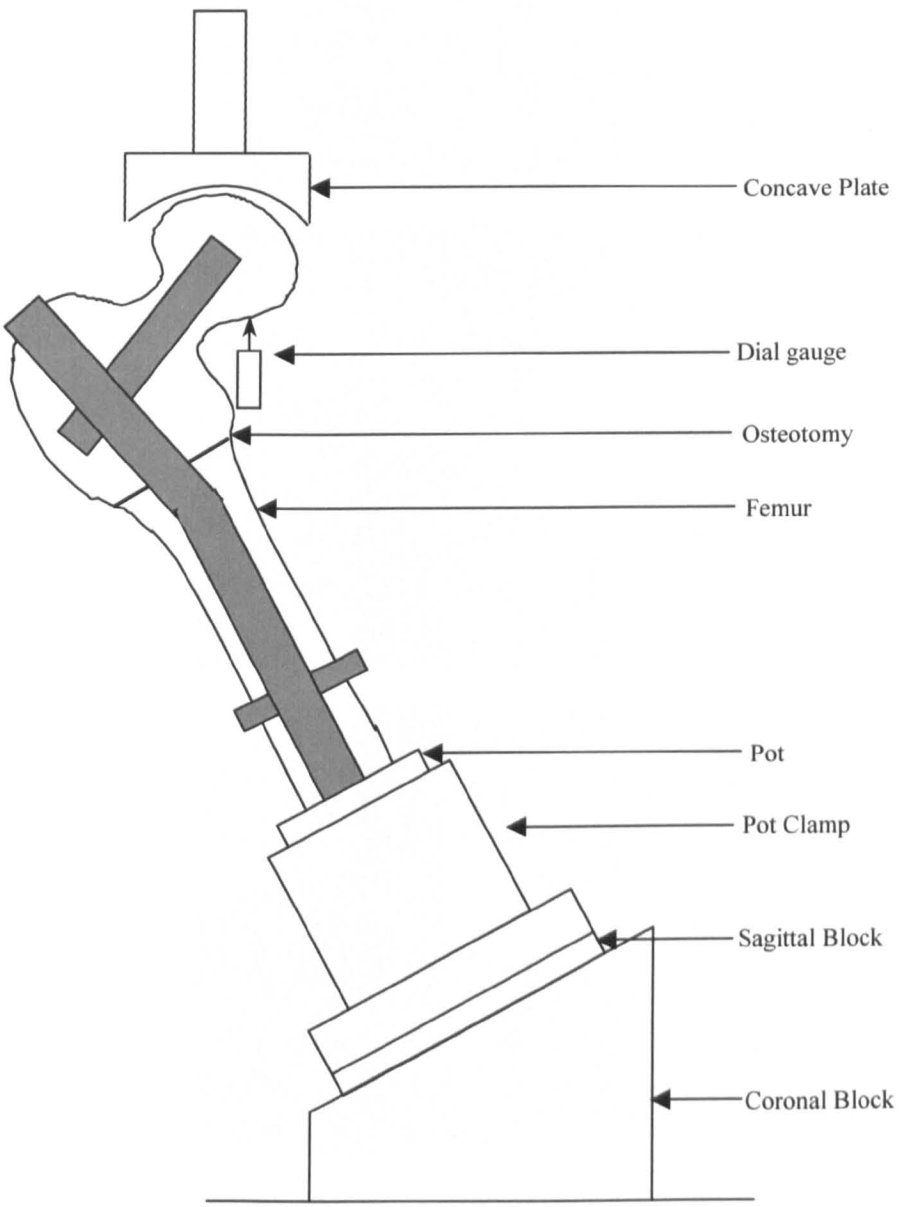

Figure 5.3 - Schematic of the experimental set-up.

Figure 5.4 – Strain gauge positions on femur 2.

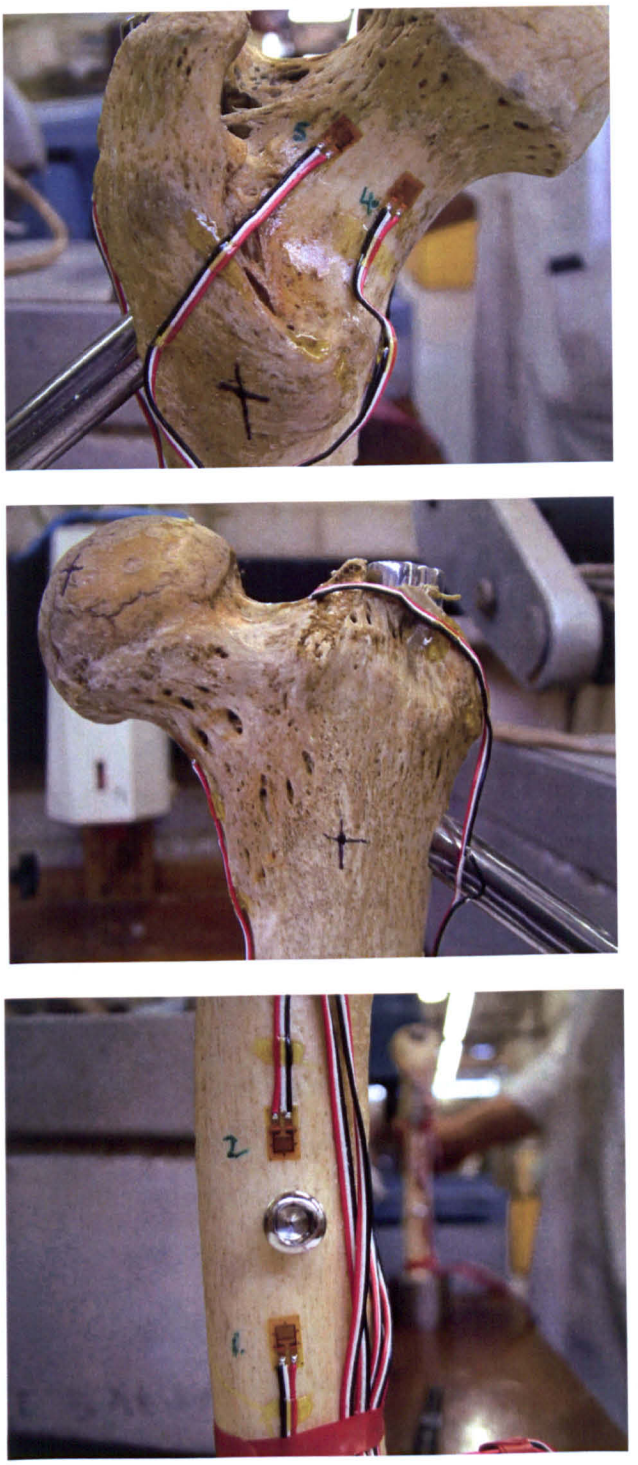

Figure 5.5 – Strain gauge positions on femur 6.

5.4.4 Dial gauge measurement

A dial gauge is positioned under the femoral head, in line with the point and direction of load application. This is used to determine if there is any localised deformation of the femoral head at the point where the load is applied. The Instron testing machine measures the displacement at the point of load and any difference between the two readings will be due to localised deflection on the femoral head due to the load. The dial gauge is shown schematically in figure 5.3.

5.4.5 Loading and data capture

Both femora were subjected to a compressive load in the Instron material testing machine. Each femur however was subjected to a different load due to the perceived quality of the bone.

Femur 2 was of the better quality with no visible cracking and little signs of general wear. Cracking was visible in the cortical shaft of femur 6 and also at the lateral edge of the trochanter. There was also a substantial amount of dust coming out of this specimen and therefore it was tested at a smaller load than femur 2.

Femur 2 was subjected to a maximum compressive load of 2.8kN, which corresponds to 4 times the body weight of a person weighing 700N. Femur 6 was subjected to a maximum compressive load of 1.3kN, due to the perceived quality of the bone.

The load and deflection data were recorded with a Schlumberger SI 3535D data logger controlled from a PC using Scorpio data acquisition software (both Schlumberger Technologies Ltd., Farnborough, UK). The load rate in each case was 0.02kN per second. This load rate was chosen for the steady application of load, enabling 30 data points to be collected. The tests were repeated three times each to check for repeatability, with about 4 minutes between each test to ensure no residual strain remained, a practice used by Cristofolini *et al.*, (1996).

5.4.6 Material properties

5.4.7 Cortical bone modulus

A small sample of cortical bone was taken from the unused distal diaphysis of the femora and loaded in compression to determine the elastic modulus of cortical bone. The modulus measured for femur 2 and 6 was 5.3GPa and 5.4GPa respectively. Values for cortical bone, in the literature are typically around 17GPa, (Reilly *et al.*, 1974., Knets *et al.*, 1975., Taylor *et al.*, 2002). Precise heat treatment methods for the femora used in this experiment are not known, and dried bone can have different material properties from live bone depending on the treatment and storage. It is in the comparison with the finite element analysis that the experimental data will be used, and as such so long as the same material properties are entered into the model, a comparison may be drawn from the two data sets.

5.4.8 Cortical shell thickness

A method for measuring the cortical shell thickness surrounding the femoral head has been devised. Small holes of 0.5mm diameter are drilled at points about the trochanter and femoral head. A dial gauge measures the distance the drill has travelled, and indicates the point at which the drill bit 'cuts-through' the hard cortical shell and passes into the soft cancellous bone.

The method is based on the fact that when the drill bit passes through a harder medium to a softer one, there is a reduction in the force required to continue drilling. The method used in this work relies on the operator 'feeling' the point at which the force is reduced, and reading off the dial gauge the distance that the drill has travelled. Figure 5.6 demonstrates this method.

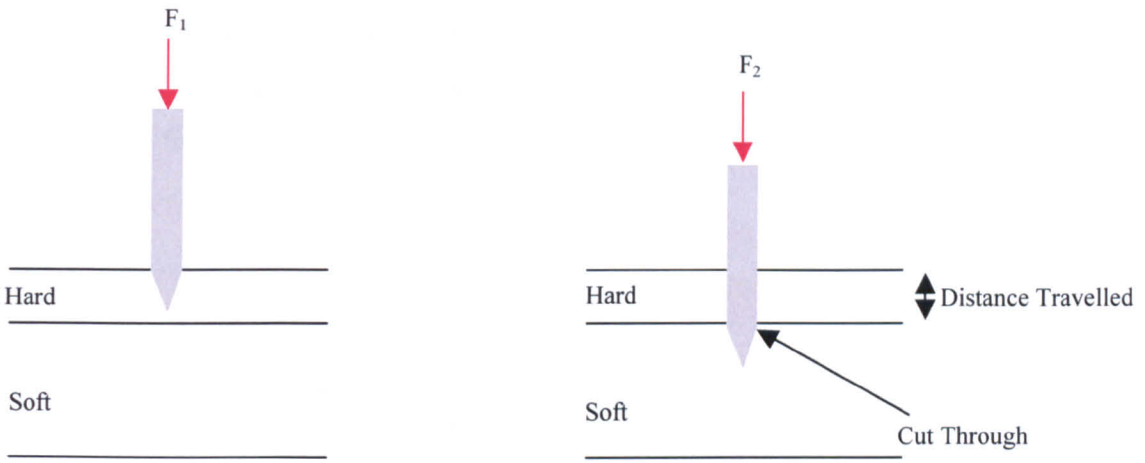

Figure 5.6 – Schematic of 'drill-through' method.

Figure 5.6 shows a drill bit cutting through a hard material, such as the cortical shell, with a force required to keep the drill cutting. As the drill 'cuts through' the hard material and enters the soft material there is a sudden reduction in the force required to keep drilling. The sudden reduction in force is greater if there is nothing the other side of the hard material. If the soft material is porous as with cancellous bone, the force reduction is emphasised and able to be 'felt' by the user with ease.

The method is validated on a sample bone by drilling 6 holes about the proximal femur and measuring the shell thickness. The proximal femur is then dissected and the shell thickness measured with Vernier callipers at the points where the bone was drilled. A sample drill hole is shown in figure 5.7.

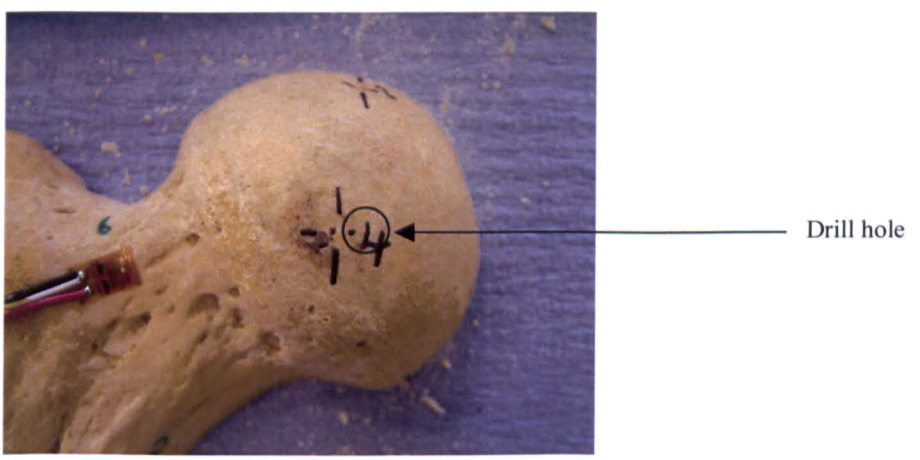

Figure 5.7 – Drill hole in femoral head.

When using this method to measure the cortical shell thickness, only six holes are drilled to minimise the damage to each femur. The cortical shell thickness measured from each method on the sample bone is presented in table 5.1.

Cortical Shell Thickness (mm)			
Dial gauge	Vernier	% Difference	Location
0.8	0.78	+3	femoral head
0.6	0.60	0	femoral head
0.8	0.81	-1	femoral head
0.9	0.83	+8	femoral head
1.2	1.29	-7	lateral trochanter
1.9	2.13	-11	medial trochanter

Table 5.1 – Measured cortical shell thickness with Vernier callipers and dial gauge.

The method is designed to determine the cortical shell thickness whilst minimising the damage to the cadaveric femora. The shell thickness may vary about the femoral head and trochanter, and a value will be assumed for the thickness of the shell in regions of the proximal femur. This assumption is based on the idea that the experiment will be used to validate a finite element model, and that the finite element model will assume a constant thickness about regions of the proximal femur. It is noted that the finite element model is an approximation of the anatomical femur.

The six drill holes used to measure the cortical shell thickness are chosen by inspection of the sample proximal femur. By measuring the cortical shell thickness around the entire cross section of the sample proximal femur with Vernier callipers, three regions of the proximal femur can be identified that each have a similar thickness. The three regions are defined as the femoral head, medial trochanter and lateral trochanter in this study. These regions are shown in figure 5.9.

The measured cortical shell thickness for femurs 2 and 6 are given in table 5.2, the points of drilling are shown in figure 5.8. Points 1 to 4 are used to measure the thickness of the femoral head, point 5 measures the thickness of the lateral trochanter and point 6 measures the medial trochanter.

	Femur	
	2	6
Point	Shell thickness (mm)	
1	1.2	1.1
2	0.8	0.6
3	0.6	0.5
4	0.7	0.6
5	1.1	0.8
6	1.6	0.9

Table 5.2 – cortical shell thickness.

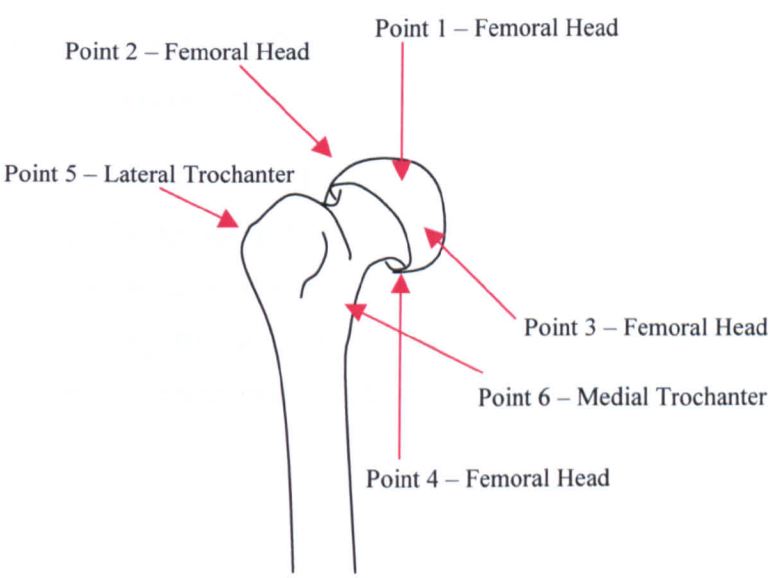

Figure 5.8 – Schematic of Drill positions for cortical shell thickness measurement.

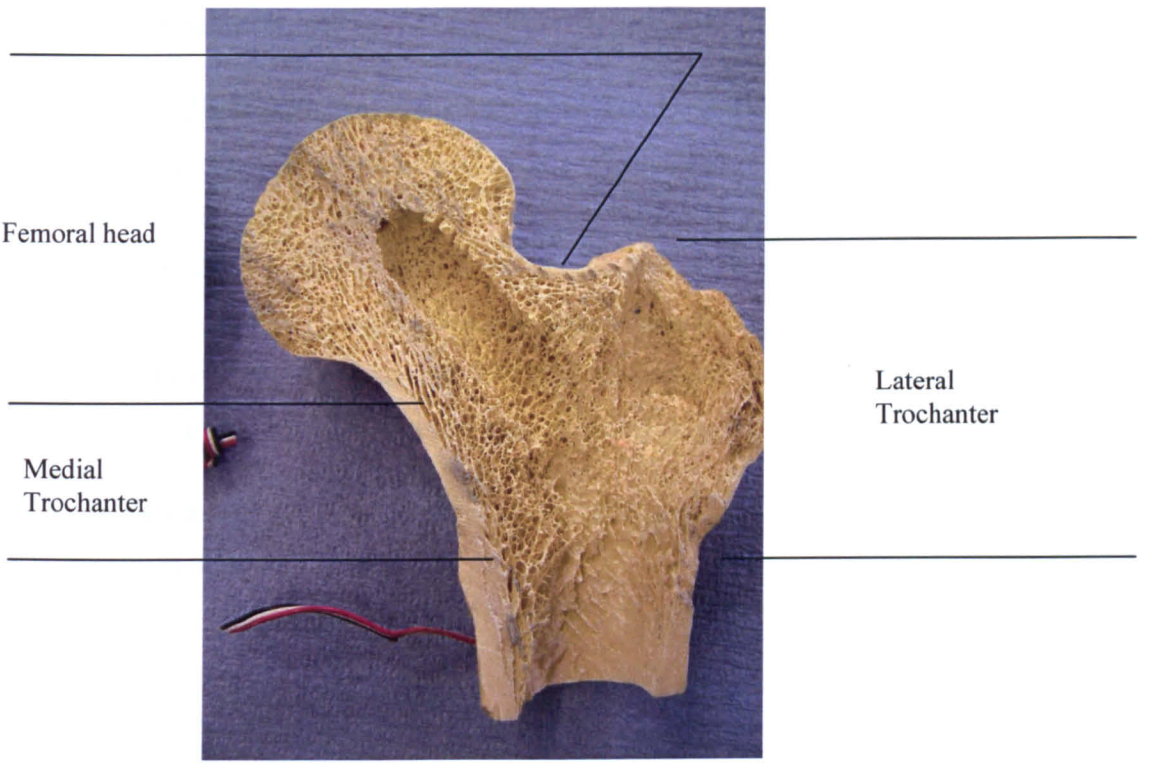

Figure 5.9 – The three regions of similar thickness for the cortical shell.

It is assumed that the cortical shell thickness has one value in the three regions described in the proximal femur for this experiment.

When modelling the experiment with finite elements, it will be argued that the medial and lateral trochanter shell thickness will have a small effect on the stiffness and deflection of the system. These simplified regions are considered justified when considering that the femoral head thickness will be a major influencing parameter on the maximum displacement of the system.

5.5 Experimental Results

Given in Appendix II are tables of the load-displacement and strain-displacement data for femur 2 and 6, for each test. This data is presented in Figures 5.10-5.13 below. The displacement measured is at the load point in the direction of the load. Data for strain gauge 2 and 1 on femurs 2 and 6 respectively is not presented, as these strain gauges were not functioning during the experiment. The strain data is used in proceeding chapters to compare with the numerical results and as such the use of five strain gauge readings is appropriate.

Deflection data measured from the dial gauge, and compared to the deflection at the load point is presented in table 5.3.

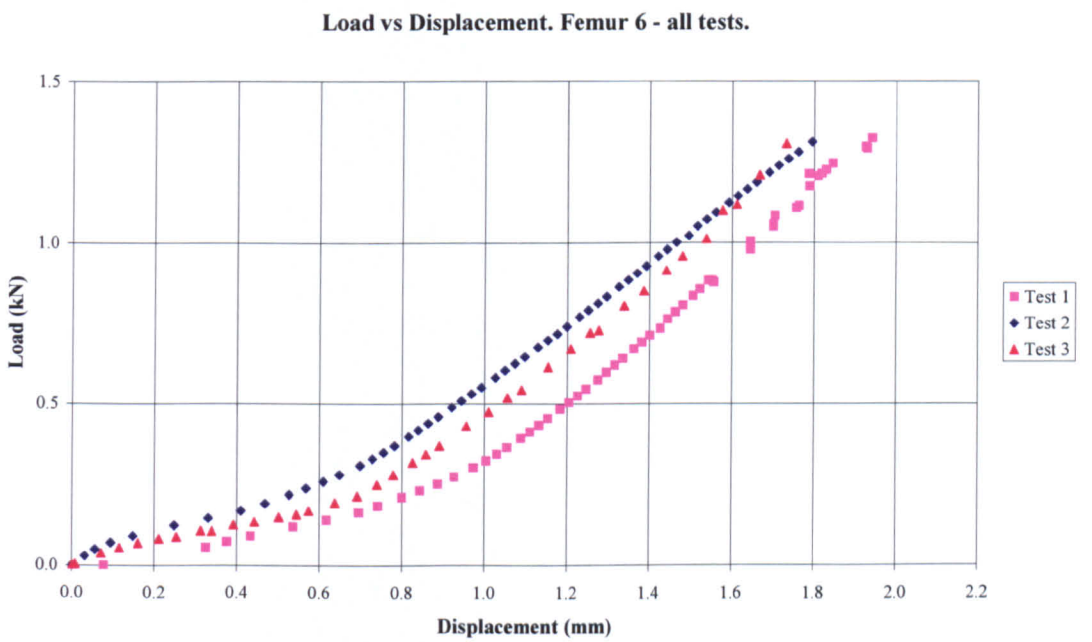

Figure 5.10-5.11 - Load-displacement distribution for each femur – all tests.

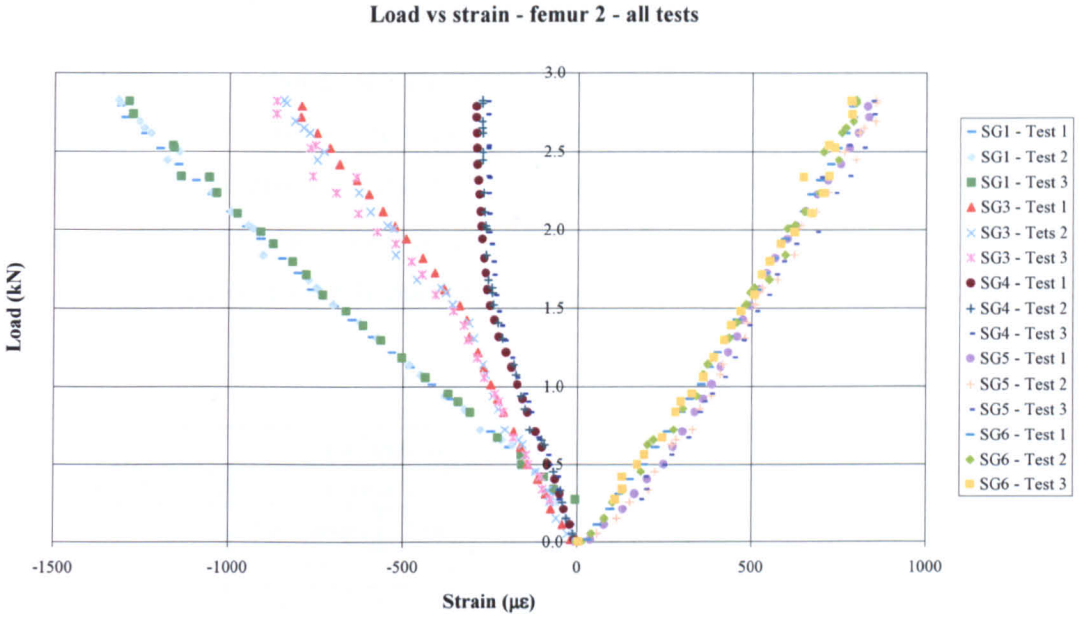

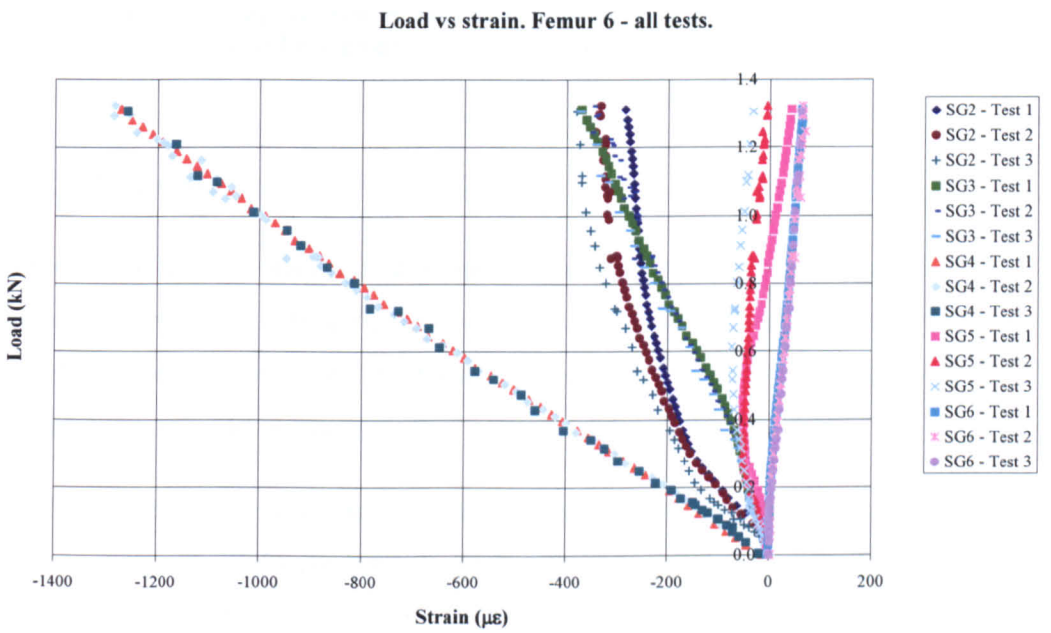

Figure 5.12-5.13 - Load-strain distribution for each femur – all tests.

5.5.1 Deflection data

Measurements from a dial gauge are taken at the maximum load, and compared to the displacement of the Instron testing machine at the point of loading. The values measured are given in table 5.3. The data is not presented to show load dependency but is tabulated to record the fact that localised deformation does occur, and was visible in each femur after testing.

Deflection of femoral head (mm)					
	Femur 2			Femur 6	
Test	Dial Gauge	Instron		Dial Gauge	Instron
1	0.81	1.43		0.92	1.94
2	0.72	1.33		0.86	1.80
3	0.70	1.29		0.81	1.73

Table 5.3 – Deflection of the femoral head in the direction of load; measured from the Instron machine and dial gauge.

5.5.2 Discussion

Inspection of the load-displacement graphs demonstrates that both femora exhibit a non-linear response. The construct gets stiffer as the load is applied; this effect is more noticeable with femur 6. A two-phase response can be identified, which may be considered as bi-linear.

The first phase is predominantly a result of the localised deformation, and the second phase is predominantly a result of the gaps being closed, and the construct being stiffer.

There are two sources of gaps in the construct. Mechanical gaps exist between the components of the implant, between the implant and bone and at the osteotomy. Material gaps exist due to the porous structure of cancellous bone.

The mechanical gaps will close after a certain load, the most influential being that in the osteotomy, where load is shared into the femoral shaft. Material gaps

will close over the entire load range. Therefore there is a monotonic response over the load range.

During testing of femur 6, cracking on the femoral shaft and trochanter were visible and audible, which is one reason for the difference in the response of this construct. Cracking of the bone will cause further non-linearity as large deformation can occur for a small increase in the load.

Strain data provides evidence that the gap in the osteotomy closes and the stiffness of the system changes. The effects are the same for both femora, but the response is clearer in femur 2.

Strain gauge 3 shows that the construct decreases in stiffness and strain gauge 4 shows that the construct increases in stiffness. Strain gauges 1 and 2 demonstrate that the stiffness of the construct increases and strain gauges 5 and 6 show very little change in the stiffness of the system.

The osteotomy for each femur is not symmetric, and the anterior and posterior gap closes at different times. Strain gauge 4 is located on the posterior surface of the femur, which is the side of the Osteotomy with the smaller gap. This gap will close first, resulting in a general increase in stiffness of the system as load is shared into the femoral shaft. As the femoral shaft shares some of the load, a smaller increase in strain at strain gauge 4 is observed for an increase in load. There is effectively more support from the bone beneath the trochanter when the posterior gap is closed and thus strain gauge 4 indicates an increase in stiffness.

Strain gauge 3 is placed on the anterior surface of the femur, which is the side of the osteotomy with the larger gap. The increased load shared by the femoral shaft, due to the posterior gap closing, results in more load being transferred into the proximal femur. However, the anterior osteotomy gap does not close at the same time and thus there is an increase in load shared into the proximal femur for the same support from the femoral shaft, on the anterior side. This has the effect of having a greater increase in strain for an increase in load, or seeming to make the construct softer, which is measured by strain gauge 3. Once the anterior gap has closed the stiffness of the system increases, and thus strain gauge 3 indicates an increase in stiffness as the maximum load is reached.

The load is shared via the femoral head into the lag screw and nail and lower trochanter. The Gamma nail has the greater stiffness and thus the majority of the load must pass through it. Once the Osteotomy gap has closed less load is carried by the Gamma nail, and more is carried by the lower trochanter, through the lag screw. The upper trochanter will carry a similar load regardless of the Osteotomy closing due to the nature of the load path. Strain gauges 5 and 6 therefore, which are located on the upper trochanter, measure a relatively constant stiffness for the construct as the load is applied.

Strain gauges 1 and 2 are located superior and inferior to the distal locking screw. As the Osteotomy closes the femoral shaft shares more of the load, increasing the stiffness of the construct. The load transferred into the distal locking screws via the nail is thus decreased, but the load transferred from the femoral shaft is increased. Strain gauges 1 and 2 therefore measure an increase in the stiffness of the system. This increase is subtle due to the majority of the load being carried by the nail.

The predominant change in stiffness of the system begins in a particular load range for each femur. For femur 2 the load at which the stiffness first changes significantly is at approximately 1.4kN. The load at which femur 6 noticeably stiffens is approximately 0.4kN.

The bi-linear load-displacement response of the system is shown more clearly in chapter 6, where the finite modelling technique is validated by comparison to the experimental data reported in this chapter.

The measured deflection data for the femoral head are given in table 5.3, from the dial gauge and Instron machine. There is a difference in the two measured deflection values due to localised deformation at the point of load application. Permanent deformation is observed at the load point from inspection of the femora after each test. Localised deformation is caused from the femoral head yielding, resulting in plastic deformation and crushing. This yielding results in the permanent deformation of the femoral head, visible after testing.

6.0 Introduction

Verification of the novel finite element modelling technique described in Chapter 3 is provided in this chapter by comparison with the experimental data presented in Chapter 5. The stiffness of the experimental construct will be matched to that of the finite element model, over a specific load range. Maximum deflection and strain data will be compared to check the validity of the finite element model.

6.1 Finite element model construction

6.1.1 The femur

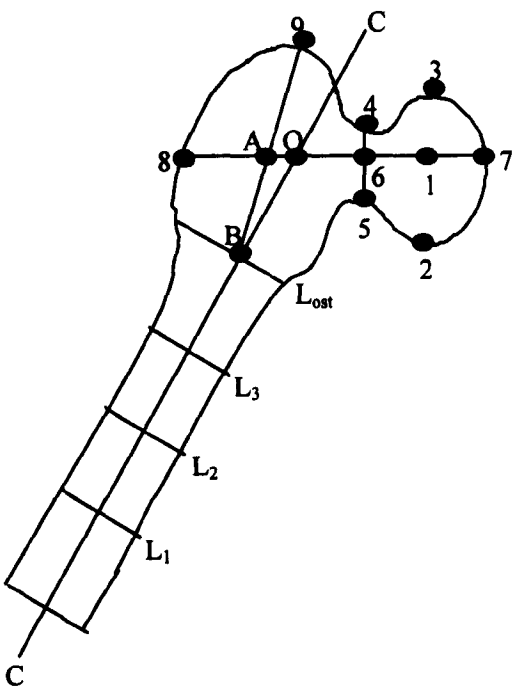

Figure 6.1 – Femur Geometry.

The construction of the femur is described in chapter 3, section 3.4. Figure 3.6 is repeated here for clarity. Measurements of line 2-3, 4-5, 7-8, B-9, and L_{ost} are taken and entered into the finite element model for femur 2 and femur 6. Measurements of the diameter at points along the femoral shaft are taken and entered for L_1, L_2, L_3 and L_{ost}.

The femur is modelled as having three distinct regions, the femoral head, trochanter and cortical shaft. Figure 6.2 shows a cross section of the idealised

femur with the three regions that are modelled. Two volumes are displayed, coloured blue and green, and represent the bone contact volumes and main femur volumes respectively.

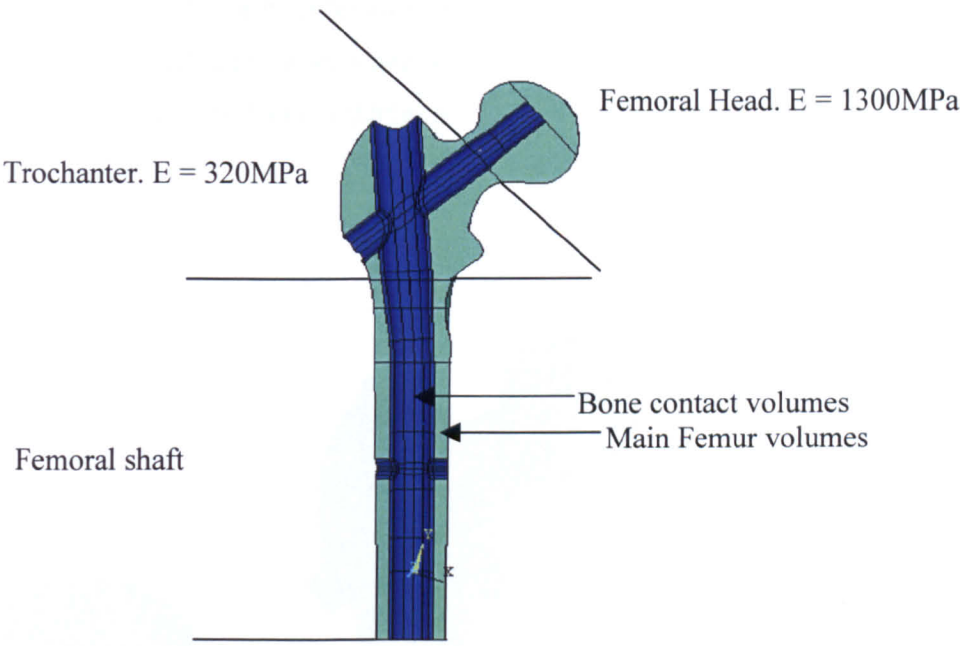

Figure 6.2 - Cross section of femur.

There is also a layer of cortical bone that surrounds the proximal femur. This layer is split into three sections of constant thickness, the medial and lateral trochanter and the femoral head, as described in chapter 5, section 5.1.8.

6.1.2 Gamma nail

The dimensions of the Gamma nails used in the experiment are given in chapter 5, section 5.1.4. The parameters that are used in the construction of the finite element model are shown in chapter 3, section 3.3. There is a small radial gap between the lag screw and nail of 0.02mm, and the same gap exists between the distal locking screw and nail.

6.1.3 Complete model

The complete model is shown in figure 6.3. A fracture plane is inserted into the femur to represent the osteotomy. The position of the fracture plane is determined by its position from the distal locking screw. The gap in the Osteotomy is 0.1mm, for both femora, as measured. The Osteotomy is modelled as having a constant gap on all sides of the femur. There is a small radial gap between the nail and the bone of 0.05mm.

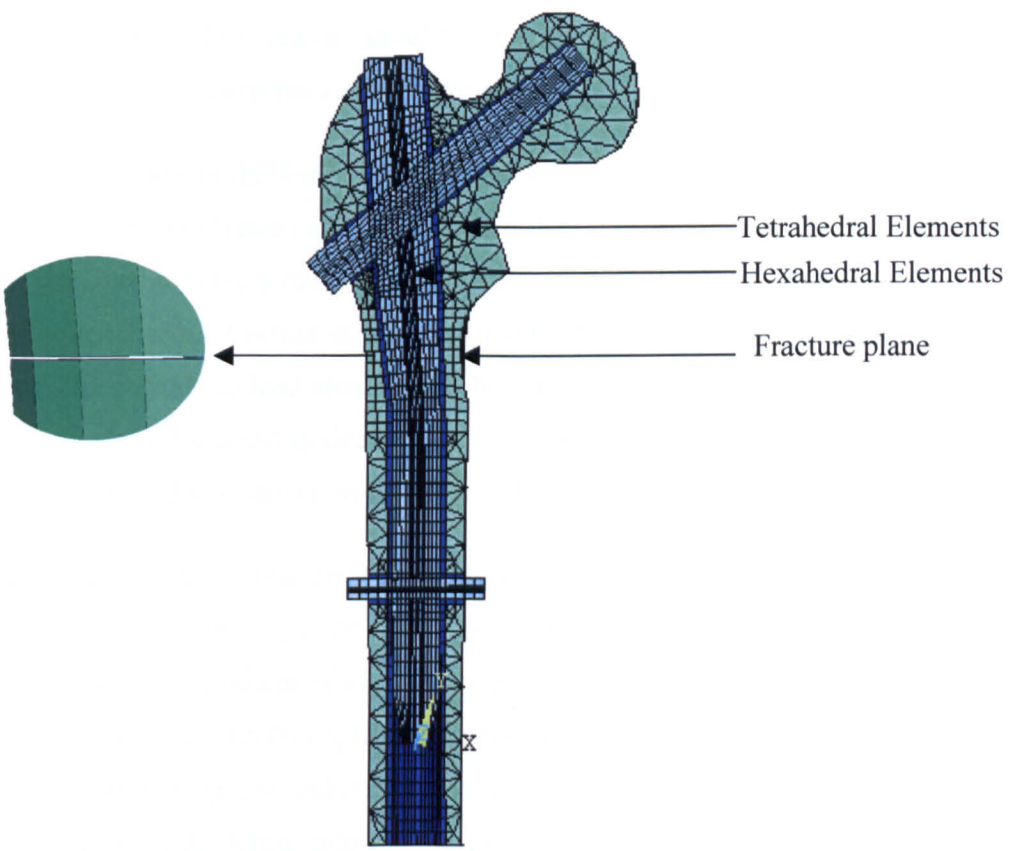

Figure 6.3 - Cross-section of finite element model and exploded view of osteotomy.

6.1.4 Material properties

A value for cortical bone of 5.3GPa is entered into the finite element model from experimental testing for femur 2, and 5.4GPa for femur 6.

There is an argument that the modulus of cancellous bone has a negligible effect on the stiffness of an implant and bone construct, (Cheung *et al.*, 2003, McNamara *et al.*, 1995, Rohlmann *et al.*, 1983). The modulus of the trochanter is typically 10 to 15 times smaller than the cortical bone modulus, and is expected to have a negligible effect on the stiffness of the construct. An appropriate estimate for this material property is required for this particular comparison. A value of 320MPa is entered into the finite element model for the elastic modulus of the trochanter. The reader should refer to chapter 2, section 2.9 for documented material properties of the femur.

The elastic modulus in the femoral head is not known and will be determined by comparison of finite element and experimental data. The modulus of the femoral head is expected to have a more significant effect on the stiffness of the system due to the localised deflection at the load point. The contribution to the overall stiffness with regards to load sharing will be relatively small, but the maximum displacement and localised deflection will be considerably affected. An initial estimate for this value is shown in figure 6.1, of 1300MPa.

The material properties and divisions shown in figure 6.1 are those used by Wang *et al.*, (1998, 2000). Taylor *et al.*, (1996) divided the cancellous bone into five groups with the modulus of elasticity varying from 250MPa to 1250MPa. A study by Seral *et al.*, (2003) split the femur into only two sections with the cancellous bone having a modulus of 100MPa, and the work by Sitthiseripratip *et al.*, (2003) divided the femur into four sections, with the femoral head having a modulus of 900MPa, the neck being 620MPa and the trochanteric region having a modulus of 260MPa.

A value for the cortical shell thickness is assigned to the three regions that have a similar thickness as described in chapter 5, section 5.1.8. The thickness of the medial trochanter is entered as 1.6mm and the lateral trochanter is 1.1mm for femur 2. The thickness of the femoral head entered for femur 2 is 0.8mm. For

femur 6 the respective cortical shell thickness is assigned as 0.9mm, 0.8mm and 0.7mm.

It is not the intention to model the exact anatomical femur, but to model a close approximation with a similar global stiffness. It is noted that the actual value of cortical shell thickness will vary about the proximal femur more considerably than modelled, however it is argued that the relative stiffness change for each region identified as having a similar thickness will have a negligible effect on the overall stiffness of the system. Moreover, the thickness of the femoral head will be a more important parameter to enter, as this will have a significant effect on the localised deflection at the load point. An investigation of varying the femoral head stiffness is given in chapter 7. Indeed, it can be argued that the cortical shell thickness around the proximal femur can be modelled as having a constant thickness.

The gamma nail used in the experiment is made from stainless steel whose properties are taken as: elastic modulus 210GPa, Poisson's ratio 0.33.

Values between bone and metal are between 0.1 and 0.2 (Orthoteers, 2004). Friction is sensitive to atmospheric dust and humidity, oxide films, surface finish, velocity of sliding, temperature, vibration and contamination. Indeed in many cases the degree of contamination can be the limiting factor. These factors may have an influence on the coefficient between the implant and bone in the experiment. A value of 0.1 has been entered into the finite element model for all contact pairs and an investigation into the importance of the coefficient of friction is provided in chapter 7.

A contact stiffness value of 0.1 is used for faster solution convergence. Chapter 4 details the effect of changing this parameter.

6.1.5 Boundary conditions

The finite element model is offset in the same orientations as the experiment, and the load is applied in the global y-direction of the system at a single point on the top of the femoral head. When the load is applied in the experiment, no lateral movement of the femur is allowed due to the restraint imposed from the

experimental apparatus. To account for this action in the finite element model the point of load application is restrained in the two orthogonal directions. The lateral free surface of the distal locking screw is restrained in all directions, as is the base of the femur. This accounts for the locking action of the distal screw in the bone, and the restraint that the potting compound imposes on the base of the femur.

6.2 Finite element solution

The solution technique used in ANSYS is static (steady-state) and non-linear. To gain contact, non-linear monitoring is used on all contact pairs. The analysis uses a chosen number of substeps to gain solution convergence with predictive time stepping.

During the solution process any contact surfaces that may come into contact have their gaps closed during the first few substeps. Contact penetration is monitored throughout the rest of the solution process, and additional contact can be made or existing contact broken. A typical force-displacement response of the finite element model used in this chapter is shown in Figure 6.4. The system demonstrates non-linearity at the beginning of the solution, at the first few substeps. Once contact is achieved and any gaps are closed, the system response is linear because the material properties are linear. The number of substeps used in the solution has no effect on the final deflection data, only on the degree of non-linearity at the beginning of the solution routine. There are a maximum number of substeps that can be used, whereby any number of substeps above this will yield the same solution response. When predictive sub-stepping is used there are a maximum number of substeps that will be used depending on the amount initially stipulated.

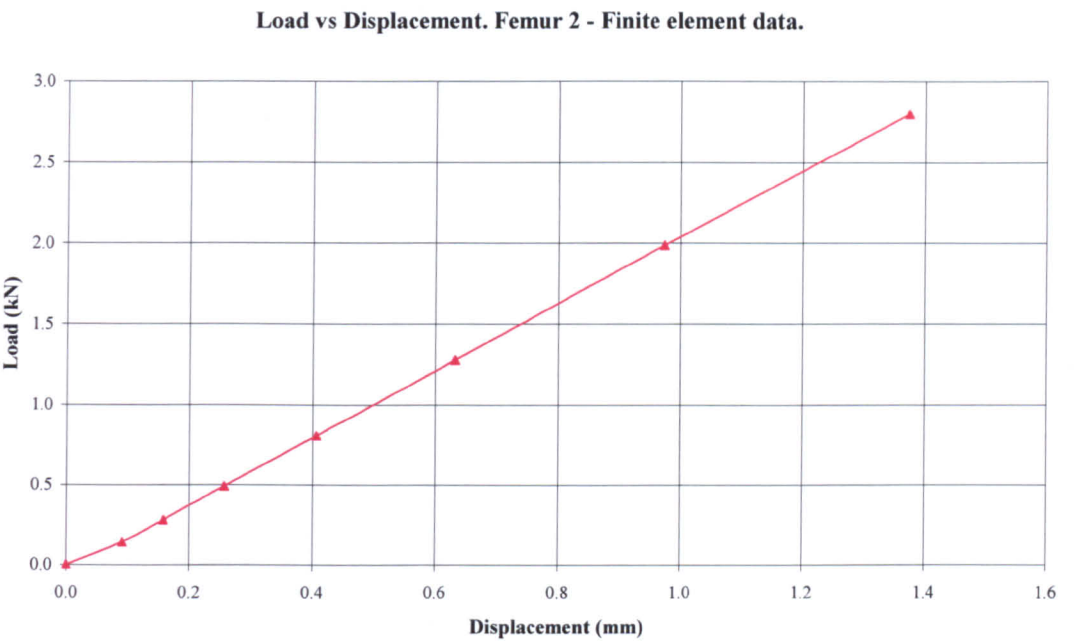

Figure 6.4 – Typical finite element solution response.

6.3 Finite element and Experimental data comparison

The experimental data response can be considered as approximately bi-linear for both femora. The second linear response occurs at about 1.4kN for femur 2 and 0.4kN for femur 6. The nature of this response is attributed to mechanical gaps closing in the system, as described in chapter 5, section 5.5.2. Finite element data can also be considered as approximately bi-linear, but it is not as clear and depends on the number of substeps defined. There is an obvious difference therefore, of how the gaps are closed in reality and in the finite element model.

The stiffness of the finite element and experimental data will be matched over a chosen load range from determination of the elastic modulus for the femoral head. Maximum and local deflection data and strain data are compared. The data range for the stiffness of each system is from 1.4kN to 2.8kN for femur 2, and from 0.4kN to 1.3kN for femur 6. The data range for each femur is chosen as the range where the system responds linearly, and all mechanical gaps are closed, as indicated from the load-deflection and strain-deflection data. The region of comparison is shown in Figure 6.5, for femur 2.

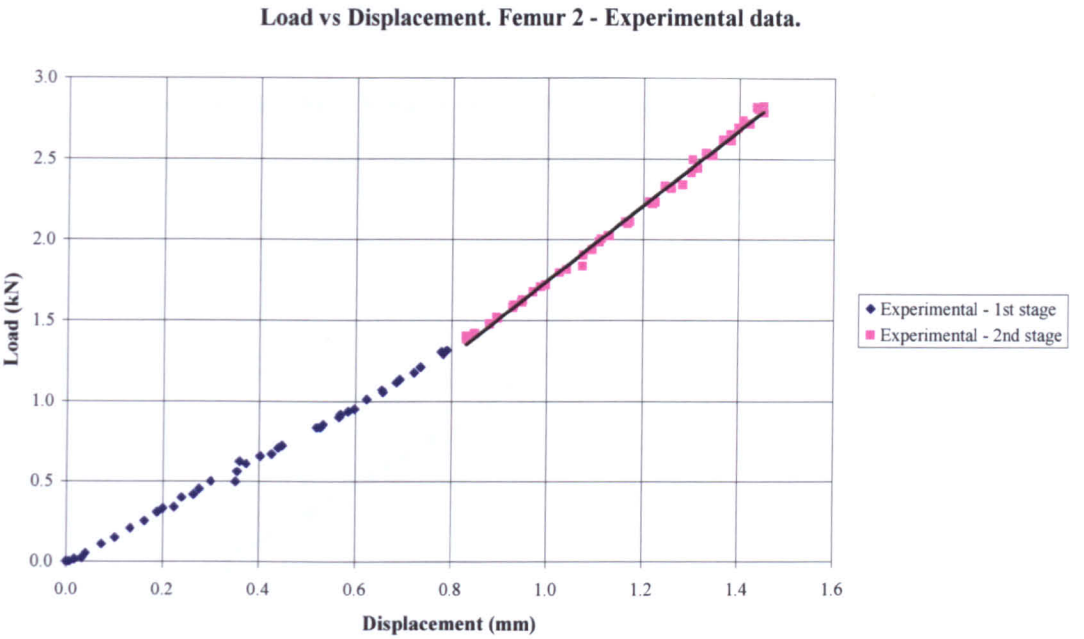

Figure 6.5 – Load – displacement data for femur 2 showing an approximately bi-linear response and data range used for the validation of the finite element model.

6.4 Results

The comparison of the experimental and finite element data is shown graphically in Figures 6.6 and 6.7. Finite element data is tabulated in Appendix III. Experimental data is tabulated in Appendix II.

Material properties entered into the finite element model to gain the best match with the experimental data are given in table 6.1. The difference between the finite element and experimental data is tabulated in table 6.2.

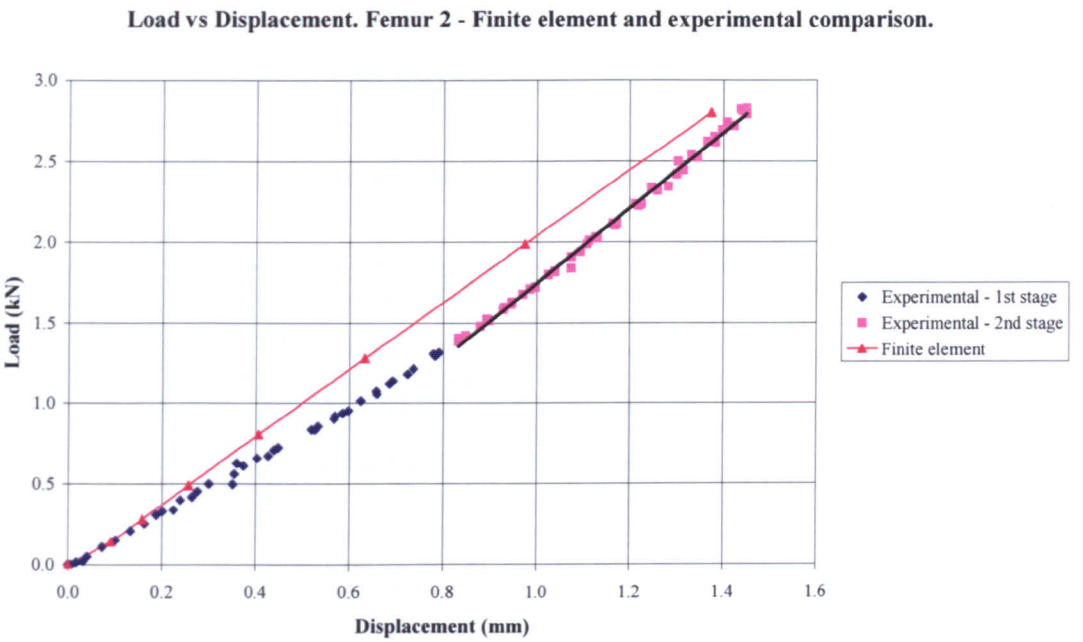

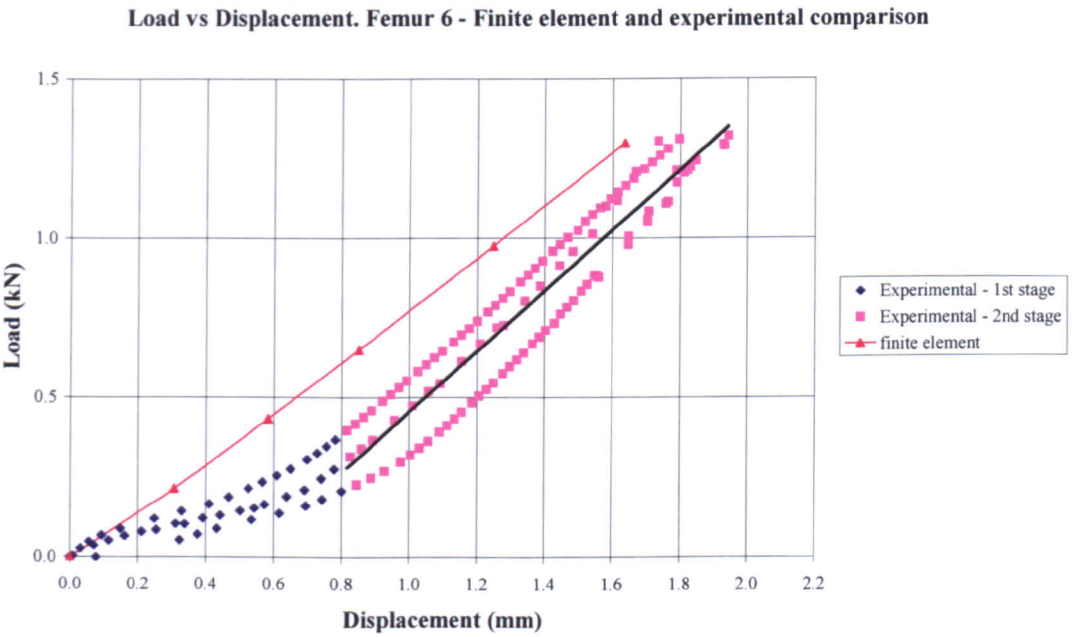

Figures 6.6 and 6.7 – Load-displacement response for femur 2 and femur 6, finite element and experimental data.

Material Properties for each femur						
	Cortical Shell Thickness (mm)			Elastic Modulus (GPa)		
	Femoral Head	Medial Trochanter	Lateral trochanter	Cortical Bone	Trochanter	Femoral Head
Femur 2	0.8	1.6	1.1	5.3	0.32	0.72
Femur 6	0.7	0.9	0.8	5.4	0.1	0.1

Table 6.1 – Material properties used to gain best match with experimental data.

		Deflection data			Strain data				
		Stiffness (kN/mm)	Maximum Deflection (mm)	Localised deflection (mm)	Strain (με)				
					Strain gauge number				
					1	3	4	5	6
Femur 2	Finite element	2.10	1.37	0.79	-971	-937	-236	382	742
	Experimental	2.31	1.45	0.62	-1350	-875	-305	850	800
	Difference (%)	9	5	-27	28	-7	23	55	7
					Strain gauge number				
					2	3	4	5	6
Femur 6	Finite element	0.80	1.64	1.25	-593	-342	-1408	-174	112
	Experimental	0.96	1.90	1.02	-360	-380	-1260	-100	100
	Difference (%)	17	14	-23	-65	10	-12	-74	-12

Table 6.2 – Finite element and experimental stiffness and deflection results.

6.5 Discussion

The measured data in the experiment were the maximum displacement in the system in the y-direction, the strain recorded from uni-axial strain gauges about the femur surfaces and the deflection under the femoral head, indicating localised deflection.

The stiffness of the finite element model is accurately matched to that of the experiment over a chosen load range where the mechanical gaps are considered closed and where both systems exhibit a similar behaviour. Matching the stiffness of the two methods is used for the validation of the finite element modelling technique.

The same point of load application is used in the experiment and the finite element model. An accurate comparison of the maximum y-displacement from the experiment is made to the maximum y-displacement in the finite element model. The maximum loading of the finite element model is the same as that in

the experiment, and is measured in the experiment to a discrimination of 1N. Furthermore the experimental displacement is notionally accurate to 10μm, and thus an adequately accurate agreement can be found.

The strain gauges are uni-axial and placed at arbitrary locations on the femora. Thus it is not obvious to compare principal strains or stresses. Furthermore, finite element results for strain on the femoral neck are taken from shell elements that have different axes of origin from the global Cartesian system, thus rendering it almost impossible to resolve the strains in the global coordinate system accurately. Instead, working planes are created in the finite element model and aligned to the strain gauge positions in the experiment. Results are then mapped onto this orientation and a direct comparison of measured strain is achieved.

6.5.1 Femur 2

Table 6.1 provides the material properties used in the finite element model. An elastic modulus of 720MPa for the femoral head provided the best comparison with experimental data. Strain gauge 5 has the worst comparison, with a difference of 55% to the experiment. This is attributed to the positioning of the strain gauge in the system. Strain gauge 5 is positioned on the anterior side of the femoral neck. This is the region on the finite element model that deviates greatest from the experiment due to the symmetry of the modelled system. A good comparison is thus not expected here.

All other strains in the system show a reasonable comparison to the experiment. The best comparison to the experiment uses a femoral head modulus of 720MPa, a trochanter modulus of 320MPa, and a varying cortical shell thickness as outlined in section 6.1.5. The cortical bone modulus is 5.4GPa. With these material properties there is an accurate match of the stiffness of the two data sets, with a difference of 9%. The finite element model is softer than the experiment. There is also an agreeable maximum displacement in the femur (5% difference), and a good match for strain gauges 3, 4 and 6 with a difference of 7%, 23% and 7% respectively compared to the experimental data. Strain gauge 1 has a 28% difference with the experimental data.

6.5.2 Femur 6

The comparison to femur 6 is not as accurate as femur 2. Table 6.1 shows the material properties that give the best match with the experiment. Strain gauge 2 and 5 in this case show the greatest deviation from the experimental data. Strain gauge 2 is placed just proximally above the distal locking screw. The reason for the vast difference (maximum 65%) is that there is a crack on the lateral side of the femoral shaft for this femur, which will influence the deflection data for this femur. Strain gauge 5 is placed on the femoral neck adjacent to a cavity in the bone. The comparison with the finite element data is thus less accurate with a difference of 74%. This strain gauge is also placed in a position that is least comparable to the finite element model, the same as femur 2.

Femur 6 was more dried out than femur 2, with a lot of bone dust escaping from it. Its properties were thus far more degraded than femur 2. This is apparent from the use of a lower load causing a greater deflection in a femur that is larger, with a slightly higher modulus for the cortical bone.

The elastic modulus of the trochanter and femoral head used in the finite element model for femur 6 were thus quite low; a modulus of 100MPa was used. The cortical shell thickness is also smaller for this femur.

Comparison between the finite element model and experiment for strain gauges 3, 4 and 6 are however encouraging with a difference of 10%, 12% and 12% respectively. The maximum deflection in the system at the load point between the two data sets is comparable, with a difference of 14%.

Matching the stiffness of the finite element and experimental data used the linear line of best fit for all three experiments, as shown in graph 6.2. This gave a difference in the stiffness of the two data sets of 17% with the finite element model being softer than the experiment. The maximum deflection difference for this stiffness is 14%.

If the linear trend line of each individual experiment is used, then the greatest stiffness of the experiment is 1.1kN/mm. With this value the difference between the two stiffness values is increased to 27%. However, due to the increased

stiffness of the system the maximum deflection is decreased and the difference between the finite element and experimental data is reduced to 9%.

6.6 Localised deflection data

The experiment measured both the maximum deflection and the deflection under the femoral head in the direction of the load. This provided evidence for localised deformation on the femoral head where the load is applied, at the maximum load. The finite element model predicts this localised deformation at the point of load application. A comparison between the experiment and finite element model is given in table 6.3 for the two models that best match the experiment.

	Experiment				Finite element			
	Deflection of femoral head (mm)							
	Femur 2		Femur 6		Femur 2		Femur 6	
Test	Dial Gauge (under femoral head)	Instron	Dial Gauge (under femoral head)	Instron	Under femoral head	Load point	Under femoral head	Load point
1	0.81	1.43	0.92	1.94				
2	0.72	1.33	0.86	1.8				
3	0.7	1.29	0.81	1.73	0.59	1.37	0.39	1.64
	Local deformation (mm)							
1	0.62		1.02					
2	0.61		0.94					
3	0.59		0.92		0.79		1.25	

Table 6.3 – Deflection data for both experimental and finite element methods.

The finite element model for both femora overestimates the local deflection at the load point. The localised deflection observed in the experimental and finite element data is due to the constraints imposed on the femoral head; no lateral movement is possible, only longitudinal. It is expected that the localised deflection on the femoral head will be influenced by the thickness of the cortical shell and the elastic modulus of the femoral head.

6.7 Summary

By estimation of the elastic modulus of the trochanter and femoral head, the stiffness of the finite element construct has been matched within 10% of the

experimental data for femur 2 and within 20% for femur 6. A comparison of the maximum displacement and strain data has been made with a reasonable difference for the maximum displacement. In both cases the finite element model is softer than the experiment.

A comparison of localised deflection data at the maximum load has been made, with a difference of within 30% for each femur. In both cases the finite element model overestimates the localised deflection.

Due to the way that the gaps are closed in the finite element model, it is not possible to match both the stiffness and the maximum deflection with a linear elastic material model. By increasing any modulus in the finite element model, the stiffness of the construct will increase, but the maximum deflection will decrease. Increasing the modulus of the trochanter however will arguably have a negligible affect on the stiffness and thus the maximum deflection of the system. Effectively the choice of matching the stiffness of the construct will inevitably increase the difference in the maximum deflection of the system. Therefore an appropriate stiffness has been used whereby both the stiffness and the maximum deflection are within a range small enough to consider the finite element model validated for this application.

The anatomical femora have not been modelled, but a close approximation to the femur stiffness has been shown. Although one particular model can be identified as having the best match with the experiment, there is in fact a range of material properties that can be considered that have a reasonable fit with the experimental data. The importance of each parameter on the stiffness of the construct is given in chapter 7, by way of a sensitivity study.

The finite element model has closely approximated the global stiffness and local deflection of the experiment. The aims of this study, when weighed carefully against the inevitable compromises necessary for the application of a numerical model, show that the novel modelling technique used has been validated.

7.0 Sensitivity Study

7.1 Introduction

This chapter presents a sensitivity study for the finite element model validated in chapter 6. An investigation will be given to establish the importance of each parameter used in the finite element model. This will identify which parameters must be modelled accurately in order to predict the stiffness of an intramedullary nail inserted into a proximal femur.

The sensitivity study will compare relative stiffness, maximum deflection and localised deflection data.

Whether femur 2 or femur 6 is used, the linear elastic finite element model will have the same relative change for each parameter. Coupled with the fact that the modelling technique is the same for both femora, only one femur will be considered. Femur 2 is chosen to investigate the variation of each parameter as this femur has the closest match with the experimental data.

An analysis of the relative change in peak von Mises stress and strain energy data for constituent parts of the model will also be provided as an assessment of the importance of certain parameters. This analysis is an assessment of the effect that a parameter may have on the internal stresses within the construct, where no significant effect on stiffness data were found.

An analysis of the trochanter modulus is expected to have a negligible effect on the global stiffness of the construct due to the large difference in stiffness compared to cortical bone and the steel nail. There may be different implications on the stress in the insertion hole due to the load being shared along the length of the lag screw and not transferred directly into the insertion hole. Compatibility at the lag screw thread results in the load being transferred into the lag screw. The trochanter modulus may have an influence on the internal forces between the lag screw and trochanter.

7.2 Stiffness and deflection investigation

The following parameters are investigated:

- Cancellous bone modulus in the femoral head
- Cancellous bone modulus in the trochanter
- Cortical bone modulus in the femoral shaft and cortical shell
- Cortical shell thickness in the proximal femur
- Osteotomy gap
- Contact stiffness
- Coefficient of friction

By varying each of the above parameters and comparing relative stiffness, displacement and local deflection data, the importance of each parameter will be determined. The influence of each parameter is investigated for femur 2, because this femur had the closest match to the experimental data given in chapter 6.

Two values for the femoral head modulus are used in addition to that used in chapter 6. A modulus of 320MPa, and 1440MPa are used. 320MPa is the same modulus as the trochanter, and 1440MPa is twice the modulus used in chapter 6. The lower limit for the modulus of the femoral head is that of the trochanter, and the upper limit is arbitrarily chosen.

To investigate the effect of changing the trochanter modulus a value of 0.001MPa is used. This simulates having no trochanter modulus. A small value is required for solution stability.

A value of 17GPa is used to investigate the effect of changing the cortical bone modulus. This value is representative of the modulus of bone *in-vivo* and is approximately 3 times greater than the modulus used in chapter 6.

To investigate varying the thickness of the cortical shell four separate investigations are used. The femoral head, lateral and medial trochanter are

investigated systematically, with the thickness being varied in increments of 0.3mm. Three thickness values are used for each region and they are investigated independently of each other. A further investigation is provided for modelling the proximal femur with one constant value for the cortical shell thickness.

A contact stiffness factor of 1 is used to confirm the hypothesis in chapter 4 that this value has no effect on the displacement of the system. In chapter 6 a contact stiffness of 0.1 was used.

The effect of doubling the gap in the Osteotomy from 0.1mm to 0.2mm is investigated.

An investigation into the influence the friction coefficient has on the deflection and stiffness of the system is provided for all contact pairs.

7.2.1 Stiffness and deflection results

The results for varying the femoral head, trochanter and cortical bone modulus are given in table 7.1. Results for varying the cortical shell thickness are given in table 7.2. Results for varying the contact stiffness and Osteotomy gap are given in table 7.3. Results for varying the coefficient of friction are presented in table 7.4. The results are represented graphically in the discussion.

	Finite Element Data										
	Material Properties						Results				
	Cortical Shell Thickness (mm)			Elastic Modulus (GPa)							
	Femoral Head	Medial Trochanter	Lateral trochanter	Cortical Bone	Trochanter	Femoral Head	Load (kN)	Displacement (mm)	Stiffness (kN/mm)	Displacement under femoral head (mm)	Local Deflection (mm)
Agreement with experimental data	0.8	1.6	1.1	5.3	0.32	0.72	0.0 0.1 0.3 0.5 0.8 1.3 2.0 2.8	0.0 0.1 0.2 0.3 0.4 0.6 1.0 1.4	2.10	0.59	0.79
Vary modulus of femoral head	0.8	1.6	1.1	5.3	0.32	0.32	0.0 0.5 0.9 1.6 2.2 2.8	0.0 0.4 0.7 1.3 1.8 2.2	1.23	0.59	1.65
	0.8	1.6	1.1	5.3	0.32	1.44	0.0 0.5 0.9 1.6 2.2 2.8	0.0 0.2 0.3 0.6 0.8 1.0	2.96	0.60	0.36
Vary modulus of trochanter	0.8	1.6	1.1	5.3	0.32	1E-06	0.0 0.1 0.3 0.5 0.8 1.3 2.0 2.8	0.0 0.1 0.2 0.3 0.4 0.7 1.1 1.5	1.94	0.72	0.75
Vary modulus of cortical bone	0.8	1.6	1.1	17	0.32	0.72	0.0 0.1 0.3 0.5 0.8 1.3 2.0 2.8	0.0 0.1 0.1 0.2 0.3 0.4 0.7 1.0	2.94	0.38	0.58

Table 7.1 – Results for varying the femoral head, trochanter and cortical bone modulus.

	Finite Element Data											
	Material Properties						Results					
	Cortical Shell Thickness			Elastic Modulus (GPa)								
	Femoral Head	Medial Trochanter	Lateral trochanter	Cortical Bone	Trochanter	Femoral Head	Load (kN)	Displacement (mm)	Stiffness (kN/mm)	Displacement under femoral head (mm)	Local Deflection (mm)
Vary femoral head shell thickness	0.50	1.60	1.10	5.30	0.32	0.72	0.00 0.47 0.93 1.63 2.22 2.80	0.00 0.28 0.53 0.90 1.22 1.54	1.84	0.60	0.93
	1.10	1.60	1.10	5.30	0.32	0.72	0.00 0.47 0.93 1.63 2.22 2.80	0.00 0.23 0.43 0.73 0.99 1.25	2.24	0.60	0.66
Vary medial trochanter shell thickness	0.80	1.30	1.10	5.30	0.32	0.72	0.00 0.56 1.12 1.96 2.80	0.00 0.29 0.56 0.97 1.39	2.01	0.60	0.78
	0.80	1.90	1.10	5.30	0.32	0.72	0.00 0.56 1.12 1.96 2.80	0.00 0.29 0.56 0.96 1.37	2.05	0.58	0.79
Vary lateral trochanter shell thickness	0.80	1.60	0.80	5.30	0.32	0.72	0.00 0.28 0.56 0.98 1.61 2.56 2.80	0.00 0.16 0.29 0.49 0.79 1.25 1.38	2.04	0.59	0.79
	0.80	1.60	1.40	5.30	0.32	0.72	0.00 0.28 0.56 0.98 1.61 2.56 2.80	0.00 0.16 0.29 0.49 0.79 1.25 1.38	2.04	0.59	0.79
Shell thickness of 1mm	1.00	1.00	1.00	5.30	0.32	0.72	0.00 0.56 1.12 1.96 2.80	0.00 0.28 0.53 0.91 1.30	2.16	0.60	0.69

Table 7.2 – Results for varying the cortical shell thickness.

	Finite Element Data										
	Material Properties						Results				
	Cortical Shell Thickness			Elastic Modulus (GPa)							
	Femoral Head	Medial Trochanter	Lateral trochanter	Cortical Bone	Trochanter	Femoral Head	Load (kN)	Displacement (mm)	Stiffness (kN/mm)	Displacement under femoral head (mm)	Local Deflection (mm)
Vary contact stiffness (FKN = 1)	0.80	1.60	1.10	5.30	0.32	0.72	0.00	0.00			
							0.28	0.16			
							0.56	0.29			
							0.98	0.49			
							1.61	0.79			
							2.56	1.25	2.10		
							2.80	1.37		0.59	0.78
Osteotomy gap = 0.2mm	0.80	1.60	1.10	5.30	0.32	0.72	0.00	0.00			
							0.14	0.12			
							0.28	0.20			
							0.42	0.27			
							0.63	0.38			
							0.94	0.55			
							1.42	0.79			
							2.13	1.14	2.34		
							2.80	1.47		0.68	0.79

Table 7.3 – Varying the contact stiffness and Osteotomy gap.

	Finite Element Data											
	Material Properties						Results					
	Cortical Shell Thickness			Elastic Modulus (GPa)								
	Femoral Head	Medial Trochanter	Lateral trochanter	Cortical Bone	Trochanter	Femoral Head	Load (kN)	Displacement (mm)	Stiffness (kN/mm)	Displacement under femoral head (mm)	Local Deflection (mm)
Nail coefficient of friction = 0.5	0.80	1.60	1.10	5.30	0.32	0.72	0.00 0.47 0.93 1.63 2.22 2.80	0.00 0.25 0.47 0.80 1.09 1.38	2.10	0.59	0.79
Lag screw coefficient of friction = 0.5	0.80	1.60	1.10	5.30	0.32	0.72	0.00 0.47 0.93 1.63 2.22 2.80	0.00 0.24 0.45 0.77 1.04 1.31	2.15	0.51	0.80
Distal locking screw coefficient of friction = 0.5	0.80	1.60	1.10	5.30	0.32	0.72	0.00 0.47 0.93 1.63 2.22 2.80	0.00 0.23 0.45 0.77 1.04 1.32	2.15	0.48	0.84
Osteotomy coefficient of friction = 0.5	0.80	1.60	1.10	5.30	0.32	0.72	0.00 0.47 0.93 1.63 2.22 2.80	0.00 0.23 0.46 0.79 1.08 1.38	2.00	0.59	0.79
Gamma nail coefficient of friction = 0.5	0.80	1.60	1.10	5.30	0.32	0.72	0.00 0.47 0.93 1.63 2.22 2.80	0.00 0.22 0.42 0.72 0.97 1.22	2.34	0.37	0.85
Friction coefficient = 0.5 on all surfaces	0.80	1.60	1.10	5.30	0.32	0.72	0.00 0.47 0.93 1.63 2.22 2.80	0.00 0.21 0.41 0.71 0.96 1.21	2.34	0.35	0.86

Table 7.4 – Varying the coefficient of friction.

7.3 Stiffness and deflection discussion

7.3.1 Varying the modulus of the femoral head

Doubling the modulus of the femoral head increases the stiffness of the system, by 41%. There is a subsequent decrease in the maximum deflection of the system by 30%. The local deflection at the load point decreases by 54%.

A reduction in the femoral head modulus to that of the trochanter results in a decrease in the stiffness of the system, with a difference of 41%, and an increase in the maximum deflection, with a difference of 63%. The localised deflection increases to over double that of the best match with the experiment, with a difference of 108%.

By increasing the femoral head modulus the stiffness of the system is increased due to the load carrying capacity of this region increasing. The maximum deflection decreases due to the increased stiffness, resulting in a decrease in the localised deflection, as shown from table 7.1.

Reducing the stiffness of the femoral head has a significant effect on the maximum deflection of the system, and on the local deflection. A reduction in the femoral head modulus results in the same deflection under the femoral head but the deflection at the load point significantly increases. This results in a large increase in the localised deflection, which renders the stiffness of the construct inaccurate.

Due to the load being applied on the femoral head, the modulus attributed to this parameter has a significant effect of the stiffness and local deflection of the system. An appropriate value for the modulus of the femoral head must therefore be used to accurately predict the stiffness of the construct and the localised deflection on the femoral head. A value for the modulus that is too small will produce a large localised deflection and a reduced stiffness, both of which may be wholly inaccurate.

The effect of changing the femoral head modulus is shown in figure 7.1, demonstrating that this is a critical parameter.

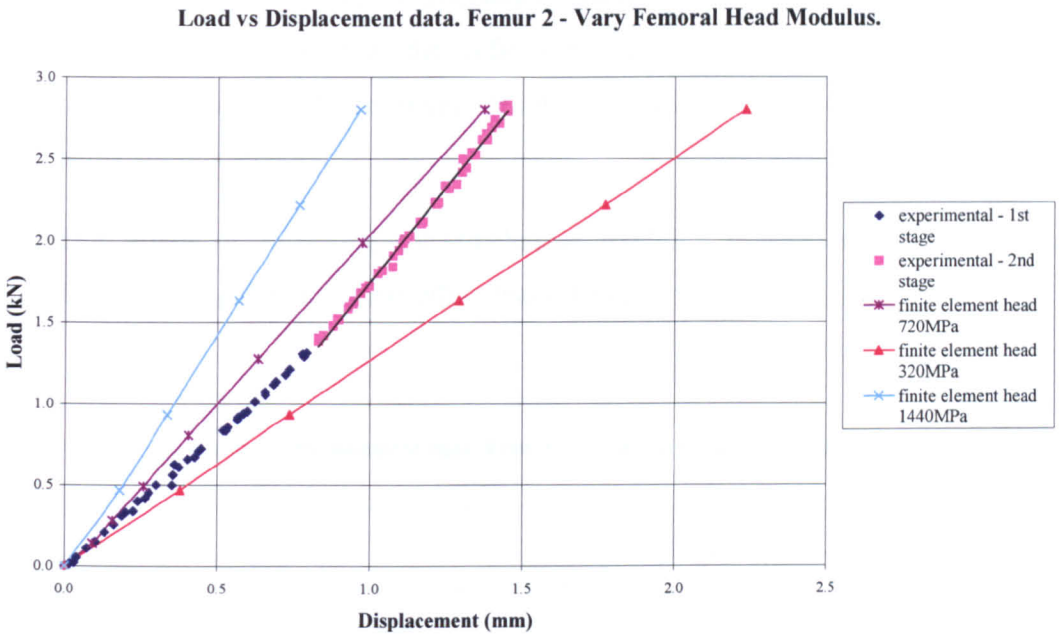

Figure 7.1 – Load-displacement data. Varying the modulus of the femoral head.

7.3.2 Varying the modulus of the trochanter

A trochanter modulus of effectively zero decreases the stiffness of the system and increases the maximum deflection. The local deflection decreases. The difference can be considered negligible however. By effectively removing the trochanter from the system the stiffness decreases by 16%, the maximum deflection increases by 10% and the local deflection decreases by 5%.

Changing the trochanter modulus changes the load carrying capacity of the proximal femur and therefore affects the stiffness of the system. The effect is small however due to the relative stiffness of the trochanter, nail and cortical bone. The steel lag screw is in the region of 600 times stiffer than the trochanter, per unit volume, as is the nail, meaning that the load is shared predominantly into the nail and lag screw. This results in the trochanter stiffness having a negligible effect on the global stiffness of the system.

Furthermore, the load is shared into the cortical shell and shaft, which have a modulus in the region of 16 or more times that of the trochanter modulus.

By effectively removing the trochanter modulus the maximum deflection of the system increases, as does the deflection under the femoral head, due to the reduced stiffness of the proximal femur. This results in the localised deflection being slightly smaller.

The effect of removing the trochanter modulus is shown in Figure 7.2, demonstrating the negligible effect that it has on the global stiffness.

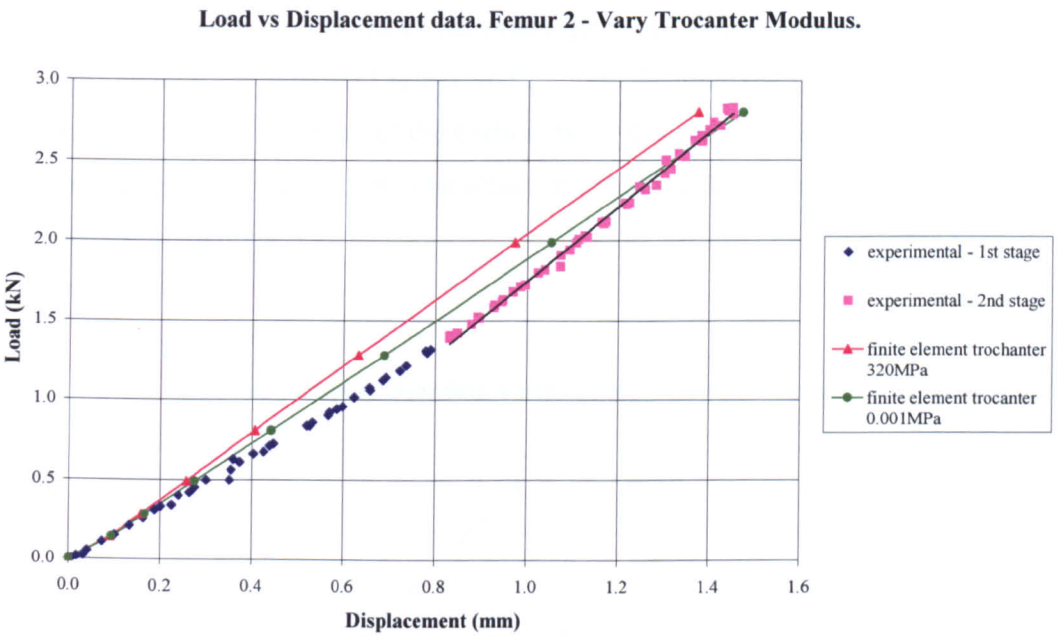

Figure 7.2 – Load-displacement data. Varying the modulus of the trochanter.

7.3.3 Varying the modulus of the cortical bone

Increasing the modulus of the cortical bone by a factor of 3.2 yields an increase in the stiffness of the system, with a difference of 30% when compared to the best match with the experimental data. The resultant increase in stiffness causes a decrease in the maximum deflection of the system and localised deflection, with a difference of 30% and 27% respectively. The cortical modulus has two main influences on the system. The first is that it will effect the local deflection and maximum deflection due to the load being applied on the cortical shell surrounding the femoral head. Secondly the load is shared about the cortical shell surrounding the proximal femur and into the femoral shaft once the Osteotomy has closed. The modulus of the cortical bone therefore has a significant effect on the stiffness of the system. The effect of changing the cortical bone modulus is shown in Figure 7.3.

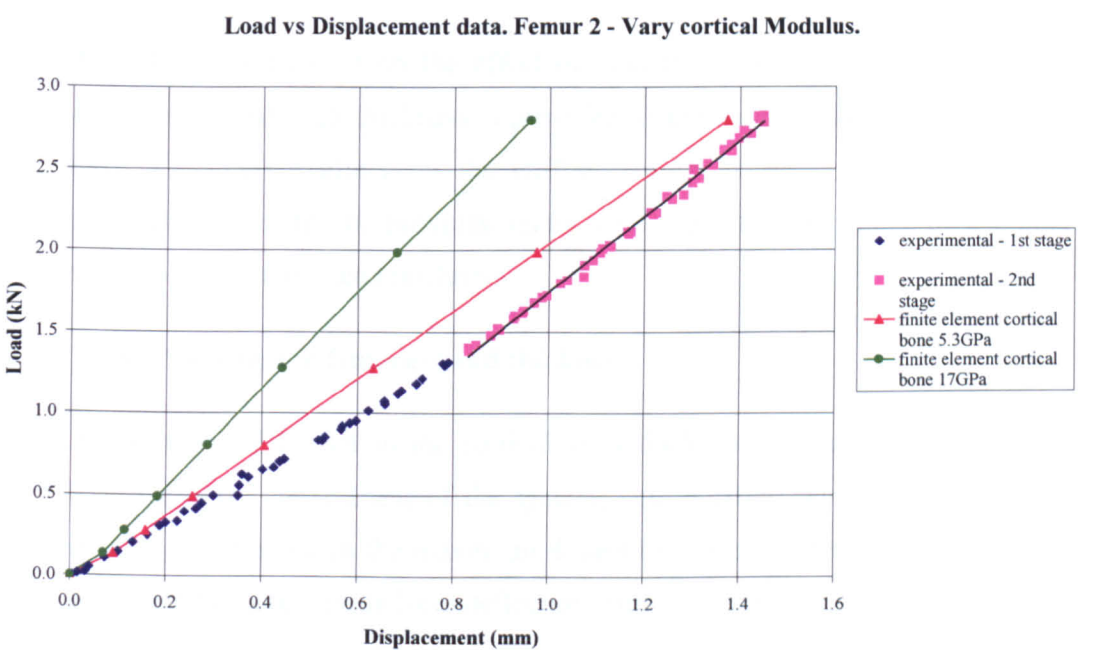

Figure 7.3 – Load-displacement data. Varying the modulus of the cortical bone.

7.3.4 Varying the cortical shell thickness

The three regions considered to have a similar thickness shown in chapter 5, section 5.4.8, are varied to investigate the importance of each parameter. Consideration is given to the fact that the femoral head thickness will not be greater than the medial or lateral trochanter thickness. Each parameter is varied independently, with three values being used for each parameter, in increments of 0.3mm. A total of 9 different sets of results are thus provided. Each parameter could be varied with respect to each other, providing a more comprehensive study. However it is argued that although each thickness is not independent of the next, the relative change between each parameter will be the same. Furthermore it is expected that the femoral head thickness will have the most significance on the deflection data and stiffness of the system, as the load is applied their. The medial and lateral trochanter thickness will have a negligible effect on the stiffness and deflection data, as the load will be carried predominantly by the lag screw, nail and shaft of the femur.

A further investigation on the effect of modelling the proximal femur with a constant cortical shell thickness is provided. If the medial and lateral trochanter have a negligible effect on the stiffness of the system than it is entirely reasonable to model the proximal femur with a constant thickness, of a similar value to the femoral head thickness.

7.3.5 Varying the femoral head thickness

An increase of 0.3mm in the cortical shell thickness surrounding the femoral head increases the stiffness of the system, with a difference of 7%. There is a subsequent decrease in the maximum deflection, with a difference of 9%, and a corresponding decrease in local deflection with a difference of 16%.

A decrease of 0.3mm in the cortical shell thickness surrounding the femoral head has the opposite effect. The stiffness decreases, with a difference of 12%, the maximum deflection increases with a difference of 12% and the local deflection increases with a difference of 18%.

The cortical shell thickness surrounding the femoral head has a significant effect on the maximum deflection and local deflection of the system due to the load being applied on the femoral head. A thinner cortical shell thickness will result in a larger maximum deflection and local deflection. The effect on the stiffness of the system is not as significant however. The effect of changing the femoral head cortical shell thickness is shown in figure 7.4.

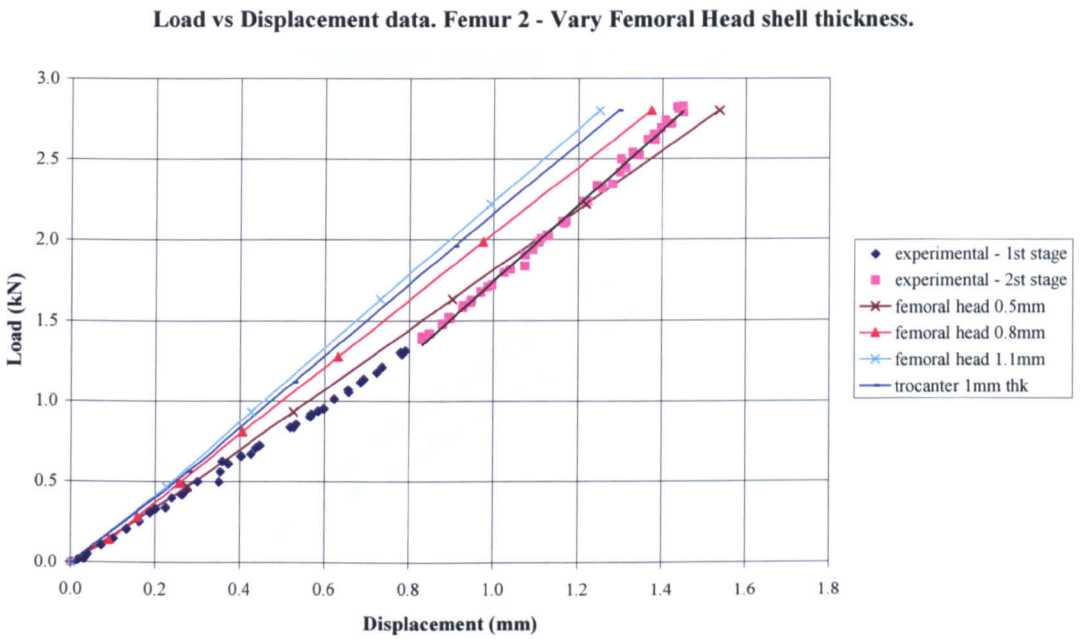

Figure 7.4 – Load-displacement data. Varying the thickness of the femoral head thickness.

7.3.6 Varying the medial trochanter thickness

An increase in stiffness of the system is observed as the thickness of the medial trochanter is increased, with a corresponding decrease in the maximum displacement at the load point. The opposite is observed with a decreasing medial trochanteric stiffness. A 20% difference in thickness of the medial trochanter has a negligible effect on the stiffness and maximum deflection of the system, with a difference of 4% and 1% respectively. The corresponding difference in local deflection is less than 1% whether increasing or decreasing the thickness.

The load is shared between all parts of the system, through the femoral head. As the load is carried into the medial trochanter it is also being shared into the lag screw and nail. The vast difference in stiffness of these parts results in the medial trochanter thickness having a negligible effect on the stiffness of the system. This effect will be further realised when the osteotomy is closed, as the femoral shaft also shares the load. The effect of changing the medial trochanter thickness is shown in figure 7.5.

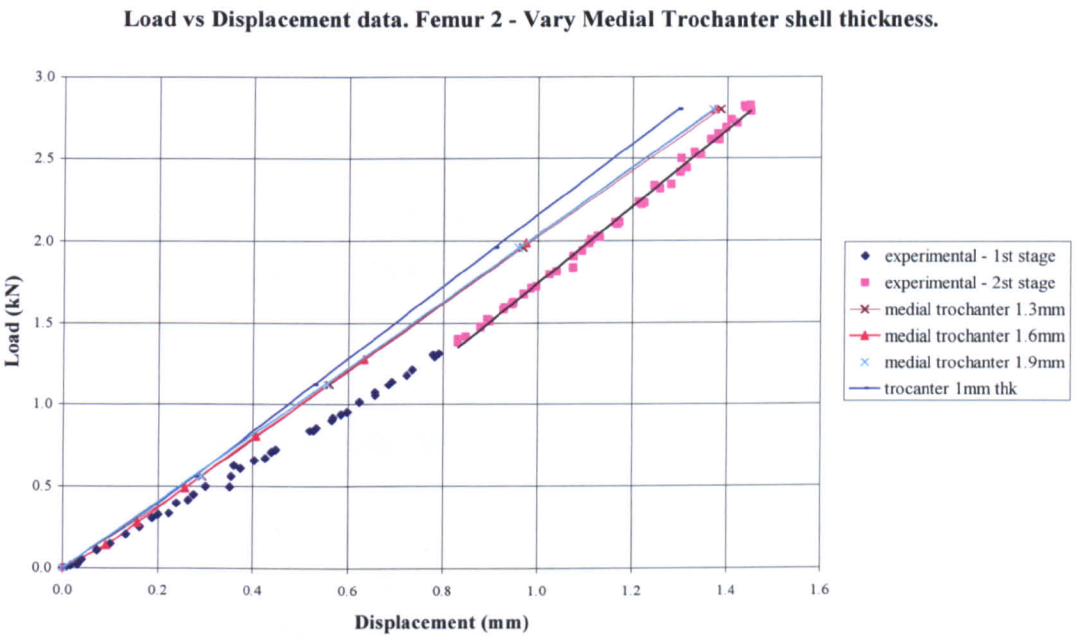

Figure 7.5 – Load-displacement data. Varying the thickness of the medial trochanter.

7.3.7 Varying the lateral trochanter thickness

As with the medial trochanter there is an increase in stiffness of the system as the lateral trochanter thickness is increased, with a corresponding decrease in the maximum displacement at the load point. The increased stiffness is considered negligible with a difference in stiffness of 4%, and in deflection of 1%, regardless of an increasing or decreasing thickness.

The argument is again made that the load is carried into the lag screw and nail, which have a much greater load carrying capacity than the lateral trochanter. The effect of changing the lateral trochanter thickness is shown in figure 7.6.

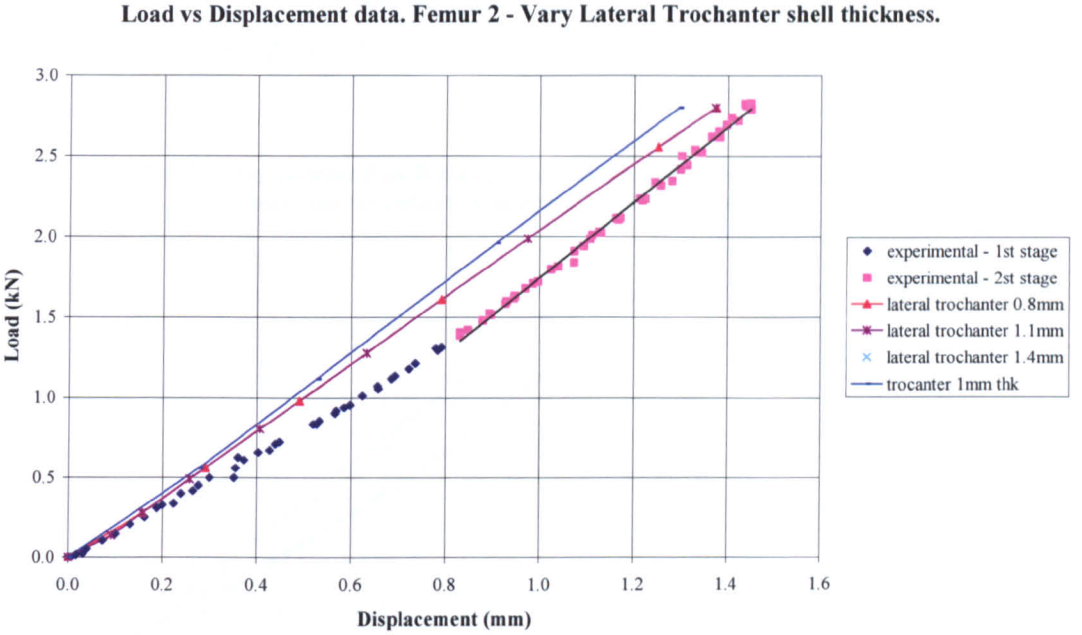

Figure 7.6 – Load-displacement data. Varying the thickness of the upper trochanter cortical shell thickness.

7.3.8 Using a constant cortical shell thickness

A constant thickness of 1mm is used for the cortical shell surrounding the proximal femur. This is an arbitrary choice made from consideration of the measured cortical thickness values given in chapter 5, section 5.1.8. It has been shown that the medial and lateral trochanter thickness has a negligible effect on the stiffness of the system. The cortical shell surrounding the proximal femur can therefore be modelled as having a constant thickness.

By using a constant cortical shell thickness of 1mm, the stiffness of the system increases, with a difference of 3%, and the maximum deflection of the system decreases, with a difference of 6%. Due to the lateral and medial trochanter thickness having a negligible effect on the stiffness of the system, this change is due to the increased thickness of the femoral head. When compared to the best match with the experimental data, the use of a constant thickness of 1mm provides a better match for the stiffness, with almost the same maximum deflection. It is therefore reasonable to model the proximal femur as having a

constant cortical shell thickness. The effect of using a constant cortical shell thickness is shown in figure 7.7.

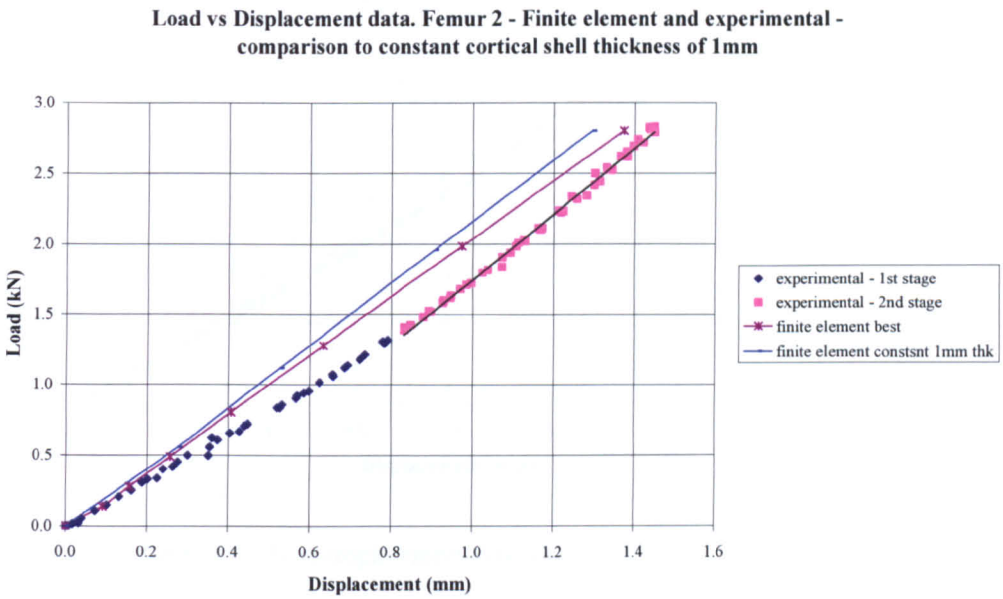

Figure 7.7 – Load-displacement data. Using a constant cortical shell thickness.

7.3.9 Varying the gap in the osteotomy

Doubling the gap in the Osteotomy decreases the initial stiffness of the system, as there is less bone to carry the load in the femoral shaft. The stiffness decreases is negligible however with a difference of 2%. Once the gap closes the stiffness will revert back to near the initial value, although there is slightly less bone material present to carry the load. There is a corresponding increase in the maximum displacement of the system with a difference of 7%. The increase in displacement is equal to the increase in the gap of the Osteotomy.

The load-displacement response is the same for both gap sizes. The gap is closed in the first few substeps and the load-displacement in that range is non-linear. Once the gaps are closed, the system exhibits a linear response. If the gap were to be increased so that it cannot close, the response would be different and the solution becomes unstable.

The effect of doubling the gap in the Osteotomy is shown in figure 7.8.

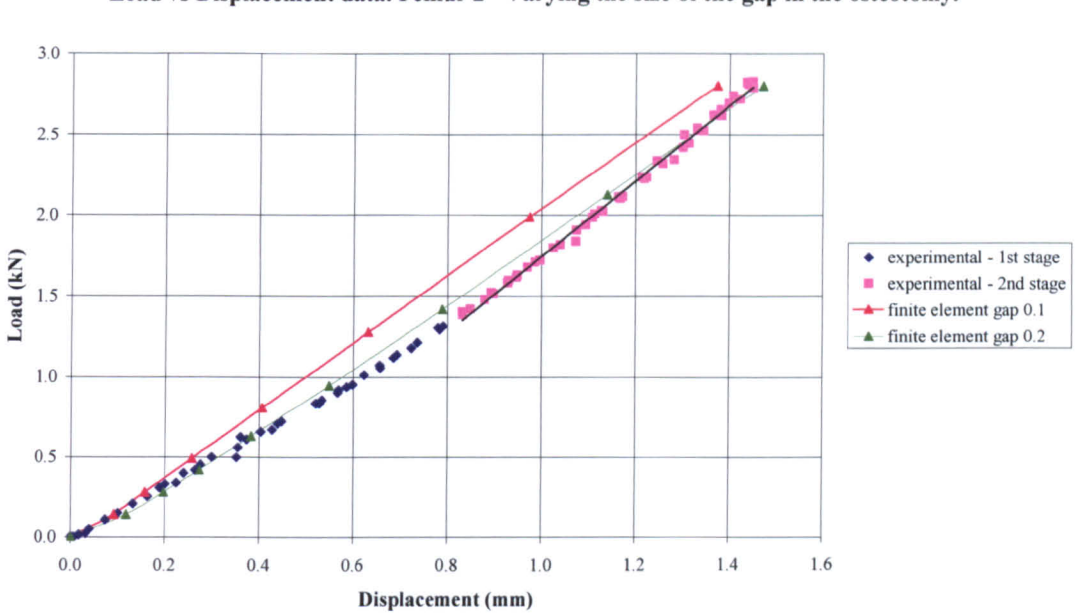

Figure 7.8 – Load-displacement data. Varying the gap in the osteotomy.

7.3.10 Varying the contact stiffness

Increasing the contact stiffness factor in ANSYS by a factor of 10, to a value of 1, has no effect on the maximum deflection or the stiffness of the construct. There is a difference in the time taken to obtain solution convergence and the amount of penetration. However, the penetration is negligible in both cases, as the maximum deflection is identical.

The effect of varying the contact stiffness is shown in figure 7.9. Contact stiffness is defined as 'FKN' in ANSYS.

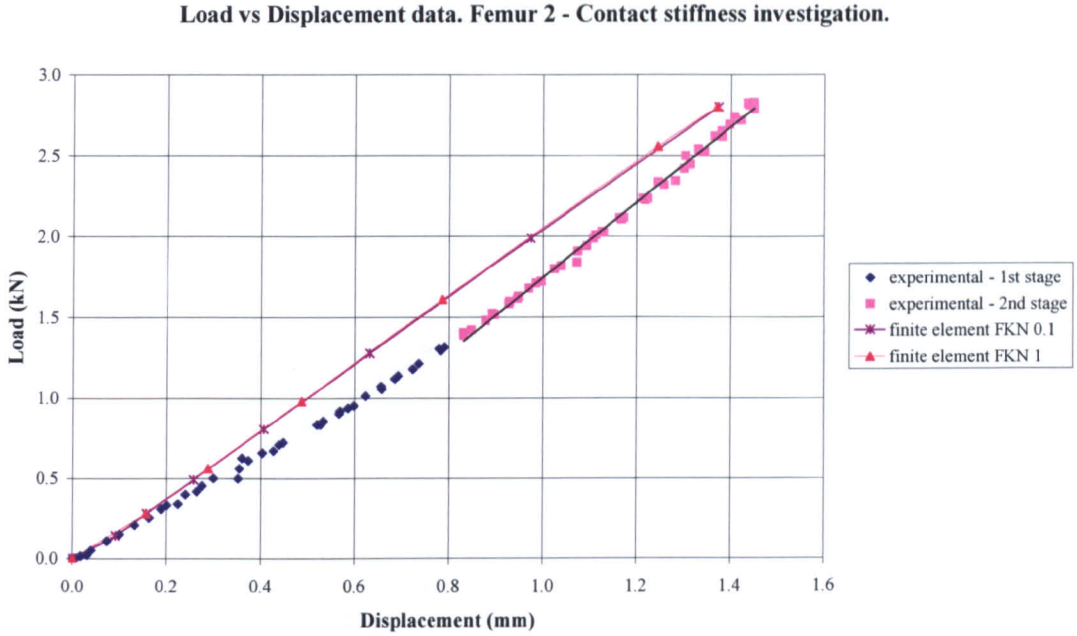

Figure 7.9 – Load-displacement data. Varying the value of contact stiffness.

7.3.11 Varying the coefficient of friction

In chapter 6 a value of 0.1 was used for the coefficient of friction on all contact pairs. An investigation into increasing this value by five times, to 0.5, is provided for each contact pair.

7.3.12 Varying the coefficient of friction on the nail contact surface

Increasing the contact coefficient to 0.5 on the nail contact surface only, has a negligible effect on the deflection data and stiffness of the construct. The effect of changing this friction value is plotted in figure 7.10.

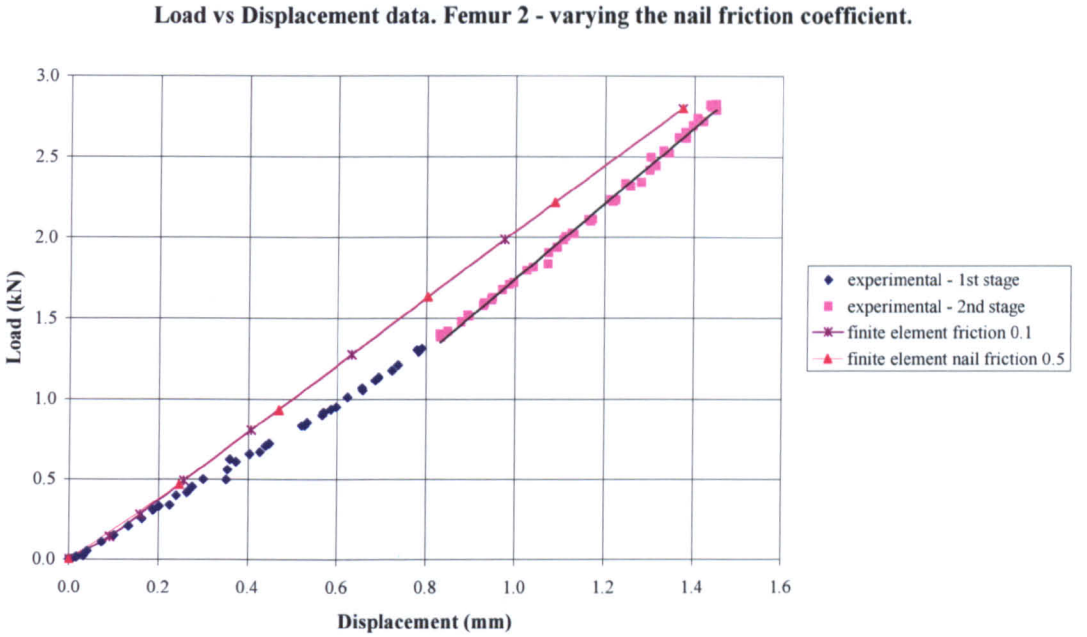

Figure 7.10 – Load-displacement data. Varying the nail coefficient of friction.

7.3.13 Varying the coefficient of friction on the lag screw contact surface

Increasing the friction coefficient on the lag screw contact pair to 0.5, increases the stiffness of the system by 2%, and decreases the maximum deflection of the system, with a difference of 5%.

The effect of increasing the coefficient of friction on the lag screw surface only is considered negligible, when comparing the maximum deflection and stiffness data of the construct.

The effect of increasing the friction coefficient is shown in figure 7.11.

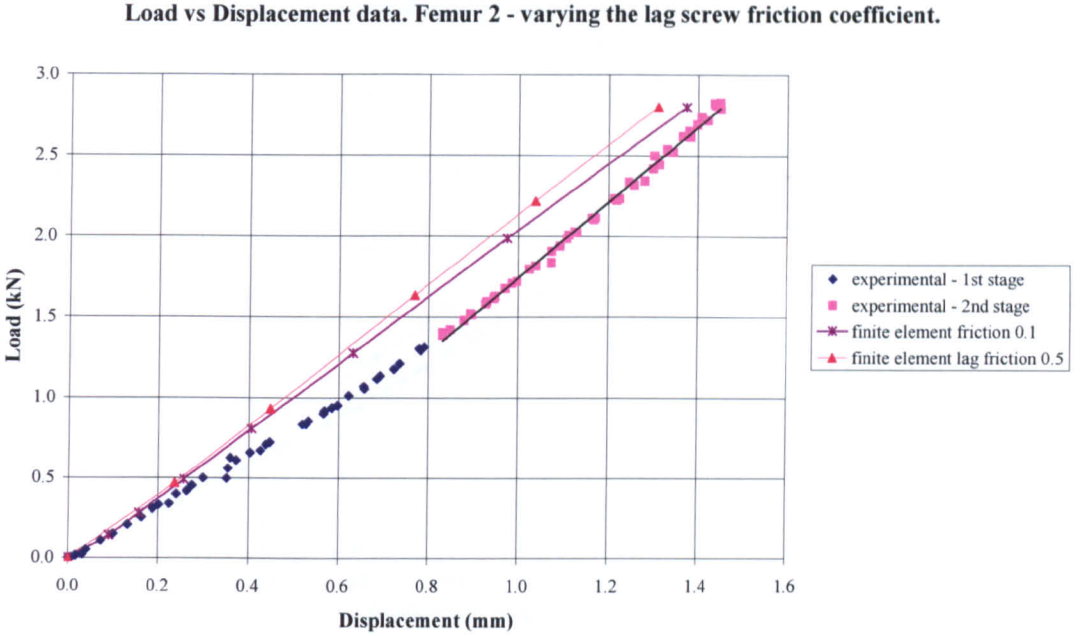

Figure 7.11 – Load-displacement data. Varying the lag screw coefficient of friction.

7.3.14 Varying the coefficient of friction on the distal screw contact surface

Increasing the coefficient of friction on the distal locking screw contact pair has the same effect as increasing the friction on the lag screw contact pair. The system stiffness increases with a difference of 2%, and the maximum deflection decreases with a difference of 5%.

The effect of varying the friction on the distal locking screw contact pair is shown in figure 7.12.

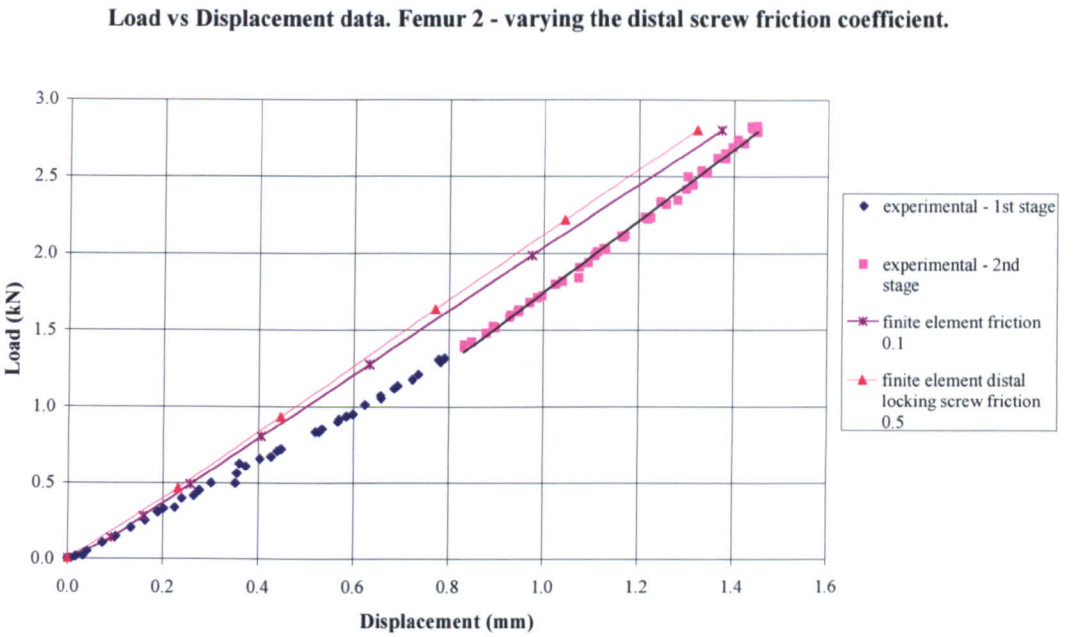

Figure 7.12 – Load-displacement data. Varying the distal locking screw coefficient of friction.

7.3.15 Varying the coefficient of friction on the osteotomy contact surfaces

Increasing the contact coefficient to 0.5 on the osteotomy contact surfaces only, has a negligible effect on the deflection data and stiffness of the construct. The effect of changing this friction value is plotted in figure 7.13.

Figure 7.13 – Load-displacement data. Varying the distal locking screw coefficient of friction.

7.3.16 Varying the coefficient of friction on all contact surfaces

Increasing the coefficient of friction on the nail, lag screw, distal locking screw and osteotomy contact pairs increases the maximum deflection of the system, with a difference of 11%, and decreases the stiffness of the of the system with a difference of 10%. There is a 6% increase in the localised deflection of the system.

It is the combined effect of the lag screw and distal locking screw friction increasing that results in a more significant change in the deflection and stiffness data.

The effect of increasing the friction coefficient on all surfaces is shown in figure 7.14.

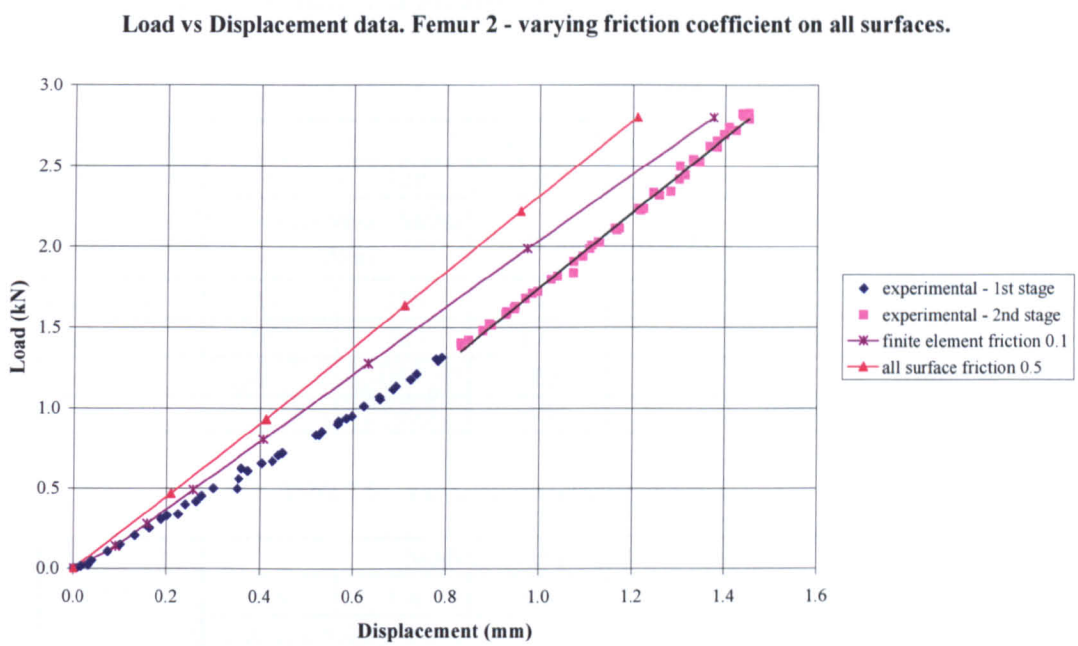

Figure 7.14 – Load-displacement data. Varying the coefficient of friction on all contact surfaces.

7.4 Internal stress and load sharing investigation

It has been shown above that the trochanter modulus, medial and lateral cortical shell thickness and contact stiffness factor have a negligible effect on the stiffness and deflection data of the system.

An additional analysis is provided to determine the effect that these parameters have on the peak von Mises stress in the lag screw and lag screw insertion hole.

Consideration is given to the strain energy and strain energy density of the lag screw, nail and femur. The applied load is shared between the system components differently, due to their relative stiffness. Therefore strain energy and strain energy density data provide an indication of the load carried, and general stress in each component.

7.4.1 Internal stress and load sharing results

Peak von Mises stress and strain energy data for the parameters that have a negligible effect on the stiffness of the system are presented in tables 7.5 to 7.8.

Data for varying the coefficient of friction on all contact surfaces is given in table 7.9.

	Trochanter Modulus (MPa)					
	0	320	0	320	0	320
	Peak von Mises Stress (MPa)		Strain energy (Nmm)		Strain energy density (N/mm^2)	
Lag screw	290	229	124	78	0.012	0.007
Nail	953	765	175	117	0.006	0.004
Trochanter			105	114	0.001	0.001
Femur			1505	1525	0.008	0.008

Table 7.5 – Varying the trochanter modulus.

	Medial Trochanter thickness (mm)					
	0.8	1.4	0.8	1.4	0.8	1.4
	Peak von Mises Stress (MPa)		Strain energy (Nmm)		Strain energy density (N/mm^2)	
Lag screw	230	228	79	77	0.008	0.007
Nail	770	761	119	117	0.004	0.004
Trochanter			113	115	0.001	0.001
Femur			1434	1436	0.007	0.007

Table 7.6 – Varying the medial trochanter thickness.

	Lateral Trochanter thickness (mm)					
	1.3	1.9	1.3	1.9	1.3	1.9
	Peak von Mises Stress (MPa)		Strain energy (Nmm)		Strain energy density (N/mm^2)	
Lag screw	232	225	80	76	0.008	0.007
Nail	773	753	120	114	0.004	0.004
Trochanter			118	112	0.001	0.001
Femur			1440	1433	0.007	0.007

Table 7.7 – Varying the lateral trochanter thickness.

	Contact stiffness factor ( )							
	0.1	1.0	0.1	1.0	0.1	1.0	0.1	1.0
	Peak von Mises Stress (MPa)		Strain energy (Nmm)		Strain energy density (N/mm^2)		Total contact stress (MPa)	
Lag screw	229	228	78	79	0.007	0.008		
Nail	765	759	117	118	0.004	0.004		
Osteotomy							6.7	6.9

Table 7.8 – Varying the contact stiffness.

	Coefficient of friction (μ)					
	0.1	0.5	0.1	0.5	0.1	0.5
	Peak von Mises Stress (MPa)		Strain energy (Nmm)		Strain energy density (N/mm^2)	
Lag screw	229	313	78	68	0.007	0.006
Nail	765	571	117	76	0.004	0.002
Trochanter			114	76	0.001	0.001
Femur			1525	1424	0.008	0.007

Table 7.9 – Varying the coefficient of friction on all surfaces.

7.4.2 Internal stress and load sharing discussion

7.4.3 Varying the trochanter modulus

By effectively removing the trochanter modulus the peak von Mises stress in the lag screw is increased with a difference of 26% and the peak von Mises stress in the lag screw insertion hole increases with a difference of 25%. The strain energy in the trochanter decreases, with a difference of 7%. The strain energy in the lag screw increases, with a difference of 59%, and the strain energy in the nail increases with a difference of 49%.

The strain energy data shows that for a trochanter modulus of 320MPa, the lag screw carries a smaller load than the trochanter, with a difference of 30%. This is because the trochanter has a larger volume than the lag screw. Due to the lag screw having a smaller volume, the strain energy density is larger, with a difference of 82%. This indicates that the lag screw carries a greater load per unit volume and is under more stress.

When the trochanter modulus is effectively removed, the lag screw has a greater strain energy, and strain energy density with a difference of 15% and 89% respectively, indicating that the lag screw carries a greater load and is under more stress.

The load is carried by the lag screw and nail, and the combined strain energy of these two components is greater than that of the trochanter with a difference of 42% and 65% for a trochanter modulus of 320MPa and 0.001MPa respectively.

The load carried by these components is significantly greater than that of the trochanter, and the increased load shared into the lag screw results in an increased load share into the nail, with an increase in the strain energy density and peak von Mises stress in the lag screw and lag screw insertion hole. The load share should therefore be considered between the Gamma nail, trochanter, femoral head and femoral shaft.

By removing the modulus of the trochanter, an increased load is carried by the Gamma nail, in total and per unit volume, and thus the peak von Mises stress in the lag screw and lag screw insertion hole increases.

It is argued that there are two main influences that the trochanter has on the load shared into the Gamma nail and femoral shaft. The first is that the trochanter provides support beneath the lag screw, and the second is that the load is shared into the femoral shaft from the trochanter via the Osteotomy. By reducing the trochanter modulus the support is reduced, as is the load shared into the cortical shaft.

The trochanter modulus therefore has a significant effect on the peak von Mises stress in the lag screw and lag screw insertion hole. The stress distribution in the trochanter will also be significantly affected.

However, the strain energy of the trochanter is only 7% of the total strain energy of the femur. Due to the trochanter carrying a small percentage of the total load carried by the whole femur, the stiffness and deflection data are not significantly influenced by a change in the trochanter modulus. Furthermore the combined strain energy of the lag screw and nail is between 42% and 65% greater than that of the trochanter, proving that the load is carried predominantly by the Gamma nail.

7.4.4 Medial and lateral cortical shell thickness

By varying the thickness of the cortical shell surrounding the medial and lateral trochanter, there is a negligible effect on the strain energy and peak von Mises stress of the system. A variation of between 30% and 40% produces an increased

difference of approximately 1% in the peak von Mises stress in the lag screw and lag screw insertion hole.

7.4.5 Contact stiffness

An increase in the contact stiffness of ten times has a negligible effect on the peak von Mises stress and strain energy in the lag screw, nail and femur. There is also a negligible effect on the total stress at the Osteotomy from contact.

7.4.6 Coefficient of friction

By varying the coefficient of friction on each contact pair, a negligible effect on the stiffness and deflection of the system has been found. An investigation into the effect that the coefficient of friction has on the peak von Mises stress is given for the case where all contact surfaces have a friction coefficient of 0.5, as this case has the greatest effect on the deflection and stiffness data.

Increasing the friction coefficient on all contact surfaces has a significant effect on the peak von Mises stress in the lag screw insertion hole. There is a decrease in the peak von Mises stress, with a difference of 25%. There is also an increase in the von Mises stress in the lag screw, with a difference of 36%.

The strain energy in the lag screw and nail decreases with a difference of 13% and 35% respectively. The femur strain energy of the system decreases with a difference of 7%. As the coefficient of friction is increased, the deflection of the system decreases as the contacting points seize more easily, therefore the strain energy decreases. Strain energy density for the lag screw and femur remain relatively constant, as the load carried per unit volume is the same. The strain energy density of the nail is halved for a five-fold increase in the friction coefficient due to the large contact area between the bone and nail.

7.5 Discussion Summary

The applied load is carried through the cortical shell surrounding the femoral head, into the femoral head and shared between the lag screw, trochanter, nail, medial and lateral shell, and into the cortical bone of the femoral shaft once the gap in the osteotomy is closed.

The load path is shown schematically in figure 7.1. The size of the force lines give an indication of the magnitude of the load at each point, but are not drawn to scale.

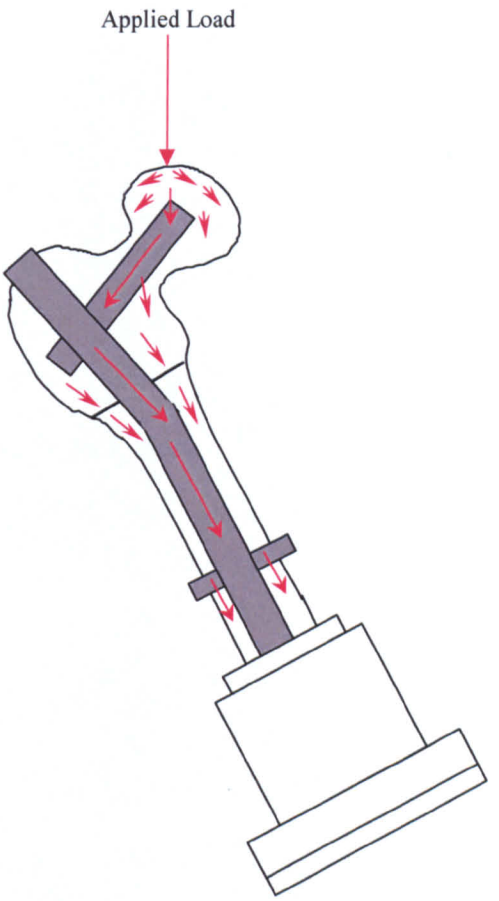

Figure 7.15 – Load path through construct.

This load path dictates that it is important to model the properties in the region where the load is applied to predict the maximum displacement and local deformation of the system. When the local deformation of the system is modelled correctly, an accurate prediction for the stiffness of the system can be achieved.

If the region where the load is applied is too soft, for example, the maximum displacement will be relatively large due to localised deformation. This will indicate a smaller value for the stiffness of the construct, which will not be accurate because the stiffness value is gained from the maximum deflection.

The femoral head modulus, cortical bone modulus and cortical shell thickness are essential parameters that have to be modelled accurately in order to predict the local deformation. The cortical bone modulus is also important in the prediction of the stiffness of the model as the load is shared into the femoral shaft, which is entirely cortical bone.

Increasing the stiffness of the system reduces the maximum deflection. It is not possible to match both the stiffness of the system and the deflection data due to the solution routine. There has, therefore, to be a balance between matching the stiffness of the system and having an accurate comparison with the local and maximum deflection data.

The gap in the Osteotomy has an insignificant effect on the maximum displacement of the system, and the stiffness. By increasing the Osteotomy gap there is more material removed from the cortical shaft and thus the stiffness is reduced. The maximum deflection increases by the increase in the Osteotomy gap.

The trochanter modulus has an insignificant effect on the stiffness and deflection data of the system. This is because the relative stiffness between the Gamma nail and trochanter, per unit volume, is substantial enough for the majority of the load to be carried by the Gamma nail. Furthermore the load is carried into the cortical shell and shaft, and again the relative stiffness between cortical bone and cancellous bone is large enough for the trochanter modulus to have an insignificant influence on the stiffness of the system.

A significant effect on the peak von Mises stress in the lag screw and lag screw insertion hole is observed by changing the trochanter modulus. Support is provided by the trochanter beneath the lag screw, and thus by reducing the modulus of the trochanter, the support is reduced, the load carried into the lag screw increases and the peak von Mises stress increases. Furthermore the trochanter transfers load into the femoral shaft, via the Osteotomy. Reducing the trochanter modulus thus reduces the load carried into the shaft resulting in the lag screw carrying a greater load.

If the trochanter were to be completely removed, the entire load must pass via the lag screw into the nail, and into the femoral shaft at the distal locking screw. This will increase the peak von Mises stress in the lag screw and lag screw insertion hole significantly. Removal of the trochanter has an insignificant effect on the stiffness of the system due to the relative stiffness of the trochanter, cortical bone and nail.

Where absolute stress values in the trochanter region are required, an accurate modulus should be used. For parametric studies using relative data a reasonable value is necessary.

Due to the load being carried predominantly in the Gamma nail the medial and lateral trochanter shell thickness have a negligible effect on the stiffness of the system and the deflection data. Unlike the femoral head shell thickness, these thickness values do not influence the local deformation at the load point, and have no effect on the displacement measured under the femoral head.

Increasing the coefficient of friction of each contact pair individually has a negligible effect on the stiffness of the system and maximum displacement. Increasing all surface coefficients has a more substantial effect on the stiffness of the system and maximum deflection data. A coefficient of friction of 0.5 on all surfaces increases the stiffness of the system. The maximum deflection increases in difference from the experimental data by 16%. The coefficient of friction is clearly an important parameter, and the relative change in deflection and stiffness data is small when compared to the increase in friction. It is therefore of greater importance to model the material properties about the load point. There is, however a significant effect on the peak von Mises stress in the lag screw and lag screw insertion hole.

It is entirely reasonable to ignore the local deformation effects, and to use the displacement under the femoral head to gain a value for the stiffness of the construct. However, by ignoring the local deformation at the load point the finite element model is simplified and further removed from reality. In addition, the comparison with the experiment would have to use the displacement measured

under the femoral head, which is not as accurate as that measured by the Instron machine at the load point.

A steel Gamma nail has been used in this study. It is noted that the modulus of the steel will affect the stiffness of the system, and the maximum displacement. The relative stiffness between the cancellous bone and stainless steel will remain an order of magnitude larger. The modulus of the steel Gamma nail is considered to have a negligible effect on the stiffness of the system and deflection data, however the use of a titanium nail will have a more significant effect.

7.6 Conclusion

To model the stiffness, maximum displacement and local deflection accurately, there are three parameters that have the most importance. These are: the femoral head cancellous modulus, the thickness of the cortical shell surrounding the femoral head and the cortical bone modulus.

Having defined the thickness for the femoral head cortical shell, the medial and lateral trochanter thickness values can be assigned. Either a constant thickness may be used to model the shell surrounding the proximal femur, or a varying thickness can be used. Consideration should be given to the fact that the femoral head shell thickness is less than the medial and lateral trochanter thickness.

The value of the trochanter cancellous modulus need not be entered accurately for the prediction of global stiffness and displacement data. For studies involving implant migration, for example, a more accurate value of the trochanter modulus may be required. The volume of the trochanter under the lag screw provides support, and can act to ameliorate peak von Mises stress in the lag screw and lag screw insertion hole.

A contact stiffness value must be assigned with consideration to solution time and penetration. A reasonable value of between 0.1 and 1 in ANSYS has no effect on the stiffness, deflection or stress data.

A reasonable value for the coefficient of friction must be entered into the finite element model. However, this value is difficult to measure for implant and bone

constructs, and will be subject to a high degree of variance due to contamination on the contact surfaces and natural body lubrication when considering an implant in the human body.

The finite element model presented in the last three chapters allows for rapid generation of multiple constructs, concerning intramedullary nails and fracture fixation. This modelling technique is considered reliable and valid for the particular application given. The novel modelling approach can be used for the development of finite element analysis as a methodology to generate clinically relevant knowledge and indeed, to further pre-clinical trials.

The novel modelling strategy presented can be applied to any fractures of long bones where an intramedullary nail is required.

In General:

- The femoral head cancellous modulus is a critical parameter in modelling the local deflection at the load point and maximum deflection. It is an important parameter in modelling the stiffness of the system when calculated using the maximum deflection of the system.

- Accurate modelling of the thickness of the cortical shell surrounding the femoral head is essential in predicting the local deformation and stiffness of the construct.

- The cortical bone modulus is a critical parameter in modelling the local deformation, maximum displacement and stiffness of the construct.

- The trochanter cancellous modulus has a negligible effect on the global stiffness of the construct, but a more pronounced effect on the peak stress at the lag screw insertion hole.

8.0 Introduction

This chapter applies the validated finite element model to one aspect of an intramedullary device, the method of fixation at the distal end.

Intramedullary nails used for the fixation of a trochanteric fracture in the human femur usually require fixation of the distal end into the femoral shaft to ensure stability of the implanted device. Locking screws inserted through the distal end of the nail and screwed into the surrounding cortical bone typically achieve this fixation.

The configuration of the screws within the distal end may be paramount to the stability of the device, and there are many devices available commercially that use a variety of distal locking techniques with screws locked into the cortical bone. It is the purpose of this investigation to assess the load carrying capacity in the distal end of an intramedullary device used for femoral fractures. The parameters under investigation are:

1. The number of distal screws
2. The screw configuration within the nail
3. The material properties of the screws

These parameters are investigated with three load conditions; an axial load, and a couple applied about each of the two orthogonal axes normal to the (long) axis of the nail. The key areas of interest are:

- The screw arrangement in the distal end and its affect on the nail's capacity to carry the load for each load condition.
- The load shared and carried in the distal screws for each load condition and screw configuration.

8.1 Method

The finite element model is used to simulate the distal end of the device, with representation of the structural stiffness of the various components and the inclusion of contact surfaces and their inherent characteristics. The modelling technique described in chapter 3 is used to construct the distal end model.

Shown schematically in Figure 8.1 is the distal end of the nail with dimensions. The area shown in blue is designated V_f (function volume). This is the part of the model that can be changed rapidly to generate the configurations shown in Figure 8.2.

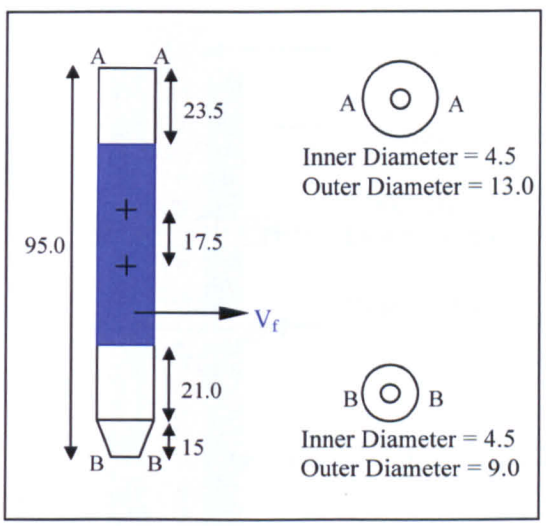

Figure 8.1 – Dimensions of distal nail end (mm).

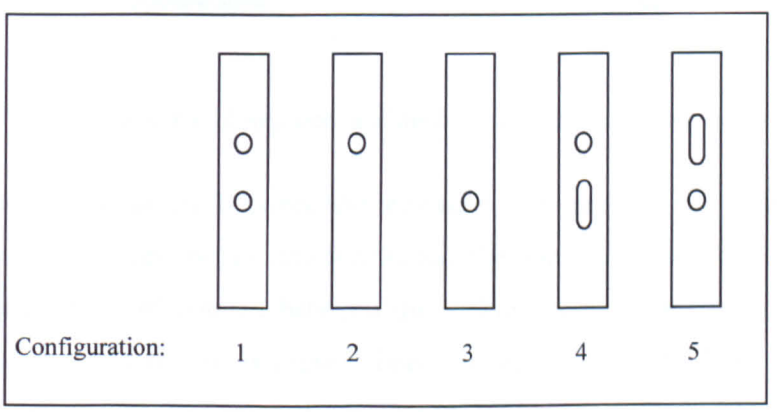

Figure 8.2 – Nail configurations under investigation.

The distal locking screws have a diameter of 6mm and the insertion hole is 6.02mm to provide clearance for the locking screws. The length of the locking screws is 40mm. The length of the slotted region is 8mm, and in configurations where screws are in the slot they are assumed to be centrally located. The bone surrounding the nail is given a diameter of 30mm, and is modelled as a concentric tube about the nail.

The complete model is shown in Figure 8.3, for configuration 4. Throughout this chapter the distal locking screws will be referred to as locking screws. Where there are two screws present they will be referred to as the proximal locking screw and distal locking screw (see Figure 8.3).

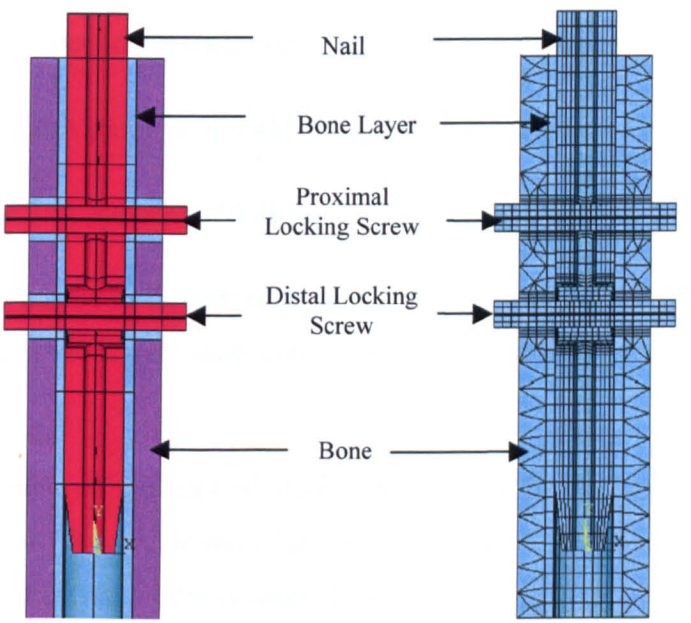

Figure 8.3 – Cross section of the complete model showing volumes and mesh.

There is a radial gap between the locking screws and the nail of 0.01mm. There is no gap between the locking screws and the bone. Contact elements are present to simulate fixed contact between the locking screws and the cortical bone. A radial gap of 0.05mm is present between the nail and the bone layer. Contact elements are used at all surfaces that may achieve contact. These are: locking screw(s) / nail insertion hole(s), locking screw(s) / bone layer and nail / bone

layer surfaces. The nature of this model is such that there is no pre-assignment of contact.

8.2 Boundary Conditions and Material Properties

The load applied to the distal end is somewhat arbitrary as the interest of this study is in the load carrying capacity of the nail and the load sharing of the screws. It is the relative benefits of each fixation type that are of interest. The loading of the femur in previous work has been described in chapter 2 and chapter 3. Based on these load regimes the following loads are applied to the model:

- Load case 1: A force of 1kN is applied in the S-I direction (axially in negative y-direction of nail) evenly distributed on the proximal surface.
- Load case 2: A moment of 0.4kNm is applied about the A-P (z) axis.
- Load case 3: A moment of 0.4kNm is applied about the M-L (x) axis.

The base of the bone is restrained in all degrees of freedom. The relevant anatomical directions and load conditions for the present study are given in Figure 8.4.

The cortical bone of the femoral shaft is assumed to be an isotropic and linear elastic material. The elastic modulus taken for steel is 210GPa, and 17GPa for cortical bone. Poisson's ratio is taken as 0.33 for all materials. A value of 0.1 is assigned to the contact stiffness and a coefficient of friction.

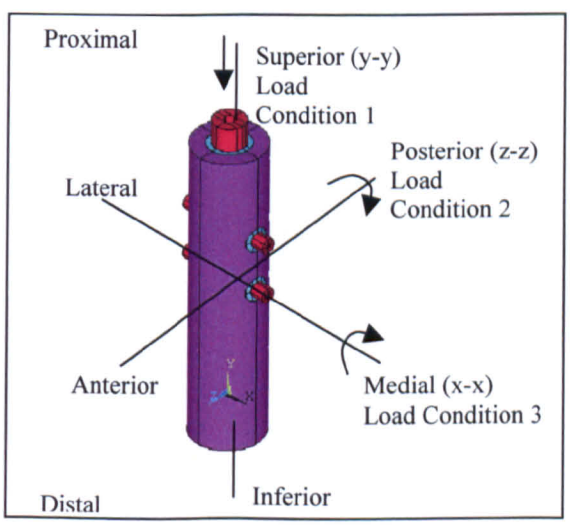

Figure 8.4 – Orientation of axes and anatomical directions.

8.3 Results

Table 8.1 provides results for all screw configurations under load condition 1. Table 8.2 displays information for all screw configurations under load condition 2 and Table 8.3 shows results for load condition 3 and all screw configurations. Maximum von Mises stress in the nail, screw and bone are shown along with the major influencing constituent stress and the maximum contact pressure.

Strain energy is a measure of the internal work done by elements of a system under the action of an external load. The total work done on any component of the system is the integral of each elemental strain energy. The total strain energy is considered for the locking screws, nail and cortical bone. This gives an indication of their load carrying and sharing capacity, relative to the total strain energy in the system. Table 8.4a, 8.4b and 8.4c show the total strain energy in each component for each configuration.

load condition 1 - all results in MPa or mm

		Maximum von Mises stress	Maximum Tensile y - stress	Maximum Compressive y-stress	Maximum Contact Pressure	Maximum displacement in y-direction
Configuration. 1	Nail	79	21	-70	n/a	-0.013
	Prox'l screw	33	5	-38	31	-0.011
	Distal screw	33	5	-38	32	-0.010
	Bone	19	4	-17	n/a	-0.009
Configuration. 2	Nail	154	43	-137	n/a	-0.017
	Prox'l screw	64	11	-72	60	-0.016
	Bone	35	10	-31	n/a	-0.012
Configuration. 3	Nail	154	43	-137	n/a	-0.016
	Distal screw	64	10	-72	60	-0.014
	Bone	35	10	-31	n/a	-0.010
Configuration. 4	Nail	153	42	-136	n/a	-0.018
	Prox'l screw	65	10	-72	60	-0.016
	Distal screw	5	0.5	-6	-	n/a
	Bone	35	10	-31	n/a	-0.012
	Slot	-	-	-	-	-
Configuration. 5	Nail	146	41	-129	n/a	-0.011
	Prox'l screw	0.05	0.02	-0.05	-	n/a
	Distal screw	61	10	-70	60	-0.008
	Bone	30	7	-27	n/a	-0.001
	Slot	36	4	-30	-	-

Table 8.1: Results for load condition 1 – Load in y-direction.

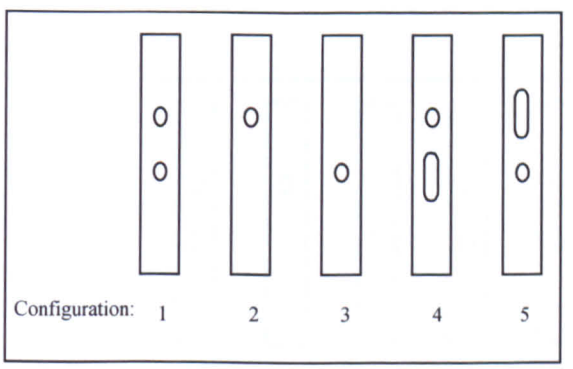

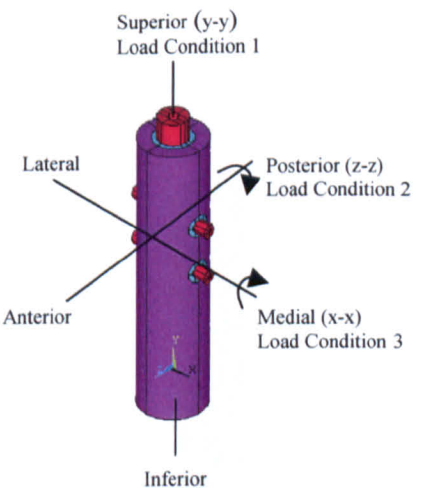

load condition 2 - all results in MPa or mm

		Maximum von Mises stress	Maximum Tensile y - stress	Maximum Compressive y-stress	Maximum Contact Pressure	Maximum displacement in x-direction
Configuration. 1	Nail	57	46	-51	n/a	-0.049
	Prox screw	17	3	-30	24	-0.017
	Distal screw	8	1	-11	10	-0.006
	Bone	4	3	-2	n/a	-0.026
Configuration. 2	Nail	76	43	-68	n/a	-0.054
	Prox'l screw	25	5	-37	30	-0.017
	Bone	5	4	-4	n/a	-0.027
Configuration. 3	Nail	76	43	-68	n/a	-0.067
	Distal screw	25	5	-37	30	-0.010
	Bone	5	4	-4	n/a	-0.024
Configuration. 4	Nail	75	43	-67	n/a	-0.051
	Prox'l screw	25	5	-37	30	-0.018
	Distal screw	2	0.2	-2	n/a	-0.011
	Bone	5	4	-4	n/a	-0.027
	Slot	3	0.7	-0.5	n/a	-
Configuration. 5	Nail	74	50	-66	n/a	-0.06
	Prox'l screw	0.06	-	-	n/a	-0.001
	Distal screw	24	5	-37	30	-0.001
	Bone	5	4	-4	n/a	-0.003
	Slot	49	50	-50	n/a	-

Table 8.2: Results for load condition 2 – moment about A-P axis (z-z).

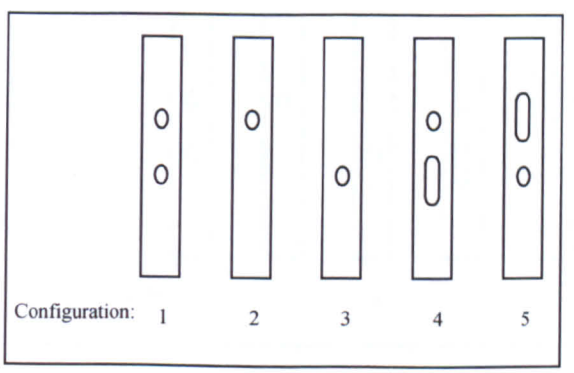

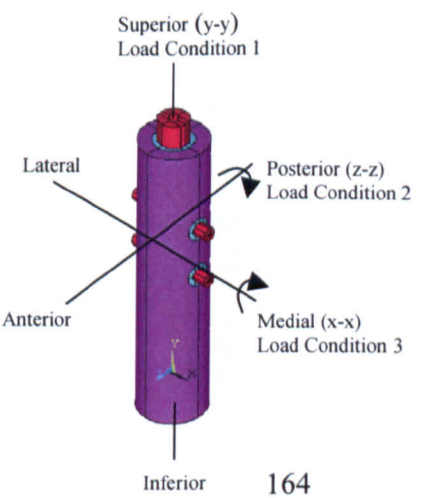

load condition 3 - all results in MPa or mm

		Maximum von Mises stress	Maximum Tensile y - stress	Maximum Compressive y-stress	Maximum Contact Pressure	Maximum displacement in z-direction
Configuration. 1	Nail	28	21	-26	n/a	-0.051
	Prox'l screw	21	2	-18	39	-0.017
	Distal screw	18	2	-17	33	-0.007
	Bone	4	2	-2	n/a	-0.026
Configuration. 2	Nail	17	15	-15	12	-0.082
	Prox'l screw	10	0.8	-11	18	-0.017
	Bone	7	2	-5	n/a	-0.021
Configuration. 3	Nail	9	15	-19	11	-0.096
	Distal screw	7	0.6	-7	13	-0.012
	Bone	15	1.5	-2.5	n/a	-0.030
Configuration. 4	Nail	19	16	-16	11	-0.084
	Prox'l screw	11	0.8	-12	22	-0.018
	Distal screw	1	-	-	2	-0.009
	Bone	6	2	-4	-	-0.022
	Slot	16	16	-16	-	-
Configuration. 5	Nail	12	12	-12	15	-0.067
	Prox'l screw	0.2	-	-	-	-0.004
	Distal screw	7	0.6	-6	-13	-0.002
	Bone	18	1.5	-5	-	-0.005
	Slot	12	12	-12	-	-

Table 8.3: Results for load condition 3 – moment about the M-L axis (x-x).

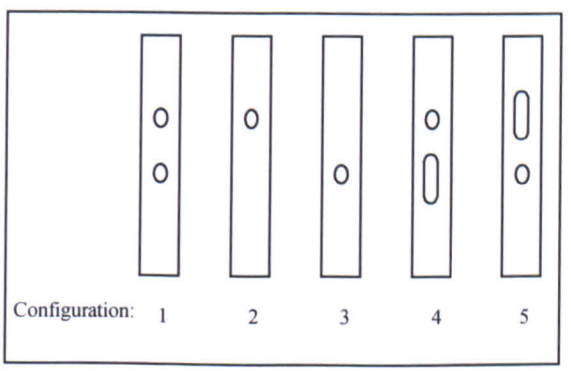

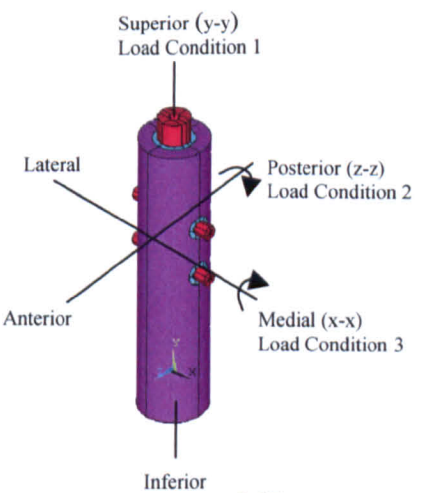

Load condition 1 - Strain energy (Nmm)

		Strain Energy	% of total Strain energy
Configuration 1	Nail	1.21	19.6
	Prox'l Screw	0.45	7.3
	Distal screw	0.54	8.7
	Bone	3.98	64.4
	Total	6.18	
Configuration 2	Nail	1.24	14.3
	Prox'l screw	1.94	22.3
	Bone	5.51	63.4
	Total	8.69	
Configuration 3	Nail	1.70	20.9
	Distal screw	1.93	23.8
	Bone	4.49	55.3
	Total	8.12	
Configuration 4	Nail	1.23	14.0
	Prox'l Screw	2.04	23.3
	Distal screw	0.03	0.3
	Bone	5.47	62.4
	Total	8.77	
Configuration 5	Nail	2.1	38.8
	Prox'l Screw	-	-
	Distal screw	1.92	35.5
	Bone	1.39	25.7
	Total	5.41	

Table 8.4a- Strain energy comparison for load condition 1.

Load condition 2 - Strain energy (Nmm)

		Strain Energy	% of total Strain energy
Configuration 1	Nail	0.69	56.7
	Prox'l Screw	0.083	6.8
	Distal screw	0.034	2.8
	Bone	0.41	33.7
	Total	1.22	
Configuration 2	Nail	0.66	48.5
	Prox'l screw	0.20	14.7
	Bone	0.50	36.8
	Total	1.36	
Configuration 3	Nail	0.92	60.5
	Distal screw	0.20	13.2
	Bone	0.40	26.3
	Total	1.52	
Configuration 4	Nail	0.66	47.7
	Prox'l Screw	0.21	15.2
	Distal screw	0.003	0.2
	Bone	0.51	36.9
	Total	1.38	
Configuration 5	Nail	1.34	82.7
	Prox'l Screw	-	
	Distal screw	0.20	12.3
	Bone	0.08	4.9
	Total	1.62	

Table 8.4b- Strain energy comparison for load condition 2.

Load condition 3 - Strain energy (Nmm)

		Strain Energy	% of total Strain energy
Configuration 1	Nail	0.68	56.3
	Prox'l Screw	0.046	3.8
	Distal screw	0.042	3.5
	Bone	0.44	36.4
	Total	1.21	
Configuration 2	Nail	0.77	72.8
	Prox'l screw	0.017	1.6
	Bone	0.27	25.5
	Total	1.06	
Configuration 3	Nail	0.38	44.5
	Distal screw	0.013	1.5
	Bone	0.46	53.9
	Total	0.85	
Configuration 4	Nail	0.81	72.7
	Prox'l Screw	0.022	2.0
	Distal screw	0.0021	0.2
	Bone	0.28	25.1
	Total	1.11	
Configuration 5	Nail	0.41	83.7
	Prox'l Screw	-	-
	Distal screw	0.011	2.2
	Bone	0.069	14.1
	Total	0.49	

Table 8.4c- Strain energy comparison for load condition 3.

8.4 Discussion

8.4.1 Load Condition 1

In each configuration the maximum von Mises stress occurs at the contact point on the nail insertion hole(s) with the locking screw(s). This von Mises stress is dominated by the maximum axial compressive stress in the nail. The load path for this configuration is shown in figure 8.5.

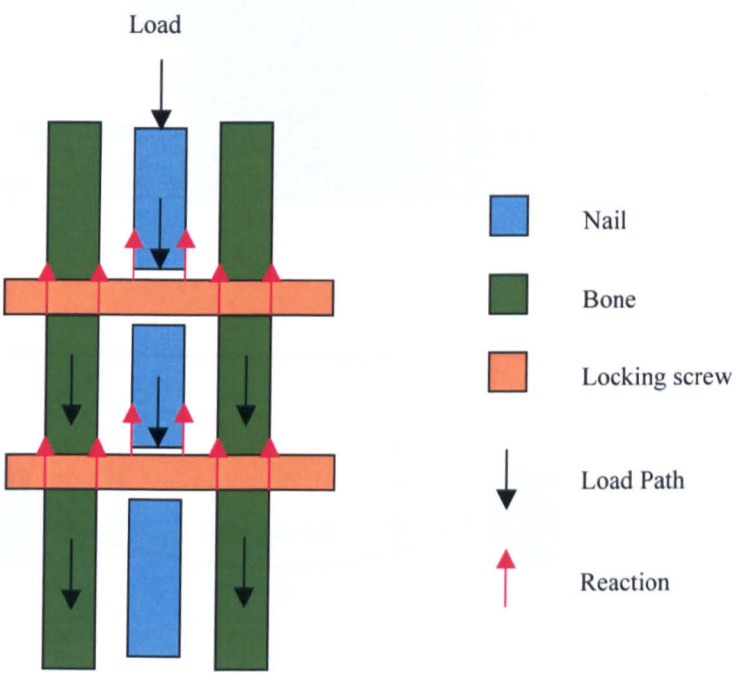

Figure 8.5 – Load path and locking screw reactions for load condition 1, configuration 1.

The maximum von Mises stress in the locking screws is on the most inferior surface of the screw(s). The screws deform like end-supported beams with the maximum bending moment at their mid point. The supports are fixed from the action of the bone on the locking screws. The superior portions of the locking screws are in compression and the inferior portions are in tension. The greater y-directional compressive stress occurs at the contact point with the nail, as does the greater x-directional stress. The deflection of the distal locking screws is shown in Figure 8.6, with a schematic.

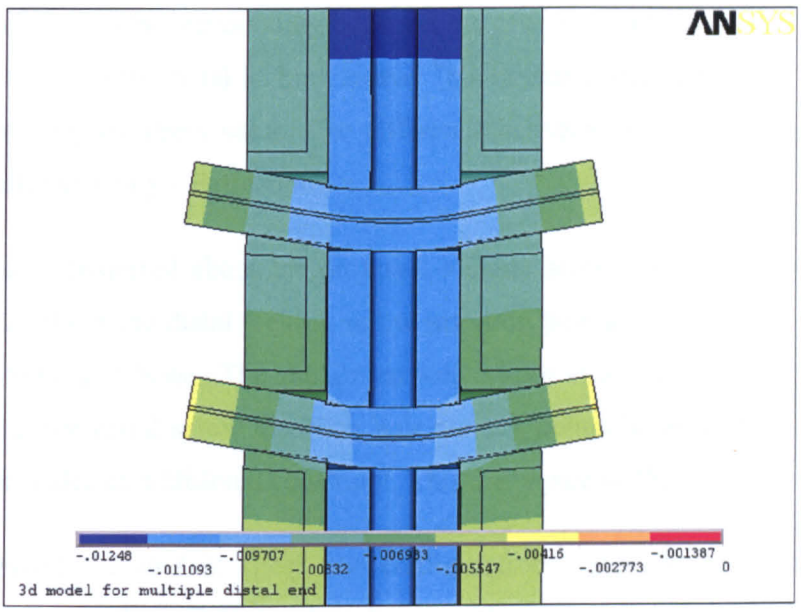

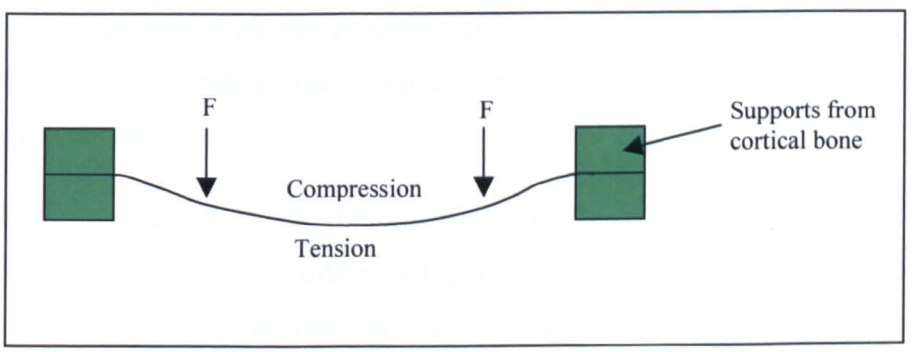

Figure 8.6- Deflection of the distal locking screw under the influence of load condition 1. Top showing scaled version of displacement of locking screws in ANSYS, bottom showing schematic of deflection.

The maximum von Mises stress in the bone occurs at the contact points with the locking screws. There is no contact between the nail and the bone as the deflection is in the axial direction of the nail and there is no lateral force.

Configuration 1: The load is not shared evenly between the two screws with a 20% difference in the strain energy between the two locking screws. The maximum von Mises stress occurs at the distal locking screw and the maximum

deflection is present in the proximal locking screw. Some of the load is transmitted into the surrounding bone via the proximal locking screw, increasing the restraint on the distal locking screw. This causes a greater reaction and hence a slightly higher stress value. The difference between these values is negligible (5% difference in y – deflection).

The load transferred about the proximal locking screw insertion hole is greater than that about the distal locking screw insertion hole due to the load sharing of the surrounding bone. The maximum von Mises stress in the nail is slightly higher at the distal screw insertion hole contact points because the surrounding bone provides an additional constraint. This difference is 2%.

Configuration 2 and 3: These two configurations have almost identical stress distributions and maximum values because the placement of the locking screw for axial loading does not have any influence on the amount of load being carried by the single locking screw and nail. The value of the maximum von Mises stress is almost double that realised in configuration 1 because one locking screw is now carrying the entire load. Contact pressure within the system is also approximately double.

Configuration 4 and 5: Configuration 4 has a slightly greater stress in the locking screw carrying the load than that in configuration 5 (4.5% difference). The values are very similar to those found in configuration 2 and 3 as the axial load is being carried by one locking screw. It is noted that the slot is a more significant stress raiser in configuration 5. In configuration 4 the load path is such that the surrounding cortical bone carries some of the load as well as the slot, with the proximal locking screw carrying the majority of the load. In configuration 5 the entire load passes around the proximal slot before being carried by the distal locking screw and surrounding cortical bone. Figure 8.7 shows the load path for configurations 4 and 5.

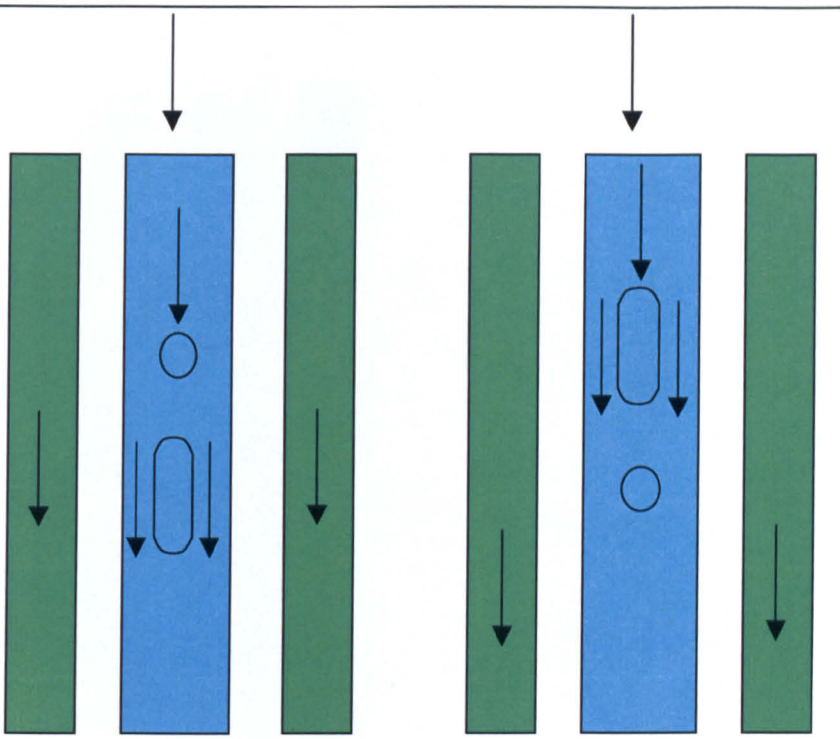

Configuration 4 Configuration 5

Figure 8.7 - Load path for slotted configurations. The slot in configuration 5 is a greater stress raiser as the entire load passes around it.

8.4.2 Load Condition 2

The peak von Mises stress occurs at the contact points with the locking screw(s) and the insertion hole(s). The maximum compressive stress is at the contact point with the proximal locking screw. The medial side of the nail (most positive x) has two peak positive values of axial stress about the locking screw insertion holes from the axial stress in the nail. There is no contact between the nail and the bone for this load condition under any configuration as the deflection of the nail is not substantial enough with respect to the deflection of the bone. Figure 8.8 displays the load path and reactions under this load condition.

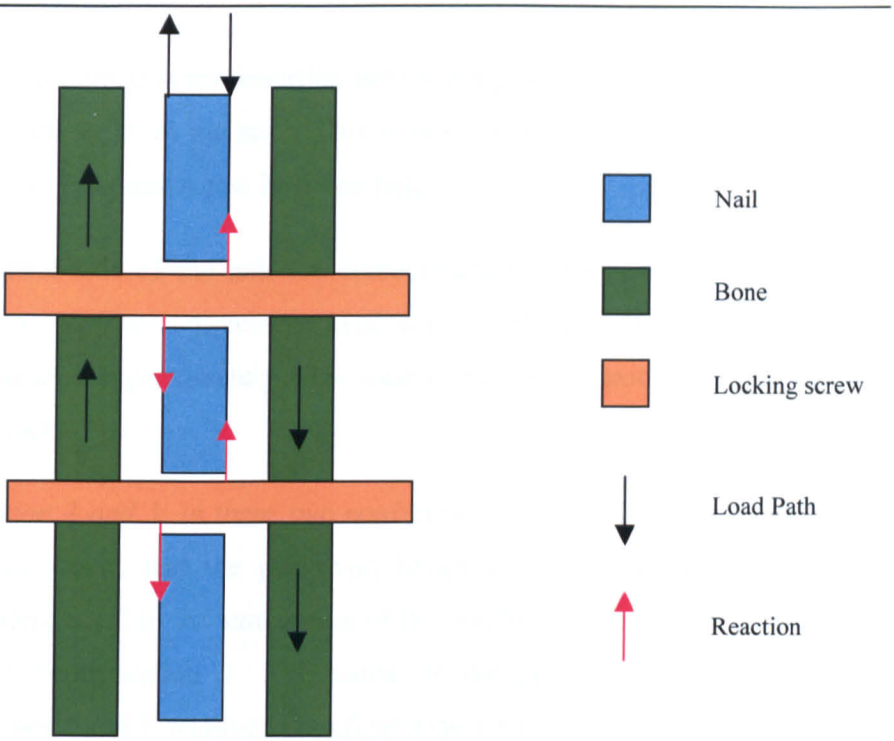

Figure 8.8 - Load path and locking screw reactions for load condition 2, configuration 1.

Configuration 1: The two screws do not share the load evenly due to the deflection of the system and load sharing of the surrounding bone. The proximal locking screw has nearly three times more strain energy than the distal locking screw. The peak von Mises stress in the proximal locking screw is just over double that of the distal locking screw and the proximal screw deflects by just under three times that of the distal locking screw.

Load is transferred to the surrounding cortical bone from the four contact reaction points between nail and locking screws. The load path increases the restraint on the distal locking screw and the action of the medial bone causes a greater deflection on the proximal locking screw.

Contact points are achieved on both locking screws from the deflection of the nail. The contact stress in the more proximal screw is approximately twice that on the distal locking screw because the bone carries some of the load below the proximal screw.

The medial proximal screw insertion hole has a peak stress value that is tensile from the axial stress in the nail. This is more dominant than the stress due to contact on the proximal screw insertion hole.

On the lateral side of the nail the contact between the screw and nail is the dominant stress. The compressive axial stress in the nail at the locking screw insertion hole is approximately 40% smaller than the maximum stress present due to contact.

Configuration 2 and 3: In these two configurations the entire load is carried by one locking screw, and the peak von Mises stress in the locking screw is approximately equal to the summation of the von Mises stress carried in the two screws for configuration 1. The value of the peak von Mises stress for configurations 2 and 3, relative to configuration 1 has increased by 25%.

The strain energy of the distal and proximal locking screws is the same for each configuration. The strain energy for the proximal screw in configuration 1 is one third of that in configurations 2 and 3.

The axial compressive stress at the lateral points of contact for the insertion holes is a maximum. The medial side of the nail insertion holes has a significant tensile stress peak, which is slightly less (11%) than the stress due to contact.

Configuration 4 and 5: The peak stress in the nail is the same as the previous configuration because one screw is carrying the load. The locking screw in the slotted portion has no capacity to carry load from the nail. The significant load carrying locking screws in both configurations have the same strain energy. The slot in configuration 5 is the greater stress raiser. In configuration 4 the proximal locking screw and surrounding bone prevents significant load being passed into the slot. Indeed, the maximum compressive and tensile stresses occur at the slot in configuration 5.

8.4.3 Load Condition 3

The nail pivots about the locking screw(s) in the radial direction and contact is achieved between the nail and bone for configurations 2, 3, 4 and 5. Because of

the freedom to rotate about the distal locking screw(s) there is a smaller peak von Mises stress in the nail and screws and the peak contact stress occurs between the cannulation of the nail and locking screw(s).

Configuration 1: The two locking screws do not share the load evenly. The proximal screw has more strain energy than the distal screw with a difference of 9%. There is a 14% higher peak von Mises stress in the proximal locking screw than in the distal locking screw. In the proximal locking screw the peak stress occurs where contact is made with it, on the cannulation of the nail. The peak stress in the distal screw occurs at the contacting point with the nail on the cannulation. For both peak values it is the compressive stress from the nail contacting the screw that is dominant.

The maximum von Mises stress is in the proximal insertion hole and is 50% greater than in the distal insertion hole. This peak stress is at the contacting point with the locking screw at the cannulation. Peak tensile stress concentrations on the insertion holes from the axial stress in the nail are 20% smaller than the peak compressive stress due to contact.

No contact is achieved between the nail and bone because the distal locking screw restrains the pivoting deflection of the nail. The proximal locking screw has a 15% greater maximum von Mises stress than the distal locking screw.

Configuration 2 and 3: The stress values in the single locking screws are approximately half that of the corresponding locking screw in configuration 1. Contact is achieved between the nail and bone and thus there is a greater stress in the bone. In configuration 2 contact is present at the distal end of the nail, and in configuration 3 it is at the proximal end. The insertion hole for configuration 2 is predominantly affected by the axial stress in the nail. The insertion hole in configuration 3 has peak compressive stress values from contact with the distal locking screw.

Configurations 4 and 5: The locking screw inside the slot does not carry any significant load. Both load carrying screws in each configuration have a peak von Mises stress of approximately half that of configuration 1. Contact is achieved at the interface between bone and nail for both configurations.

For configuration 4 the maximum von Mises stress in the nail occurs at the contact point with the proximal locking screw. This von Mises stress is dominated by the axial compressive stress within the nail. Configuration 5 has a maximum von Mises stress at the proximal slot due to axial stress in the nail. There is a high von Mises stress at the contact point with the distal locking screw but it is 25% smaller than the peak von Mises stress in the slot.

8.5 Results Summary

8.5.1 Load Condition 1

Under the influence of the axial load, configuration 1 leads to a stiff construct and low stress levels in the nail. For predominantly axial load, two screws of equal stiffness placed into a nail without a slot minimises the peak stress in the nail, locking screws and cortical bone. The two locking screws do not share the load evenly due to load sharing into the surrounding cortical bone.

Configuration 1: The peak stress occurs in the nail at the contact points with the locking screws. The action of load being shared to the surrounding cortical bone is the primary cause of the 20% difference in strain energy of the locking screws. It is the distal screw that has the greater strain energy.

Configurations 2 and 3: The strain energy in each screw for these configurations is approximately four times that of configuration 1 in the locking screws due to the increased deflection from one locking screw carrying the entire load. The resultant stress is twice that of configuration 1. Contact points are the same as configuration 1.

Configurations 4 and 5: The stress distributions and peak values are very similar to configurations 2 and 3 (respectively). A locking screw in a slot carries no load from the nail. A slot in the nail is a stress raiser and is hence a weak point within it and a proximal slot is a more significant stress raiser.

8.5.2 Load Condition 2

Configuration 1 gives the lowest values of peak contact and axial stress. A slotted configuration has no structural advantage. The proximal screw in

configuration 1 carries the majority of the load. The slot in the nail acts as a stress raiser.

Configuration 1: The strain energy in the proximal screw is nearly three times greater than that in the distal screw. The medial side on the proximal screw insertion hole has an axial tensile stress that is approximately 50% greater than the compressive stress due to contact. The lateral side of the proximal screw insertion hole has the peak stress within the nail due to contact with the proximal locking screw.

Configurations 2 and 3: The peak stress in the single locking screw is approximately 30% greater than the peak stress in configuration 1. The peak stress in the nail is 25% greater than that in configuration 1. At the medial free boundary on the locking screw insertion hole the peak stress due to contact is 11% greater than the stress due to bending.

Configurations 4 and 5: Peak stresses in these configurations are very similar to configurations 2 and 3 as the load is being carried by one locking screw. The screw inserted into the slot has no significant load carrying capacity, as the screw and the insertion hole contact carry the majority of the load. The proximal slot is the greater stress raiser and it is due to the nail in shear that causes the slot to deform significantly when placed proximally. When the slot is placed distally the proximal locking screw and surrounding cortical bone carry the load.

8.5.3 Load Condition 3

One distal locking screw gives low peak stress values in the nail, locking screw and surrounding cortical bone. The slot provides some rotational stability of the nail for this load case. The distal slot in configuration 4 gives a reaction from the distal locking screw, but there is no reaction with the proximal slot for configuration 5. Configuration 4 leads to contact with both the nail and the bone at the distal end, and contact at the insertion hole is on the anterior side. This pattern is reversed in configuration 5.

Configuration 1: The load is not shared equally between the locking screws. The proximal screw undergoes a 14% greater peak stress due to contact. With

comparison to load condition 2, there is a 20% and 50% increase in von Mises stress in the proximal and distal screws respectively. The peak stress about the nail insertion hole is 50% smaller than load case 2.

Compressive stress due to contact dominates the stress regime; in the proximal screw the contact stress is 20% greater than the axial stress. However, this stress is not significant in magnitude compared to load case 1.

The proximal insertion hole realises a peak stress at the cannulation. The distal insertion hole peak stress is at the free boundary, on the anterior and posterior side due to contact.

There is no contact between the nail and bone, as the two screws prevent motion of the nail relative to the bone.

Configurations 2 and 3: Smaller peak values in the locking screws and nail for these configurations are observed in comparison to configuration 1. Configuration 3 has the greatest difference with a 60% decrease of stress in the distal locking screw and a 70% decrease in the maximum von Mises stress at the insertion hole. Configuration 3 however has a 50% increase in von Mises stress within the bone. Contact is achieved between the nail and the bone in both cases.

Configurations 3 and 4: The slot is a greater stress raiser in configuration 4, and this configuration also has a greater contact stress at the proximal screw insertion hole. The peak von Mises stress in configuration 5 occurs about the slot, and the constituent axial stress is both dominant and symmetric. The proximal slot provides more stability in the system with smaller peak values and deflections on the system but more load is transferred into the bone (70%).

8.6 Other considerations

The position of the screw in the slot will influence the way the load is carried. All configurations have utilised central positioning of the screw in the slot and thus rotational stability is the slot's primary function. Also, the finite element model is set up such that the gap about each screw is closed simultaneously and thus the load is transferred to both screws evenly. In reality the placement of the

screws may not be of equal alignment with the insertion holes, and if the gaps close differently, the load sharing may not be equal.

The loading is such that stress values do not reach magnitudes that could cause failure of the nail or screws. The peak values however are an indication of where the nail and screws are likely to fail due to the contact stress present. The load sharing capacity of the locking screw(s) has also been clearly defined.

8.7 Material Properties of locking screws

The use of a "softer" screw is investigated to establish how load-carrying mechanisms may change. The study is presented for configuration 1 for all load conditions. Configuration 1 is chosen following the outcomes described in the preceding sections. Initially both screws are modelled as Nickel Titanium with an elastic modulus of 44.4GPa. As a secondary study only the proximal screw is modelled with the properties of Nickel Titanium. This is to establish how differing the stiffness of the locking screws affects their load share.

The selection of materials used for intramedullary devices is not arbitrary due to the requirement of biocompatibility of any material with the specific environment within which it has to co-exist. Other requirements include mechanical and physical properties for the desired function and the relative ease of manufacture, production and supply of any such material. Nickel Titanium is used in biomechanical devices and thus is a suitable choice for examination here; moreover, its elastic modulus is very low relative to steel and only approximately double that of cortical bone.

8.8 Two Screws – nickel titanium

The results for both screws having a modulus of elasticity of 44.4GPa are given in Table 8.5. Table 8.6 gives the strain energy values for each screw.

Both screws with the same modulus - E=44.4GPa – all results in MPa or mm

Load Condition	Component	Maximum von Mises stress	Maximum Tensile y - stress	Maximum Compressive y-stress	Maximum Contact Pressure	Maximum displacement in y-direction
1	Nail	84	22	-74	n/a	-0.016
	Prox'l screw	26	6	-34	31	-0.015
	Distal screw	27	6	-35	33	-0.014
	Bone	27	6	-25	n/a	-0.010
2	Nail	50	50	-42	N/a	-0.060
	Prox'l screw	12	3	-19	29	-0.018
	Distal screw	9	2	-11	18	-0.007
	Bone	6	3	-5	N/a	-0.040
3	Nail	32	20	-28	N/a	-0.059
	Prox'l screw	15	2	-13	27	-0.019
	Distal screw	14	2	-13	26	-0.011
	Bone	6	2	-2	N/a	-0.026

Table 8.5- Stress and displacement for NiTi locking screws.

Strain energy (Nmm)

Both screws NiTi

Load Condition	Component	Strain Energy	% of total S.E.
1	Nail	1.22	15.3
	Prox'l Screw	1.13	14.2
	Distal screw	1.25	15.7
	Bone	4.35	54.7
	Total	7.95	
2	Nail	0.74	49.7
	Prox'l screw	0.43	28.9
	Distal screw	0.20	13.4
	Bone	0.12	8.1
	Total	1.49	
3	Nail	0.68	49.3
	Prox'l screw	0.12	8.7
	Distal screw	0.12	8.7
	Bone	0.46	33.3
	Total	1.38	

Table 8.6 - Strain energy results for both locking screws having modulus of 44.4GPa.

8.9 Discussion – two screws Nickel Titanium

8.9.1 Load Condition 1

The load is not shared evenly between the distal locking screws under the influence of the axial load condition. The strain energy of the proximal locking screw is approximately 10% smaller than that in the distal locking screw. The load is shared more evenly than when both screws have the material properties of steel. Furthermore there is a reduction in the proportion of strain energy into the surrounding cortical bone.

When using the lower modulus (softer) screws there is an 18% reduction in the peak von Mises stress in the screws. Displacements are also increased. The decrease in stress in the locking screws is countered by a 6% increase in the peak von Mises stress about the insertion hole of the nail. The nail is the same stiffness as in the previous models, and now has a modulus that is approximately five times that of the locking screws.

The peak von Mises stress in the bone has increased by 30%. The contact pressure on the locking screws remains the same, as the loading is equal to that used before. It is the deformation that increases for the same load.

8.9.2 Load Condition 2

Under the influence of load condition 2, the peak von Mises stress in the system occurs at the contact points with the locking screws and the insertion holes. This von Mises stress is predominantly compressive at the contact point with the screw. The medial side of the nail realises an axial tensile stress at the free boundary of the insertion hole. No contact is achieved between the nail and the bone in this case due to the restriction of the nail about the locking screws.

The two locking screws with a smaller stiffness share the load more evenly than before. The proximal locking screw now has approximately twice the strain energy value of the distal locking screw. The peak stress about the insertion holes is due to the axial stress in the nail and is only slightly higher than the stress due to contact (4%).

8.9.3 Load Condition 3

Load condition 3 gives the smallest stress values in the system. When using screws of a smaller stiffness the two screws carry the load evenly between them. The peak von Mises stress in the distal locking screw is 4% greater than that in the proximal locking screw. The "softer" screws have a maximum reduction in peak von Mises stress of 29%. This is attributed to the fact that they can deflect more, realising a greater strain and transmitting more of the load through to the surrounding bone. The maximum von Mises stress in the insertion hole of the nail is increased by 13% which is reasoned by the fact that the nail is the main load bearing component of the system and hence more load is carried in this case than if the screws were stiffer. There is now a 30% reduction in the contact pressure present on the distal screws.

8.10 Proximal screw Nickel Titanium, Distal screw Stainless Steel

The results for the proximal screw having a modulus of elasticity of 44.4GPa (the distal screw has a modulus of 210GPa) are given in Table 8.7. Strain energy results are given in Table 8.8.

All results in MPa or mm

Load Condition	Component	Maximum von Mises stress	Maximum Tensile y-stress	Maximum Compressive y-stress	Maximum Contact Pressure	Maximum displacement in y-direction
1	Nail	98	27	-87		-0.014
	Prox'l screw	18	4	-25	37	-0.012
	Distal screw	43	6	-47	64	-0.011
	Bone	23	5	-20		-0.009
						x-direction
2	Nail	51	52	-38		-0.057
	Prox'l screw	8	3	-16	24	-0.019
	Distal screw	12	3	-18	23	-0.009
	Bone	4	4	-4		-0.026
3	Nail	30	18	-27		-0.056
	Prox'l screw	15	2	-13	27	-0.019
	Distal screw	18	2	-18	34	-0.010
	Bone	6	1	-2		-0.026

Table 8.7- Results for proximal screw having modulus of 44.4GPa, all load conditions.

Load Condition	Component	Strain energy (Nmm) Strain Energy	% of total S.E.
1	Nail	1.34	19.8
	Prox'l Screw	0.57	8.4
	Distal screw	0.84	12.4
	Bone	4.02	59.4
	Total	6.77	
2	Nail	0.78	56.7
	Prox'l screw	0.14	10.2
	Distal screw	0.056	4.1
	Bone	0.4	29.1
	Total	1.38	
3	Nail	0.68	52.6
	Prox'l screw	0.12	9.3
	Distal screw	0.043	3.3
	Bone	0.45	34.8
	Total	1.29	

Table 8.8 - Strain energy results for proximal screw being NiTi.

8.11 Discussion – Proximal screw NiTi

8.11.1 Load Condition 1

The locking screws do not share the load evenly, as they differ considerably in their material properties and stiffness. It is the distal screw that carries the majority of the load. The proximal locking screw has greater strain energy, as the modulus is one fifth of the distal screw. Also the surrounding bone carries more of the load passing through the proximal screw, as the order of magnitude of moduli of screw and bone is comparable. The distal screw has an increase of 20% peak von Mises stress in comparison to both screws having a modulus of elasticity of 210GPa. There is an increase of von Mises stress about the distal insertion hole of 20%, and a decrease of 24% about the proximal insertion hole. This is attributed to the fact that the nail and the distal locking screw carry the

majority of the load, as they are the stiffer components within the system. The contact pressure on the distal locking screw is almost doubled than previous and the proximal screw contact pressure increases by 16%.

8.11.2 Load Condition 2

The maximum von Mises stress in the nail occurs at the proximal insertion hole from the axial stress in the nail. The peak axial stress is 22% greater than the peak von Mises stress at the contact points. The overall stress in the nail has decreased by 10%, because of the two screws sharing the load more evenly. It is the distal screw that has the greater peak von Mises stress because it is the stiffer of the two. The trend of the distal screw carrying the majority of the load is apparent from the strain energy results as the proximal screw has a 60% greater value than the distal locking screw, accounted for by the increase in deformation for the same load. The contact pressure within both locking screws is comparable to the peak stress of the proximal screw when both had material properties of steel. As the load is shared more equally between the screws, the contact pressure is also very similar in both.

8.11.3 Load Condition 3

The peak von Mises stress in the distal locking screw is 17% greater than that in the proximal locking screw. As the distal screw is the stiffer of the two it is able to carry a greater amount of the load. Again this is apparent from the proximal locking screw realising a 64% greater magnitude in strain energy from the greater deformation. The proximal screw transfers a greater amount of the load into the surrounding bone. There is a reduction in the maximum von Mises stress in the proximal screw as it is reduced in stiffness. The nail has only a slight increase in peak von Mises stress that can be considered negligible (6%). Contact pressure on the two screws has decreased slightly and is more evenly distributed over the two.

8.12 Summary of NiTi locking screw(s)

8.12.1 Load Condition 1

By reducing the stiffness of both locking screws the peak stress within them decreases by 18%. The peak von Mises stress at the screw insertion holes increases by 6%. The two screws do not share the loading equally.

By having a NiTi proximal screw a fifth of the stiffness of the distal locking screw, the majority of the load is carried by the distal screw. The von Mises stress in the distal screw is 20% greater than a stainless steel screw. There is an increase of von Mises stress about the distal insertion hole of 20% and a decrease in the von Mises stress of the proximal screw insertion hole of 24%. The proximal locking screw has a 14% increase in strain energy.

8.12.2 Load Condition 2

The maximum stress in the nail occurs at the proximal insertion hole. For both screws having the same material properties it is the proximal screw that carries the majority of the load. With a NiTi proximal screw, it is the distal screw that has the peak von Mises stress value.

8.12.3 Load Condition 3

When both screws are NiTi, the load is shared evenly between them. However the difference in strain energy and load sharing of the surrounding cortical bone results in higher peak stresses in the distal locking screw. With a NiTi proximal screw the proximal screw carries more of the load

8.13 Alignment of the locking screws in the intramedullary nail

The analysis in this chapter has been concerned with the central positioning of the locking screws within their respective insertion holes. In reality this may not be the case when the surgical procedure is completed. If the screws are misaligned within the hole in the nail then there may be an alternative load sharing mechanism. If the screws are misaligned so that contact is not achieved with one of the locking screws then the system will behave as for the one locking

screw case. This section investigates how the alignment of the screws affects the load sharing between them.

The stiffness of the screws is changed incrementally to model the effect of changing the radial gap between the locking screws and their respective insertion hole. This is a quick and effective way of assessing the load sharing between the screws without actual manipulation of changing the gap between them.

The study concerning a difference in stiffness is in two parts; keeping the proximal locking screw stiffness constant while altering that of the distal screw in the following increments:

Proximal locking screw stiffness (GPa): 210

Distal locking screw stiffness (GPa): 210, 190, 170, 150, 100

The second part keeps the distal locking screw stiffness constant while altering the proximal screw stiffness in the same increments.

This method is analogous to changing the gap between the locking screws and their respective insertion holes, and investigating how the load is shared between the two screws in each case. The method of changing the modulus of the locking screws is numerically stable and robust, changing the gap itself can lead to numerical instabilities and in some cases requires internal settings within the program to gain solution convergence. It is thus deemed appropriate to model the lack of fit of the locking screws by modelling them with varied a variable stiffness.

8.14 Results for variable stiffness of nail

Tables 8.9 and 8.10 provide information for the peak stresses and displacements for the two separate stiffness cases. Tables 8.11 and 8.12 provide strain energy data for each case. All units are in MPa for stress values and mm for displacement.

Proximal screw E = 210GPa. All results in MPa or mm
Load Condition 1

Modulus of Distal Screw (GPa)	Component	Maximum von Mises stress	Maximum Tensile y - stress	Maximum Compressive y-stress	Maximum Contact Pressure	Maximum displacement in y-direction
100	Nail	86	22	-76	-	-0.013
	Prox'l screw	37	6	-42	35	-0.011
	Distal screw	28	5	-33	28	-0.011
	Bone	21	6	-18	-	-0.009
150	Nail	80	21	-72	-	-0.013
	Prox'l screw	34	6	-40	32	-0.011
	Distal screw	30	5	-36	31	-0.010
	Bone	20	5	-18	-	-0.009
170	Nail	79	22	-71	-	-0.013
	Prox'l screw	34	5	-39	33	-0.011
	Distal screw	31	5	-37	31	-0.010
	Bone		5	-18	-	-0.009
190	Nail	79	22	-70	-	-0.013
	Prox'l screw	33	5	-38	30	-0.011
	Distal screw	32	5	-38	32	-0.011
	Bone	20	4	-18	-	-0.009
210	Nail	79	21	-70	-	-0.013
	Prox'l screw	33	5	-38	31	-0.011
	Distal screw	33	5	-38	32	-0.010
	Bone	19	4	-17	-	-0.009

Table 8.9 - Results for steel proximal locking screw and varying stiffness (misalignment) of distal screw.

Distal screw E = 210GPa. All results in MPa or mm
Load Condition 1

Proximal Screw E (GPa)	Component	Maximum von Mises stress	Maximum Tensile y - stress	Maximum Compressive y-stress	Maximum Contact Pressure	Maximum displacement in y-direction
100	Nail	87	24	-77	-	-0.013
	Prox'l screw	27	5	-33	27	-0.011
	Distal screw	37	6	-42	37	-0.011
	Bone	21	6	-18	-	-0.009
150	Nail	82	23	-73	-	-0.013
	Prox'l screw	29	5	-36	29	-0.011
	Distal screw	34	6	-39	33	-0.010
	Bone	20	5	-18	-	-0.009
170	Nail	81	22	-72	-	-0.013
	Prox'l screw	30	5	-37	30	-0.011
	Distal screw	34	6	-39	33	-0.010
	Bone	20	5	-17	-	-0.009
190	Nail	80	22	-71	-	-0.013
	Prox'l screw	32	5	-38	30	-0.011
	Distal screw	33	5	-38	32	-0.01
	Bone	20	4	-18	-	-0.009
210	Nail	79	21	-70	-	-0.013
	Prox'l screw	33	5	-38	31	-0.011
	Distal screw	33	5	-38	32	-0.010
	Bone	19	4	-17	-	-0.009

Table 8.10 - Results for steel distal screw and varying stiffness or misalignment of proximal locking screw.

load condition 1, varying stiffness of distal locking screw - Strain energy (Nmm)
Proximal screw E=210GPa

Distal Screw E (GPa)	Component	Strain Energy	% of total S.E.
100	Nail	1.18	18.2
	Prox'l Screw	0.57	8.8
	Distal screw	0.61	9.4
	Bone	4.11	63.5
	Total	6.47	
150	Nail	1.20	19.0
	Prox'l screw	0.50	7.9
	Distal screw	0.57	9.0
	Bone	4.03	64.0
	Total	6.30	
170	Nail	1.21	19.3
	Prox'l screw	0.48	7.7
	Distal screw	0.56	8.9
	Bone	4.01	64.1
	Total	6.26	
190	Nail	1.21	19.5
	Prox'l Screw	0.46	7.4
	Distal screw	0.55	8.9
	Bone	3.99	64.3
	Total	6.21	
210	Nail	1.21	19.6
	Prox'l Screw	0.45	7.3
	Distal screw	0.54	8.7
	Bone	3.98	64.4
	Total	6.18	

Table 8.11 - Strain energy results for varying stiffness of distal locking screw.

load condition 1, varying stiffness of proximal locking screw - Strain energy (Nmm)
Distal screw E=210GPa

Proximal Screw E (GPa)	*Component*	Strain Energy	% of total S.E.
100	Nail	1.26	19.6
	Prox'l Screw	0.51	7.9
	Distal screw	0.66	10.3
	Bone	4.00	62.2
	Total	6.43	
150	Nail	1.23	19.6
	Prox'l screw	0.48	7.6
	Distal screw	0.59	9.4
	Bone	3.99	63.4
	Total	6.29	
170	Nail	1.22	19.6
	Prox'l screw	0.47	7.5
	Distal screw	0.57	9.1
	Bone	3.98	63.8
	Total	6.24	
190	Nail	1.22	19.6
	Prox'l Screw	0.46	7.4
	Distal screw	0.55	8.9
	Bone	3.98	64.1
	Total	6.21	
210	Nail	1.21	19.6
	Prox'l Screw	0.45	7.3
	Distal screw	0.54	8.7
	Bone	3.98	64.4
	Total	6.18	

Table 8.12 - Strain energy results for varying stiffness of proximal locking screw.

8.15 Discussion – varying stiffness of locking screws

The peak von Mises stress in the construct occurs in the nail for any of the combination of material properties considered. The largest values occur when the moduli are greatly different. If the proximal screw is steel and the distal screw varies, then the larger stress will always occur in the proximal screw, and *vice versa*.

As the modulus of the distal non-steel screw is reduced, the strain energy values increase. When a steel proximal screw is considered, reducing the modulus of the distal screw decreases the total strain energy in the screws. However, the total strain energy is little changed for either the same pair of screws in either configuration.

The peak stress in the nail is in the insertion hole of the stiffer screw. As the difference in stiffness is increased between the two locking screws, the difference in the peak von Mises stress value between them increases to 27%. There is also an 11% increase in peak von Mises stress in the locking screws from the case of similar stiffness to that of the most varied. These figures demonstrate how the stiffer screw carries the majority of the load, or is indicative of the fact that when the gap is closed in one locking screw before the other, then that locking screw will carry the majority of the load.

There is a difference in strain energy of 18% between the locking screws when the distal locking screw has a stiffness of half that of the proximal locking screw, the distal locking screw having the larger value. This is because of the increased deformation of the "softer" screw, and hence an increase in work is done on it. When the two screws share the same stiffness, this difference is reduced to 6%, with the distal locking screw having the greater strain energy. This is because the deformation in the distal screw is greater in the x-direction, as a result of the load sharing with the surrounding cortical bone. There is a more substantial difference of 30% in strain energy of the distal locking screw from a stiffness of 100GPa to that of 210GPa.

8.16 Conclusion

This work has shown that the finite element analysis of nail/screw/bone constructs using contact analysis will yield results for stresses and displacements in the components. The analysis assumes that initially close proximity between the components exists. The distribution of stresses will be strongly affected by the initial assumptions about contact, and the use of contact elements in a finite element model. The modelling technique used allows stresses to develop as contact is achieved. Analyses that do not consider this contact problem (e.g. those that assume initial connectivity) may not lead to accurate predictions of stresses. However, using contact elements is restrictive in that large gaps cannot be accommodated. The user must therefore consider any displacements that will be needed before contact is achieved to be additional to those reported here.

Displacements reported as a result of the applied loads are small – of the order of tens of microns. If loads are larger than 1000N (for LC1) then displacements will be commensurately larger, but in non-linear analysis this is not a linear relationship.

The stresses are strongly determined by the stiffness of the various elements of the construct and this has been reported above. In general the load levels specified have not been sufficient to cause yield in any of the elements, but again comments about the magnitude of stress appropriate to the load levels applied should be borne in mind.

Screws with notional moduli have been used to represent screws of different stiffness. Load sharing in these systems has been reported. As the screws have a lower modulus deformations become larger. Strain energy levels increase (as deformations increase) and the load sharing becomes more even. This is a modelling device to overcome the problem that contact elements cannot be activated differentially.

In general:

- The total strain energy of the system for load case 1 is far greater than for any other load case.
- Deformations for a nail configuration with a proximal slot (and a distal hole) are less than those for a distal slot and a proximal hole for axial load.
- The total strain energy using NiTi screws is greater than that for steel screws.
- Screws with lower modulus deform more than stiffer screws but the distribution of strain energy will be different for NiTi screws and stainless steel screws.
- For axial load the distal screw (of a pair of screws in slotted or round holes) is more critical, while for bending loads the proximal screw is more important. This is particularly relevant to bending about the A-P axis.
- For axial load applied to two-screw configurations with screws of different moduli, it is irrelevant whether the proximal or distal screw has the lower modulus.

9.0 Introduction

Fracture healing involves a complex series of events on a cellular and molecular level that result in structural and functional restoration of the bone involved. The optimal conditions for effective fracture healing are not known and it is unclear how biochemical and mechanical factors govern the fracture healing process.

There are some important factors that influence how a fracture heals. These are:

- The mechanical environment
- Blood supply and vascularity
- Fracture gap size
- Movement of the fracture fragments
- Loading at the fracture site (e.g. compressive and tensile)
- Load sharing between implant components and bone
- Dominant load regimes applied to the bone involved

This chapter will apply the finite element modelling strategy presented in chapter 3 to fracture healing. Finite element analysis can provide relative comparisons between different constructs fairly quickly, and can provide information about stress and strain at a fracture site. Knowledge of general stress and load shared into a fracture callus, relative to different constructs, may lead to a better understanding of trauma treatment devices used to stabilise fractures. Such knowledge could help optimise the design of implant and tissue constructs with respect to the mechanical environment imposed on a fracture callus.

A finite element model of a fractured femur, stabilised with an intramedullary nail is used in this chapter to investigate the effect that loading and mechanical environment has on a simplified fracture callus. Two fracture types are used for this investigation, a femoral neck fracture, and a femoral subtrochanteric fracture.

Results will primarily look at strain energy and strain energy density for an indication of the load carried in a fracture callus and the nail. These two quantities will provide information on load transfer, deflection, total stress, and strain. By analysing the system in this way the following will be investigated relative to different constructs and material properties:

- How the mechanical environment affects the healing callus.
- How the mechanical environment affects the load sharing as the callus stiffens.

Flexibility of a construct may have implications in the selection of trauma treatment devices for certain types of fracture. The use of one or two screws, for example, may change their load sharing characteristics as the callus heals. Eveleigh (1997) carried out simulated fracture healing on two intramedullary nails inserted into a composite femur. The work found that the two nails used had a large difference in stiffness in the fractured state, but had the same stiffness values when the fracture was healed. This led to the assertion that an AO un-reamed nail may be more appropriate for stable fractures, and a Russell-Taylor nail could be used in more severe cases.

Similar results may be apparent from the implementation of finite element analysis, whereby the stiffness of different constructs and load sharing characteristics can be assessed to provide information about what construct will best suit a particular fracture. Moreover, comparative studies can provide information for how one device performs relative to another.

This study will address callus size by using a 0.5mm and 1.5mm thick callus for each investigation. This size is chosen somewhat arbitrarily and it is noted that in practice achieving or choosing a set gap size is difficult. An indication is provided for how a larger or smaller callus will affect the load shared and stress in the callus. Two dominant load regimes are applied to the femur, bending and torsion.

9.1 A brief overview of the principles of fracture healing

The goal for any trauma treatment device is to enable the fracture healing process, and to provide returned functionality of the bone. There are two main ways of stabilising a fracture site: direct apposition of the fracture ends and dynamisation of the fracture site.

Direct apposition of the facture site results in direct, or primary fracture healing. This type of healing commences without callus formation and is a result of bone being formed directly from osteoblast activity. Osteoclasts remove bone matrix, followed directly by osteoblasts that produce osteons and restore the Haversian architecture.

In practice direct healing is hard to achieve because there is some necrosis of the bone fragments and usually some movement at the fracture site, which results in callus formation. Intramembranous ossification is the primary driver for fracture healing when the fracture ends are held in direct apposition. Intramembranous ossification begins when osteoclasts differentiate in a mesenchymal cell and compact bone is formed relatively quickly.

It is arguable that direct fracture healing cannot occur in isolation. According to Wolff's law (Wolff, J, 1892) direct fracture healing is illogical as there is no stimulus for fracture healing. Furthermore, since direct apposition of fracture ends does not occur under natural conditions of weight bearing, primary fracture healing may be regarded as an artificial form of healing.

Indirect, or secondary fracture healing involves bridging of the bone fracture fragments by callus formation at the fracture site. Typically, an internal (endosteal) and external (periosteal) callus is formed, as shown in figure 9.1. Secondary fracture healing has a series of stages that can overlap to a certain extent, including inflammation (large blood clot or fracture hemotoma), callus formation, ossification and remodelling.

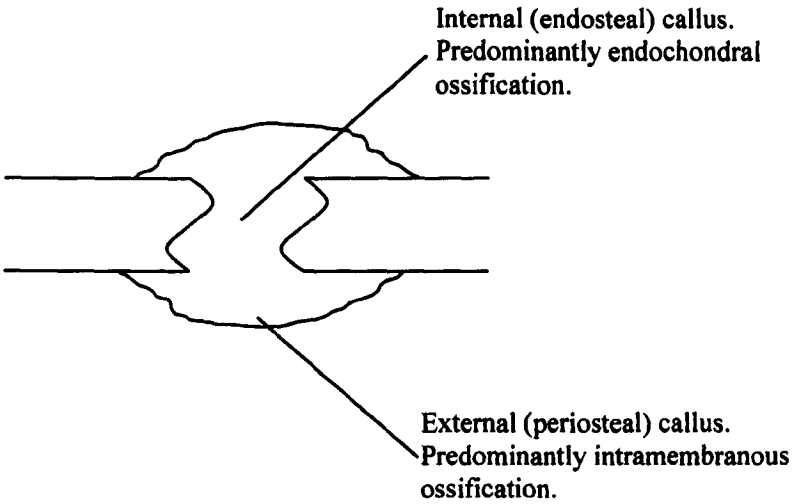

Figure 9.1 – schematic showing the internal and external callus formed between two fracture fragments.

Intramenbranous ossification is found in the external callus and is a result of direct osteoblast activity. Intramembranous woven bone is produced directly without first forming cartilage. At the same time, in the internal callus endochondral ossification commences with the formation of bone after an intermediate stage of cartilage formation. Ossification continues until all cartilage has been replaced by bone. Blood vessels and osteoblasts enter the callus, contributing to the further minerilisation of the woven bone and remodelling.

Remodelling involves the removal of bone by osteoclasts and replacement by osteoblasts, a continuing process through the life of healthy bone, and initiated in a fractured bone. Remodelling replaces randomly orientated woven bone into mature lamellae bone. As a result of remodelling normal structure and biomechanical properties of bone are restored.

With regards to an intramedullary nail used to fix fractures of the proximal femur, direct apposition of the fracture ends is very difficult to achieve, and thus a callus will more than likely form. Intramembranous and endochondrical ossification will occur, followed by bone remodelling and resorption to form a united fracture of good quality bone. It is assumed in this chapter that a callus will form at the fracture site.

9.2 A brief history of fracture healing considerations

Many studies have been carried out to ascertain the conditions that affect fracture healing, and an exhaustive account is not given here, but some important issues are highlighted. Much of the experimental work has been carried out using tibial fracture models, commonly in sheep. The controlled conditions usually include a transverse fracture held with an external fixator. External fixators have the advantage of being adapted so that strain readings can be taken *in-vivo* and the amount of dynamisation at the fracture site can be controlled relatively easily.

The optimum mechanical conditions for fracture healing remain unknown. It is certainly the case that the movement of the fracture fragments has an important effect on the healing callus. Fracture healing requires two major pre-requisites; sufficient blood supply and mechanical stability, (Claes *et al.*, 2002, Goodship *et al.*, 1985) and fracture healing is susceptible to small changes in the mechanical environment (Kenwright *et al.*, 1986).

Fracture movement, or interfragmentary movement influences the callus formation, with less fragmentary movement causing less callus formation (Claes *et al.*, 1995) and large fragmentary movement has been shown to lead to more fibrocartilage and less bone formation (Claes *et al.*, 2002). Furthermore, interfragmentary axial movement of transverse osteotomies results in improved fracture healing when compared to transverse movement, (Augat *et al.*, 2003). Augat *et al.*, (2003) used a sheep model with an external fixator, allowing pure transverse and axial movement with a 3mm osteotomy. The study found that for improved fracture healing the amount of transverse movement should be minimised.

Interfragmentary movement in an early callus tends to increase tissue proliferation and results in a larger callus size. Rigid immobilisation or internal fixation is associated with smaller callus sizes (Carter *et al* 1988).

Kenwright *et al.*, (1986) investigated 85 tibial fractures held with a highly rigid fixator. Two groups were formed, one with and one without limited micromovement. The group with micromovement had a shorter time to weight bearing and to reach a stiffness level equivalent to clinical union. They reported

that the optimum strain magnitudes and rate for different phases of fracture healing had not been determined. However, the micro movement that they applied (0.5mm-2.0mm axial displacement applied at 30Hz for 30 minutes per day) did speed up fracture healing.

The gap size used between the two fracture sites is also important in the fracture healing process. Goodship *et al.*, (1998), used ovine tibial fractures stabilised with an external fixator. Dynamisation of the fracture caused additional damage and repair cycles from the fixator, from a reduction in the osteotomy gap at variable strain rates. The yield point of the callus can easily be exceeded at the early stages of fracture healing from the gap being reduced, and thus it is important to control the gap size in fracture healing. It was also stated that inhibited healing seen in rigid fixators could be avoided from an early application of strain, such as from brisk walking.

The load that the fracture gap is subjected to also affects the fracture healing. Carter *et al.*, (1988) showed that the compressive side of an angulated fracture consisted of mainly cartilaginous material, whereas the tensile side had a smaller callus with a more fibrous character.

Finite elements allow for the evaluation of the fracture site, for different fixation devices under a variety of loads. Finite elements have been used to predict the type of fracture healing in shaft fractures. Carter *et al.*, (1988), used a 2-D finite element model of a femoral midshaft osteotomy with a callus and used simple linear, small strain isotropic modelling. They investigated asymmetric and symmetric callus formation and predicted that intermittent compressive stress inhibits ossification. More direct interfragmentary ossification was predicted on the tensile side. They predicted this from looking at the principal stress magnitudes and directions in the callus region for both axial and bending loads. An elastic modulus and Poisson's ratio of 18.5GPa and 0.33 respectively, were used for the cortical bone. An elastic modulus and Poisson's ratio of 6MPa and 0.47 respectively, were used for the fracture callus. An axial and bending load was applied to the model.

Gardner *et al.*, (2003) modelled an oblique disphyseal fracture in a male patient and based their analysis on the hypothesis presented by Claes and Heigle, (1999). A 2-D finite element model using linear elastic properties was used to determine the type of ossification present in the fracture callus. Different elastic moduli were used at four stages during fracture healing, and a Poisson's ratio of 0.33 was used for all materials. The model correctly predicted the hypothesis of fibrocartilage formation in the early stages and endochandral ossification in the latter stages. The model incorrectly predicted intramembraneous ossification during early healing.

Duda *et al.*, (2001) used a three-dimensional finite element model to understand the load sharing between the implant and bone on a fractured human tibia, using five fracture locations along the shaft. All material properties were considered linear isotropic and an elastic modulus and Poisson's ratio of 6MPa and 0.45 respectively were used for the fracture callus. Compact bone in the shaft had an elastic modulus and Poisson's ratio of 17GP and 0.30 respectively. The elastic modulus of trabecular bone in the epiphysis varied linearly from 300MPa to 700MPa over three element layers from proximal to distal. The material properties at the diaphysis were considered homogeneous, with an elastic modulus and Poisson's ratio of 700MPa and 0.2 respectively. They found unloading of the fracture callus as the load passed through the nail, with negligible forces being exchanged between the bone and nail at the fracture site. They reported that pre-clinical testing of trauma devices should include an analysis of the load sharing mechanisms under physiological-like loading conditions.

The determination of whether a fracture has healed is a subjective process, often carried out from inspection of radiographs. Some test methods have been introduced, such as measuring the bending stiffness of a bone at different points during the healing process. Certainly, time is a poor indicator of fracture healing (Chehade *et al.*, 1997). Also, at the early stages of fracture healing both stiffness and strength result from the same healing process, with relatively uniform material properties throughout the callus. After the early stages the organisation

and remodelling of bone may increase the strength of the callus with little or no effect to the stiffness.

Studies have suggested values of stress and strain that lead to certain types of ossification, and movements that have enhanced healing. Conclusions are drawn mainly from radiographs but also by some mechanical testing. These assessments are useful in determining trends, but the difference in each fracture and tendency for specimens to impart weight on the fracture vary considerably and thus the results are very difficult to quantify and are not directly transferable to other fracture situations.

Trochanteric femoral fractures are subjected to a range of movements, including transverse and axial, and are subjected to both compressive and tensile forces in different parts of the callus. The quantification of the type of ossification in a trochanteric fracture is therefore difficult to achieve. The load sharing between the device and bone would be an advantageous means of assessing how fracture healing will be affected, especially by implementation of a comparative study analysing different fixation methods.

9.3 Application of this study

An assessment is given for the load sharing between the device and bone for different fixation techniques. In particular the strain energy and strain energy density are examined in the fracture callus on a comparative basis to evaluate the use of different intramedullary configurations on two fracture modes.

9.3.1 Method

The same modelling concept used throughout this thesis is used to create a femur instrumented with an intramedullary device. The model is used to assess the load sharing in the construct for a femoral neck fracture and a trochanteric fracture.

The femoral neck fracture is stabilised with a device using four different lag screw configurations. The configurations are:

- Single lag screw of 12mm diameter, referred to as (12) in subsequent sections.

- Two lag screws of 7mm and 9mm diameter with the 7mm lag screw placed proximally to the 9mm lag screw. Referred to as (7-9) in subsequent sections.

- Two lag screws of 7mm and 9mm diameter with the 9mm lag screw placed proximally to the 7mm lag screw. Referred to as (9-7) in subsequent sections.

- Two lag screws of 8mm diameter each. Referred to as (8-8) in subsequent sections.

The two lag screw configurations have a similar cross-sectional area to the single lag screw configuration with the two-screw configuration having a 10% reduction in surface area. Also, the (7-9) lag screw configuration is the only commercially available two-screw device at this time.

The subtrochanteric fracture is stabilised with a device using a single lag screw of 12mm in diameter.

All configurations use a single distal locking screw of 6.02mm diameter.

For each fracture type, two values for the callus thickness are used: 0.5mm and 1.5mm. The fracture callus is modelled as an idealised uniform volume. Each fracture is a transverse, simple fracture in the femoral neck and subtrochanteric region. The fracture callus is modelled as internal only, with linear, isotropic material properties. The callus is modelled thus as a simplification of an actual callus. The finite element models reported earlier in section 9.2 adopted a similar strategy.

9.3.2 Material properties

Linear, isotropic material properties are used for all components of the finite element model. Material properties similar to real healthy bone are used. The properties are listed in table 9.1 and the reader should refer to chapter 3, sections 3.1 for a detailed description of bone material properties.

	E (GPa)	ν (–)
Cortical bone	17	0.33
Cancellous bone - femoral head	1.3	0.33
Cancellous bone - trochanter	0.32	0.33

Table 9.1 – material properties of bone used.

The callus is modelled as being very 'soft' for initial stages of fracture healing, increasing in increments to that of the healthy surrounding bone. The callus modulus ranges from 1MPa to 17GPa. A Poisson's ratio of 0.3 is used. The fracture callus is a simplified representation of a real callus formed at a fracture site. The callus is modelled as isotropic for simplicity and the range of elastic modulus used is representative of a healing callus increasing in stiffness. Very low elastic moduli represent 'soft' fibrous tissue, and higher moduli represent healthy bone. Time dependent behaviour has not been included in this study. The relationship between time and healing is often subjective due to the ability and willingness for a patient to impart load and therefore the study concentrates on a healing callus, which may be over differing time periods.

Two material properties for the intramedullary nail are used, titanium and steel. An elastic modulus and Poisson's ratio of 110GPa and 0.33 respectively are used for titanium. An elastic modulus of 210GPa and 0.33 respectively are used for steel.

9.3.3 Loading

Each configuration is subjected to two separate load regimes: a bending and torsion load condition. The loading is explained in more detail in chapter 3, section 3.9.

Figures 9.2 to 9.4 show the fracture callus and configurations used.

The fracture callus is a single layer in the positions shown in figure 9.2, and is one element thick. An external callus has not been modelled for simplicity and allows a like-for-like comparison with an un-fractured bone once the callus is considered 'healed'.

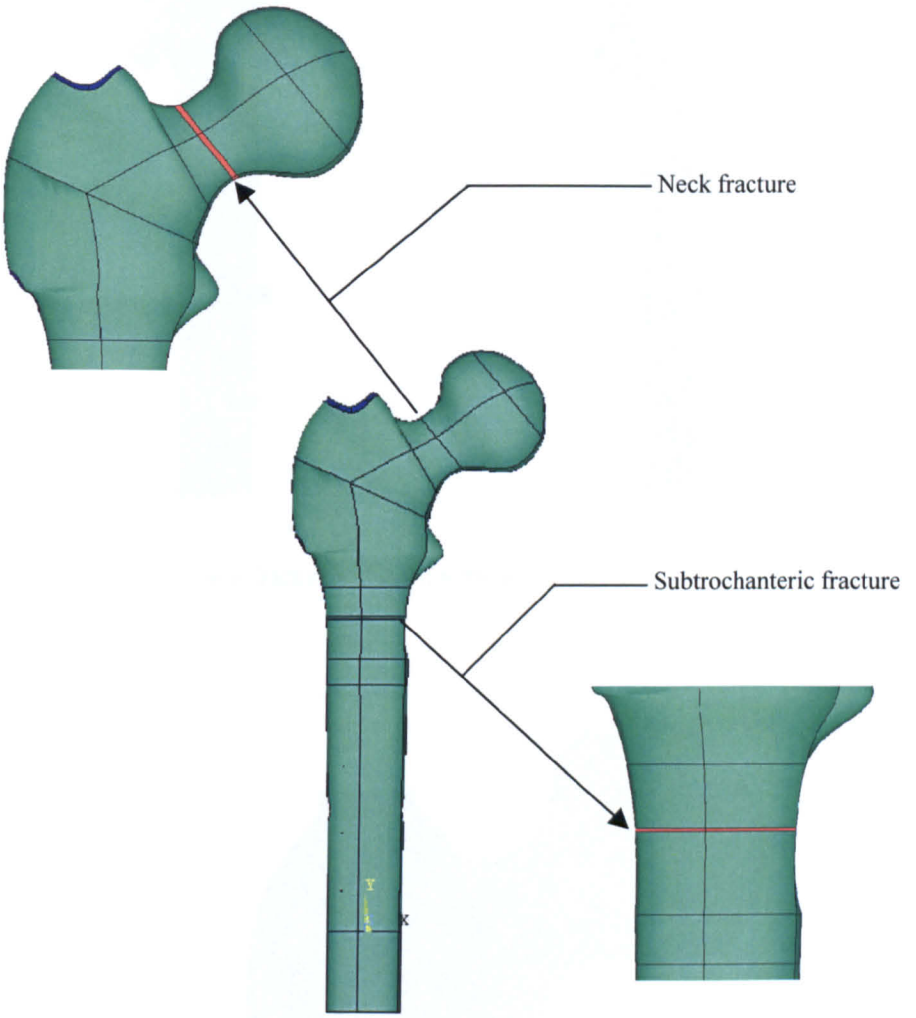

Figure 9.2 – Neck and subtrochanteric fracture are highlighted in orange.

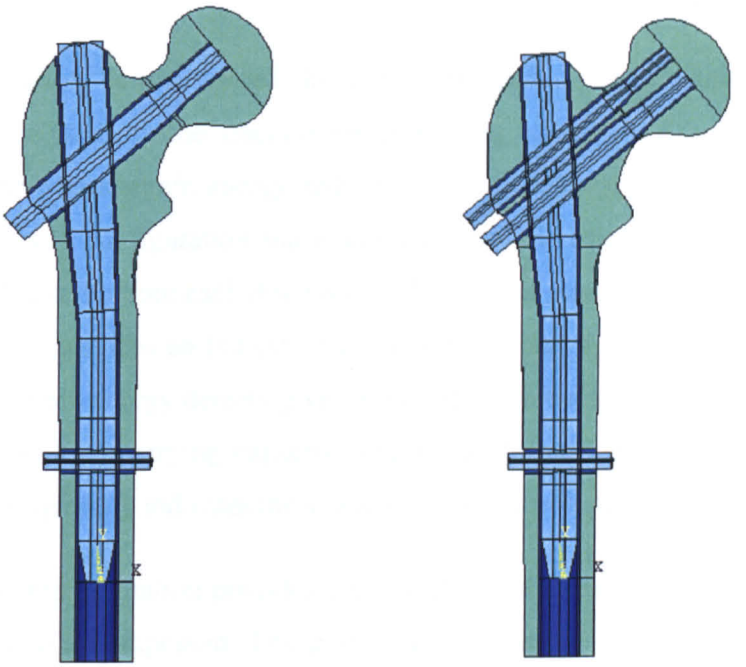

Figure 9.3 – neck fracture stabilised with single and two lag screw configuration.

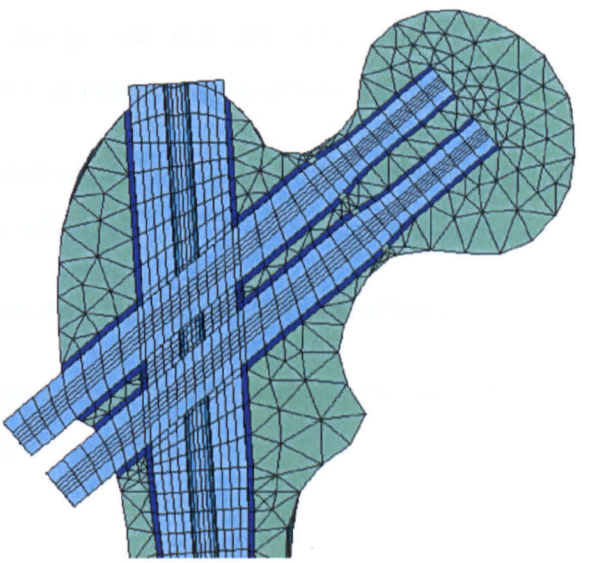

Figure 9.4 – Cross-section mesh of (8-8) configuration.

9.4 Results

Each configuration is considered in turn with each load condition. The components analysed are the fracture callus and lag screw(s), with respect to peak von Mises stress, strain energy and strain energy density. A comparison is made between each configuration and a summary provided after each discussion. Results are tabulated before each discussion. The units of strain energy are Nmm, and this quantity provides an indication of the load carried by a component, and its deflection. Strain energy density gives information on the load carried relative to a components load carrying capacity. The units of strain energy density are N/mm^2 and this quantity indicates the average stress in a component.

Each graphical representation provides data for the total strain energy and strain energy density in a component. The graphs do not clearly indicate the rate of change of a quantity relative to the increased stiffness of the callus. This is deliberate to make a clear assessment of the load share in each component, and becomes particularly important when comparing the different lag screws and material properties in each configuration for a particular callus modulus. The decrease in strain energy, for example, relative to the increase in fracture stiffness must be borne in mind when observing the results data.

Tabulated data for deflection, von Mises stress, strain energy and strain energy data is given in Appendix IV.

9.4.1 Neck fracture, two lag screws (7-9), bend load

Figures 9.5 to 9.9 represent the strain energy and strain energy density for the fracture callus, nail and lag screws.

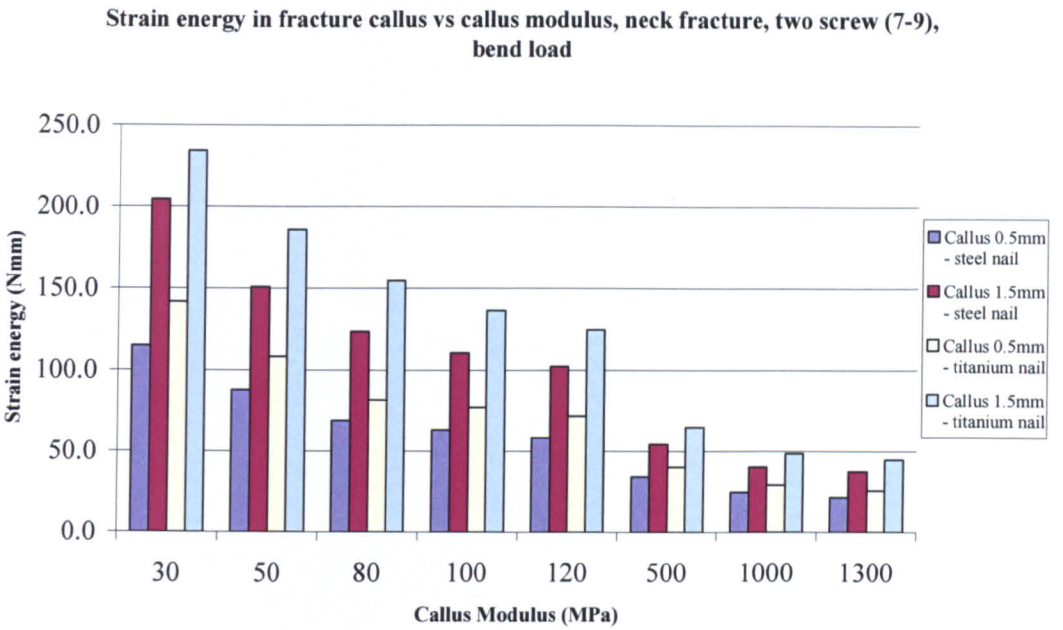

Figure 9.5 - strain energy in callus.

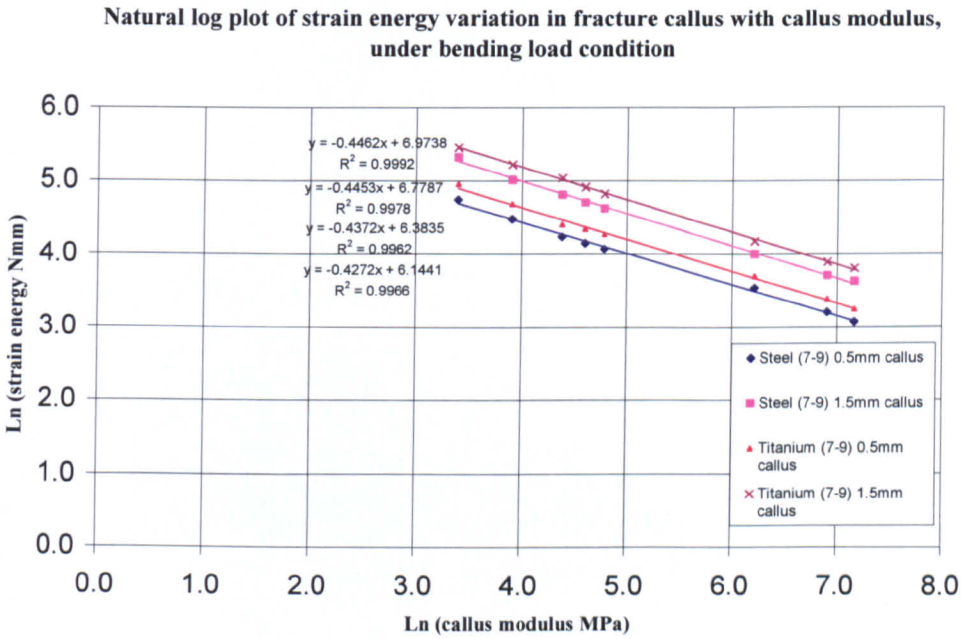

Figure 9.5a –strain energy in callus (natural log of data)

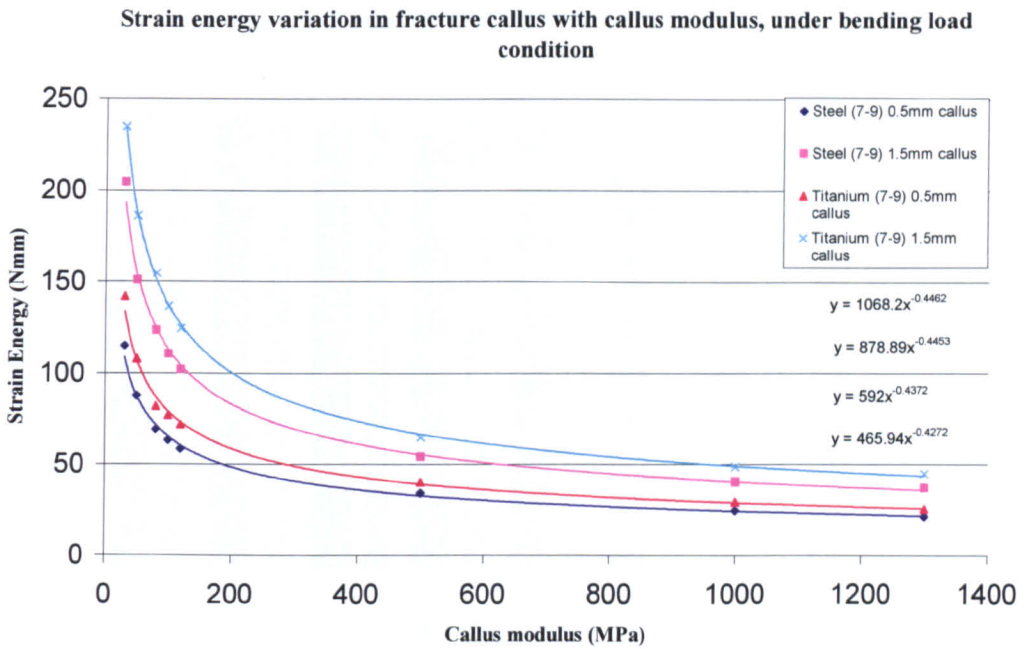

Figure 9.5b – Strain energy in callus (natural log of data)

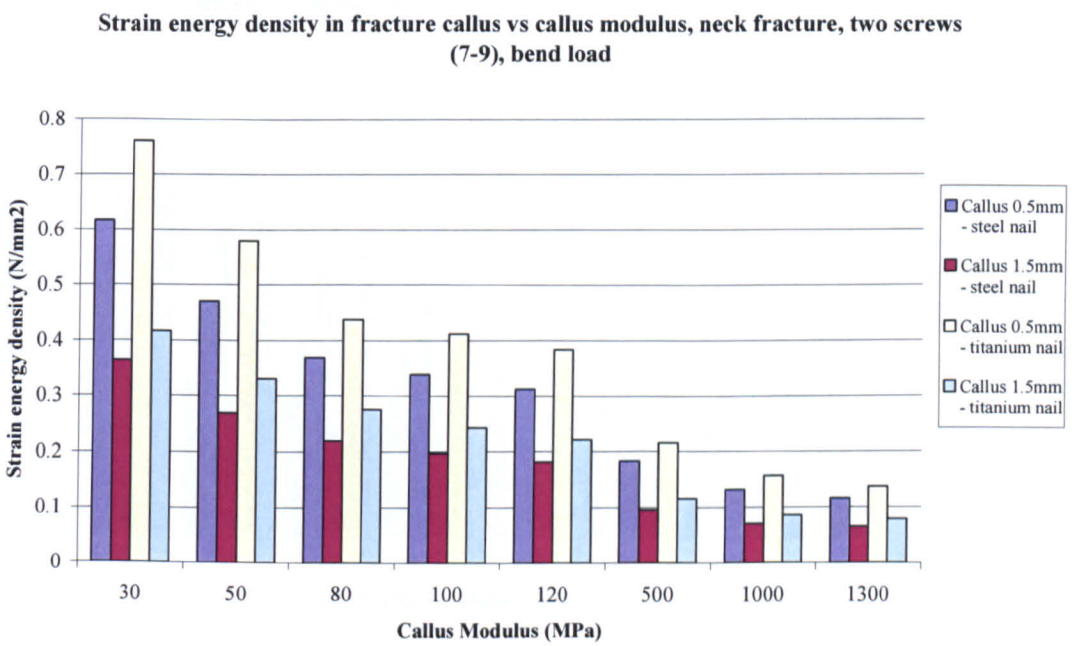

Figure 9.6 - strain energy density in callus.

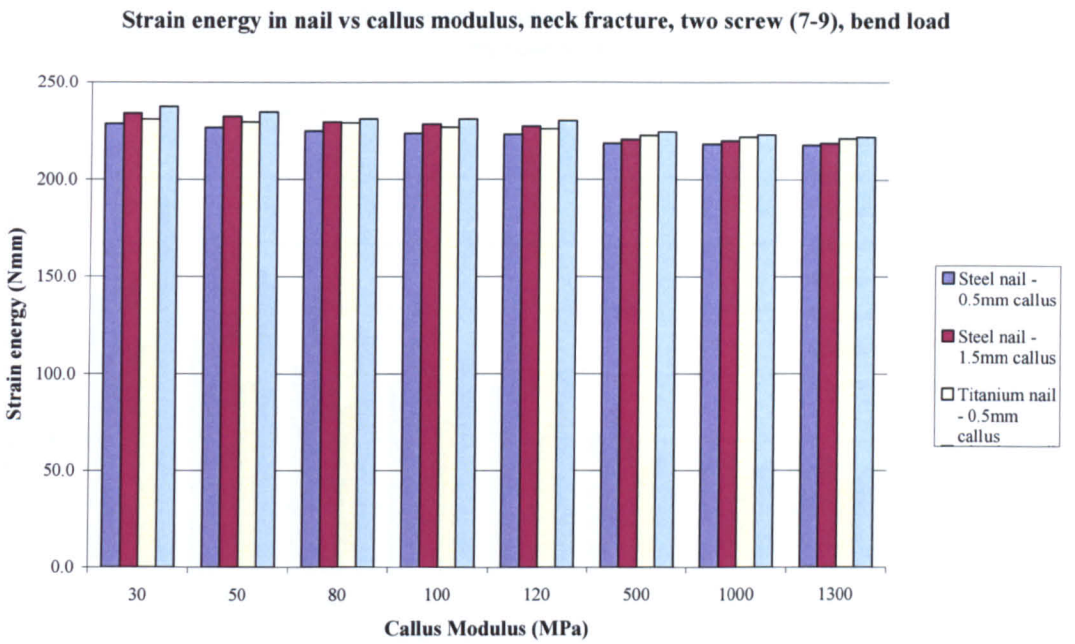

Figure 9.7 - strain energy in nail.

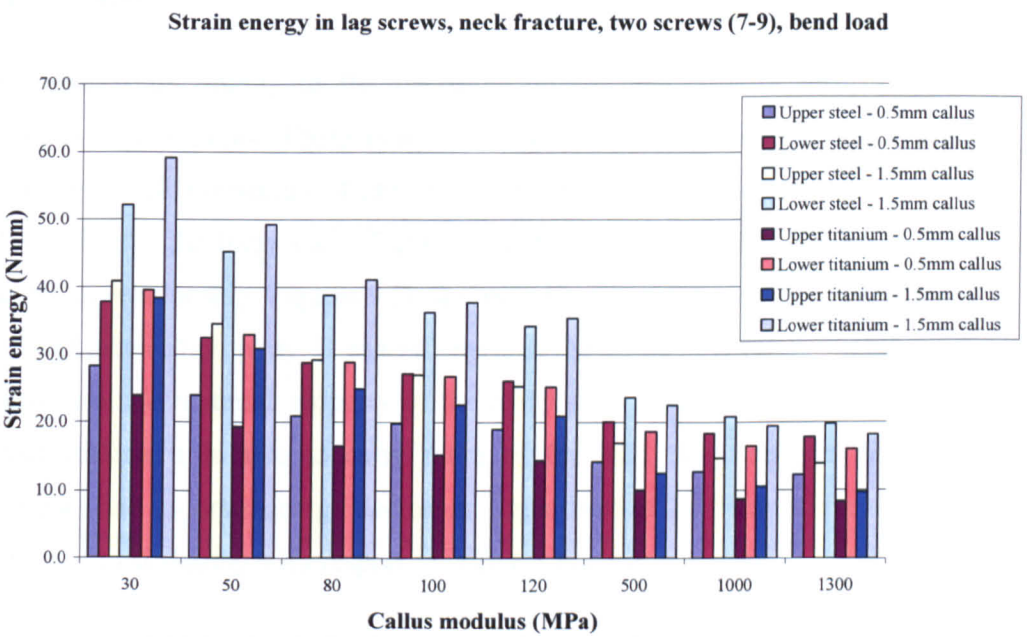

Figure 9.8 - strain energy in lag screws.

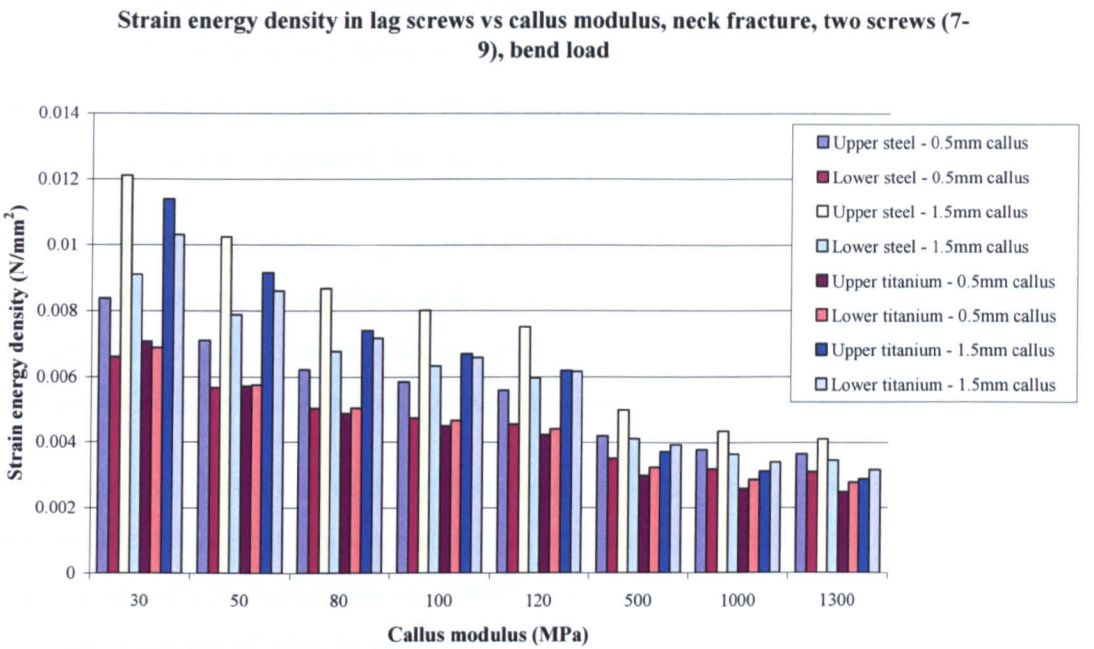

Figure 9.9 - Strain energy density in lag screws.

9.4.1.1 Callus

The total strain energy in the fracture callus decreases with respect to the modulus of the callus. There is a large decrease in strain energy for a small increase in callus modulus, at low callus moduli. The trend is an inverse power relationship of the form $1/x^n$. Figure 9.5a shows a logarithmic plot identifying the power relationship. Figures 9.5b shows the power relationship for each callus size and material property. It can be seen that the value of n varies slightly with callus size and material property of the nail but is approximately 0.43. As the callus stiffens it is able to carry more of the load, the strain in the callus decreases and its strain energy decreases. Regardless of the fracture size the same pattern of load sharing with respect to stiffness is observed.

The greatest change in strain energy is at the lowest stiffness range, indicating the importance of keeping the fracture stable at the early stages of fracture healing. At the early stages (<500MPa) the callus is rapidly able to carry more load and at these stages it would be prudent to accelerate fracture healing if possible. Once the callus can carry a significant proportion of the load (>500MPa), the strain energy is relatively constant and the callus will carry a similar proportion of the load as it stiffens.

The larger fracture callus has greater strain energy in all cases. The percentage increase from a 0.5mm to 1.5mm, 30MPa callus fixed with a steel and titanium nail is 44% and 39% respectively. The larger callus has a smaller strain energy density because it is, in general, less stressed.

A larger callus size promotes greater load sharing into the lag screws and less into the surrounding bone. There is therefore a smaller strain energy density in the larger callus. This is an indication to promote larger callus sizes to shield the callus from higher stresses, which can be detrimental to the healing process.

A titanium nail carries less of the load, transfers more into the surrounding bone and thus the callus shares more, resulting in a greater strain energy for the larger callus. A 0.5mm fracture callus of 30MPa, stabilised with a titanium nail has a difference increase of 19% in strain energy when compared with a steel nail. A corresponding 1.5mm callus has a 13% increase. Both the 0.5mm and 1.5mm callus for a fracture callus of 1300MPa have an increase of 16% in strain energy when fixed with a titanium nail compared to a steel nail. Therefore the use of a titanium nail has a greater effect on the load shared into the callus when a smaller callus size is used.

9.4.1.2 Nail

As the fracture callus stiffens more load is shared into the surrounding bone and consequently less into the lag screws and nail. This causes a decrease in the strain energy of the nail, which is small (maximum percentage difference 7%), because the nail is the main load bearing structure. The strain energy in the nail is greatest for the larger callus size as there is less good quality bone to carry the load. The increase can be considered negligible with a maximum percentage difference of 3% for an increased callus size when using a steel or titanium nail. The use of a titanium nail results in greater load sharing into the surrounding bone, the strain energy for the titanium nail is greater than that for steel, with a maximum difference of 2%.

9.4.1.3 Lag screws

The strain energy in the lag screws (combined and individual) decreases with respect to the stiffening callus. The maximum strain energy is with a large callus size because there is less good quality bone. The lower lag screw, being the larger of the two always has the greater strain energy.

At lower callus moduli the lag screws share the load between them more evenly. The percentage difference for a steel nail and a 0.5mm callus increases from 25% to 31% as the callus stiffens and the corresponding titanium percentage difference increases from 40% to 47%. The lag screws also share the load between them slightly more evenly for a larger callus size. The percentage difference between the lag screws for a steel nail with a 0.5mm and 1.5mm callus of 30MPa is 25% and 22% respectively, and a difference of 40% and 35% is observed for the titanium nail. Once the fracture callus has stiffened to above 200MPa the callus size has a negligible effect on the load sharing of the lag screws (within 1%). For low callus moduli, the callus size is more influential on the load shared between the lag screws.

At low callus moduli, the steel upper lag screw has more strain energy than the corresponding titanium upper lag screw (16% difference increase for 0.5mm, 30MPa callus). The steel lower lag screw has less strain energy than the corresponding titanium lower lag screw (4% difference decrease for 0.5mm, 30MPa callus).

Once the callus has stiffened to above 200MPa, the steel upper and lower lag screws have a greater strain energy value than the titanium lag screws (32% and 10% difference respectively for 0.5mm, 1300MPa callus). This effect is independent of the callus size.

At the early stages of fracture healing the choice of a steel nail will result in more load being shared into the upper screw and less into the lower screw. Once the callus has stiffened significantly, the choice of a steel nail will result in more load being transferred into the lag screws, with a significant increase in load being carried by the upper lag screw. A titanium nail shares a greater amount of load into the surrounding bone.

The steel lag screws carry a greater share of the load due to their increased stiffness. The proportion of load share to the surrounding bone and the deflection of the lag screws will determine the strain energy values for the steel and titanium nails. Once the fracture is 'healed' the load share is such that both the steel screws have a greater strain energy than the titanium screws. For the steel lag screws a greater force is transmitted through them, and they have a smaller deflection compared to the titanium screws. The increase in force transmittance compared to the decrease in deflection results in an overall increase in strain energy. At the early stages of fracture healing there is less load share into the surrounding bone and the lag screws carry a greater proportion. The effect is to have an increased deformation of the lower titanium lag screw for a similar force transmittance; therefore the lower titanium lag screw has greater strain energy. The effect is not present in the upper lag screw as it is not the main load-bearing component of the two lag screws.

For a smaller callus size the combined strain energy of the lag screws is reduced when using titanium nails with a difference of 4% and 19% for a 30MPa and 1300MPa callus respectively. There is an increase in strain energy when using titanium lag screws and a larger callus size with a 5% and 8% difference for a 30MPa and 1300MPa callus respectively. This increase in strain energy is attributed to the increased load share into the lag screws when a larger callus is used.

The strain energy density is always higher in the smaller lag screw at lower callus moduli, which is indicative of this screw being more highly stressed. For the steel screws this distribution is continued as the callus stiffens, and the difference in strain energy density for a 0.5mm and 1.5mm callus, as the callus stiffens is similar (between 4% and 1%). Once the callus has stiffened to 1300MPa the strain energy density is very similar in both screws for the 0.5mm and 1.5mm callus with a percentage difference of 15% and 16% respectively.

Therefore, for a steel nail, the load is shared more equally between the two screws when the callus is at 30MPa, but the screws are not equally stressed due to their geometries. When the callus has stiffened to 1300MPa, the load is not

distributed as evenly between them, and they are more equally stressed. This trend is apparent for either a 0.5mm or 1.5mm callus.

When using titanium lag screws the greater strain energy density is observed in the upper screw for low callus moduli, as with the steel screws. Again this indicates the fact that the upper screw is more highly stressed. The difference in the strain energy density values is small, with a percentage difference of 2% and 9% for a 0.5mm and 1.5mm callus respectively compared to a 21% and 25% difference for the corresponding steel screws. This demonstrates that the titanium screws are more equally stressed and the distribution of load between them is more equal.

As the fracture callus stiffens the strain energy density distribution changes in the titanium screws. The upper screw has higher strain energy density at low callus moduli, and the lower lag screw has higher strain energy density at high callus moduli. For a 0.5mm callus the strain energy density changes to a higher value in the lower lag screw once the stiffness reaches 80MPa. The same effect is observed for a 1.5mm callus with a stiffness of 500MPa. The limiting point at which the lag screws change in their strain energy density is when the load carried in the bottom screw is 1.8 times that of the upper screw.

This load sharing is not observed in the steel screws and the upper steel screw is always under more stress than the lower screw. One result of this load sharing is that the smaller callus size promotes a more even load distribution between the titanium lag screws for a softer callus, which may be beneficial to fracture healing as the load will be more evenly distributed throughout the callus tissue.

9.4.2 Neck fracture, two lag screws (7-9), torsion load

Figures 9.10 to 9.14 represent the strain energy and strain energy density in the fracture callus, nail and lag screws as the callus stiffens.

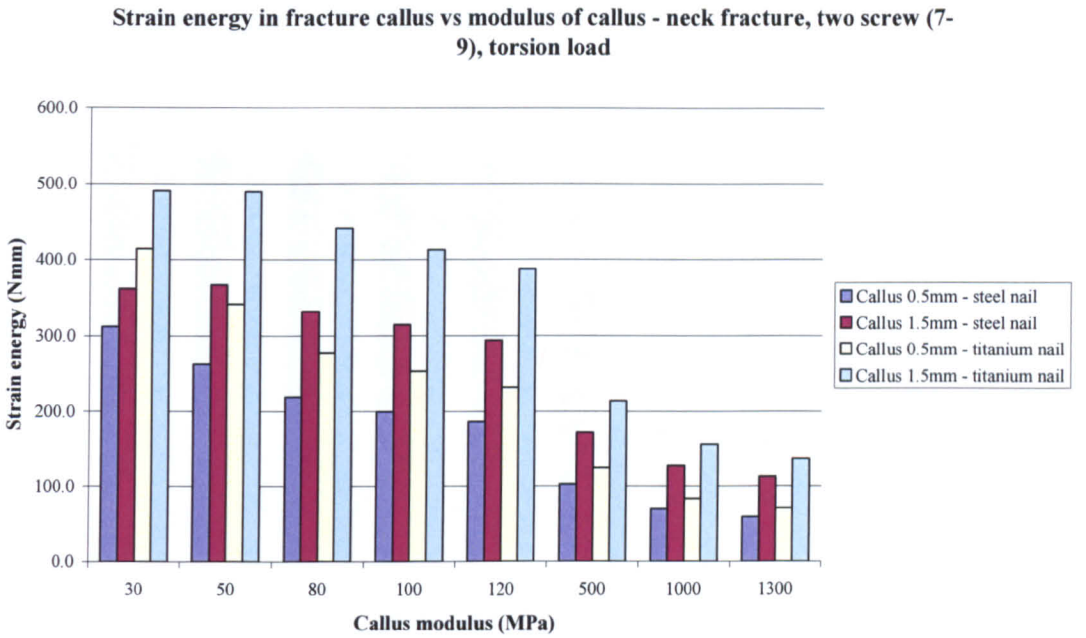

Figure 9.10 - Strain energy in callus.

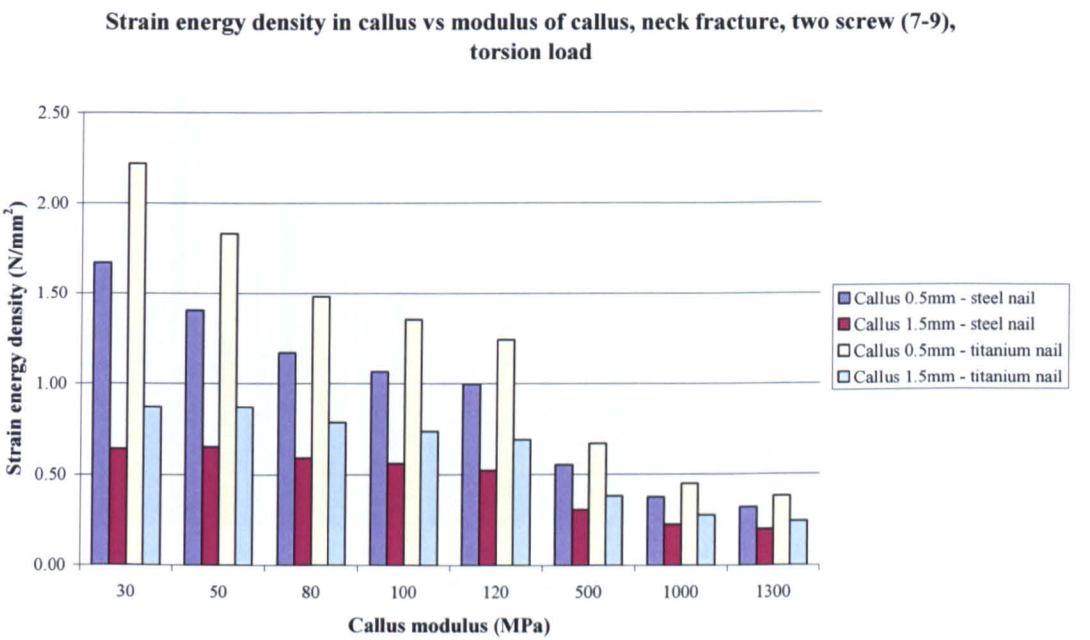

Figure 9.11 - Strain energy density in callus.

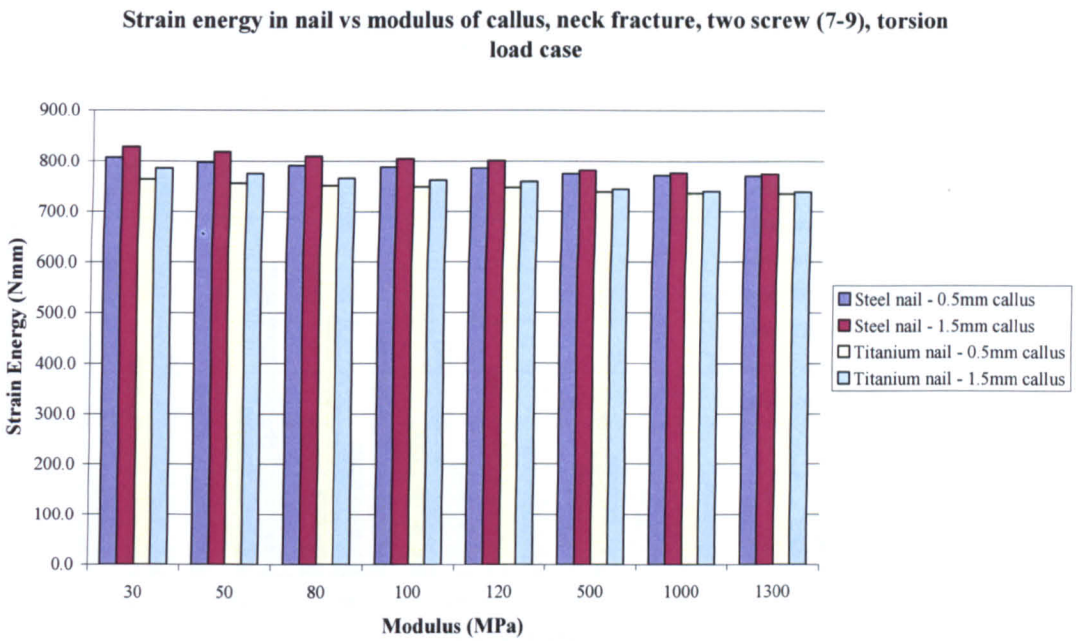

Figure 9.12 - Strain energy in nail.

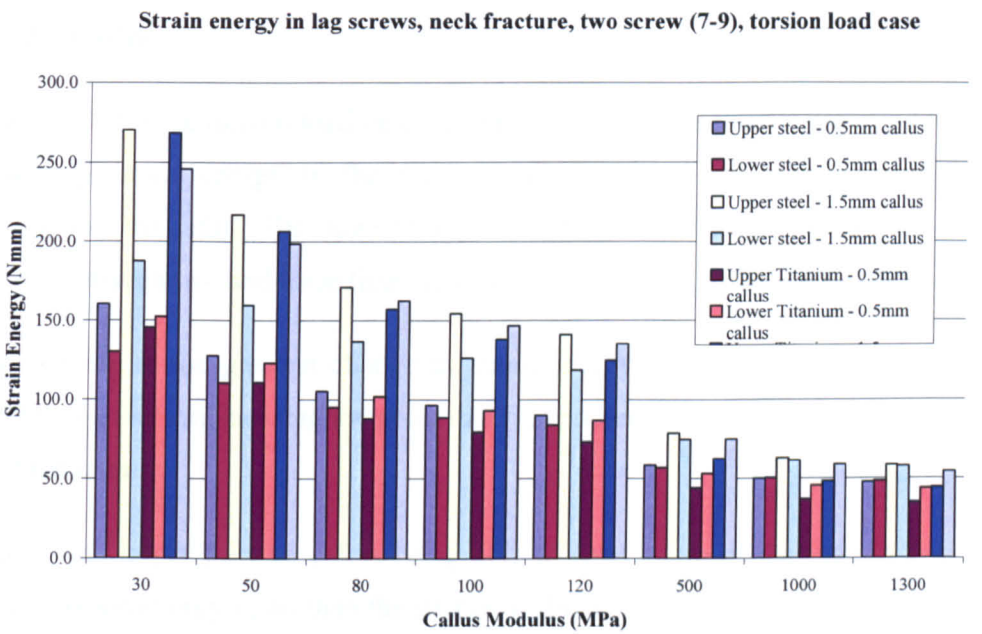

Figure 9.13 - Strain energy in lag screws.

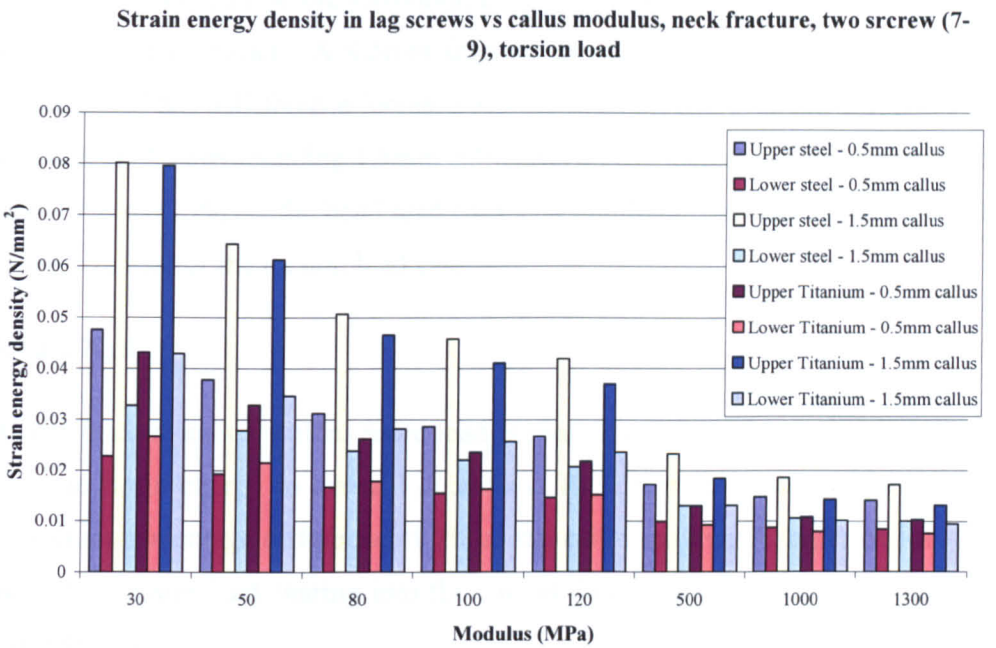

Figure 9.14 - Strain energy density in lag screws.

9.4.2.1 Callus

The trends for the torsion load case are similar to those observed in the bend load case. The strain energy in the fracture callus decreases with respect to the modulus of the callus. The strain energy in the fracture callus for the torsion load case is between two and three times that observed under the bend load condition.

Again there is the greatest change in strain energy of the callus at the lower moduli, further emphasising the point that it is prudent to have early stabilisation of the fracture.

Due to the larger fracture callus being able to carry more of the load, it has a greater strain energy value than the smaller callus size. The percentage difference increase from 0.5mm to 1.5mm for a 30MPa callus, fixed with a steel and titanium nail is 14% and 15% respectively.

More load is shared into the lag screws with a larger callus and the strain energy density in the smaller callus is greater than in the larger callus. A smaller callus results in more load share into the surrounding bone, causing a more highly stressed callus.

More load is shared into the surrounding bone when a titanium nail is used as the titanium nail is 'softer'. A 0.5mm fracture callus of 30MPa, stabilised with a titanium nail has a difference increase of 25% in strain energy when compared to a steel nail. A corresponding 1.5mm callus has a 26% increase. This is compared with 19% and 13% for the bend load case, and highlights the small effect that the callus size has for the torsion load case.

9.4.2.2 Nail

As the fracture callus stiffens more load is shared into the surrounding bone and thus the strain energy in the nail decreases. The decrease is only slight with a maximum percentage difference of 7% as the callus stiffens. A larger callus size promotes greater load sharing into the nail as there is less good quality bone to share the load.

Unlike the bend load case, the titanium nail has less strain energy than the steel nail for the torsion load case.

9.4.2.3 Lag screws

As the fracture callus stiffens the strain energy in the lag screws decreases with an inverse power relationship. The larger callus size has the greater strain energy in all cases and the titanium nail imposes further load sharing into the callus. The load sharing characteristics differ considerably from those observed for the bend load case.

For a steel nail with a 0.5mm callus, the upper lag screw has the greater strain energy at low callus moduli with a 20% difference increase for a 30MPa callus. This load share is reversed as the callus stiffens with the lower lag screw having the greater strain energy value for a callus of 1300MPa. The difference is 1%. Indeed, once the callus has stiffened, the proportion of strain energy into each lag screw is almost equal. A larger callus results in the lag screws having more strain energy, and again the upper lag screw has the higher strain energy, with a 31% difference increase for a 30MPa callus. This difference is reduced to 1% once the fracture has 'healed', and again the amount of load being carried into each screw is almost equal.

For a titanium nail with a 0.5mm callus the upper lag screw has less strain energy at low and high callus moduli. The percentage difference at 30MPa and 1300MPa is 4% and 24% respectively, showing that the load is shared more equally between the two screws at lower callus moduli.

For a 1.5mm callus size the lower lag screw has the higher strain energy at low callus moduli, and lower strain energy at high callus moduli. The percentage difference at 30MPa and 1300MPa is 8% and -23% respectively. The larger callus therefore promotes greater load sharing into the upper screw at low callus modulus, and into the lower screw for high callus modulus.

At low callus moduli the steel upper lag screw has more strain energy than the corresponding titanium upper lag screw with a 9% difference increase for 0.5mm, 30MPa callus. This difference increases to almost three fold for the 1.5mm callus with a difference of 24%. The steel lower lag screw has less strain energy than the corresponding titanium lower lag screw with a 14% difference decrease for 0.5mm, 30MPa callus. When the larger callus size is used there is an almost equal load share between the titanium and steel upper screws with a difference of 1%.

Once the callus has stiffened to above 200MPa, both the steel upper and lower lag screws have a greater strain energy value than the titanium lag screws (26% and 10% difference respectively for 0.5mm, 1300MPa callus).

At low callus moduli, the combined strain energy of the steel lag screws is less than that of the titanium lag screws, with a difference of 3% and 11% for a 0.5mm and 1.5mm callus respectively. The callus strain energy is increased by 25% when using a titanium nail. It is the upper titanium lag screw that has less strain energy than the corresponding steel lag screw and thus this is the most influential component on the fracture callus at low modului.

At high callus moduli, the combined strain energy of the steel lag screws is higher than that of the titanium lag screws with a difference of 18% and 15% for a 0.5mm and 1.5mm callus size respectively. This indicates that the callus strain energy is increased when using a titanium nail, which is observed in the 1300MPa callus with a 16% and 18% difference increase for a 0.5mm and

1.5mm callus respectively. Both the steel lag screws also have a higher strain energy than the corresponding titanium screws for a stiff callus, which indicates that the load being shared into the callus will increase.

Therefore at low callus moduli the upper lag screw in this configuration is the most influential on the fracture callus, and although the titanium lag screws combined strain energy is greater than the steel lag screws, the callus has a greater strain energy when titanium screws are used. As the callus heals, the load share between the two lag screws changes, and the combined strain energy of the two steel lag screws is higher than that of the titanium lag screws. The upper lag screw is still the more influential on the fracture callus.

The upper lag screw in all cases has the greater strain energy density indicating that it is more highly stressed. At low callus moduli the upper lag screw has typically about twice the strain energy density of the lower. The difference for a 30MPa callus and a steel nail is 52% and 59% for a 0.5mm and 1.5mm respectively, and the titanium differences are 37% and 46% respectively. This is an indication of the influence that the upper screw has on the surrounding callus, and the increased stress that it is under due to its reduced diameter. As the callus stiffens, the difference in strain energy density decreases as more load is being shared into the surrounding bone and thus the influence of the upper screw is reduced. At 1300MPa, with a steel nail the difference in strain energy density is 39% and 41% for a 0.5mm and 1.5mm callus respectively, and 24% and 27% for the titanium nail respectively.

Titanium lag screws have a smaller strain energy density than the corresponding steel lag screws for all callus moduli, and this strain energy density is also more evenly spread between the titanium lag screws than the steel.

9.4.3 Summary – bend load, (7-9) configuration

The larger callus size has a higher value of strain energy and a smaller value of strain energy density, indicating that the smaller fracture callus has a higher peak stress and that more load is shared into the surrounding bone. The use of a titanium nail results in greater load sharing into the fracture callus for all cases when compared to the steel nail.

Callus size and choice of material have a marked effect on the load shared into the callus for low callus moduli, or at the early stages of fracture healing. Once the fracture callus has stiffened, typically above 200MPa, the effect of callus size and material choice is considerably reduced. Therefore the aim of the design should be to optimise fracture healing at the early stages, when the choices available to the engineer and surgeon have their greatest impact.

The lower lag screw, being the larger of the two, always has the greater strain energy and the lag screws share the load between them more evenly at lower callus moduli for a larger callus size. The steel lag screws share the load between them more evenly than the titanium screws.

For healed fractures, both the upper and lower steel lag screws have more strain energy than the titanium lag screws and hence transmit a smaller load into the surrounding bone, resulting in a smaller strain energy in the callus. For a soft fracture callus, the lower titanium lag screw has more strain energy than the lower steel lag screw. At low moduli the choice of titanium will impart less loading into the inferior callus area and at higher moduli will impose greater loading into the region. The upper titanium screw will always impart more load into the superior callus region. Therefore as the callus always has a larger strain energy when a titanium nail is used, the upper screw is the more influential.

For low callus moduli the lag screws are under the greatest stress and share more of the load. The larger lag screw has the greater share of the load, and is under less stress at the early stages of fracture healing. When using steel screws, the upper screw is always under greater stress, and as the callus stiffens the stress-state in each screw becomes more equal. The stress distribution between the two titanium lag screws changes as the callus stiffens. Initially the smaller screw is more highly stressed, but as the callus stiffens the larger screw becomes more stressed. At low callus modulus approximately 2/5th of the load is shared into the upper and 3/5th into the lower for steel screws. For titanium screws approximately 1/3rd and 2/3rd of the load are shared into the upper and lower screws respectively.

9.4.4 Summary – torsion load, (7-9) configuration

The greatest change in strain energy of the fracture callus occurs at the early stages of fracture healing when the callus is relatively soft (<200MPa), emphasising the need for a competent fracture fixation technique at the early stages.

A smaller callus will be more highly stressed as more load is carried by the good quality surrounding bone, and transmitted through the callus. This is demonstrated from the strain energy density of the callus. The greatest load is shared into the callus when a titanium nail is used.

The steel lag screws share the load more equally between them once the callus has 'healed' and the upper lag screw always has the larger strain energy. The titanium lag screws share the load more equally between them at low callus moduli. For the 0.5mm callus the lower lag screw has the greater strain energy and the upper lag screw has more strain energy for the 1.5mm callus. For both the steel and titanium nail the screws share the load more evenly when a smaller callus size is used.

There is therefore an argument for using titanium lag screws to promote a more even load share into the callus. A smaller callus may also be preferential to share more load into the lower lag screw, which is capable of carrying higher loads. However the upper lag screw will be more highly stressed and the decision must also be balanced against the overall increase of load shared into the fracture callus.

For low callus modulus the steel upper lag screw has more strain energy than the titanium upper screw and the steel lower lag screw has less strain energy than the titanium lower screw. However, the combined strain energy of the steel lag screws is less than that of the titanium screws for low moduli and the strain energy in the callus is higher when titanium screws are used. Therefore at low callus moduli the upper lag screw is the most influential on the callus, and possibly more likely to fail. At high callus moduli the combined strain energy of the steel lag screws is higher than the titanium and thus it follows that the upper lag screw is the more influential in every case.

The upper lag screw always has the greater strain energy density and thus is always more stressed than the lower screw, substantiating the assertion that the upper lag screw is most likely to fail.

9.4.5 Neck fracture, one lag screw (12), bend load

Figures 9.15 to 9.18 represent the strain energy and strain energy density in the fracture callus, nail and lag screw as the callus stiffens.

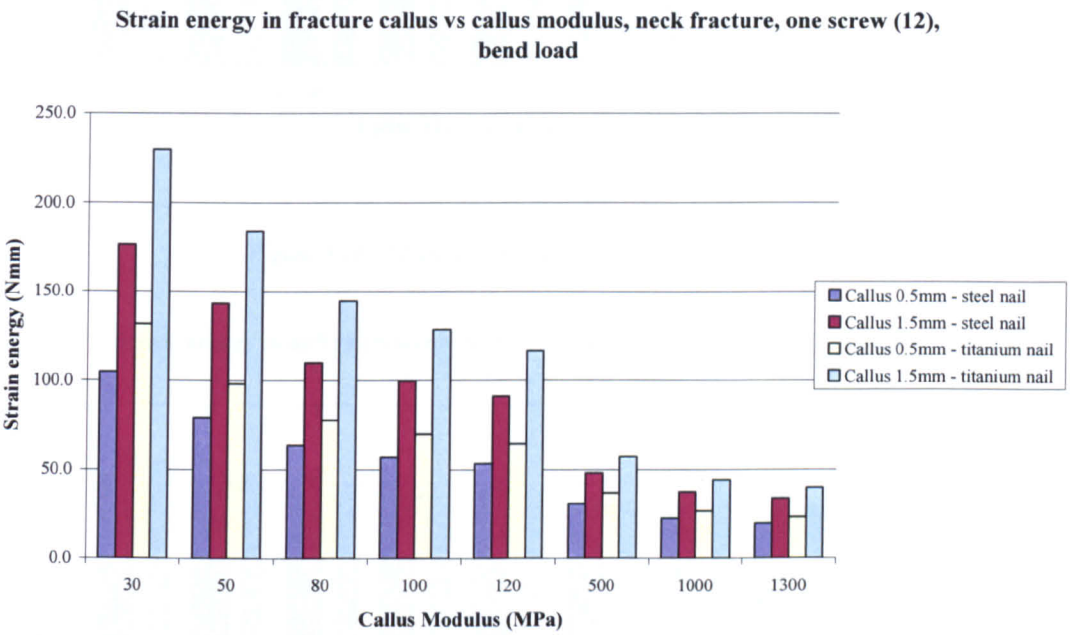

Figure 9.15 - Strain energy in callus.

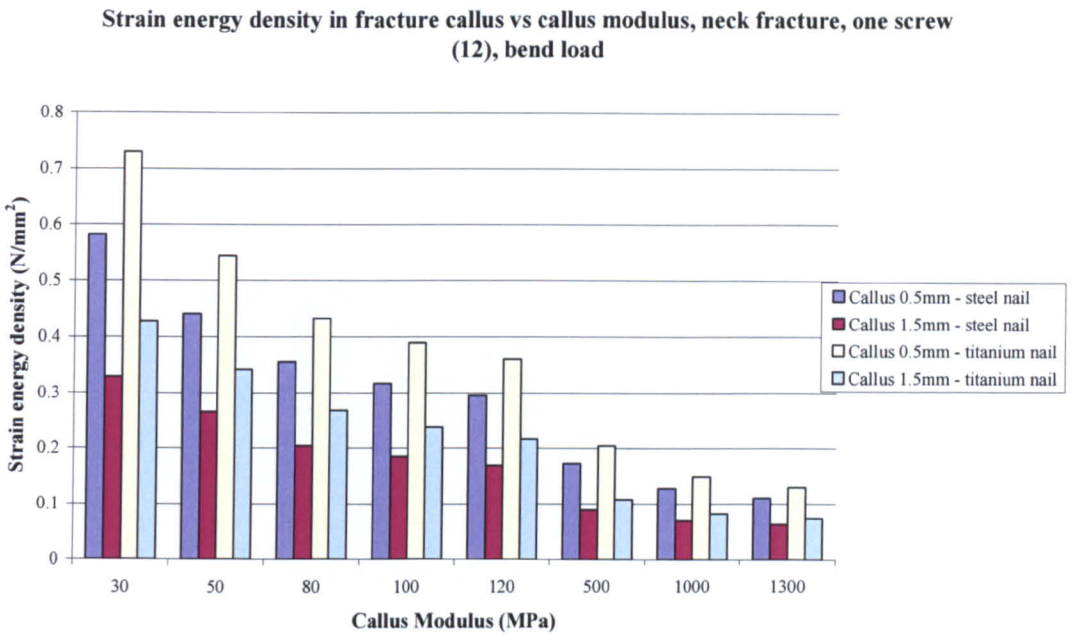

Figure 9.16 - Strain energy density in callus.

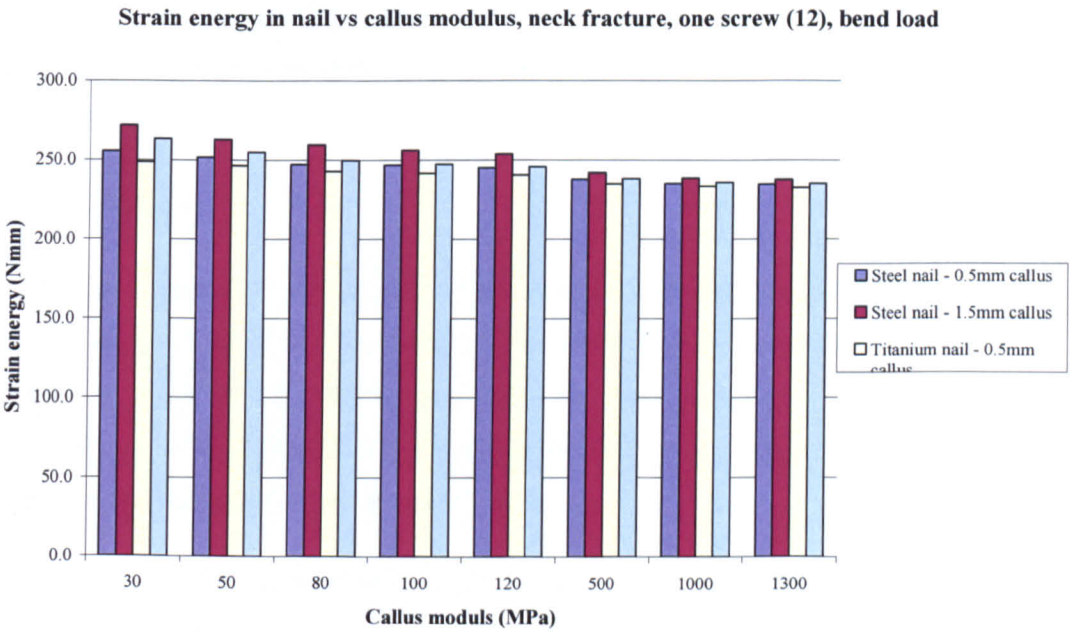

Figure 9.17 - Strain energy in nail.

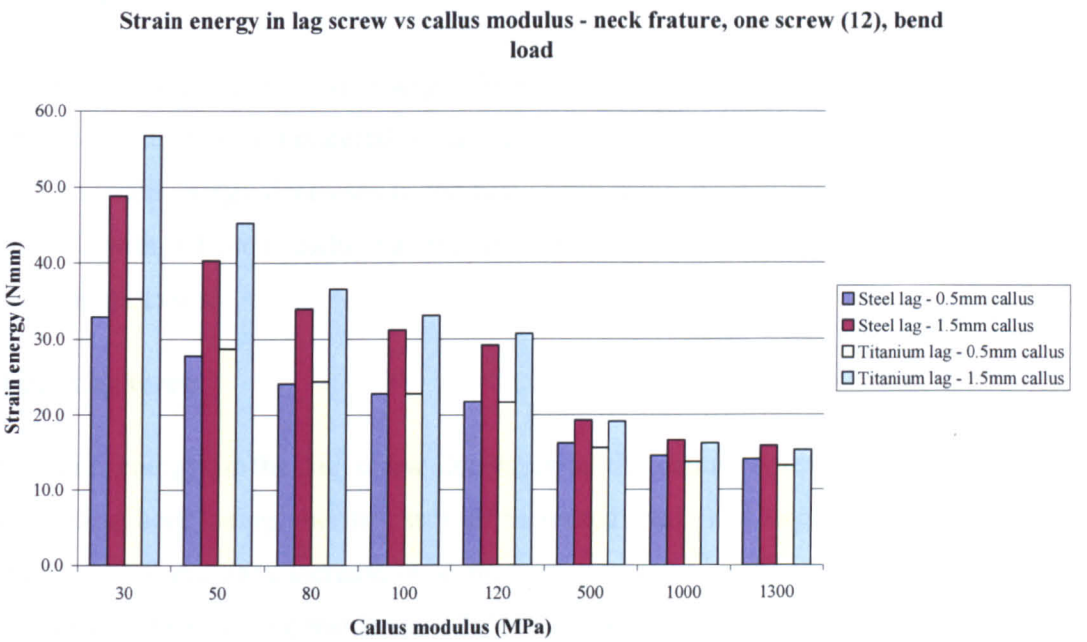

Figure 9.18 - Strain energy in lag screw.

The trends for the single screw configurations are similar to those described by the (7-9) screw configuration, and thus the same detail is not attributed to this fixation device. In the proceeding section there is a comparison between the two configurations.

9.4.5.1 Callus

The larger callus has the greater strain energy. The percentage difference increase from a 0.5mm to 1.5mm callus, for a steel nail and a fracture callus of 30MPa and 1300MPa is 41% in each case. The smaller callus is significantly more stressed, with a 40%-45% difference increase in strain energy density when comparing the callus size at each callus modulus.

It is in the use of a titanium nail and large callus size that the greatest strain energy in the callus is realised, some 23% larger than the corresponding steel nail, and it is in the use of a titanium nail and small callus size that the greatest strain energy density is imparted into the fracture callus with a 21% increase compared to the corresponding steel nail, when considering a 30MPa callus.

9.4.5.2 Nail

The strain energy and strain energy density remain relatively constant with respect to callus size and material of nail. The maximum percentage difference is 2%. The strain energy decreases in the nail as the callus moduli increases and a steel nail with a 1.5mm callus has the greatest strain energy and strain energy density in all cases.

9.4.5.3 Lag screw

The strain energy in the lag screw decreases as the callus stiffens due to the surrounding bone being able to carry an increased load. The larger callus size imparts a 33% and 38% increase in strain energy into the steel and titanium lag screw respectively when considering a 30MPa callus.

For a soft callus, the titanium lag screw has an increased load share, yielding the greater strain energy value. For a 30MPa callus the titanium screw has an increase of 7% and 14% for a 0.5mm and 1.5mm callus respectively when considering a 30MPa fracture callus. Once the callus has stiffened however the titanium lag screw has a smaller strain energy value than the corresponding steel nail, with a percentage difference of 6% and 3% decrease for the same comparison.

As the callus heals, the strain energy density in the lag screw decreases. At low callus moduli the steel lag screw has less strain energy density than the titanium lag screw, with a percentage difference of 9% and 14% for a 0.5mm and 1.5mm callus when considering a 30MPa callus. These differences between the steel and titanium lag screws are reduced to within 1% once the fracture callus has healed, indicating that for a healed fracture there is little difference in the stress state of a steel or titanium nail.

9.4.6 Neck fracture, one lag screw (12), torsion load

Figures 9.19 to 9.23 represent the strain energy and strain energy density in the fracture callus, nail and lag screw as the callus stiffens.

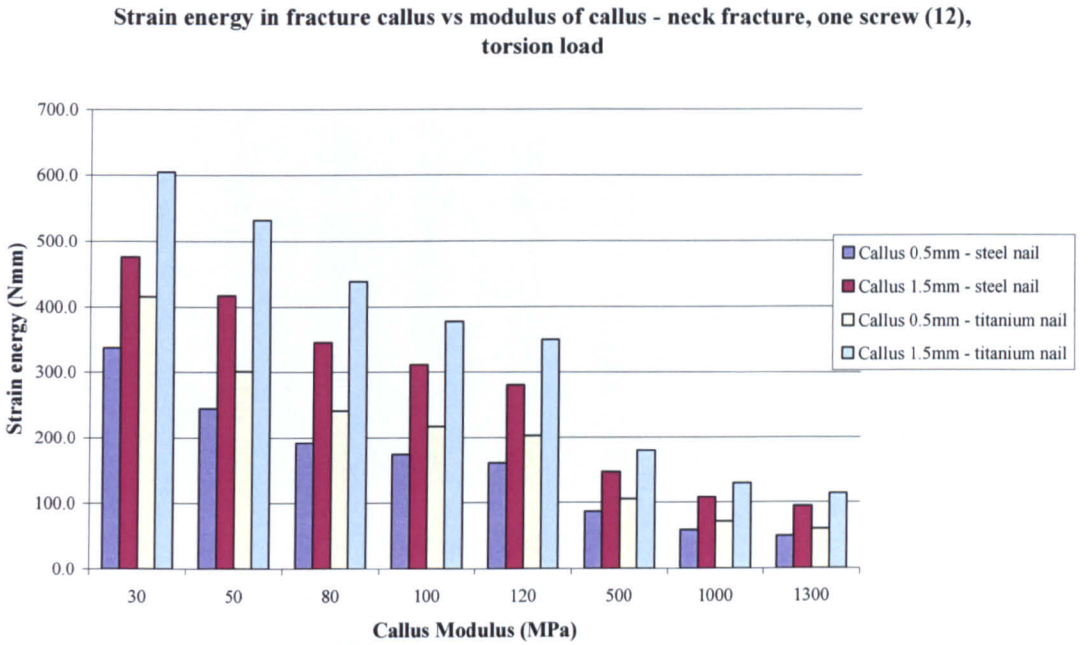

Figure 9.19 - Strain energy in callus.

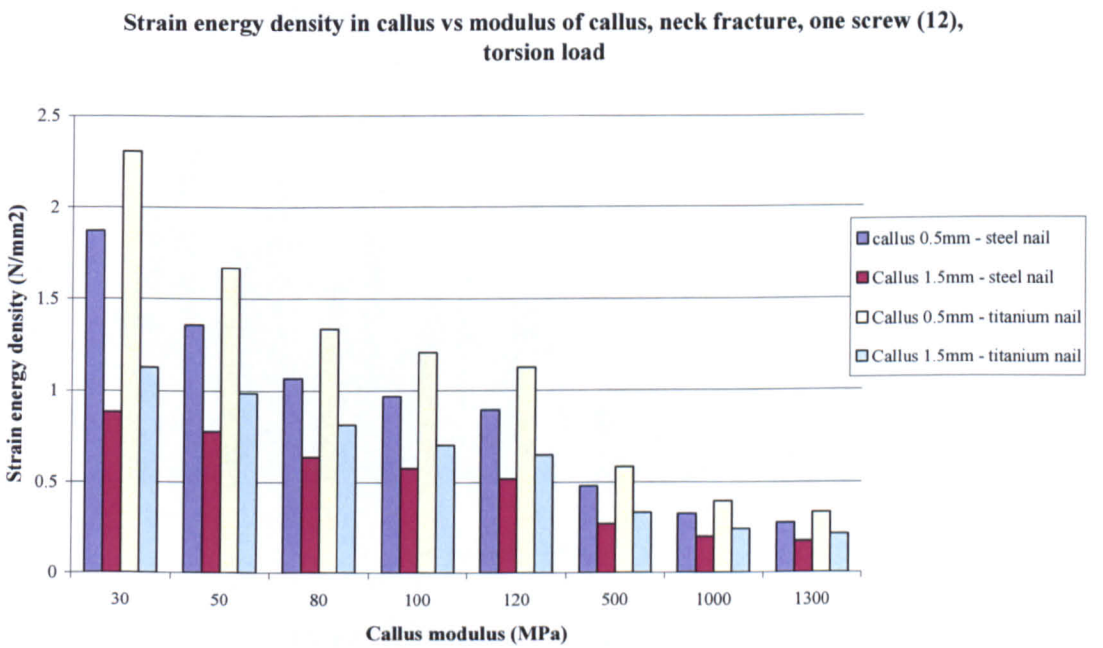

Figure 9.20 - Strain energy density in callus.

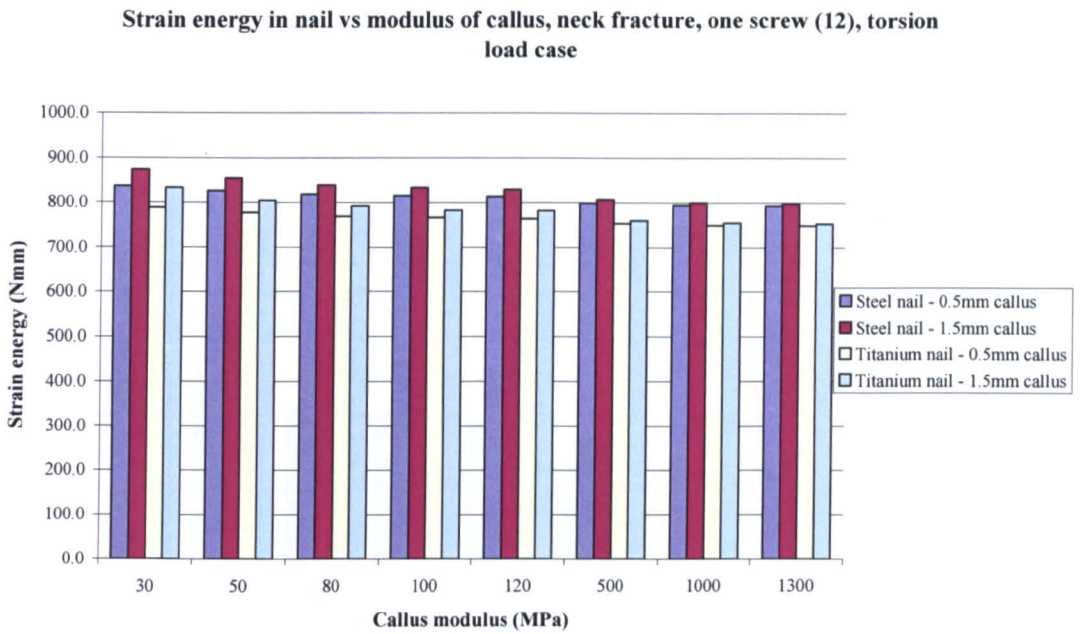

Figure 9.21 - Strain energy in nail.

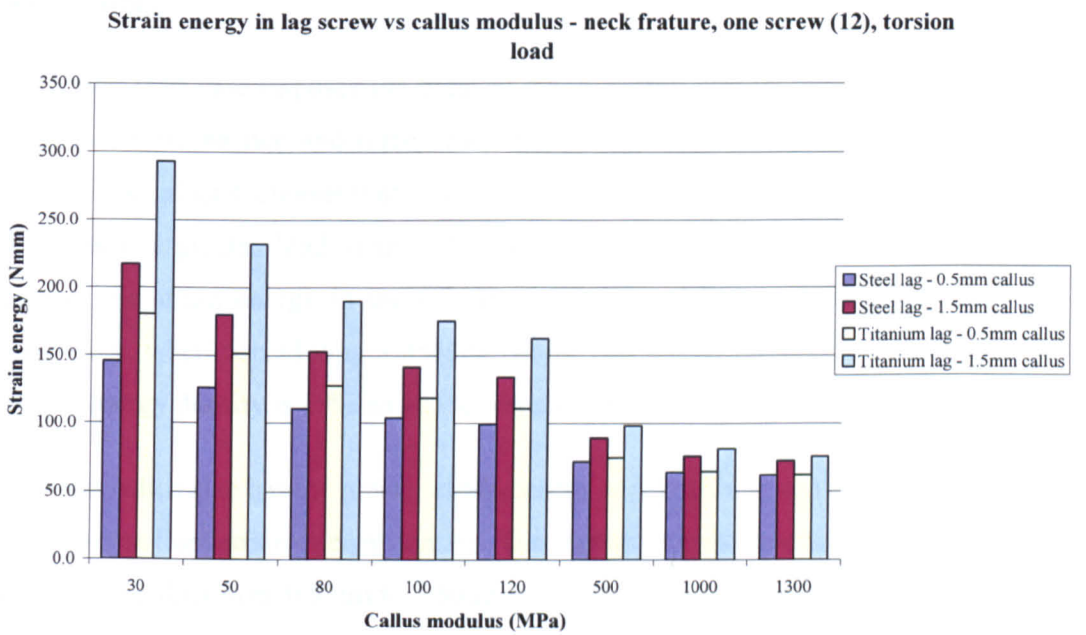

Figure 9.22 - Strain energy in lag screw.

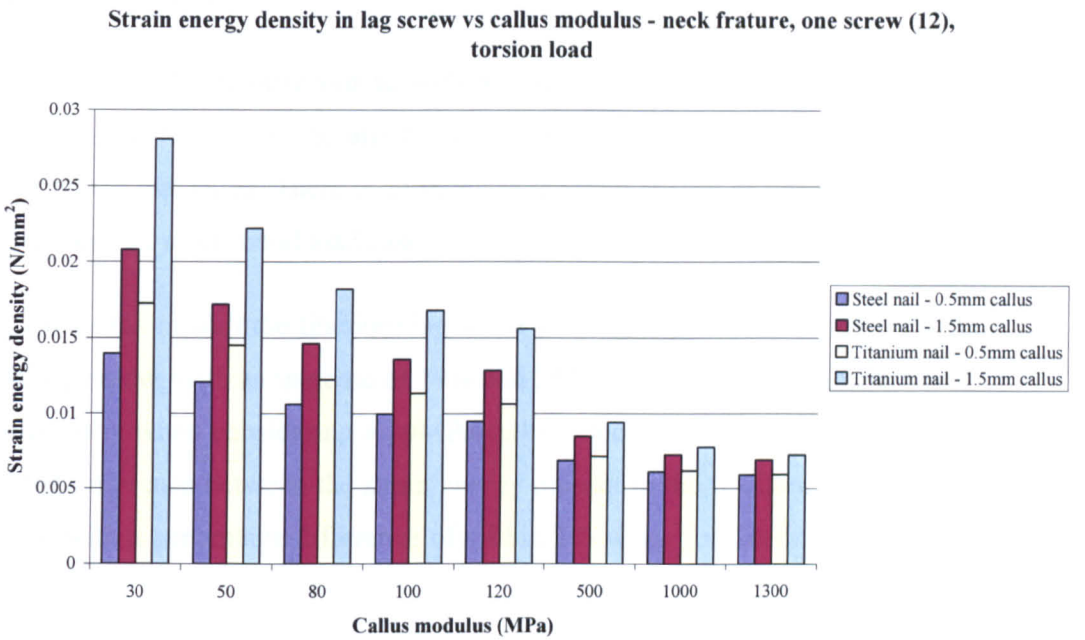

Figure 9.23 - Strain energy density in lag screw.

9.4.6.1 Callus

The torsion load case imposes the greatest strain energy into the callus, with an increase of between two and three times that of the bend load case. The strain energy in the callus decreases with respect to the callus stiffness, and the titanium nail imparts a greater load share into the callus. The use of a titanium nail increases the strain energy in the 0.5mm and 1.5mm callus by 18% and 21% respectively, when considering a 30MPa callus, and the corresponding increase in strain energy density is 19% and 21% respectively.

The larger callus size has the greater strain energy as it is able to carry more load, but yields the least strain energy density. The increase in strain energy observed for a 30MPa callus from 0.5mm to 1.5mm is 29% and 31% for steel and titanium nails respectively. The decrease in strain energy density is 53% and 52% for a 0.5mm and 1.5mm callus, steel and titanium nail respectively.

9.4.6.2 Nail

The strain energy decreases in the nail as the callus moduli increases and the steel nail with a 1.5mm callus yields the greatest strain energy and density in all cases.

9.4.6.3 Lag screws

The same trends are observed as with the bend load case. However, there is a substantial difference in the amount of strain energy imparted into the screws between the two cases. There is an increase in strain energy of between four and five times that of the bend load case.

At low callus moduli the titanium lag screw has a greater strain energy than the steel lag screw, with an increase of 19% and 26% for a 0.5mm and 1.5mm callus respectively when considering a 30MPa callus. Once the callus has healed there is little difference between the strain energy present in the titanium and steel lag screw, with a percentage difference of within 1% when considering a 1300MPa callus.

There is a similar trend with strain energy density. At the early stages of fracture healing the steel nail has less strain energy density than the titanium nail, with a difference of 18% and 25% for a 0.5mm and 1.5mm callus respectively when considering a 30MPa callus. The difference in strain energy density once the fracture has healed is considered negligible with a percentage difference of within 1%.

9.4.7 Summary – bend load, (12) configuration

When a smaller callus size is used, there is a reduced load shared into it, but it is more highly stressed. The use of a titanium nail results in greater load being shared into the fracture callus, and as such the greatest load share into the callus is achieved when using a large callus size and a titanium nail. The most highly stressed fracture callus is observed by using a titanium nail and the smaller callus size.

The steel lag screws are able to carry a greater share of the load than the titanium lag screws. At high callus modulus (>200MPa) the steel lag screw has the greater strain energy value.

At low callus modulus there is less load share into the surrounding bone and an increase in deflection of the titanium lag screw. The titanium lag screws therefore have the greater strain energy.

A titanium nail significantly increases the load carried, and resulting stress into the fracture callus. The choice of material will determine how effectively the fracture heals.

9.4.8 Summary – torsion load, (12) configuration

A titanium nail results in more strain energy in the fracture callus and lag screw because the titanium nail is not as stiff as steel. At low callus moduli this effect is more noticeable. Once the callus has healed the difference in strain energy between a steel and titanium lag screw is negligible. It is the capacity of the steel nail to carry a greater load, the load share into the surrounding bone and the increased deflection of the titanium system that yields a similar strain energy for the titanium and steel lag screw once the fracture has healed.

It is important to use an optimum design of fracture stabilisation at the early stages of fracture healing when the choice of material properties and callus size has the greatest effect on the system.

9.4.9 Bend load comparison, (12) and (7-9) configuration

Figures 9.24 to 9.26 represent the strain energy and strain energy density in the fracture callus, nail and lag screw as the callus stiffens.

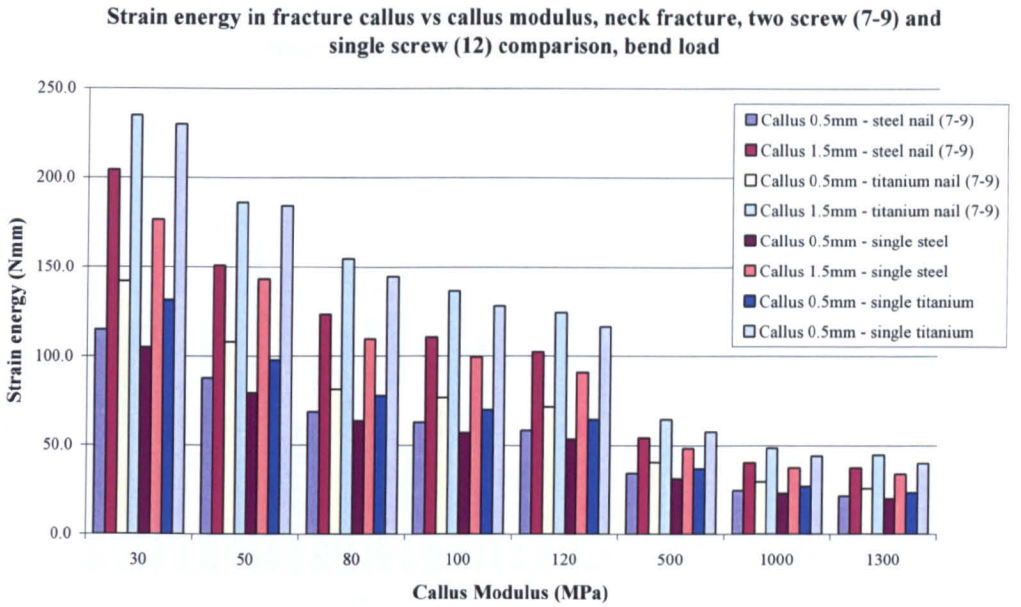

Figure 9.24 - Strain energy in callus.

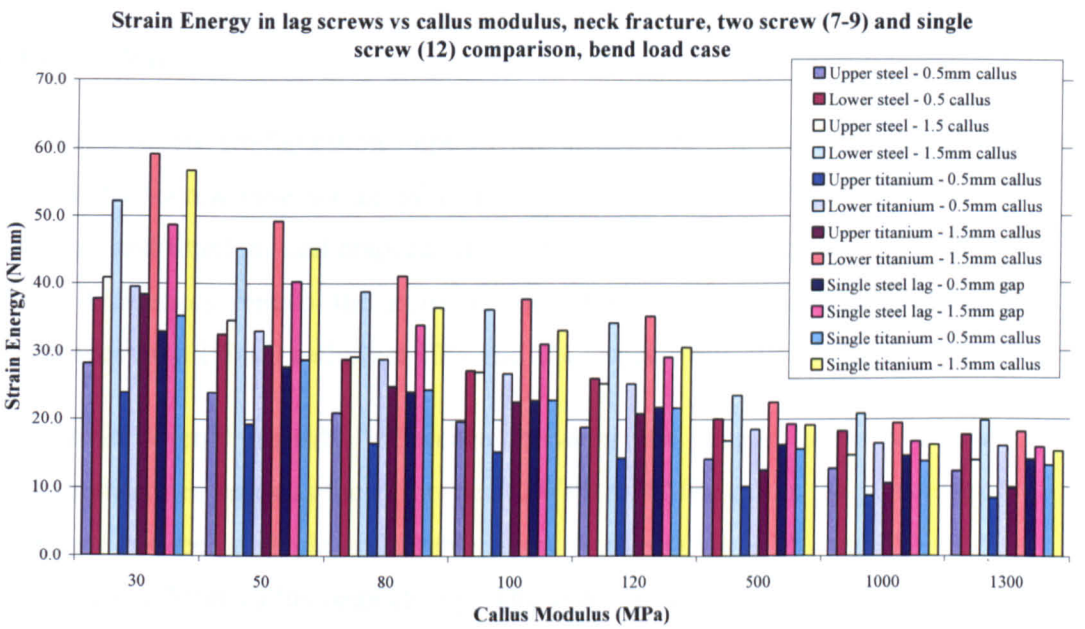

Figure 9.25 - Strain energy in lag screws.

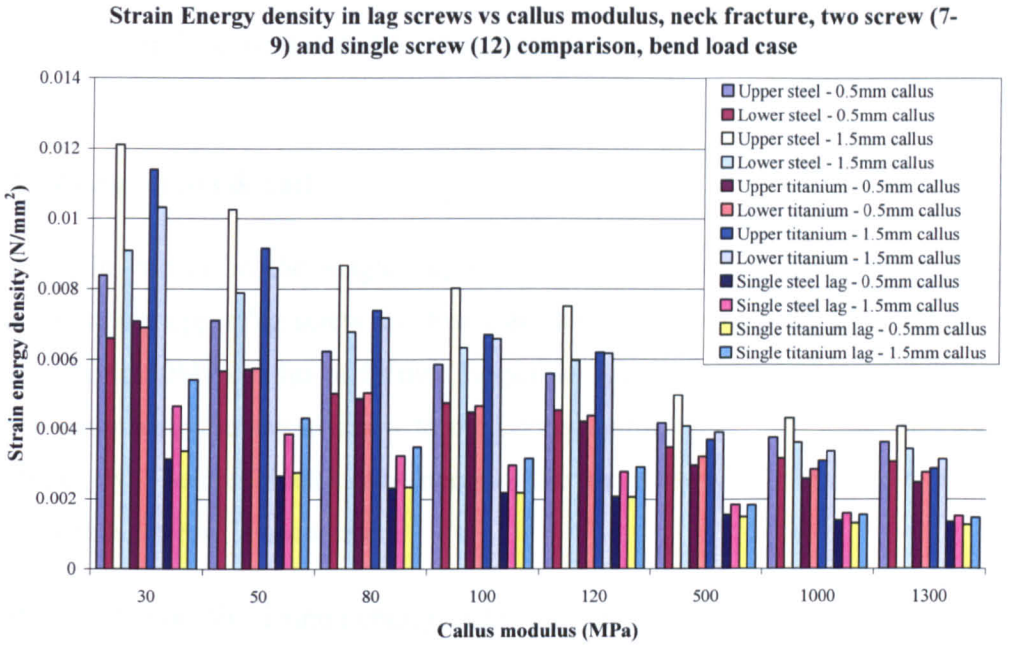

Figure 9.26 - Strain energy density in lag screws.

9.4.9.1 Callus

The single screw configuration imposes less load share into the fracture callus than the two-screw case for all callus moduli. The difference 9% and 7% for a steel nail and titanium nail respectively, considering a 0.5mm callus at 30MPa. These differences remain the same as the callus heals. The corresponding differences for a 1.5mm callus are 13% and 2% respectively.

The strain energy density difference between the single and two-screw configuration decreases as the callus heals. With a 30MPa callus the percentage difference between a single and double screw configuration is 6% and 8% for a 0.5mm and 1.5mm callus respectively. The corresponding titanium differences are 4% and 2% respectively. Once the callus has stiffened to 1300MPa, the differences between the single lag screw and two lag screw case are almost identical (<1%).

Considering a 0.5mm callus and a steel nail, the von Mises stress in the healed fracture are within 1% when comparing the single and two screw case. The difference is larger at the early stages of fracture healing, by 28%. The strain

energy density difference of 6% for the same case and is such, because the distribution of the constituent stresses are taken into account rather than the peak values.

9.4.9.2 Lag screws & nail

The strain energy in the single lag screw is always larger than that in the corresponding upper lag screw and less than that of the corresponding lower lag screw. For a 30MPa callus of 0.5mm the percentage difference is 14% and 13% when comparing the single screw to the corresponding upper and lower screws respectively. The combined strain energy of the two screws is about twice that of the single lag screw in each case.

Although the combined strain energy of the lag screws is twice that of the single lag screw, the strain energy in the callus is similar. The volume of the callus with two screws is slightly larger than that with the single lag screw, (11mm^2). It is a balance between the strain energy of the lag screws, the strain energy of the nail, the deflection of the system and the ability of the callus to carry the load in both the two screw and single screw case that causes the fracture callus to share the load equally.

Using a two-screw configuration significantly reduces the maximum von Mises stress in the lag screw insertion hole when compared to the single lag screw case. For a 0.5mm callus at 1300MPa with a steel nail, the peak von Mises stress is observed to increase by 42% when using a single lag screw.

9.4.10 Torsion load comparison, (12) and (7-9) configuration

Figures 9.27 to 9.29 represent the strain energy and strain energy density in the fracture callus, nail and lag screw as the callus stiffens.

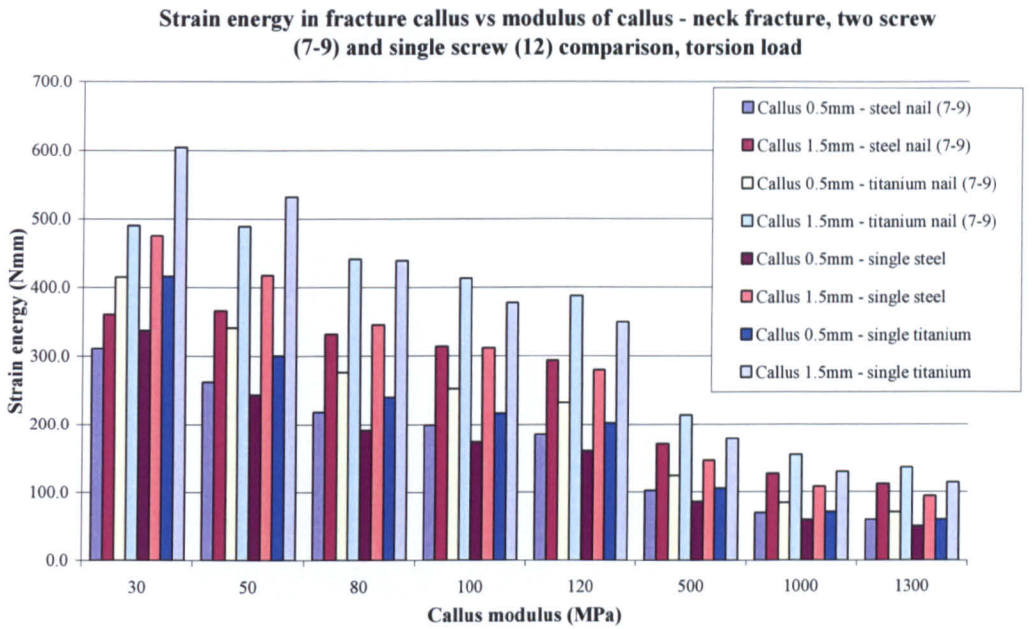

Figure 9.27 - Strain energy in callus.

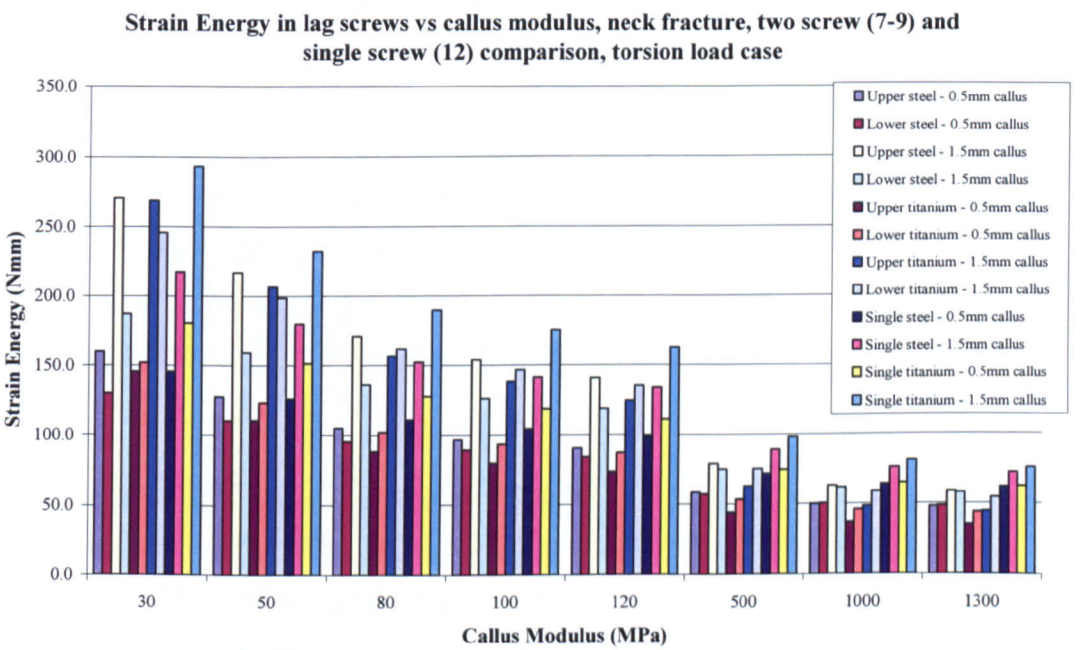

Figure 9.28 - Strain energy in lag screws.

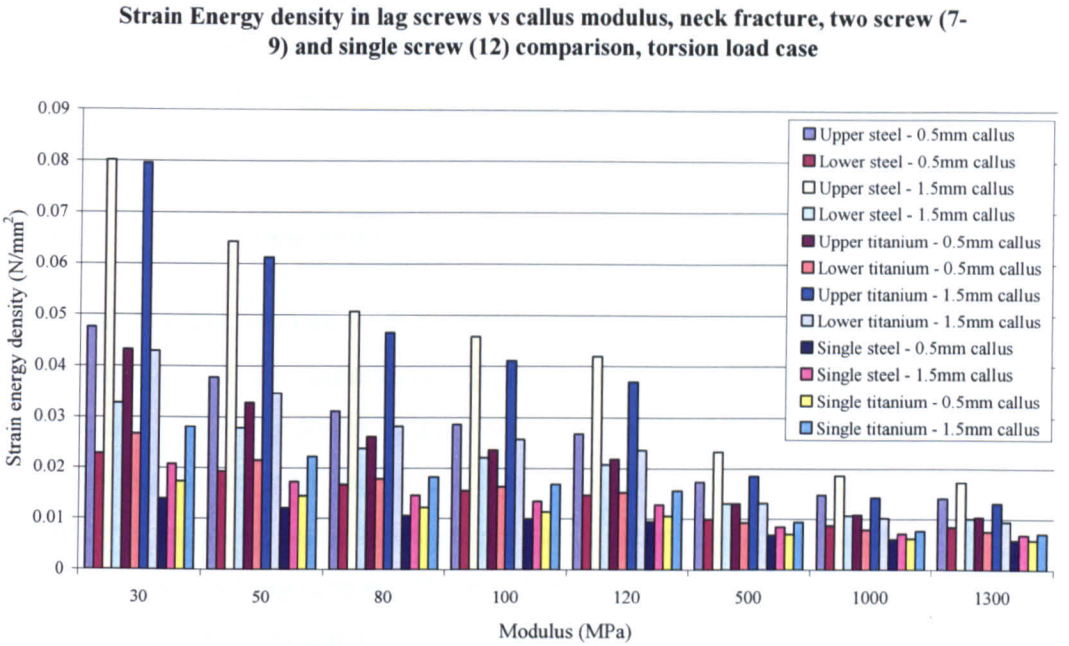

Figure 9.29 - Strain energy density in lag screws.

9.4.10.1 Callus

At low callus moduli the strain energy in the fracture callus is higher for the single lag screw than that of the two-screw configuration. For a 30MPa callus with a steel nail the difference increase is 8% and 24% for a 0.5mm and 1.5mm callus respectively, and the corresponding titanium increases are 0.3% and 19% respectively.

As the callus stiffens its strain energy is smaller for a single lag screw. For a 1300MPa callus with a steel nail the difference decrease is 16% and 17% for a 0.5mm and 1.5mm callus respectively, and the corresponding titanium decreases are 15% and 16% respectively.

A similar trend is observed with the strain energy density of the fracture callus. At low callus moduli the single screw configuration imparts a greater strain energy density into the fracture callus. There is an 11% and 32% difference increase for a 0.5mm and 1.5mm size callus of 30MPa, respectively, when fixed with a steel nail. The corresponding titanium differences are 4% and 20% respectively.

The fracture callus stabilised with the two screw configuration has the higher strain energy density once the fracture has healed, showing an increase of 13% and 10% for a steel nail and a 1300MPa callus of 0.5mm and 1.5mm respectively.

9.4.10.2 Lag screw and nail

When stabilising a fracture with a steel nail, the single lag screw has greater strain energy than the corresponding lower steel screw in the two-screw configuration. There is lower strain energy in the single lag screw than the corresponding upper steel lag screw. Once the callus has modulus is above 100MPa the single lag screw has a greater strain energy value than either of the upper or lower steel lag screws. The combined strain energy of the upper and lower screw in the two-screw case is always around twice that of the strain energy of the single lag screw. For a 30MPa callus the percentage difference between the single screw and the two-screw configuration for a 1.5mm callus is 9% and 11% for the upper and lower screw respectively.

At low callus moduli, the single steel lag screw has less strain energy than the corresponding upper lag screw, and more load is shared into the fracture callus. At high callus moduli the strain energy in the single steel lag screw is greater than that present in the upper lag screw, and the callus fixed with a single lag screw has a lower strain energy value. The pattern of strain energy in the fracture callus is limited by that shared into the upper lag screw.

The single titanium lag screw always has a higher strain energy value than either the corresponding upper or lower lag screws. For a 30MPa, 0.5mm callus the difference is 19% and 16% for the upper and lower lag screws respectively. The combination of the upper and lower strain energy of two lag screws is always approximately twice that of the single lag screw for low callus modulus and thus the two screws are capable of carrying more of the load, resulting in a smaller strain energy in the fracture callus at low callus moduli. The combined strain energy for the two screw is approximately 1.3 times that of the single screw for the 'healed' fracture and for this load share the callus observes a larger strain energy for the two screw case.

The use of a single lag screw significantly increases the peak von Mises stress in the lag screw insertion hole. For a healed callus using a titanium nail, the increase in von Mises stress with a 0.5mm callus is 57%.

9.4.11 Summary – bend load, (12) and (7-9) configuration

There is a greater load shared into the fracture callus when using a double screw (7-9) configuration compared to a single 12mm lag screw, with a difference of about 10%. The two-screw callus has a slightly smaller area, and thus is not as stiff as the single screw case, thus enabling a greater load share into the fracture callus.

By using a single lag screw to fix a neck fracture, under the bend load case, less load is shared into the fracture callus, and as a result the callus is also slightly less stressed. The difference in the two cases is only small however, and possibly can be considered negligible when considering other biocompatible effects, and stages of fracture healing.

The use of a single lag screw reduces the stress in the callus and there is the greatest difference when considering the softer callus, which again indicates that the design choice should be considered at the early stages of fracture healing.

There is more strain energy in the two lag screws combined than the single screw, which is countered by a decrease in strain energy of the nail. The deflection of the two problems is very similar and the callus with two lag screws has a larger volume, resulting in the callus being able to carry a larger share of the load. The combined effect is for the callus to carry a similar amount of load in either the single or double lag screw case, and there is little difference between these two fixation methods when considering the load carried by the callus.

The use of a single lag screw results in almost double the peak von Mises stress in the larger lag screw insertion hole and the likelihood of failure about the insertion hole is significantly increased. When using a single lag screw there is more material removed from the nail and thus the stress raiser is much more significant. This observation must clearly be weighed against any benefits that the single lag screw may have to the fracture callus.

9.4.12 Summary – torsion load, (12) and (7-9) configuration

At low callus moduli the single lag screw results in a greater amount of strain energy in the fracture callus. Once the callus has stiffened significantly (more than 100MPa), the two-screw configuration imparts more strain energy into the callus. There is thus an indication to use the two-screw configuration at the early stages of fracture healing as there is less load transferred into the callus. Once the callus has healed the increase in load being carried may be considered negligible when compared to the increased ability of the callus to carry the load. Moreover, an increased load share for the healed callus is advantageous as it aids in the prevention of stress shielding. It is also noted that a smaller fracture callus results in less of a difference between the two and single screw configuration.

There is an implication that the upper lag screw is the most significant in the torsion load case, providing rotational stability and defining the pattern of load share into the fracture callus. It would appear to be beneficial to use two lag screws for low callus modulus when considering the torsion load case as a smaller load is shared into the fracture callus.

The combined strain energy of the upper and lower lag screws is always larger than that of the single lag screw case, but the strain energy present in the fracture callus is higher at low callus modulus and lower at high callus modulus for the single screw case. Furthermore the total strain energy and deflection of the femoral head is always greater for the two lag screw configuration. It is the load share between the lag screws that determines the load shared into the callus. When the combined strain energy of the two lag screws is twice that or more than the strain energy in the single lag screw (as happens at low callus moduli), there is more strain energy shared into the callus for the single screw case. When the combined strain energy of the two lag screw configuration is twice that or lower than that of the single lag screw case (as occurs at higher callus modulus) then there is more strain energy shared into the callus fixed with the two screw configuration.

When considering the influence of a single lag screw and two screw configuration, it is essential to consider the stress concentration about the lag

screw insertion holes. A single 12mm lag screw can increase the peak von Mises stress in the insertion hole by over 50% and could be a limiting factor in the failure of an intramedullary device.

9.4.13 Two screw configurations

An assessment is given on two different two screw configurations, (9-7) and (8-8). These are compared to the (7-9) configuration with respect to the load shared into the fracture callus and the lag screws. At the end of this section all three configurations are compared with the single lag screw case (12). Results are presented before the comparison of all configurations in figures 9.30 to 9.35 for the torsion load case only and for all four configurations.

9.4.13.1 (9-7) and (7-9) comparison

The two-screw configuration above is based on the only commercially available implant at the present time, which comprises of the upper lag screw being of a smaller diameter than the lower lag screw. For completeness and in the interests of this study two further configurations have been considered. The first consists of the upper lag screw being larger in diameter (9-7) and the second has the two lag screw of equal diameter (8-8), with a total area reduction in the callus being similar to the other two configurations.

It is in the assessment of the lag screws and callus that are of most significance when considering different lag screw configurations and thus the following discussion emphasises these parts of the model.

9.4.13.2 Neck fracture, bend load (9-7) and (7-9) configurations

9.4.13.3 Callus

There is a similar general trend for the (9-7) and (7-9) configurations. The titanium nail imparts more strain energy and strain energy density into the fracture callus, and there is a decrease in strain energy as the callus stiffens. For a steel construct, the (9-7) configuration always imparts a smaller load share in to the callus, as expected due to the upper screw having a greater load carrying

capacity. The difference is small, with a 6% and 7% increase for 30MPa and 1300MPa callus respectively.

The use of a titanium nail and (9-7) configuration imparts a greater load share into the callus for low moduli, albeit small (2%), and a reduced load share for high callus moduli, again relatively small at 7%. This is because the titanium lag screws share the load more evenly between them. At higher callus modulus the surrounding bone is able to carry a greater proportion of the load and thus more load is shared into the upper screw.

9.4.13.4 Lag Screws

The larger of the two lag screws always carries the majority of the load. By observing the total strain energy of the lag screws, there is a difference of less than 1% for either configuration. This is expected due to the combination of the lag screws having the same load carrying capacity. The combined strain energy for the (9-7) configuration is larger due to less load being carried into the bone, as the load path results in the larger screw carrying a greater load in this configuration. The use of steel screws at low callus moduli results in the larger screw of the (9-7) configuration carrying 14% more load than the corresponding screw in the (7-9) case. This difference is 10% for high callus moduli.

There is little difference in the load shared into the callus and by the combined effect of the lag screws for either configuration. There is however a stark difference in the peak Von Mises stress at the insertion holes and in the lag screws due to the way in which the load is carried.

For a steel screw at low callus moduli there is a 21% increase in the peak Von Mises stress at the upper insertion hole, and a 20% increase in the upper lag screw. The corresponding differences once the callus has healed are 11% and 5% respectively. The large difference observed for a soft callus highlight the increased likelihood of failure for the (9-7) configuration. This is the case due to the upper (9) lag screw carrying the greatest amount of load, and thus transferring it to the insertion hole where the nail is weakest.

Titanium lag screws share the load more evenly between them and as a result the corresponding peak von Mises stress is different from the steel counterparts. For low callus moduli there is an increase in the von Mises stress in the screw and the insertion hole of 22% and 4% respectively. The larger insertion hole has a higher stress level, as the upper screw (9) is able to carry more load. Once the callus has healed, there is a decrease in the peak von Mises stress at the larger insertion hole of 17%, and an increase in the screw by 5%.

The (7-9) configuration shares the load between the two screws more evenly. This is independent of whether the screws are steel or titanium. For a steel screw and a 30MPa callus modulus, the larger screw carries 1.3 times the load of the smaller screw. This difference is 1.8 times for the (9-7) configuration. The increased load sharing of the (7-9) configuration results in the smaller screw observing a higher strain energy density, which is an indication of the smaller screw being more highly stressed. Indeed, the peak von Mises stress observed in the smaller steel screw is higher than that in the larger screw. This trend is observed for all callus modulus. As the load is not shared as equally for the (9-7) configuration the larger screw observes the greater strain energy density for low callus moduli. As the callus stiffens the smaller screw observes the higher strain energy density.

For a titanium nail the larger screw carries 1.5 times and 1.8 times the load for the (7-9) and (9-7) configuration respectively. The smaller screw in the (7-9) configuration and the larger screw in the (9-7) configuration observe the greater strain energy density. As the callus increases in stiffness the effect is to have the larger screw in the (7-9) configuration and the smaller screw in the (9-7) configuration having the greater strain energy density.

The above load sharing characteristics relate to how evenly spread the load will be throughout the fracture callus. The load share between the screws is not expected to be equal as they are of different sizes. The strain energy density provides an indication of the proportion of load shared into each screw with respect to its load carrying capacity. With this in mind, it is the (9-7) configuration that shares the load more evenly between the screws with respect to its load carrying capacity. The stress in the upper lag screw for this

configuration is highest as well as the peak stress in its insertion hole. Furthermore, the load is not carried into the callus evenly. There is thus a balance between the load shared between the screws, induced stress levels at the insertion holes, and the load shared relative to the capacity of the screws. If the desire is to spread the load into the callus evenly, than the (7-9) configuration is most desirable at low callus moduli. Once the fracture is considered healed than the (9-7) configuration may be more beneficial.

9.4.14 Neck fracture, torsion load, (9-7) and (7-9) configurations

9.4.14.1 Callus

The general trend for the (9-7) configuration is similar to that of the (7-9) configuration, such as the titanium nail carrying a smaller amount of the load and thus increasing the strain energy of the fracture callus. For a steel nail the lag screws in the (9-7) configuration always imparts a smaller load share into the callus as expected due to the upper screw now having a greater load carrying capacity and the load path being such that the larger upper screw will carry the greater proportion of the load. The difference is quite significant at low callus modulus with a 18% decrease, whereas at higher callus moduli the difference is 7% considering 30MPa and 1300MPa callus stiffness respectively. The same effect is observed when a titanium nail is used. The reduction in strain energy between the (9-7) and (7-9) configuration is 8% and 4% for 30MPa and 1300MPa callus modulus respectively.

9.4.14.2 Lag Screws

The upper lag screw always carries the majority of the load, and is independent of the size of the screw. The combined load carried by the two lag screws is similar for both configurations as expected. It is the (7-9) configuration that carries more of the load with a 9% and 3% increase in strain energy at a callus of 30MPa and 1300MPa respectively, when fixing the fracture with a steel nail. The same trends are observed when using a titanium nail.

The (7-9) configuration shares the load between the screws more evenly whether a titanium or steel nail is used. When considering a steel nail, the upper lag screw

has 1.4 times the strain energy of the lower, at a callus modulus of 30MPa. The upper lag screw in the (9-7) configuration has 3 times the strain energy of the lower screw for the same callus modulus. A similar trend is observed for the titanium nail and this observation would indicate that the (9-7) configuration is better suited to torsional stability for low callus modulus. Indeed, the maximum deflection at the femoral head when stabilising the fracture with a (9-7) configuration is less than when a (7-9) configuration is used.

Once the callus has reached 1300MPa, the steel lag screws in the (7-9) configuration share the load carried between them equally, with a difference in strain energy of less than 1%. For the (9-7) configuration however the upper screw (9) has 3.5 times the strain energy as the lower screw. As the callus heals more load is shared into the bone, and less is carried by the lower lag screw. The upper lag screw being the larger in the (9-7) configuration therefore carries a greater amount of the total load.

When a titanium nail is used, the load share between the lag screws for the (7-9) configuration changes as the callus heals. Initially the upper lag screw carries the majority of the load, and once the callus has stiffened to 100MPa the lower lag screw carries the majority of the load. This is attributed to the titanium lag screws sharing the load more evenly and hence a greater load is shared into the larger screw. This is not the case for the (9-7) configuration, whereby the upper screw always carries a higher proportion of the load as the callus heals.

The implication of the (9-7) configuration sharing a greater load into the upper screw is that the stress at the larger insertion hole is larger than that of the (7-9) configuration. The larger insertion hole is examined as it is the greater stress raiser and is the most likely place of nail failure.

If a steel nail is used, the peak von Mises stress observed at the larger insertion hole is significantly higher for the (9-7) configuration than that observed for the (7-9) configuration. The difference is 40% and 17% for a 30MPa and 1300MPa callus respectively.

The stress distribution is different when a titanium nail is used. For a 30MPa modulus there is an increase of 34% in the peak von Mises stress at the larger

insertion hole when using the (9-7) configuration. For a callus modulus of 1300MPa the peak von Mises stress at the larger insertion hole is reduced by 12%.

9.4.15 Summary - Bend load, (7-9) and (9-7) configurations

The load shared into the callus with either configuration is similar. This is expected, as the load carrying capacity for each case is the same, with the same removal of material from the callus.

If a decision were based on the load share into the callus than the (7-9) case would be advised, form a stress-shielding aspect at low callus moduli.

The combined strain energy of the lag screws is very similar regardless of the configuration used. It is the load shared to each that is different. The configuration with the smaller lag screw above the larger (7-9) shares the load more evenly between the two lag screws.

For a steel nail, the smaller screw is always more highly stressed in the (7-9) configuration. In the (9-7) configuration the larger screw is more highly stressed for low callus moduli and less stressed for high callus moduli.

For a titanium nail, the smaller screw is more highly stressed in the (7-9) configuration, and the larger screw is more stressed in the (9-7) configuration. This reverses once the callus has stiffened to a healed condition.

There is a significant increase in the peak von Mises stress observed at the insertion hole when using the (9-7) configuration with a steel nail. This increase is more pronounced at low callus modulus, when stabilisation of the fracture site is important. A titanium nail has a relatively small increase in von Mises stress at the larger insertion hole for low callus modulus, but a relatively large decrease for the healed fracture.

The use of a (7-9) configuration shares the total load more evenly throughout the callus, but the lag screws are not carrying the load as equally with respect to their load carrying capacity. The smaller screw is more highly stressed in the (7-9) configuration, but the larger insertion hole is more stressed in the (9-7)

configuration. It is the difference in peak von Mises stress at the insertion holes that is more significant than the small changes in load sharing into the fracture callus.

The indication is to favour a (9-7) configuration when titanium screws are used, as at low callus moduli there is little difference in the von Mises stress at the insertion holes, whereas at higher callus modulus there is a reduction in the von Mises stress and thus less likelihood of failure. The use of steel nails would favour a (7-9) configuration, as at low callus modulus there is a significant decrease in the peak von Mises stress observed at the larger insertion hole.

9.4.16 Summary - Torsion load, (7-9) and (9-7) configurations

The (9-7) configuration shares a smaller load into the callus for low callus moduli, which may be beneficial to facture healing. The reduction in load share is more pronounced at the early stages of fracture healing and with the use of a steel nail. The use of a titanium nail shares a smaller load into the callus. In the interests of minimising the stress levels into the fracture callus a (9-7) configuration could be beneficial however the reduction in strain energy is relatively small and thus other factors must also be considered such as the peak stress at the insertion holes.

The combined strain energy in the lag screws for both configurations is very similar, with the (7-9) configuration sharing the total load more evenly between the two screws. It is the upper lag screw that carries the majority of the load in all cases at low callus moduli, regardless of the configuration of the screws. When a titanium nail is used the lower lag screw in the (7-9) configuration carries a greater load once the callus modulus is above 100MPa. There is little difference between the load shared into each screw with respect to their capacity to carry the load.

As a result of the load share into the two lag screws the use of a steel nail with a (9-7) configuration significantly increases the peak von Mises stress at the insertion hole for the larger screw, and thus for this criteria it is not advisable to use a configuration where the upper screw is larger than the lower. The use of a titanium nail results in the same scenario for low callus moduli. Once the callus

has 'healed' the insertion hole for the (9-7) configuration has a reduced peak von Mises stress. Given that at the early stages of fracture healing the device has its most critical influence on fracture healing, and at this point the lag screws and nail carry the greatest load, it is not advisable to use a configuration with the larger lag screw placed above the smaller.

9.4.17 (7-9) and (8-8) Comparison

9.4.17.1 Neck fracture, bend load,

9.4.17.2 Callus

The use of a steel nail results in a smaller load being passed into the fracture callus for the (8-8) configuration. This reduction occurs for all callus moduli and is relatively small. There is a 6% and 13% reduction in the strain energy at 30MPa and 1300MPa respectively.

A greater amount of strain energy is imparted on the fracture callus when a titanium nail is used, at low callus moduli for the (8-8) configuration. The difference is relatively small at 4%, and the trend reverses once the callus has stiffened to 500MPa. There is a 4% reduction in the strain energy of the callus once it has healed.

The combined load carrying capacity for the (8-8) configuration is smaller than that of the (7-9) arrangement, however the load path is such that upper screw is able to carry a greater load and transmit it to the nail in the (8-8) configuration. The load path and sharing between the screws differs depending on the amount of load that the callus is able to carry, and on the material properties of the screws. However the difference in strain energy and strain energy density in the callus for both configurations is relatively small, and would not play a decisive role in the choice for either configuration.

9.4.17.3 Lag screws

Both lag screws in the (8-8) configuration are of the same length and diameter, and thus have the same load carrying capacity. They don't share the load equally between them because the load path into the surrounding bone. The load share

varies as the callus stiffens and is able to carry a greater share of the load. Unlike the (7-9) configuration it is the upper lag screw that carries the majority of the load, a trend repeated as the callus stiffens for both the steel and titanium nails.

The use of a steel nail results in the upper screw carrying 29% more load in the (8-8) configuration and the lower screw carries 12% less at a callus of 30MPa. This is expected due to the load carrying capacities of each screw. The combined strain energy in both lag screws is 11% greater for the (8-8) configuration at low callus moduli, which is the reason for there being less strain energy in the fracture callus. Once the fracture callus has healed, the lower screws in both configurations carry a similar load (within 1%), whereas the upper screw in the (8-8) configuration has a 36% greater strain energy. The combined strain energy of the (8-8) configuration is 20% greater than the (7-9) configuration once the callus is considered healed.

The (7-9) and (8-8) configurations share the load relative to their load carrying capacity relatively equally, with the upper screw in each case having a 1.3 times greater strain energy density than the lower screw for a steel nail and a 30MPa callus. The strain energy density for each screw in the (8-8) configuration is larger, indicating that the screws in this case are more highly stressed. This is a pattern repeated for all callus modulus and for the use of a titanium nail.

There is an increase in load carried by the upper screw in the (8-8) configuration, and this translates to an increase in the peak von Mises stress at the upper screw insertion hole of 16% at low and high callus moduli. There is therefore an increase in the peak von Mises stress at a larger insertion hole and thus the (8-8) configuration is more likely to fail at this point. The lower lag screw in the (8-8) configuration carries a smaller load and thus the insertion hole at this point decreases in peak von Mises stress, with a difference of 8% and 2% for a 30MPa and 1300MPa callus respectively.

9.4.18 Neck fracture, torsion load, (7-9) and (8-8) configurations

9.4.18.1 Callus

Both a titanium and steel nail with the (8-8) configuration impart a smaller load into the fracture callus compared with the (7-9) configuration. The difference is small with the steel nail having a 13% and 3% difference for a 30MPa and 1300MPa callus respectively. The corresponding percentage difference in load share for the titanium nail is 4% and 2% respectively.

The torsion load is the design case with a significant increase in the deflection and strain energy of the system. Once the callus has effectively 'healed' there is little difference between the load shared into the fracture callus and thus this may not be the criteria used for selecting a particular device configuration. The load share into the fracture callus is more significant when considering a soft callus and a steel nail. It is also noted that the (8-8) configuration transfers a greater load into the callus than the (9-7) configuration but less than the (7-9) configuration.

The load carrying capacity of the (8-8) configuration is smaller than that of the (7-9) configuration, however the upper screw is able to carry a greater share of the load and hence a smaller load is transferred into the fracture callus. The volume of the fracture callus for the two configurations is very similar and thus the strain energy density in the callus follows the same pattern as the strain energy.

9.4.18.2 Lag Screws

It is the upper lag screw in both configurations that carry the majority of the load, and thus the upper screw has the greater value of strain energy. This trend is consistent for the (8-8) configuration, but reversed for the (7-9) configuration once the callus has 'healed'. This effect is observed for both titanium and steel nails. The upper lag screw in the (8-8) configuration carries more load than that of the (7-9) configuration due to its increased load carrying capacity. The increase is 12% and 26% for a steel nail, with a 30MPa and 1300MPa callus respectively, and 20% and 30% for a titanium nail respectively. The lower lag

screw in the (8-8) configuration has a smaller load carrying capacity than that in the (7-9) configuration and thus has a smaller strain energy value. The difference for a steel nail at a 30MPa and 1300MPa callus is 19% and 28% respectively, and 23% and 30% for a titanium nail respectively.

In the (8-8) configuration the two screws have the same load carrying capacity, however share the load differently due to the load path and the load carrying capacity of the fracture callus, as it stiffens. The upper lag screw in the (8-8) configuration carries approximately twice the load as the lower screw at low callus moduli. As the callus stiffens, this difference reduces. The percentage difference for a steel nail is 50% and 46% for a 30MPa and 1300MPa callus respectively. The same trend occurs when using titanium nails.

The load carrying capacity of each lag screw for the (7-9) configuration is different, and as the callus stiffens the load share between the two screws changes. Although the total load carried by the two screws changes as the callus stiffens, the strain energy density is always higher for the upper lag screw in both configurations.

The combined strain energy of the lag screws is similar for both configurations, with the (8-8) configuration having a slightly larger value. The percentage difference is less than 5% for both the titanium and steel nails.

There is a greater peak von Mises stress at the upper screw insertion hole when the (8-8) configuration is used due to the upper lag screw carrying a greater load. The increase in von Mises stress for a steel nail is 5% and 18% for a steel nail with a 30MPa and 1300MPa callus respectively, and 8% and 15% for a titanium nail respectively. There is an increased chance of failure of the implant at this insertion hole as there is less material to carry an increased load.

The peak von Mises stress at the lower insertion hole is reduced when using the (8-8) configuration. The reduction in peak von Mises stress for a steel nail is 11% and 10% for a 30MPa and 1300MPa callus respectively, and a 16% and 22% for a titanium nail respectively. The reduced load share into the lower lag screw and insertion hole reduce the implants likelihood of failure with the

reduction in the peak von Mises stress being greatest for a titanium nail and once the callus has 'healed'.

9.4.19 Summary – bend load, (7-9) and (8-8) configurations

In the (7-9) configuration the lower screw carries 1.3 times the load of the upper, whereas in the (8-8) configuration the upper screw carries 1.3 times the load of the lower. Therefore the screws share the load between them equally, but it is shared into each differently due to their load carrying capacity. The load-sharing trend for both configurations is repeated as the callus stiffens.

The lag screws in the (8-8) configuration have a higher strain energy density and are thus more highly stressed than the (7-9) case. The peak stress at the insertion hole is larger for the upper screw in the (8-8) configuration due to the increased load carried by the screw. That of the lower insertion hole is reduced due to there being more material in the (8-8) configuration to carry the load.

Strain energy and strain energy density in the fracture callus are smaller when using the (8-8) configuration, regardless of the callus stiffness or material of the nail. The largest difference in the load carried by the callus occurs at the early stages of fracture healing. This indicates that as the callus stiffens stress shielding effects may be enhanced from the use of the (8-8) configuration, however at low callus moduli the decrease in load carried by the callus may be beneficial to allowing the callus to heal.

9.4.20 Summary – torsion load, (7-9) and (8-8) configurations

The (8-8) configuration shares a smaller load into the fracture callus for both a titanium and steel nail, for all callus moduli. The difference in load share is relatively small when a titanium nail is used, being under 5% for all callus moduli, but is more significant when a steel nail is used and for low callus modulus (13% difference). Once the callus has healed however there is again a relatively small influence on the load share into the fracture callus (under 5%).

The combined load sharing of the two lag screws in each configuration is very similar, and thus the total strain energy of the two lag screws is comparable. The

individual lag screws have different load carrying capacities and thus the load shared into the callus varies for each configuration. It is the upper lag screw in each case that carries the majority of the load at low callus modulus, and it is the upper lag screw that has the greater value of strain energy density for all callus moduli and material properties. As the callus stiffens the two configurations vary in their load sharing characteristics. The (7-9) configuration shares the load between the two lag screws more evenly as the callus heals, and once the callus is healed the lower screw carries the majority of the load. For the (8-8) configuration the upper screw carries the majority of the load as the callus heals and the proportion of load carried by the two screws remains relatively constant.

Due to the difference in load share for each screw between the two configurations, the upper lag screw insertion hole for the (8-8) configuration has a greater peak von Mises stress. The peak von Mises stress at the lower insertion hole is however reduced.

With comparison to the second moment of area of the insertion holes, the nail reduces it ability to carry load by 41% when using an upper lag screw of 8mm rather than 7mm. The maximum increase in von Mises stress for the insertion hole is 18%. The nail increases its ability to carry load by 38% when using a 8mm lower lag screw instead of a 9mm screw, and the maximum decrease in peak von Mises stress at this insertion hole is 22%. On balance there would seem little difference in the choice of implant based on the peak von Mises stress considerations.

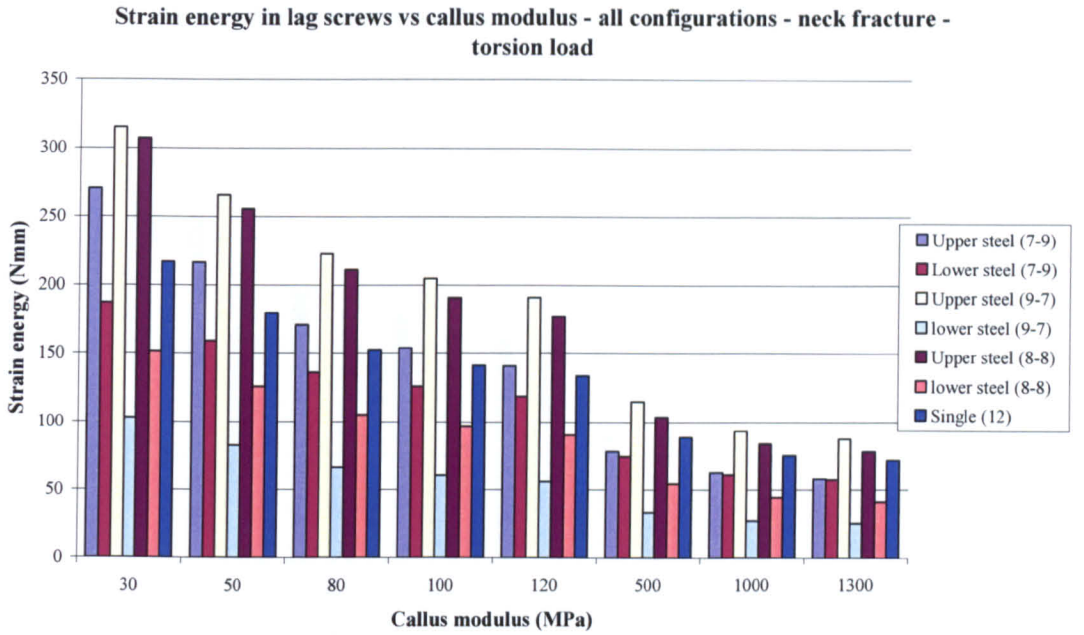

Figure 9.30 - Strain energy in lag screws.

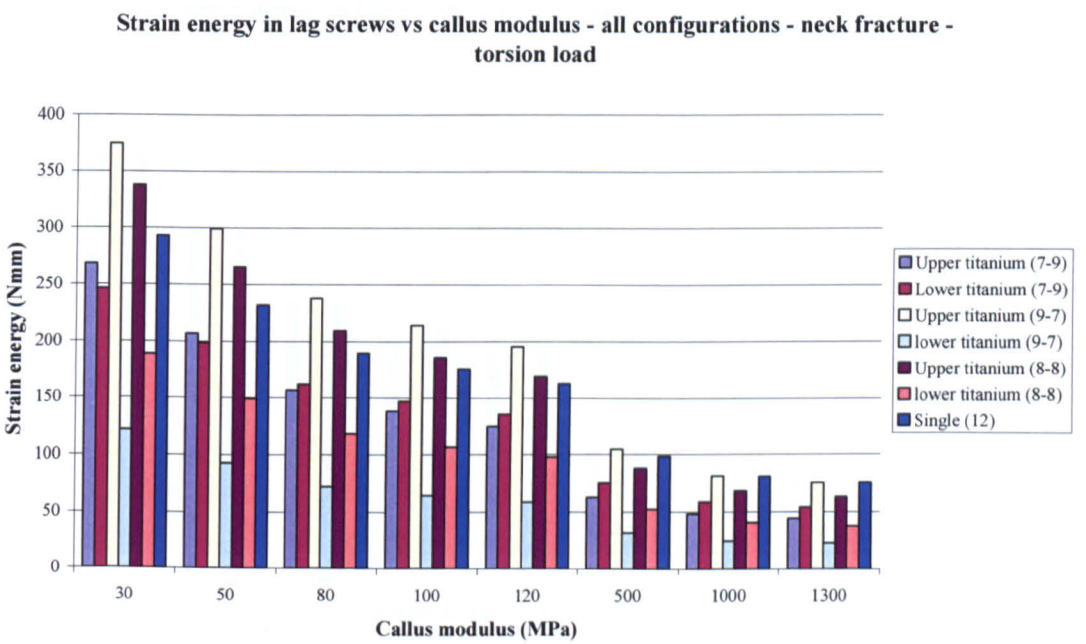

Figure 9.31 - Strain energy in lag screws.

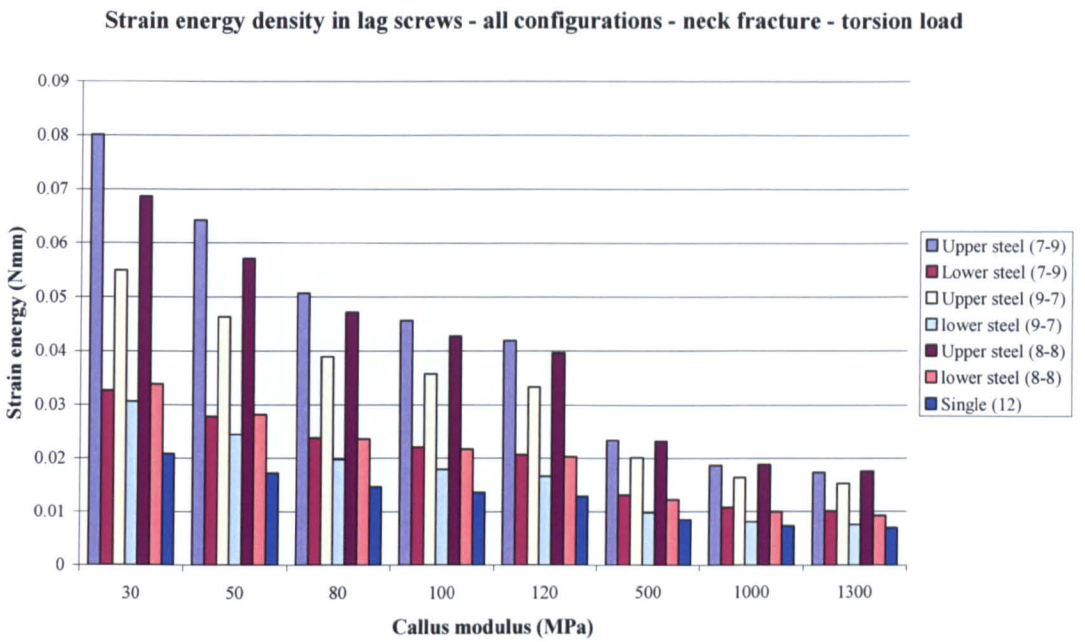

Figure 9.32 - Strain energy density in lag screws.

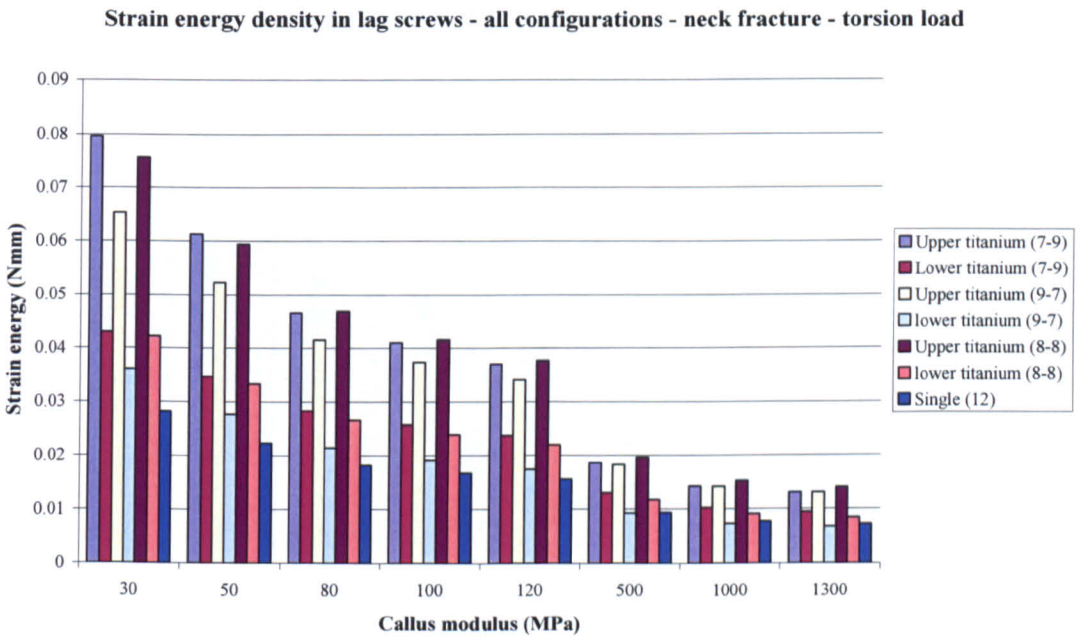

Figure 9.33 - Strain energy density in lag screws.

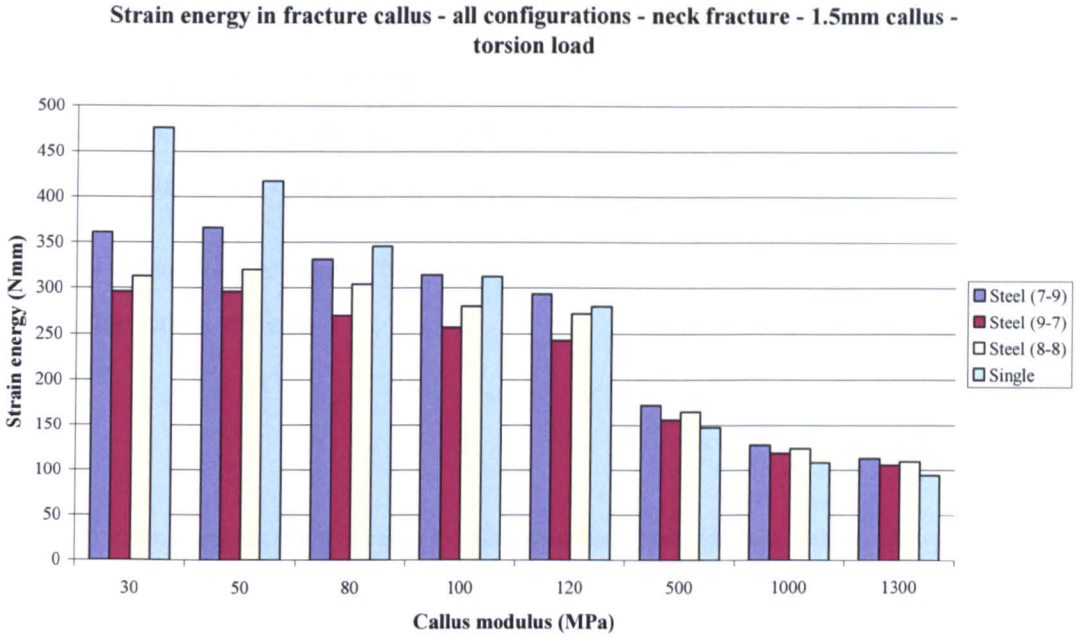

Figure 9.34 - Strain energy in callus.

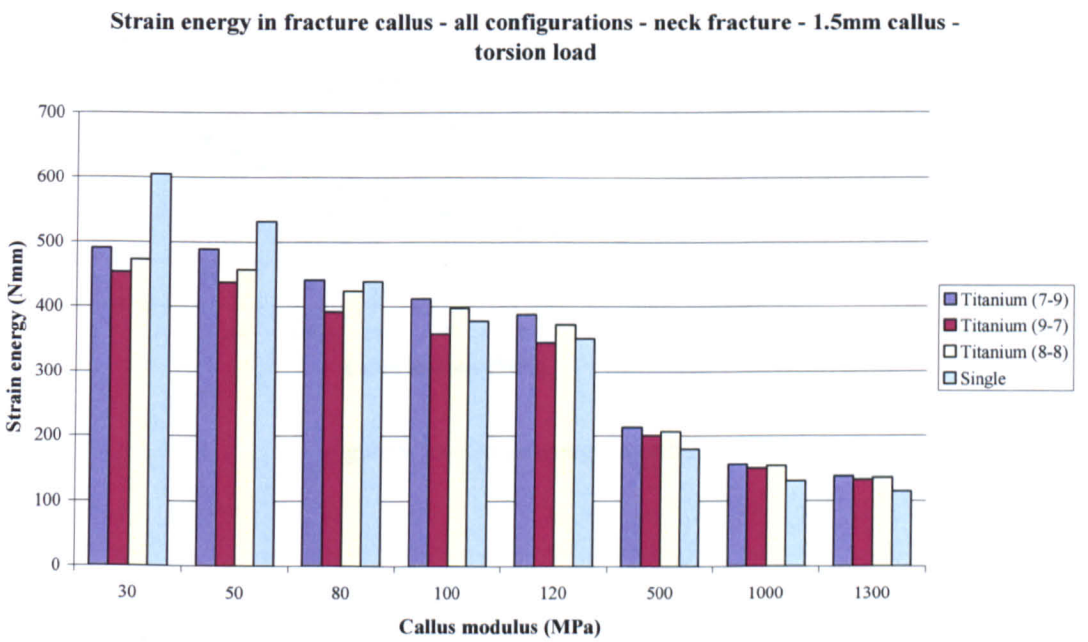

Figure 9.35 - Strain energy in callus.

9.4.21 Subtrochanteric fracture, bend and torsion load

The bend and torsion load case have the same trends. The maximum values are different but the relative change remains the same. The torsion load case has larger maximum strain energy values and is the design case.

Figures 9.36 to 9.41 represent the strain energy in the fracture callus, and lag screw as the callus stiffens.

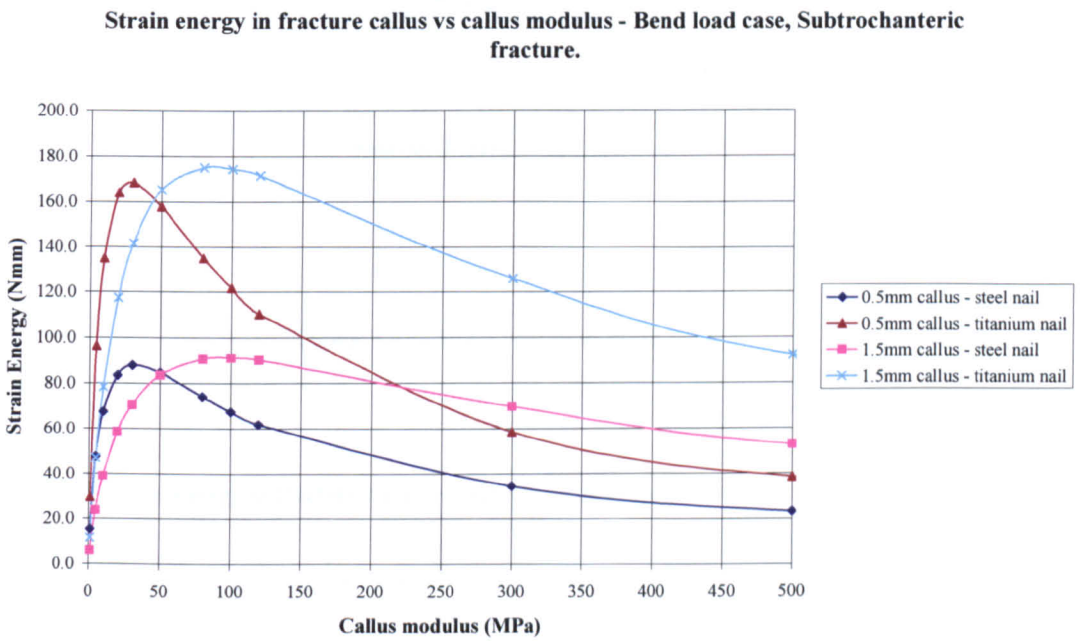

Figure 9.36 – Strain energy in callus.

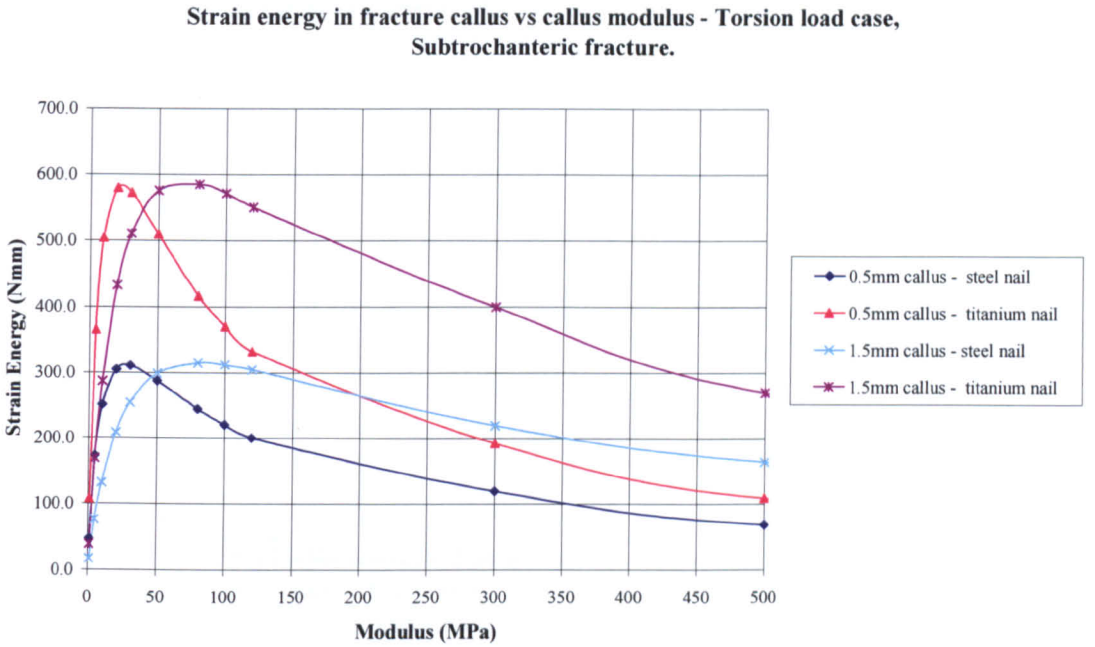

Figure 9.37 - Strain energy in callus.

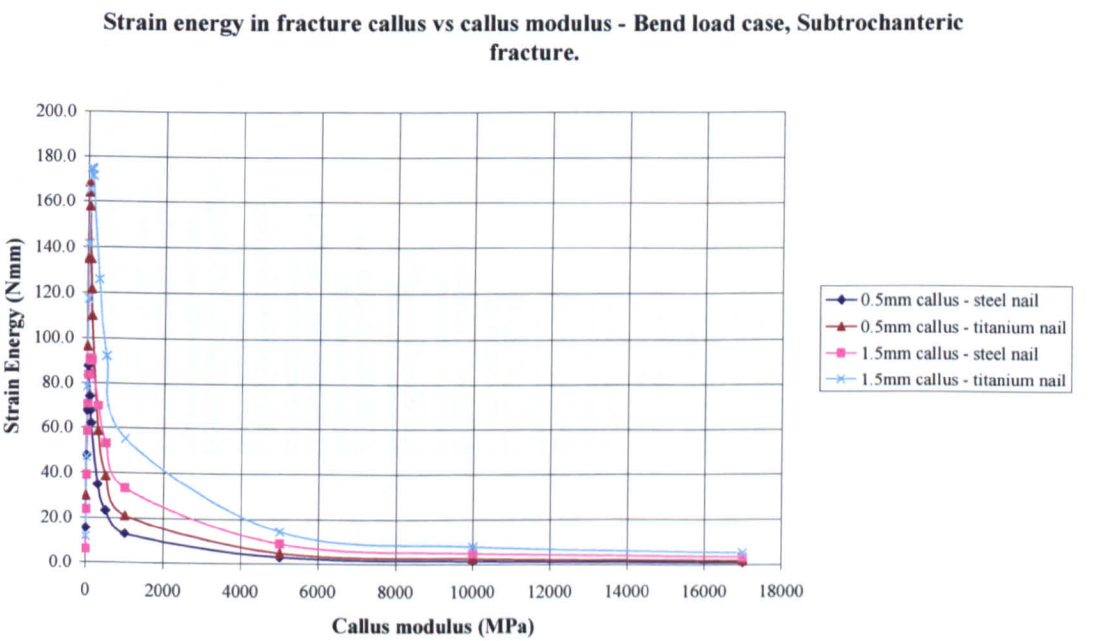

Figure 9.38 – Strain energy in callus.

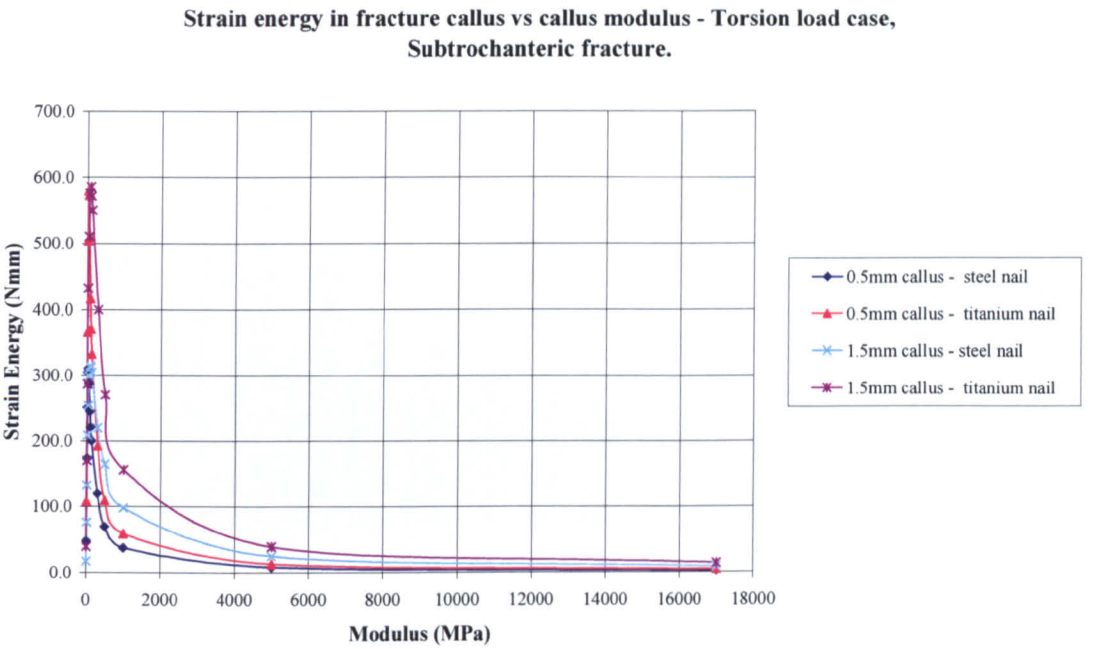

Figure 9.39 - Strain energy in callus.

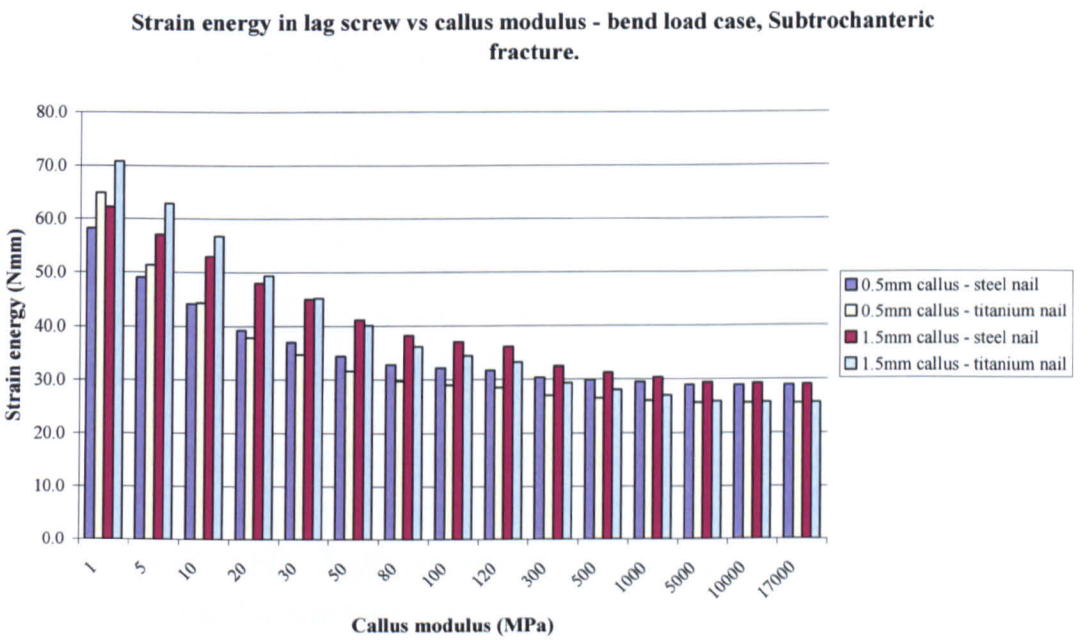

Figure 9.40 - Strain energy in callus.

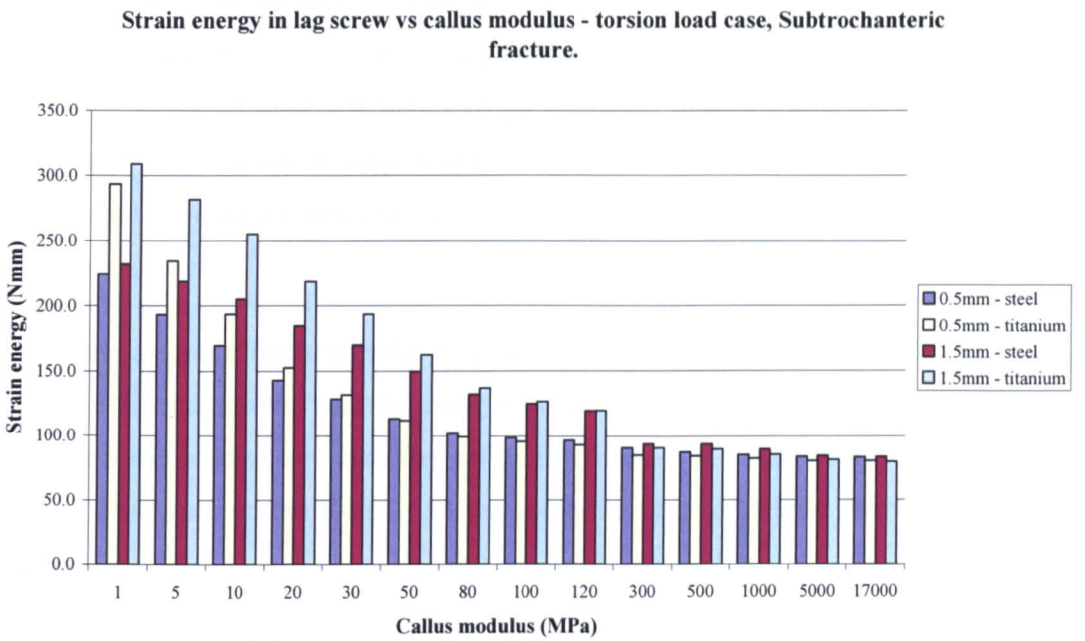

Figure 9.41 - Strain energy in callus.

9.4.21.1 Callus

As the callus stiffens the strain energy increases up to a certain value of elastic modulus, then decreases as the callus modulus increases to that of the surrounding bone. This effect is observed for both callus sizes and material property of the nail. The implication is that there is a particular value of elastic modulus for the fracture callus where the load shared into the bone can be carried. This value of elastic modulus is dependent on the size of the fracture callus and independent of the nail material properties.

The load share is limited by the ability of the callus to carry load. If no callus is present, the entire load must be transmitted through the nail, at the fracture site. When the fracture callus is present load can be carried by it, and the force transmitted through the callus will increase as the stiffness increases. There is a point where the load shared into the callus remains relatively constant, at an elastic modulus that is capable of carrying the load shared into the bone by the lag screw.

For a relatively constant load, as the elastic modulus increases, the deflection of the callus decreases and the strain energy decreases. This is observed in figures 9.30 and 9.32 for an elastic modulus of greater than 30MPa and 80MPa for a 0.5mm and 1.5mm callus thickness respectively. After 5GPa the strain energy remains relatively constant because the load is shared relatively equally between the nail and callus.

At the early stages of fracture healing, for very low callus moduli, the majority of the load is shared into the nail and partly into the callus. As the callus increases in stiffness the load shared into the callus increases. The strain energy of the callus is dependent on the increase of the force transmitted and the decrease in deflection.

The trend in strain energy as the callus stiffens can be broken into 4 parts for each callus size. The first is an increase in strain energy for very small callus moduli. In this region the nail carries almost the entire load. The second is a decrease in strain energy that mirrors the increase for small callus moduli, as the callus carries some of the load. The strain energy then decreases at a smaller rate as the callus stiffens to 500MPa, and the final stage is a decrease in strain energy as the callus modulus increases to that of the surrounding bone. In the final stages the callus is carrying its maximum amount of load relative to the nail. An inspection of the strain energy for a callus size of 0.5mm is given for an explanation of this trend.

The relative increase in stiffness for the callus from 1MPa to 30MPa is large compared to the decrease in deflection (30 times increase for a 1.2 times decrease). Therefore the strain energy increases over this range. The relative stiffness from 30MPa to 500MPa is relatively small compared to a similar decrease in deflection (17 times increase for a 1.5 times decrease). Therefore the strain energy decreases. As the callus stiffens from 500MPa to 5000MPa, there is a smaller increase in the stiffness of the callus for a relatively constant deflection of the callus (10 times decrease for a 1.1 times decrease). The strain energy therefore decreases at a larger rate. There is a 3.4 times increase in the stiffness of the callus from 5GPa to 17GPa, for a relatively constant displacement and therefore the strain energy decreases by a smaller rate.

The strain energy in the callus is dependent on the rate of increase in stiffness (and thus load carried) to the rate of decrease in deflection. The point at which the callus is able to carry a significant amount of the load is the point where the strain energy of the callus begins to decrease. This point is 30MPa and 80MPa for a 0.5mm and 1.5mm callus respectively.

The increase in strain energy in the fracture callus is more significant when using titanium. There is a 48% and 38% difference increase for a 0.5mm callus with a modulus of 1MPa and 5GPa respectively. The increase in strain energy for a healed fracture is beneficial when trying to minimise stress shielding, however the increased load imparted into the bone when the callus is very soft may hinder the healing process.

At the early stages of fracture healing the smaller callus has the greater strain energy. This is because the larger callus transfers more load into the nail, as there is more material removed from the cortical bone. Once the callus is able to carry a significant proportion of the load share, the larger callus has the greater strain energy, as there is more material able to carry a greater load. For a steel nail with a callus modulus of 1MPa, the difference is 61%. For a callus modulus of 50MPa this difference has reduced to 1%, and once the callus has healed the larger callus has a greater strain energy with a difference of 66%.

The effect of having more strain energy in the 0.5mm callus at low callus moduli results in a the smaller callus having a significantly higher strain energy density in this region. The smaller callus has an 83% increase in strain energy density for the steel nail at a callus modulus of 1MPa, the corresponding difference for the titanium nail is 87%. As the callus stiffens the difference in strain energy density decreases, and once the callus has healed to 5GPa and above, the difference is negligible (within 1%). The reason for this is that the force transmitted into the callus remains relatively constant for high callus moduli. The smaller callus has a greater average stress for the early stages of fracture healing, which is quite significant. A larger callus may therefore be more beneficial to fracture healing, with respect to keeping the stress and strain to a minimum, however the larger callus requires a larger modulus before it can be considered as load bearing, which will inevitably increase the time required for the fracture to heal.

9.4.21.2 Nail and lag screw

Strain energy in the nail decreases as the fracture callus increases in stiffness. At the early stages of healing the majority of the load is transmitted into the nail, and thus the deflection and strain energy are maximum at this point. The larger fracture callus shares more load into the nail, as there is less good quality bone to carry the load and therefore the strain energy in the nail is greatest when a larger callus size is used. The difference is small, varying from a maximum difference of 10% to less than 1%, as the callus stiffens.

As the callus stiffens, the strain energy in the lag screw decreases because the increased stiffness of the callus results in the surrounding bone carrying more load. The rate of change of the strain energy varies as the callus stiffens due to the amount of load that can be carried by the callus. The decrease in strain energy of the lag screws is greatest at the early stages of fracture healing when the relative stiffness of the callus and nail is the largest. Once the callus is able to carry load, the force transmitted into it increases by a smaller amount, and eventually becomes constant, resulting in a smaller amount of load being shared into the callus and thus less into the lag screws as the callus stiffens.

There is a greater strain energy in the lag screw with the larger fracture callus due to there being less good quality bone to carry load. The difference is relatively small, ranging from 17% to virtually nothing.

The titanium nail has a smaller elastic modulus than steel, and thus for the same load will deflect a larger amount and have more strain energy. The majority of the load at the early stages of fracture healing is shared into the nail, and this results in a larger deflection and strain energy in the nail and lag screw when titanium is used. As the callus stiffens, the steel nail and lag screw have more strain energy than the titanium nail and lag screw. This is due to the increased load share that the titanium construct imparts onto the surrounding bone. When the fracture is healed, the steel nail and lag screw carry more load, and share less into the surrounding bone, resulting in the steel construct having a larger strain energy than the titanium. With regards to fracture healing, the titanium could be

beneficial as it minimises stress-shielding, however more load is shared into the callus at low moduli which may be detrimental to the healing process.

For a callus modulus of 1MPa, the titanium lag screw has a 10% and 12% increase in strain energy for a 0.5mm and 1.5mm callus respectively, due to the deflection of the titanium lag screw being greater. Once the callus has healed and can carry the load shared into the bone, the steel lag screw carries a greater load and has a 12% increase in the strain energy for both callus sizes.

9.4.22 Summary – subtrochanteric fracture

As the fracture callus stiffens, there is a value of elastic modulus where the load shared into the bone can be carried. This value of elastic modulus is dependent on the size of the fracture callus and independent of the nail material properties. At very low callus modulus (<80MPa) the strain energy in the fracture callus increases as the modulus increases because of the load transfer through the callus and increased stiffness of it.

The use of a titanium construct significantly increases the strain energy in the fracture callus. This is beneficial for a healed fracture as stress shielding is limited, however at the early stages of fracture healing this may be detrimental.

The use of a larger callus size reduces the stress state of the callus, which may be beneficial to fracture healing. A larger callus requires a higher modulus before it can significantly carry any load however, which will result in a longer healing time.

9.5 Discussion

9.5.1 (12) and (7-9) comparison (Neck Fracture)

There is a small increase in the amount of load carried by the fracture callus for the (7-9) configuration under the bend load condition (maximum 10%). If the design choice were to be based on this criteria than there is an argument for the use of two lag screws as there is less stress shielding on the proximal femur. However, this configuration also incurs a greater average stress in the fracture callus, which may be a hindrance to effective fracture healing. The differences

between the two configurations are relatively small, and when other biomechanical effects are considered such as resorption and vascularity at the fracture site, the decision to use either one or two lag screws under the bend load condition may become a moot point.

The torsion load case results in a significantly larger strain energy and strain energy density for all components and thus is the dominant design case. A two-screw configuration imparts less strain energy into the callus at low callus moduli and more at high callus modulus. There is thus a sound argument for the use of two lag screws, because of the advantages of stress shielding on the callus at the early stages of healing and of preventing such phenomena once the fracture has healed.

A larger fracture callus observes greater strain energy differences between the single and double lag screw configurations and thus a smaller callus is beneficial for having similar load sharing characteristics regardless of the configuration used. A larger callus carries significantly more load for the bend load condition and has almost half the strain energy density. Similar trends occur for the torsion load case but the significance is greatly reduced. In the interest of keeping the stress in the callus at a minimum and increasing its load share to minimise stress shielding, a large callus size would be of benefit.

Titanium allows for more load share into the surrounding bone due to its smaller modulus of elasticity. The increase in load share into the callus is not trivial and must be considered in any design case, as is the subsequent increase in strain energy density. The differences that occur are far more pronounced when considering the early stages of fracture healing or low callus moduli, especially for the torsion load case. Once the fracture is considered 'healed' there is a negligible difference in the average stress of the fracture callus and a relatively small increase in the load carried. Titanium lag screws share the load more evenly between them at low callus moduli imparting a more even load path into the fracture callus at the most sensitive time of fracture healing. Steel lag screws share the load between them more evenly at high callus moduli, imposing an uneven load path into the fracture callus at the early stages. There is thus an argument for the beneficial use of titanium lag screws, allowing a more even load

share into the callus, however this must be assessed with the increase in load carried by the callus, and consideration must be given to the fact that the smaller upper lag screw carries a greater proportion of the load at lower callus moduli.

A further advantage of using two lag screws is the reduction in peak von Mises stress at the larger lag screw insertion hole. There is a maximum reduction of 50% when using two screws. Each insertion hole in a two-screw configuration requires the removal of less material from the nail. Therefore the stress-raising effect is reduced. Two titanium screws would be an optimum design choice, when considering load sharing of the lag screws and stress shielding implications. The use of two lag screws certainly has benefits in reducing the peak stress due to physical contact at the insertion holes, producing a construct that is less likely to fail.

9.5.2 (7-9) and (9-7) configurations

The (7-9) configuration imparts the greater strain energy into the callus, and as the callus volume is constant for either configuration, the overall stress distribution follows the same trend. The difference in load share is significant for a steel nail, with a maximum difference of 18%. The difference for a titanium nail is greatly reduced with a maximum increase of 8%. The (7-9) configuration may be preferential as it reduces stress-shielding effects once the callus has healed.

The combined load carried by the lag screws is very similar for both configurations as they have the same total load carrying capacity; it is the proportion of load carried by each screw relative to its load carrying capacity that alters.

For the bend load case the (9-7) configuration carries the load between the lag screws more equally with respect to their capacity, and the (7-9) configuration share the total load between the screws more evenly, resulting in a more even load share into the fracture callus. The peak von Mises stress incurred at the larger insertion hole for the (9-7) configuration is significantly increased (maximum difference 40%), and may be more influential than the load sharing characteristics. An ideal configuration under the bend load case would be for (9-

7) when titanium screws are used and (7-9) for steel screws, due to the reduced stress at the insertion holes.

Under the torsion load case the (7-9) configuration carries the total load more evenly between the lag screws, and thus distribute the load henceforth into the fracture callus. The upper screw in either configuration carries the majority of the load at the early stages of fracture healing and as a result the use of the (9-7) configuration significantly increases the peak von Mises stress at the larger insertion hole. The use of a titanium nail reduces the peak von Mises stress in the larger insertion hole once the fracture is healed, however the increase in stress at the early stages of fracture healing indicates that the better screw configuration is (7-9).

Considering that the torsion load case is the design case, as the stress levels and load shared into the lag screws and callus is significantly increased, a (7-9) configuration may be the optimum choice for fixation of femoral neck fractures. The total load is shared more evenly by the screws, and thus into the callus. The load share with respect to each screws load carrying capacity remains relatively equal, and the peak von Mises stress in the larger insertion hole is significantly reduced, minimising failure at this point. A (7-9) configuration has the advantages of using the upper screw for torsional stability, whilst keeping the stress at the larger insertion hole to a minimum, and reducing stress shielding effects once the callus has healed.

9.5.3 (7-9) and (8-8) configurations

The total load carrying capacity of these configurations is very similar, and this is apparent from the combined strain energy of both lag screws. The load path and sharing of the individual lag screws in each configuration is different. As the fracture callus heals, the load sharing for the (7-9) configuration changes, whereas that of the (8-8) configuration remains relatively constant.

For both configurations the upper lag screw has the greater strain energy density as the fracture callus heals. The (7-9) configuration shares the load between them relative to their load carrying capacity more evenly as the callus heals. Therefore at the early stages of fracture healing the upper screw carries about twice the load

as the lower screw, and once the callus has healed the upper lag screw has about one and a half times the strain energy density of the lower screw. As the callus heals the strain energy in the upper lag screw reduces by a greater amount than that in the lower lag screw and the load sharing is switched so that the lower lag screw has the greater strain energy.

The difference in value of the strain energy density for the (8-8) configuration remains the same as the callus heals, and there is no increase in the sharing of the load between the two screws. The upper screw always has the greater strain energy and strain energy density, and the load share between the two screws does not vary as the callus stiffens. Therefore if the desire is to have the load shared equally between the lag screws, the (7-9) configuration is the design choice. The two configurations have very similar load sharing characteristics at the early stages of fracture healing, however as the callus heals the (7-9) configuration shares the load more equally, both with respect to the total load and the screws load carrying capacity.

9.5.4 (7-9), (8-8), (9-7) and (12) configurations

As the fracture callus stiffens, the strain energy in the callus decreases, as does that in the lag screws. It has been shown that the stiffness of the callus increases exponentially with time (Kenwright *et al.,* 1986), and thus it is essential to maintain good fracture fixation at the early stages.

The critical design case is for low callus moduli, under the torsion load case. It is at low callus moduli that the greatest changes in strain energy and stress levels occur for the configurations considered, and it is under the torsion load case that the highest values of strain energy and stress are found. In the following assessment of which configuration would best suit the fracture healing process, only the torsion load case is considered. It is stipulated that once the design is optimised for the torsion load case, then that design will also be suitable for the bend load condition.

Titanium lag screws share the load more evenly between them, especially at low callus moduli and the use of titanium significantly reduces the overall stress state of the system, and the peak von Mises stress present at the lag screw insertion

holes. The use of titanium nails has the advantage of sharing a greater amount of load into the bone, which can minimise stress shielding. The table below demonstrates the reduction in peak von Mises stress at the larger or upper lag screw insertion hole when using titanium instead of steel. There is however a relatively large increase in the strain energy of the fracture callus. Considering the 1300MPa callus, the increase in strain energy into the callus is beneficial in preventing stress shielding of the surrounding bone. It is for the 30MPa callus that an increase in strain energy may have detrimental effects to the healing callus.

	Configuration							
	(7-9)		**(9-7)**		**(8-8)**		**(12)**	
Callus Modulus (MPa)	**30**	**1300**	**30**	**1300**	**30**	**1300**	**30**	**1300**
% reduction in stress	22	13	30	37	31	37	26	29
% increase in callus strain energy	27	18	35	20	34	19	21	18

Table 9.2 – All configuration comparison.

Two-screw configurations impart less strain energy into the fracture callus at the early stages of healing and more into the healed fracture callus. It may be advantageous to use a two-screw construct to minimise the load carried by the callus at the early stages of healing and prevent stress shielding once the callus has healed. Which two-screw configuration will optimise or least hamper the fracture healing process, when considering the load sharing and peak stress between the bone-implant construct must be considered.

By comparing the total strain energy of the two lag screws with that of the single lag screw, each two-screw configuration has a larger value of strain energy, and carries a greater proportion of the load. The difference in strain energy is reduced as the fracture callus heals. The percentage increase for the (7-9), (9-7) and (8-8) configurations, with a steel nail and a 30MPa callus is 53%, 48% and 53% respectively, and the corresponding values when using a titanium nail are 43%, 41% and 44% respectively. Once the callus has reached 1300MPa and considered healed, the increase in strain energy for the (7-9), (9-7) and (8-8) configurations is 38%, 36% and 40% respectively for the steel nail and 23%, 23% and 25% respectively for the titanium nail. The titanium has the most comparable strain energy to the single lag screw case and in every instance the

difference between the two-screw configurations is relatively small. Each two-screw configuration therefore transfers a similar load into the fracture callus.

The upper screw in the (8-8), and (9-7) configurations always has a higher strain energy and carries the greater load as the callus stiffens. This is not the case for the (7-9) configuration, whereby the upper and lower lag screws have a varying difference in strain energy and strain energy density as the fracture callus heals. The strain energy in the upper lag screw for the titanium nail is higher than that of the lower screw for low callus moduli and is less than that of the lower screw once the callus has healed. For the steel nail, the upper screw carries more load then the lower at low callus modulus, and once the callus has healed the strain energy in each is virtually the same.

At the early stages of fracture healing the smaller insertion hole for the (7-9) configuration, with a third of the second moment of area, has the maximum von Mises stress. Once the fracture has healed and the bone is carrying a significant proportion of the load the larger insertion hole has the peak von Mises stress, which is comparable to that in the upper insertion hole.

When comparing the peak von Mises stress in the system, it is the value in the larger insertion hole that is of interest, as this is where the nail is most likely to fail. The larger lag screw insertion hole of the (7-9) configuration has a significantly reduced peak von Mises stress compared to that in the (9-7) configuration (maximum difference 40%). The peak stress for low callus moduli occurs in the upper insertion hole for the (7-9) configuration and is less than that in the larger screw for the (9-7) configuration. The second moment of area for the 7mm insertion hole is approximately a third of that of the 9mm hole, thus it is able to carry more load, leading to the conclusion that the (9-7) configuration is more likely to fail about the nail. Once the callus has healed the peak von Mises stress occurs at the lower insertion hole for the (7-9) configuration and at the upper for the (9-7) case. The peak von Mises stress is greater in the (9-7) case.

A similar effect is observed when comparing the (7-9) to the (8-8) configuration, whereby the upper lag screw insertion hole in the (8-8) case has a larger peak von Mises stress than upper lag screw insertion hole in the (7-9) configuration,

and thus more likely to fail. The peak von Mises stress in the (7-9) configuration is therefore the most favourable with respect to having a smaller hole observing the peak von Mises stress, and having significantly less von Mises stress at the larger insertion hole.

Under the torsion load case the upper lag screw is always the more stressed. At the early stages of fracture healing the upper screw carries a greater load and therefore if there is non-bony union, or indeed mal-union of the bony fragments, it is quite likely that this upper screw could migrate in the femoral head. It is also the case that this screw may fail at the early stages. The smaller upper screw in the (7-9) configuration has less of a contact area when screwed into the cancellous bone, and thus may be more likely to cut-out than the other configurations.

Consideration must be given to the potential for lag screw cut-out. The use of two screws results in a greater load being carried into them, and thus the potential for cut-out is increased. If the bone were of good quality, with little or no degree of osteoporosis, than two screws would certainly seem the preferred choice of fixation for femoral neck fractures (Wang *et al.*, 2000). It was also cited that the use of two lag screws can increase the likelihood of screw cut out, especially in osteoporotic bone, which is obviously a serious consideration when deciding on the type of implant used.

Furthermore, the use of two screws can result in more favoured facture healing, by reducing the load carried into the callus at the early stages and countering stress shielding at the latter.

9.5.5 Subtrochanteric fracture

Early stabilisation of a fracture callus for a subtrochanteric fracture is essential in ensuring that the fracture will heal. At the beginning of the healing process there is a large increase in strain energy of the callus for a small increase in the elastic modulus. After this time the callus decreases sharply in strain energy as it is able to carry a significant proportion of the load. The point at which the callus can carry a significant amount of the load is independent on the material property of the nail, and dependent on the size of the fracture callus.

A larger callus size may be of benefit to the healing process because it reduces the stresses in the callus significantly at the early stages of fracture healing. As the callus stiffens the difference in strain energy density reduces, until the fracture has healed and the difference is negligible. A larger callus requires a larger modulus before being able to carry a significant proportion of the load and thus will take longer to heal, or require a more stable fixation in the early stages.

The use of titanium significantly increases the strain energy in the callus and may be detrimental to healing in the early stages. Once the callus has healed the titanium nail is of benefit to the bone because it transmits more load into it, limiting stress-shielding effects. The implication is for a stiff construct to be utilised at the early stages of fracture healing to reduce the load carried by the callus. Alternatively, a 'softer' construct could be used with limited weight bearing, until the callus stiffens.

The choice of implant must be weighed against the quality of the surrounding bone, the fracture that is to be fixed and the load sharing characteristics of the lag screw configurations that may be used. Furthermore, consideration must be given to the workability of each material and the manufacturing implications for the desired device. There is also the question of what type of fracture healing is desirable for a particular patient. The choice of implant for an elderly patient, who may carry the same implant for the rest of their lives, may be limited by the requirement not to fail mechanically, and thus the considerations for direct apposition of the fracture surfaces and micromovement may become moot points. In this case a more cost effective and higher load bearing steel device may be preferential. When considering patients where the implant may be removed at a later stage, the choice of dynamisation of the lag screw, fracture gap size and load sharing will be critical for the callus formation and degree of secondary bone healing. Information provided in this chapter is on a relative basis, generated from a simplification of an actual fracture and thus the values presented may need to be compared to data associated with bony union, an arduous task complicated by the lack of fracture healing information concerning proximal femoral fractures.

9.6 Conclusion

Neck fracture:

- The strain energy in the callus decreases as the fracture callus stiffens. The trend is an inverse power relationship. The stiffness of the callus increases exponentially with time, and thus it is essential to have optimal fracture fixation at the early stages.

- A larger callus is beneficial in keeping the stress to a minimum and reducing 'stress-shielding' as the callus stiffens.

- The critical design case is for low callus modulus, under the torsion load case.

- Titanium lag screws share the load more evenly between them, particularly at low callus moduli and the use of titanium significantly reduces the peak stress in the lag screw insertion hole.

- Titanium nails share a greater amount of load into the bone, minimising stress shielding.

- Two-screw configurations impart less strain energy into the fracture callus at the early stages of healing and more into the healed fracture callus. The use of two screws results in more favoured facture healing, by reducing the load carried into the callus at the early stages and countering stress shielding at the latter.

- The combined strain energy of the two-screw configuration is larger than the single screw. Two titanium screws have similar strain energy to the single screw case.

- Each two-screw configuration transfers a similar load into the fracture callus.

- The upper screw in the (8-8), and (9-7) configurations always has a higher strain energy and carries the greater load as the callus stiffens.

- For the (7-9) configuration: The strain energy in the upper lag screw is higher than that of the lower screw for low callus moduli. The strain energy in the upper lag screw is less than that of the lower screw once the callus has healed.

- The larger lag screw insertion hole of the (7-9) configuration has a significantly reduced peak von Mises stress compared to that in the (9-7) configuration (maximum difference 40%). The (9-7) configuration is more likely to fail about the nail.

Subtrochanteric fracture:

- At the beginning of the healing process there is a large increase in strain energy of the callus for a small increase in the elastic modulus. After this point the callus decreases in strain energy.

- The point at which the callus can carry a significant amount of the load is independent on the material property of the nail, and dependent on the size of the fracture callus.

- A larger callus size may be of benefit to the healing process because it reduces the stresses in the callus significantly at the early stages of fracture healing. A larger callus requires a larger modulus before being able to carry a significant proportion of the load and may take longer to heal.

- The use of titanium significantly increases the strain energy in the callus and may be detrimental to healing in the early stages.

- An optimum design may be to use a stiff construct at the early stages of fracture healing, and a 'softer' construct once the callus has healed. Alternatively, a 'softer' construct could be used with limited weight bearing, until the callus stiffens.

10.0 Conclusions

A novel finite element technique for the analysis of long bone fractures stabilised with an intramedullary nail has been developed. The technique is generic, and may be extended to other trauma treatment devices inserted into a medullary canal.

Finite element data has been compared to experimental data for verification, and an acceptable agreement found. An assessment has been made for the important parameters required to model a bone and implant construct.

An analysis of different distal end screw configurations has been provided, and the finite element model has been applied to fracture healing to ascertain relative benefits of different constructs with respect to the mechanical environment of a fracture. Implementation of the finite element model in this thesis has led to the following outcomes:

- Contact stiffness is an essential parameter in a contact analysis.
- An experimental set-up using cadaver specimens and only allowing axial movement can lead to localised deformation on the tip of the femoral head. This localised deformation can also be permanent.
- The finite element model has been validated against a cadaver test. Stiffness of the constructs matches to within 5%. The finite element model predicts local deformations.

A sensitivity study found:

- The cortical bone modulus, femoral head cancellous modulus and cortical shell thickness surrounding the femoral head are critical physiological parameters required to model the stiffness of an intramedullary nailing system.
- The femoral head modulus is critical for modelling the local deformation on the femoral head.

- The trochanter modulus has a negligible effect on the global stiffness of the construct but has a more significant effect on the peak von Mises stress in the lag screw and lag screw insertion hole.

- The cortical shell thickness can be modelled as constant about the proximal femur. The shell thickness at the load point is important in predicting local deflection and can be used as the value for a constant thickness if required.

Application to the distal screw end found:

- The axial load case produces the greatest strain energy in the system.

- The distribution of stresses will be strongly affected by the initial assumptions about contact, and the use of contact elements in a finite element model.

- A proximal slot has no structural advantage.

- Screws with lower modulus deform more than stiffer screws but the distribution of strain energy will be different for NiTi screws and stainless steel screws.

- For axial load the distal screw (of a pair of screws in slotted or round holes) is more critical, while for bending loads the proximal screw is more important. This is particularly relevant to bending about the A-P axis.

- For axial load applied to two-screw configurations with screws of different moduli, it is irrelevant whether the proximal or distal screw has the lower modulus.

Application to fracture healing found:

Neck Fracture.

- The strain energy in the callus decreases rapidly as the fracture callus stiffens, for low callus moduli. The stiffness of the callus increases with

time, and thus it is essential to have optimal fracture fixation at the early stages.

- The critical design case is for low callus modulus, under the torsion load case.
- Titanium lag screws share the load more evenly between them, particularly at low callus moduli and the use of titanium significantly reduces the peak stress in the lag screw insertion hole.
- The use of two screws results in more favoured facture healing, by reducing the load carried into the callus at the early stages and countering stress shielding at the latter.
- Each two-screw configuration transfers a similar load into the fracture callus.
- For the (7-9) configuration: The strain energy in the upper lag screw is higher than that of the lower screw for low callus moduli. The strain energy in the upper lag screw is less than that of the lower screw once the callus has healed.
- The (9-7) configuration is more likely to fail about the nail.

Subtrochanteric fractures.

- At the beginning of the healing process there is a large increase in strain energy of the callus for a small increase in the elastic modulus. After this point the callus decreases in strain energy.
- The point at which the callus can carry a significant amount of the load is independent of the material property of the nail, and dependent on the size of the fracture callus.
- The use of titanium significantly increases the strain energy in the callus and may be detrimental to healing in the early stages.

- An optimum design may be to use a stiff construct at the early stages of fracture healing, and a 'stiffer' construct once the callus has healed. Alternatively, a 'softer' construct could be used with limited weight bearing, until the callus stiffens.

10.1 Future Work

This research has provided validation of a numerical analysis, which can be used, in the longer term, as a tool for assessing which intramedullary device is best suited to a particular fracture. The results can be used to optimise the design of existing devices.

Future studies should include a comparison with exact anatomical femoral geometry, to evaluate the importance of visual observation and modelling techniques.

More accurate material modelling of a fracture callus at critical times during the healing process would provide a means of assessing the actual stress state in a callus, and indicate the type of ossification that may occur. The results of which would lead to optimising the design of an intramedullary nail to suit the mechanical environment required for optimum fracture healing.

The work presented here has been applied to fractures of the proximal femur. Equally, the numerical modelling technique can be applied to any long bone in the body stabilised with an intramedullary nail. Future work could use the methods presented here for analysing fractures of the tibia. There is a great wealth of data concerning fracture healing in tibial fractures and application of the finite element modelling technique could provide comparable results for the optimisation of an intramedullary nail.

Finally, corroboration with a good surgical team would develop the work here to a stage where specific clinical needs can be addressed.

References

Ahrengart, L., Tornkvist, H., Fornander, P., et al., 2002. A randomised study of the compression hip screw and Gamma nail in 426 fractures. Clin. Orthop, 1:209-222.

Al-yassari, G., Langstaff, R.J., Jones, W.M., Al-Lami, M., 2002. The AO/ASIF proximal femoral nail (PFN) for the treatment of unstable trochanteric femoral fracture. Injury, 33:395-399.

ANSYS, Swanson Analysis Systems, 1993.

Ashby, M., Johnson, K., 2002. Materials and Dessign, the Art and Science of Materials Selection in Product Design. Butterworth Heinemann, Oxford.

Ashman, R. B., Rho, J. Y., Turner, C.H., 1989. Anatomical variation of orthotropic elastic moduli of the proximal human tibia. J. Biomechanics. 22:895-900.

Askew, M., Lewis, J., 1981. Analysis of model variables and fixation post length effects on stresses around a prosthesis in the proximal tibia. J. Biomechanics, 103:239-245.

Audit Commission. United they stand: co-ordinating care for elderly patients with hip fracture. London: HMSO, 1995

Augat, P., Burger, J., Schorlemmer, S., Henke, T., Peraus, M., Claes, L., 2003. Shear movement at the fracture site delays healing in a diaphyseal fracture model. J. Orthop. Res, 21:1011-1017.

Bellabarba, C., Herscovici, D., Ricci, W.M., 2000. Percutaneous treatment of peritrochanteric fractures using the Gamma nail. Clin Orthop, 375:30-42.

Bernakiewicz, M., Viceconti, M., 2002. The role of parameter identification in finite element contact analyses with reference to orthopaedic biomechanics applications. J. Biomechanics, 35:61-67.

Bergmann, G., Graichen, F., Rohlmann, A., 1993. Hip joint loading during walking and running, measured in two patients. J. Biomechanics, 26:969-990.

Bergmann, G., Silva, M.C., Neff, G., Rohlmann, A., Graichen, F., 1994. Evaluation of ischial weight-bearing orthoses, based on in-vivo hip joint force measurements. Clin Biomechanics, 9:225-234.

Bergmann, G., Deuretzbacher, G., Heller, M., Graichen, F., Rohlmann, A., Strauss, J., Duda, G.N., 2001. Hip contact forces and gait patterns from routine activities. J. Biomechanics, 34:859-871.

Bonfield, W., 1981. Biomechanics of bone. Queen Mary College, London, UK, 16 March Biomaterials, 2:188.

Bourgery., 1832. De motu animalium. Rome.

Brandt, S.E., Lefever, S., Janzing, H.M.J., Broos, P.L.O., Pilot, P., Houben, B.J.J., 2002. Percutaneous compression plating (PCCP) versus the dynamic hip screw for pertrochanteric hip fractures: preliminary results. Injury, 33:413-418.

Bridle, S.H., Patel, A.D., Bircher, M., Calvert, P.T., 1991. Fixation of intertrochanteric fractures of the femur. J. Bone Jt Surg, 73-B:330:334.

Brown, T.D., Ferguson, A.B., 1980. Mechanical property distribution in the cancellous bone of the human proximal femur. Acta Orthop. Scand, 51:429-437.

Brown, C.J., Wang, C.J., Yettram, A.L., Procter, P., 2004. Intramedullary nails with two lag screws. Clin Biomechanics, 19:519-525.

Brunn von, W., 1929. Johann Friedrich Dieffenbach. Chirurg, 1:315-318.

Carter, D.R., Schwab, G.H., Spengler, D.M., 1980. Tensile fracture of cancellous bone. Acta Orthopaedica Scandinavica. 51:733-741.

Carter, D.R., Blenman, P.R., Beaupre, G.S., 1988. Correlations between mechanical stress history and tissue differentiation in initial fracture healing. J. Orthop. Res, 6:736-748.

Catanese, J., Iverson, E.P., Ramford, K.N., Keaveny, T.M., 1999. Heterogeneity of the mechanical properties of demineralised bone. J. Biomechanics, 32:1365-1369.

Chehade, M.J., Pohl, A.P., Pearcy, M.J., Nawana, N., 1997. Clinical implications of stiffness and strength changes in fracture healing. J. Bone & Jt. Surg, 79-B:9-12.

Cheung, G., Zalzal, P., Bhandari, M., Spelt, J.K., Papini, M., 2004. Finite element analysis of a femoral retrograde intramedullary nail subject to gait loading. Med. Eng & Phys, 26:93-108.

Chinoy, M.A., Parker, M.J., 1999. Fixed nail plates versus sliding hip systems for the treatment of trochanteric femoral fractures: a meta analysis of 14 studies. Injury, 30:157-163.

Claes, L.E., Wilke, H.J., Augat, P., Rubenacker, S., Margevicius, K.J., 1995. Effect of Dynamisation on gap healing of diaphyseal fractures under external fixation. Clin. Biomechanics, 10:227-234.

Claes, L.E., Heigele, C.A., 1999. Magnitude of local stress and strain along bony surfaces predict the course and type of fracture healing. J. Biomechanics, 32:255-266.

Claes, L., Eckert-Hubner, K., Augat, P., 2002. The effect of mechanical stability on local vascularization and tissue differentiation in callus healing. J. Orphop. Res, 20:1099-1105.

Cook, R.D., 1995. Finite element modelling for stress analysis. John Wiley & sons, INC.

Couteau, B., Labey, L., Hobatho, M.C., Vander Sloten, J., Arlaud, J.Y., Brignola, J.C., 1988. Validation of a three dimensional finite element model of a femur with a customised hip implant. In: Middleton, J., Jones, M.J., Pande, G.N. (Eds.), Computer Methods in Biomechanics & Biomedical Engineering. Gorden & Breach, Amsterdam: 77-86.

Cowin, S. C., Mehrabadi, M. M., 1989. Identification of the elastic symmetry of bone and other materials. J. Biomechanics, 22:503-515.

Cristofolini, L., Viceconti, M., Cappello, A., Toni, A., 1996. Mechanical validation of whole bone composite femur models. J. Biomechanics, 29:525-535.

Crowninshield, R.D., Pedersen, D.R., Brand, R.A., 1980. A measurement of proximal femur strain with total hip arthroplasty. J. Biomechanical Engineering, 102:230-233.

Curtis, M.J., Jinnah, R.H., Wilson, V., Cunningham, B.W., 1994. Proximal femoral fractures: a biomechanical study to compare intramedullary and extramedullary fixation. Injury, 25:99-104.

Dalstra M: Biomechanical aspects of the pelvic bone and design criteria for acetabular prostheses. PhD thesis, University of Nijmegen, 1993.

Dandy, D.J., Edwards, D.J., 1998. Essential orthopaedics and trauma. Churchill Livingstone.

Davis, T.R.C., Sher, J.L., Checketts, R.G., Porter, B.B., 1988. Intertrochanteric fractures of the femur: a prospective study comparing the use of the Kuntscher-Y nail and a sliding hip screw. Injury, 19:421-426.

Davis, J., Harris, M.B., Duval, M., Ambroisia, R., 1991. Pertrochanteric fractures treated with the Gamma nail: Technique and report of early results. Orthopaedic, 14:939-942.

Davy, D.T., Kotzar, G.M., Brown, R.H., Heiple, K.G., Goldberg, V.M., Heiple, J.K.G., Berilla, J., Burnstein A., 1988. Telemetric force measurements across the hip after total arthroplasty. J. Bone Jt Surg, 70A:45-50.

Dubbeld, J., Den Outer, A.J., 2000. Proximal femoral nail-first Experience with a new technique in a teaching hospital. Poster: Hip Fractures-State-of-the-Art. Meeting at Amsterdam 28th/29th May 2000.

Duda, G.N., Schneider, E., Chao, E.Y.S., 1997. Internal forces and moments in the femur during walking. J. Biomechanics, 30:933-941.

Duda, G.N., Mandruzzato, F., Heller, M., et al., 2001. Mechanical boundary conditions of fracture healing: borderline indications in the treatment of undreamed tibial nailing. J. Biomechanics, 34:639-650.

English, T.A., Kilvington, M., 1979. In vivo records of hip loads using a femoral implant with telemetric output (a preliminary report). J. Biomechanics. Eng, 1:111-115.

Eveleigh, R.J., 1995. A review of biomechanical studies of intramedullary nails. Med. Eng & Phys, 17:323-331.

Eveleigh, R.J., 1997. A biomechanical evaluation of intramedullary nails during simulated fracture healing. PhD theses, University of Bath.

Genda, E., Iwasaki, N., Li, G., Bruce, A. MacWilliams, P.J., Barrance, E., Chao, Y.S., 2001. Normal hip joint contact pressure distribution in single-leg standing-effect of gender and anatomic parameters. J. Biomechanics, 34: 895-905.

Fagan, M.J., Lee, A.J.C., 1986. Role of the collar on the femoral stem of cemented total hip replacements. J. Biomed. Eng, 8:295-304.

Fergusen, E.S., 1992. Engineering in the Mind's Eye. The MIT press, Cambridge, MA.

Gahr, R.H., Leung, K.S., Rosenwasser, M.P., Roth, W., 1999. The Gamma locking nail – ten years results and surgical experience. Einhorn-Presse Verlag.

Gallilei., 1638. Mechanic, dialog. 1.

Gardner, T.N., Mishra, S., 2003. The biomechanical environment of a bone fracture and its influence upon the morphology of healing. Med. Eng & Phys, 25:455-464.

Gluck, T., 1930. Bernhard von Langenbeck. Chirurg, 2:25-32.

Goldhagen, P.R., O'Conner, D.R., Schwarz, D., Schwarz, E., 1994. A prospective comparative study of the compression hip screw and the gamma nail. J. Orthop. Trauma, 8:367-372.

Goldstein, S.A., Wilson, D.L., Sonstegard, D.A., Matthews, L.S., 1983. The mechanical properties of human tibial trabecular bone as a function of metaphyseal location. J. Biomechanics. 16:965-969.

Goodship, A.E., Kenwright, J., 1985. The influence of induced micromovement upon the healing of experimental tibial fractures. J. Bone & Jt Surg, 67-B:650-655.

Goodship, A.E., Cunningham, J.L., Kenwright, J., 1998. Strain rate and timing of stimulation in mechanical modulation of fracture healing. Clin. Orthop. & related Res, 355S:105-115.

Gullberg, B., Johnell, O., Kanis, J.A., 1997. World-wide projections for hip fracture. Osteoporos Int, 7:407-413.

Guyer, P., Landolt, M., Keller, H., Eberle, C., 1991. The Gamma nail in per- and intertrochanteric femoral fractures – alternative or supplement to the dynamic hip screw? A prospective randomised study of 100 patients with per- and intertrochanteric femoral fractures in the surgical clinic of the City Hospital of Triemli, Zurich, September 1989 – June 1990. Aktuelle Traumatol, 21:242-9.

Guyton, J.L., 1998. In: Canale ST, editor. Campbell's operative orthopaedics, vol. 3. Missouri: Mosby.

Halder, S.C., 1992. The Gamma nail for peritrochanteric fractures. J. Bone Jt Surg, 74B:340-344.

Harman, M.K., Toni, A., Cristofolini, L., Viceconti, M., 1995. Initial stability of uncemented hip stems: an in vitro protocol to measure torsional interface motion. Med. Eng. Phys, 17:163-171.

Harrigan, T.P., Harris, W.H., 1991. A three dimensional non-linear finite element study of the effect of cement-prosthesis debonding in cemented femoral total hip components. J. Biomechanics, 24:1047-1058.

Hayes, W.C., Snyder, B., Levine, B.M., Ramaswamy, S., 1982. Stress-morphology relationships in trabecular bone of the patella. Finite Elements in Biomechanics, 223-268. John Wiley, New York.

Haynes, R.C., Poll, R.G., Miles, A.W., Weston, R.B., 1997. An experimental study of the failure modes of the gamma locking nail and AO dynamic hip screw under static loading: a cadaveric study. Med. Eng & Phys, 19:446-453.

Haynes, R.C., Poll, R.G., Miles, A.W., Weston, R.B., 1997. Failure of femoral head fixation: a cadaveric analysis of lag screw cut-out with the gamma locking nail and AO dynamic hip screw. Injury, 28:337-341.

Hefzy, M.S., Singh, S.P., 1997. Comparison between two techniques for modelling interface conditions in a porous coated hip endoprosthesis. Med Eng & Phys, 19:50-62.

Heiner, A.D., Brown, T.D., 2001. Structural properties of a new design of composite replicate femurs and tibias. J. Biomechanics, 34:773-781.

Heller, M.O., Bergmann, G., Deuretzbacher, G., Claes, L., Haas, N.P., Duda, G.N., 2001. Influence of femoral anteversion on proximal femoral loading: measurement and simulation in four patients. Clin. Biomechanics, 16:644-649.

Hoffmann, C.W., Lynskey, T.G., 1996. Intertrochanteric fractures of the femur: a randomised prospective comparison of the Gamma nail and the Ambi hip screw. NZJ Surg, 66:151-155.

Hohle, P.G., 1952. Nachuntersuchungen an gebolzten Schenkelhalsfrakturen. Chirurg, 23:306-310.

Huiskes, R., 1979. Some fundamental aspects of human joint replacement; Part III: Stress analysis of intramedullary fixation systems. Acta orthop. Scand, 185:109-200.

Huiskes, R., Chao, E.Y.S., 1983. A survey of finite element analysis in orthopaedic biomechanics: The first decade. J. Biomechanics, 16:385-409.

Huiskes, R., Strens, P., Vroemen, W., Sloof, T.J., 1990. Post-loosening mechanical behaviour of femoral resurfacing prosthesis. Clin Mater, 6:37-55.

Humphry, G.M., 1858. A treatise of the human skeleton. Cambridge.

Jinn Lin, Son-Jyh Lin, Po-Quang Chen, Shu-Hua Yang., 2001. Stress analysis of the distal locking screws for femoral interlocking nailing. J. Ortho. Res. Vol. 19, Issue 1, 57-63.

Joyce, H.K., Stephen, A.R., 2000. Prediction of femoral fracture load using finite element models: an examination of stress- and strain-based failure theories. J. Biomechanics, 33:209-214.

Keaveny T.M and Hayes W.C., 1993. A 20 year perspective on the mechanical properties of trabecular bone. Trans. ASME, 115:534-542.

Kenwright, J., Goodship, A.E., Kelly, D.L., et al., 1986. Effect of controlled axial micromovement on healing of tibial fractures. The Lancet, 1185-1187.

Keyak, J.H., 2001. Improved prediction of proximal femoral fracture load using nonlinear finite element models. Med. Eng. Phys, 23:165-173.

Knets, I.V., Krauya, U.E., Vilks, Y.K., 1975. Acoustic emission in human bone tissue subjected to longitudinal extension. Mechanika Polimerov, 11:685-190.

Koch, J.C., 1917. The laws of bone architecture. American Journal of Anatomy, 21(2).

Koslowski, L., 1960. Zur Technik der Schenkelhalsnagelung mit dem Drei-LamellenNagel. Chirurg, 31:306-308.

Kotzar, G.M., Davy, D.T., Goldberg, V.M., Heiple, K.G., Berilla, K.G.J., Brown, R.H., Burnstein, A.H., 1991. Telemeterized in vivo hip joint force data: a report on two patients after total hip surgery. J. Orthopaedic Research, 5:621-623.

Kulkarni, S.S., Moran, C.G., 2003. Results of dynamic condylar screw for subtrochanteric fractures. Injury, 34:117-122.

Kuntscher, G., 1970. A new method of treatment of pertrochanteric fractures. Proc. Roy. Soc. Med, 63:44-45.

Kuntscher, G., 1986. Praxis der Marknagelung. Handschriftlich nach 1. Auflage 1962 uberarbeitete, bisher unveroffentlichte 2. Ausgabe von 1972.

Lacroix, H., Arwert, H., Snuders, C.J., Fontijne, W.P.J., 1995. Prevention of fracture at the distal locking site of the gamma nail. J. Bone Jt Surg, 77B:274-276.

Lentz, W., 1990. Die Geschichte der Marknagelung – Ein kurzer Ruckblick. Chirurg, 61:474-480.

Leung, K.S., So, W.S., Shen, W.Y., Hui, P.W., 1992. Gamma nails and dynamic hip screws for pertrochanteric fractures, J. Bone Jt Surg, 74-B:345-51.

Lisbeth, R., Ejnar, L., Frank, L., Anders, O., Jorgen, J., 1991. Tensile and compressive properties of cancellous bone. J. Biomechanics. 24:1143-1149.

Mahomed, N., Harrington, I., Kellam, J., et al., 1994. Biomechanical analysis of the Gamma nail and sliding hip system. Clin Orthop, 304:280-288.

Mann, K., Bartel, D., Wright, T., Burstein, A., 1995. Coulomb frictional interfaces in modelling cemented total hip replacements: a more realistic model. J. Biomechanics, 28: 1067-1078.

Martens, M., Van Audekercke, R., Delport, P., De Meester, P., Mulier, C., 1983. The mechanical characterisation of cancellous bone at the upper femoral region. J. Biomechanics, 16:971-983.

Martini F.H, Fundamentals of Anatomy & Physiology, 5th ed. Prentice Hall, New Jersey.

Marwege, H., Teichert, G., 1957. Weitere Erfahrungen mit der verbundenen Dopelschraube bei der Versorgung medialer Schenkelhalsbruche. Chirurg, 28:505-510.

McNamara, B.P., Cristofolini, L., Toni, A., Taylor, D., 1994. Evaluation of experimental and finite element models of synthetic and cadaveric femora for pre-clinical design analysis. Cvlin Mat, 17:131-140.

McRae, R., Practical Fracture Treatment, 3rd ed. Churchill Livingstone, London. 1996.

Moaveni, S., 1999. Finite element analysis, theory and application with ANSYS. Prentice Hall.

Muller, M.E., Allgower, M., Schneider, R., Willenegger, H., 1979. Manual of internal fixation. Springer-Verlag, Berlin.

Parker, M.J., Pryor, G.A., 1996. Gamma versus DHS nailing for extracapsular femoral fractures. Meta-analysis of ten randomised trials. Int Orthop, 20:163-168.

Prendergast, P.J., Taylor, D., 1990. Stress analysis of the proximo-medial femur after total hip replacement. J. Biomed. Eng, 12:379-382.

Prendergast, P. J., 1997. Finite element models in tissue mechanics and orthopaedic implant design. Clin. Biomechanics, 12:343-366.

Radford, P.J., Needoff, M., Webb, J.K., 1993. A prospective randomised comparison of the dynamic hip screw and the gamma locking nail, J. Bone Jt. Surg, 75-B, 789-93.

Ramakrishnan, M., Prasad, S.S., Parkinson, R.W., Kaye, J.C., 2004. Management of subtrochanteric femoral fractures and metastases using long proximal femoral nail. Injury, 35:184-190.

Ramaniraka, N.A., Leyvraz, P.F., Rakotomana, L.R., P.J, R., Zysst, P.K., 1996. Micromotion at the bone-implant interface during the gait cycle after cementless total hip replacement: influence of stem design and loading level. Hip International, 6:51-58.

Randle, J.A., Meisami-Fard, B., McKee, M.D., 1999. Mechanical failure of a Gamma nail in a patient with an impending pathologic subtrochanteric fracture. Can. J. Surg. 42, 384-386.

Rauber., 1876. Elasticitat und Festigkeit der Knocken. Leipsig.

Reilly, D.T., Burstein, A.H., Frankel, V.H., 1974. The elastic modulus for bone. J. Biomechanics, 7:271-272.

Reilly, D.T., Burstein, A.H., 1975. The elastic and ultimate properties of compact bone tissue. Journal of Biomechanics, 9:393-396.

Rohlmann, A., Mossner, U., Bergmann, G., 1983. Finite element analysis and experimental investigation in a femur with hip endoprosthesis. J. Biomechanics, 16:727-742.

Rosenblum, S.F., Zuckerman, J.D., Kummer, F.J., Tam, B.S., 1992. A biomechanical evaluation of the Gamma nail. J. Bone Jt Surg, 74-B:352-357.

Rubin, P.J., Rakotomanana, R.L., Leyvraz, P.F., Zysst, P.K., Curnier, A., Heegaard, J.H., 1993. Frictional interface micromotions and anisotropic stress-distribution in a femoral total hip component. J. Biomechanics, 26:725-739.

Rybicki, E.F., Simonen, F.A., Weis, B., 1972. On the mathematical analysis of stress in the human femur. J. Biomechanics, 5:203-215.

Sanchez, G.M., Albareda A.J., Cardona, V.J.M., Fuentelsalz, G.J., Fernandez, J.J., Seral, I.F., 1997. Biomechanical study of the Gross-Kempf femoral nail. Int. Orthop, 21:115-118.

Schatzker, J., Wadell, J.P., 1980. Subtrochanteric fractures of the femur. Orthop Clin North Am, 11:539-534.

Schick, C.H., Wolfel, R., Walther, M., Hennig, F., 1996. Early mobilisation and long-term results of treatment of trochanteric fractures with the dynamic hip screw and the Gamma Nail. Langenbecks Archiv Fur Chirurgie, S2:991-993.

Schmitt, J., Meiforth, J., Lengsfeld, M., 2001. Development of a hybrid finite element model for individual simulation of intertrochanteric osteotomies. Med Eng & Phys, 23:529-539.

Sedel, L., Cabanela, M.E., 1998. Hip Surgery, materials and developments. Martin Dunitz.

Seral, B., Garcia, J.M., Cegonino, J., Doblare, M., Seral, F., 2003. Finite element study of intramedullary osteosynthesis in the treatment of trochanteric fractures of the hip: Gamma and PFN. Int. J. Care Injured, 35:130-135.

Shybut, G.T., Askew, M., Hori, R.Y., Stulberg, S.D., 1980. Theoretical and experimental studies on femoral stresses following surface replacement hip arthroplasty. Proc. Inst. Med. Chir. 33:95-106.

Simpson, A.H.R.W., Varty, K., Dodd, C.A.F., 1989. Sliding hip screws: modes of failure. Injury, 20:227-231.

Sitthiseripratip, K., Van Oosterwyk, H., Vander Sloten, J., Mahaisavariya, B., Bohez, E.L.J., Suwanprateeb, J., Van Audekercke, R., Oris, P., 2003. Finite element study of trochanteric gamma nail for trochanteric fracture. Med. Eng. Phys, 25:99-106.

Steinberg, E.L., Blumberg, N., Dekel, S., 1998. The fixion proximal femur nailing system: biomechanical properties of the nail and a cadaveric study. J. Biomechanics.

Stolk, J., Verdonschot, N., Cristofolini, L., Toni, A., Huiskes, R., 2002. Finite element and experimental models of cemented hip joint reconstructions can produce similar bone and cement strains in pre-clinical tests. J. Biomechanics, 35:499-510.

Stone, J.L., Beaupre, G.S., Hayes, W.C., 1983. Multiaxial strength characteristics of trabecular bone, J. Biomechanics. 16:743-747.

Szivek, J.A., Weng, M., Karpman, R., 1990. Variability in the torsional and bending response of a commercially available composite femur. J. Appl. Biomaterials, 1:183-186.

Szivek, J.A., Gealer, R.L., 1991. Comparison of the deformation response of synthetic and cadaveric femora during simulated one-legged stance. J. Appl. Biomaterials, 1:277-280.

Taylor, W.R., Roland, E., Ploeg, H., Hertig, D., Klabunde, R., Warner, M.D., et al., 2002. Determination of orthotropic bone elastic constants using FEA and modal analysis. J. Biomechanics, 35:767-773.

Taylor, M., Tanner, K.E., Freeman, M., Yettram, A.L., 1996. Stress and strain distribution within the intact femur: compression or bending. Med. Eng. Phys, 2:122-131.

Taylor, M., 1997. Finite element analysis of cancellous bone stresses within an implanted proximal femur and their relationship to implant migration. PhD thesis, University of London.

Tornetta, P., 2002. Subtrochanteric femur Fracture. J. Orthop. Trauma, 16:280-283.

Ungern-sternberg, von F.W., 1966. Die durchbohrte Pohlsche Schraube zur operativen Fixation von Schenkelhalsfrakturen. Chirurg, 37:186.

Van Buskirk W.C and Ashman R.B: The elastic modulus of bone. In Cowin S. C. ed. Mechanical properties of bone, 1981, 45:131-143.

Van der Sloten, J., Van der Perre J., 1989. Trabecular structure compared to stress trajectories in the proximal femur and the calcaneus. J. Biomed. Eng., 11:203-208.

VanRietbergen, B., Huiskes, R., Weinans, H., Summer, D.R., Turner, T.M., Galante, J.O., 1993. ESB Research Award 1992. The mechanism of bone remodelling and resorption around press-fitted THA stems. J. Biomechanics, 26:369-382.

Verdonschot, N., Huiskes, R., Freeman, M.A.R., 1993. Pre-clinical testing of hip prosthetic designs: a comparison of finite element calculations and laboratory tests. Proceedings of the Institution of Mechanical Engineers Part H. Journal of Engineering in Medicine, 207:149-154.

Viceconti, M., McNamara, M., Toni, B.P., Giunti., 1996. A FEM analysis of the static stresses induced in a THR femoral component during a standardised fatigue test. Computer Methods in Biomechanics, 57-66.

Viceconti, M., Casali, M., Massari, B., Cristofolini, L., Bassini, S., Toni, A., 1996a. The 'standardised femur program' proposal for a reference geometry to be used for the creation of finite element models of the femur. J. Biomechanics, 29:1241.

Viceconti, M., Bellingeri, L., Cristofolini, L., Toni, A., 1998. A comparative study on different methods of automatic mesh generation of human femurs. Med Eng Phys, 20:1-10.

Viceconti, M., Muccini, R., Bernakiewicz, M., Massimiliano, B., Cristofolini, L., 2000. Large-sliding contact elements accurately predict levels of bone-implant micromotion relevant to osseointegration. J. Biomechanics, 33:1611-1618.

Wang, C.J., Yettram, A.L., Yao, M.S., Procter, P., 1998. Finite element analysis of a gamma nail within a fractured femur. Med. Eng Phys, 20:677-683.

Wang, C.J., 1999. Structural behaviour of femoral intramedullary fracture stabilising devices. PhD Thesis, Brunel University.

Wang, C.J., Brown, C.J., Yettram, A.L., Procter. P., 2000. Intramedullary femoral nails: one or two lag screws? A preliminary study. Med. Eng Phys, 22:613-624.

Wang, C.J., Brown, C.J., Yettram, A.L., Procter, P., 2003. Intramedullary nails: some design features of the distal end. Med Eng Phys, 25:789-794.

Wassner, U.J., 1955. Zur operativen Versorgung der medialen Schenkelhalsfraktur. Chirurg, 26:83-85.

Wolff, J., 1892. Das Gesetz der Transformation der Knocken. Quarto. Berlin.

Wyman, J., 1857. On the cancellated structure of the bones of the human body. Boston Jour. Of Natural History, 6.

Yoon, H.S, and Katz J.L., 1976. Ultrasonic wave propogation in human cortical bone, measurements of elastic properties and microhardness. J. Biomechanics. 17:459-464.

Zafiropoulos, G., Pratt, D.J., 1994. Fractured Gamma Nail. Injury: International Journal of care of the Injured, 25:331-336.

Experimental components.

Concave Plate

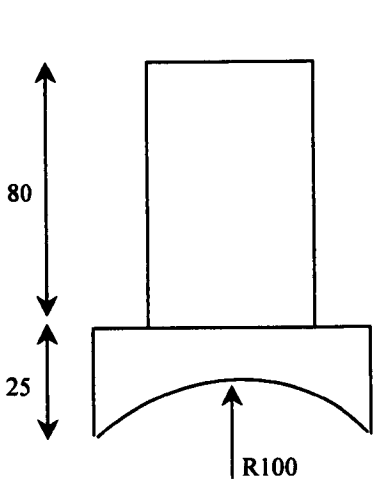

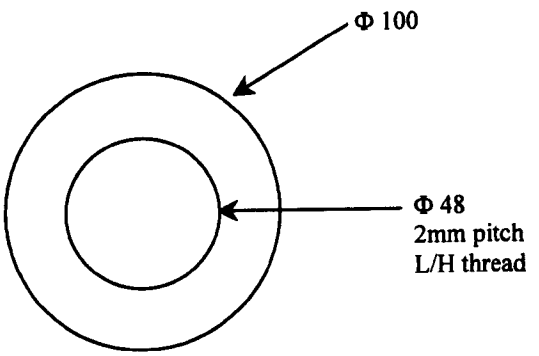

Pot

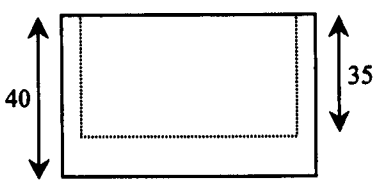

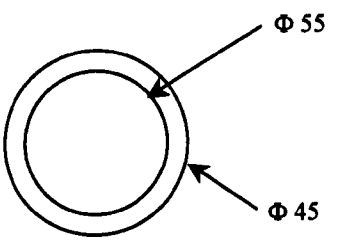

Pot Clamp

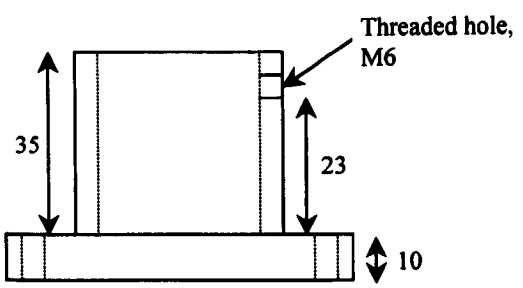

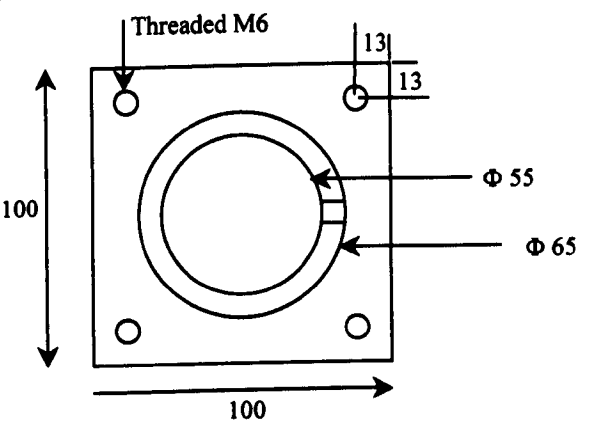

Sagittal Block

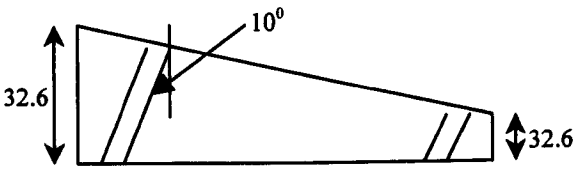

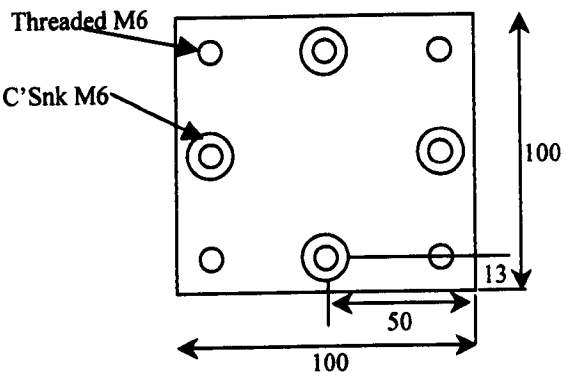

Coronal Block

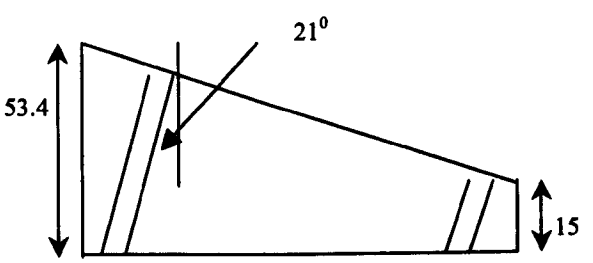

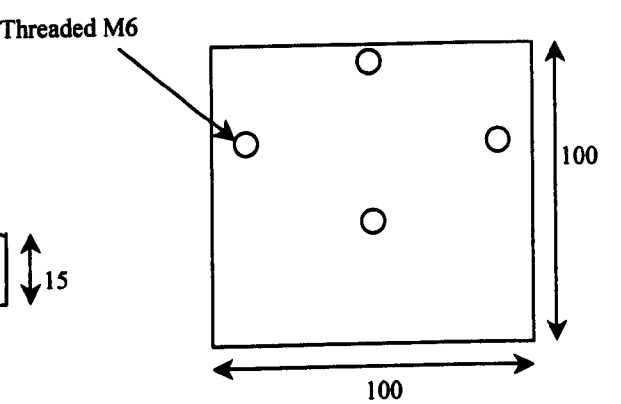

X Carriage

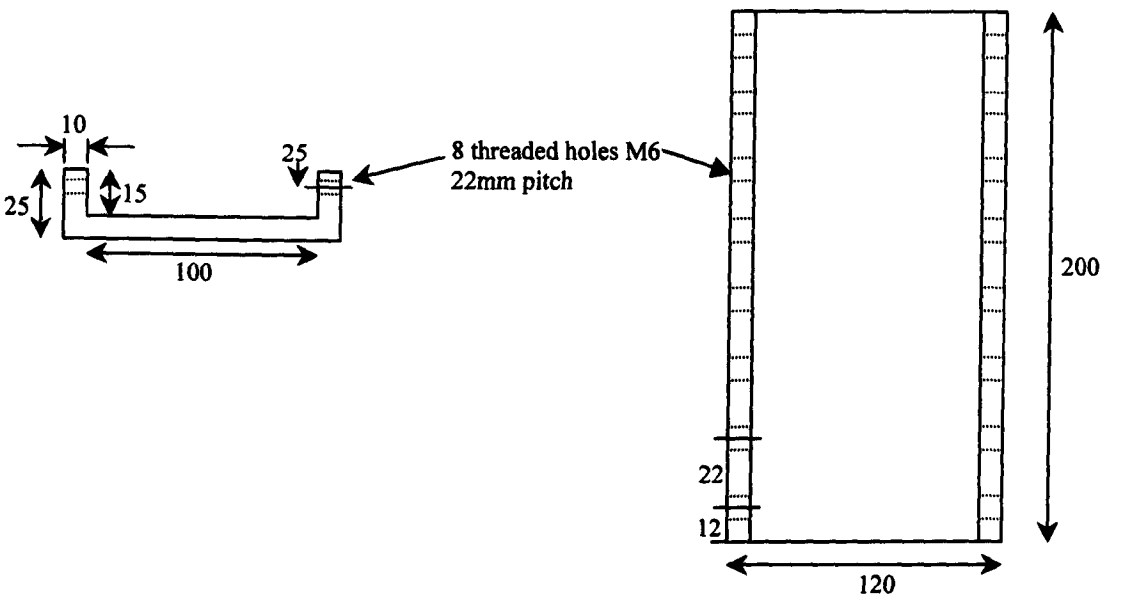

Y Carriage

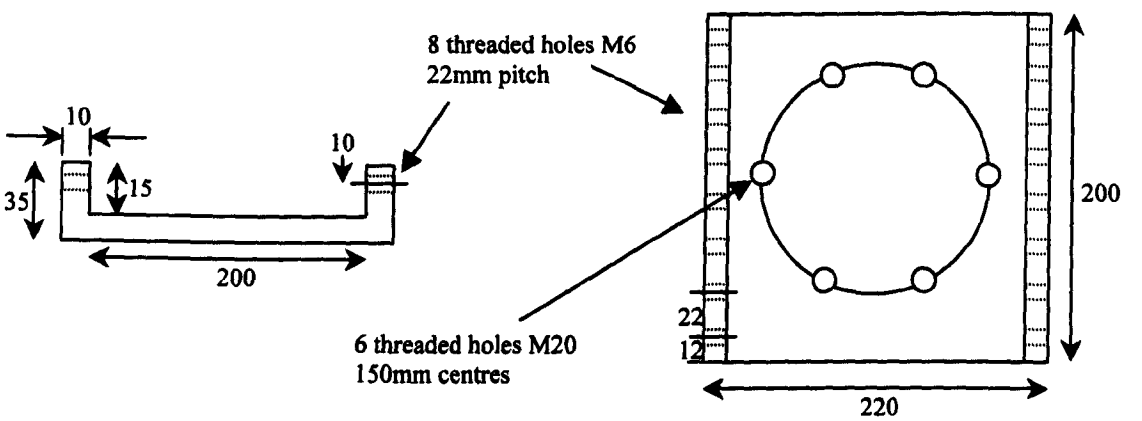

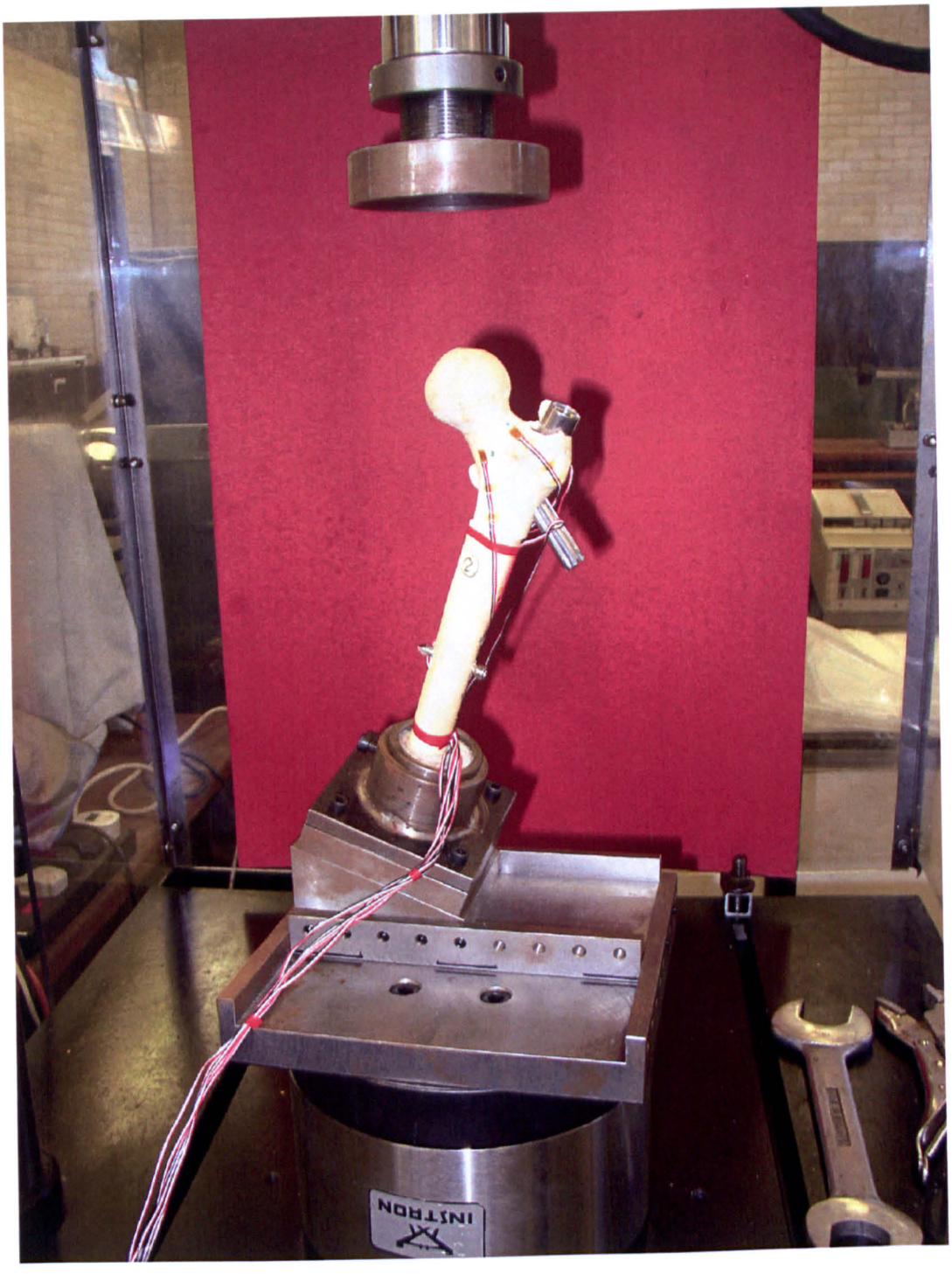
INSTRON

Test 1 Femur 2

Load (kN)	Displacement in y-direction (mm)	SG1 (με)	SG3 (με)	SG4 (με)	SG5 (με)	SG6 (με)
0.00	0.00	1.30	2.30	1.40	-2.80	-0.50
0.02	0.02	-3.70	-17.70	-7.70	37.90	28.70
0.11	0.07	-18.80	-43.10	-20.00	78.10	57.60
0.21	0.13	-39.50	-76.70	-38.40	131.20	95.20
0.31	0.19	-65.50	-91.30	-50.30	164.50	120.00
0.40	0.24	-96.90	-113.20	-64.10	201.40	149.00
0.50	0.30	-153.10	-142.70	-85.20	247.70	192.20
0.61	0.37	-196.80	-162.40	-101.60	274.80	224.30
0.71	0.44	-248.70	-183.40	-119.60	303.10	258.30
0.84	0.52	-318.90	-211.60	-142.30	338.10	298.80
0.92	0.57	-364.40	-229.20	-156.40	360.00	323.20
1.01	0.62	-417.60	-248.60	-171.90	384.80	355.30
1.12	0.69	-479.30	-269.40	-190.00	410.90	378.10
1.21	0.74	-532.20	-286.70	-205.10	432.50	402.60
1.31	0.79	-588.40	-310.40	-225.70	458.60	434.90
1.42	0.85	-648.00	-318.40	-238.60	474.60	456.70
1.51	0.90	-699.20	-338.10	-250.60	493.40	481.50
1.62	0.95	-764.70	-381.10	-259.90	522.20	514.60
1.72	1.00	-803.30	-410.20	-264.90	542.90	536.30
1.82	1.04	-847.90	-444.80	-269.40	566.30	560.70
1.94	1.09	-909.10	-492.50	-274.80	600.80	593.80
2.02	1.13	-949.80	-524.30	-277.80	624.70	616.10
2.12	1.17	-996.40	-560.30	-281.00	653.50	646.80
2.22	1.22	-1049.40	-600.00	-284.20	686.80	669.50
2.32	1.26	-1095.60	-635.10	-286.80	716.10	693.20
2.42	1.30	-1145.00	-685.00	-290.40	754.70	724.40
2.52	1.34	-1197.10	-712.30	-291.20	779.00	745.30
2.62	1.38	-1240.90	-748.30	-292.50	804.80	768.00
2.72	1.42	-1299.40	-796.30	-294.20	833.60	790.30
2.79	1.45	-1312.40	-793.80	-294.00	830.30	788.00

Test 2 Femur 2

Load (kN)	Displacement in y-direction (mm)	SG1 (με)	SG3 (με)	SG4 (με)	SG5 (με)	SG6 (με)
0.00	0.00	0.90	0.90	0.30	0.80	0.00
0.00	0.00	1.50	0.50	1.00	1.00	0.00
0.00	0.00	1.90	0.90	1.00	1.10	-0.60
0.00	0.00	2.00	-1.40	-0.80	13.70	11.40
0.05	0.04	-11.60	-28.00	-12.80	57.20	40.50
0.15	0.10	-32.20	-60.50	-31.30	114.00	78.40
0.25	0.16	-58.40	-78.80	-42.70	150.00	102.50
0.33	0.20	-73.50	-85.20	-47.90	205.20	131.20
0.45	0.28	-119.40	-119.60	-68.90	223.00	182.30
0.63	0.36	-186.80	-156.30	-94.60	270.30	202.30
0.66	0.40	-217.60	-167.70	-102.60	284.20	218.40
0.72	0.45	-278.90	-207.50	-135.50	330.30	276.70
0.86	0.53	-324.40	-226.90	-149.90	352.20	303.40
0.94	0.58	-380.40	-241.90	-160.40	383.90	342.00
1.07	0.66	-450.30	-263.00	-176.70	408.80	361.30
1.14	0.69	-482.60	-271.70	-182.80	418.30	373.40
1.31	0.78	-573.80	-298.10	-215.60	480.30	435.00
1.40	0.83	-624.70	-313.00	-228.30	486.60	456.60
1.52	0.89	-701.40	-359.10	-241.70	510.20	483.40
1.60	0.93	-735.60	-377.70	-244.80	519.30	495.00
1.63	0.95	-748.30	-391.90	-246.80	530.50	506.30
1.68	0.97	-772.90	-461.90	-256.90	573.30	549.40
1.84	1.07	-903.40	-522.00	-263.00	620.80	595.10
2.01	1.11	-929.40	-527.70	-262.90	623.20	600.80
2.03	1.13	-943.40	-546.70	-264.50	640.00	622.40
2.11	1.16	-994.20	-595.60	-268.60	684.30	651.10
2.23	1.21	-1048.80	-629.30	-271.20	717.80	693.80
2.50	1.30	-1142.60	-728.90	-275.50	765.00	705.00
2.44	1.31	-1176.60	-748.80	-275.30	797.60	747.80
2.62	1.37	-1225.80	-771.10	-275.60	808.60	757.20
2.65	1.38	-1243.80	-788.00	-276.10	819.90	768.70
2.69	1.40	-1257.00	-812.00	-277.00	852.10	789.80
2.81	1.44	-1311.90	-837.40	-277.10	854.10	797.60
2.83	1.45	-1318.30	-844.30	-277.40	854.20	797.70

Test 3 Femur 2

Load (kN)	Displacement in y-direction (mm)	SG1 (με)	SG3 (με)	SG4 (με)	SG5 (με)	SG6 (με)
0.00	0.01	1.40	0.60	0.70	5.90	4.30
0.27	0.03	-5.60	-77.80	-57.40	180.50	108.40
0.34	0.22	-67.60	-100.70	-58.00	195.50	129.40
0.42	0.26	-96.50	-106.00	-59.10	193.80	128.40
0.50	0.35	-159.10	-139.90	-82.40	246.10	171.50
0.56	0.35	-160.40	-147.00	-87.50	267.00	191.90
0.67	0.43	-228.60	-184.80	-115.00	315.20	243.80
0.84	0.53	-308.30	-213.80	-135.60	348.40	281.80
0.90	0.57	-342.40	-225.30	-143.90	362.10	297.10
0.95	0.60	-371.00	-237.90	-153.30	381.50	328.30
1.06	0.66	-437.20	-268.00	-176.10	420.40	361.20
1.18	0.72	-502.70	-289.00	-192.30	448.00	390.60
1.29	0.78	-564.20	-314.80	-211.30	472.50	420.60
1.39	0.83	-615.00	-326.30	-221.30	489.50	441.50
1.48	0.88	-665.30	-356.50	-230.20	511.30	468.80
1.58	0.93	-730.90	-407.50	-238.70	545.30	506.70
1.71	0.99	-779.30	-446.50	-243.60	566.60	529.00
1.80	1.02	-818.00	-476.60	-246.60	587.00	551.30
1.91	1.07	-873.90	-523.20	-251.40	621.00	582.10
1.98	1.11	-909.50	-576.90	-258.90	684.20	621.40
2.10	1.17	-975.50	-631.40	-258.70	667.30	670.20
2.33	1.25	-1056.60	-638.10	-259.60	695.00	646.80
2.23	1.22	-1035.70	-693.70	-261.70	737.50	704.40
2.34	1.28	-1137.90	-760.80	-262.80	776.70	720.50
2.54	1.33	-1161.10	-752.90	-262.10	772.80	718.60
2.52	1.33	-1157.70	-769.40	-263.50	817.20	737.40
2.74	1.41	-1276.20	-867.10	-264.00	844.60	786.40
2.82	1.44	-1286.30	-866.20	-263.70	840.90	784.40

Test 1 Femur 6

Load (kN)	Displacement in y-direction (mm)	SG2 (με)	SG3 (με)	SG4 (με)	SG5 (με)	SG6 (με)
0.00	0.08	1.8	1.1	-25.3	-1.2	3.2
0.06	0.32	-9.9	-5.5	-59.5	-5.9	3.5
0.07	0.38	-19.2	-8.6	-75.5	-10.1	3.2
0.09	0.43	-31.1	-11.5	-94.1	-17.9	2.9
0.12	0.54	-53.1	-18.6	-124	-20	2.9
0.14	0.62	-70	-25.4	-144.3	-23	3.1
0.16	0.69	-82	-29.7	-162.4	-27.5	3.5
0.21	0.80	-104.7	-33	-207.5	-40.1	5.3
0.25	0.89	-130.3	-40.4	-251.1	-47.9	7.3
0.27	0.93	-141.8	-45	-281.7	-49.6	8.4
0.30	0.97	-154.4	-53.5	-303.2	-49.7	9.7
0.32	1.00	-162.4	-59.9	-325.1	-49.2	11.3
0.34	1.03	-169.4	-66.5	-346.8	-48.8	12.6
0.36	1.06	-175.9	-76	-378.2	-49.3	13.9
0.39	1.09	-184.9	-80.8	-399.4	-49	15.8
0.41	1.11	-191	-87.4	-420.5	-48.8	17.1
0.45	1.15	-206.3	-104.3	-474	-47.4	19.9
0.48	1.18	-210.9	-111.4	-496.6	-46.7	21.4
0.52	1.23	-222.7	-126	-541.2	-45.7	24.3
0.55	1.25	-230.9	-136.2	-572.7	-44.4	25.8
0.60	1.30	-242.5	-150.2	-612.4	-43.2	28.8
0.64	1.34	-255.4	-167.6	-671	-41.4	31.5
0.69	1.38	-265.2	-181	-715.6	-40.4	34.3
0.73	1.43	-276.4	-197	-767.6	-39.3	36.9
0.80	1.48	-289	-215.4	-831.6	-38	40.9
0.83	1.51	-294.1	-223.6	-859.5	-37.1	41.7
0.88	1.54	-301.3	-234.1	-895.2	-34.7	43.9
1.00	1.65	-320	-263.5	-996.4	-27.2	48.6
1.07	1.65	-314	-268.4	-1091.4	-27.1	53.7
1.16	1.79	-328.4	-297.7	-1114.8	-15.4	55
1.18	1.79	-323.4	-309	-1170.5	-14.4	59.7
1.21	1.81	-324.2	-311	-1179.6	-12.9	60.1
1.22	1.83	-323.6	-316.9	-1202.6	-11.2	61.6
1.25	1.85	-343.2	-352.4	-1241	-15.4	68.8
1.30	1.93	-335.9	-340.8	-1253.9	-5.9	62.6
1.29	1.93	-335.1	-346	-1285.6	-6.8	64.4
1.32	1.94	-333.1	-348.2	-1284.1	-5.6	63.6

Test 2 Femur 6

Load (kN)	Displacement in y-direction (mm)	SG2 (με)	SG3 (με)	SG4 (με)	SG5 (με)	SG6 (με)
0.00	0.00	-1.4	1.2	-14.2	-2	-0.4
0.07	0.09	-14.3	-6.9	-84.4	-8.7	1.6
0.09	0.15	-25.2	-12.6	-105.4	-11.1	1.2
0.12	0.25	-45.9	-23.4	-136.2	-13.3	2.3
0.15	0.33	-62.4	-31.7	-157.5	-13.9	2.6
0.19	0.47	-91	-39.2	-195.1	-21.3	2.2
0.22	0.53	-106.6	-41.9	-222.8	-28.4	3.5
0.26	0.61	-130.4	-48.3	-264.3	-38.5	5.2
0.31	0.70	-151.9	-56.2	-314.5	-46.5	7.3
0.35	0.76	-163.6	-63.7	-355.1	-49.3	9.9
0.37	0.78	-169.2	-68.2	-376.3	-50.8	11.2
0.40	0.82	-175.9	-75.5	-406.1	-50.1	12.7
0.44	0.86	-184.7	-86.7	-448.6	-50.8	15.4
0.49	0.92	-195.4	-102.2	-501.9	-49.5	18.4
0.51	0.94	-199.8	-109.3	-523.5	-48.4	20
0.55	0.99	-208.1	-124.2	-577.2	-45.4	23.1
0.60	1.05	-218.4	-142.3	-620.2	-40	26
0.65	1.10	-225.9	-163.6	-669.2	-31.4	29.4
0.70	1.15	-234.7	-179.6	-709.6	-23.7	32.3
0.74	1.20	-242.6	-198	-756.7	-16.1	35
0.77	1.23	-244.1	-204.7	-775.8	-13.5	36.4
0.81	1.27	-249	-219	-815	-7.8	38.8
0.86	1.33	-253.9	-235.4	-863.9	-3.5	40.9
0.91	1.37	-256.7	-248.5	-903.3	1.2	43.1
0.96	1.42	-259.6	-264.1	-950.6	7	45.5
0.98	1.44	-260.7	-270.5	-969.9	8.9	46.7
1.00	1.47	-261.9	-277.2	-988.6	11.1	48.2
1.05	1.52	-265	-292.6	-1035.5	17.2	50.4
1.07	1.54	-266.2	-298.2	-1055.2	19.7	51.3
1.12	1.59	-268.8	-311.6	-1102.6	25.9	53.7
1.17	1.64	-271.4	-323.2	-1143	29.1	55.8
1.22	1.69	-275.4	-339.9	-1190.2	33.8	58.8
1.24	1.72	-276.8	-346.9	-1209.5	35.9	60
1.26	1.74	-278.9	-354	-1229.8	37.8	61.1
1.28	1.76	-280.9	-361	-1250.4	39.2	62.4
1.31	1.80	-284.2	-370.3	-1271.7	41.3	62.2

Test 3 Femur 6

Load (kN)	Displacement in y-direction (mm)	SG2 (με)	SG3 (με)	SG4 (με)	SG5 (με)	SG6 (με)
0.00	-0.01	-0.6	-0.4	-2.6	-0.2	0.1
0.00	0.00	-0.4	0	-3.8	0	1
0.00	-0.01	-0.6	-0.4	-2.6	-0.2	0.1
0.00	0.01	-1.4	-0.3	-18.9	-1.4	0.2
0.04	0.07	-9.5	-2.2	-44.2	-8.1	2.1
0.05	0.11	-18.1	-4	-57.4	-12.1	2.1
0.07	0.16	-27.6	-5	-70.4	-16	2
0.08	0.21	-38	-5.8	-69.8	-16.9	1.1
0.09	0.25	-48.1	-6.9	-82.6	-22.7	1.8
0.11	0.31	-54.6	-6.8	-99.8	-25.9	1.4
0.11	0.34	-67.9	-8.3	-99	-27.7	1.8
0.12	0.39	-71.9	-9	-119.6	-32.6	1.3
0.13	0.44	-86.2	-11.2	-129.9	-35	1.8
0.15	0.50	-99.3	-13.5	-142.9	-37.2	2.5
0.16	0.54	-106.7	-15	-148.6	-37.6	3.2
0.17	0.57	-115.1	-19.3	-172.4	-38.9	4.1
0.19	0.64	-132.2	-28.2	-191.2	-38.8	5.5
0.21	0.69	-144.6	-35.2	-221.5	-43.7	7.3
0.25	0.74	-156	-42.7	-254.5	-47.9	9.3
0.28	0.78	-165.4	-54.2	-295.7	-52.8	11.2
0.32	0.83	-177.9	-60.6	-323	-55.5	13.5
0.34	0.86	-185.9	-67.6	-349.5	-58.1	14.7
0.37	0.89	-195.1	-88.3	-403.7	-62	18.8
0.43	0.96	-218.2	-99.8	-459.3	-68.1	20.6
0.47	1.01	-228.6	-109.7	-486.3	-70.2	24
0.52	1.06	-247.7	-128.8	-540.7	-72.6	24.9
0.54	1.09	-259.9	-144.9	-577.8	-71.8	27.6
0.61	1.15	-270.5	-156.3	-647.2	-74	31.6
0.67	1.21	-283	-172.6	-667.6	-71.3	33.2
0.72	1.26	-300	-194.3	-727.6	-69.3	35.3
0.73	1.28	-303.6	-210.9	-782.9	-67.9	39
0.80	1.34	-322	-228	-814.5	-63.2	40.5
0.85	1.39	-334.7	-247	-867	-60.2	42.5
0.91	1.44	-344.3	-266.2	-918.8	-57.5	45.5
0.96	1.48	-352.3	-274.9	-946.2	-54.8	47.2
1.01	1.54	-362.2	-296.8	-1011.4	-50	48.9
1.10	1.58	-369.9	-317.4	-1082.8	-46.5	52
1.12	1.61	-369.1	-333.7	-1121.8	-43.4	55.2
1.21	1.67	-374.1	-342	-1163	-39.7	57.6
1.31	1.73	-380.3	-372	-1258.7	-33.7	60.4

Finite element data for experimental comparison.

Finite Element Data	
Femur 2	
Load (kN)	Displacement (mm)
0.00	0.00
0.14	0.09
0.28	0.16
0.49	0.26
0.80	0.41
1.28	0.63
1.99	0.97
2.80	1.37

Finite Element Data	
Femur 6	
Load (kN)	Displacement (mm)
0.00	0.00
0.22	0.31
0.43	0.58
0.65	0.85
0.98	1.25
1.30	1.64

Neck fracture data

Neck fracture. Two lag screw Gamma nail (7-9). E = 210GPa
Cortical bone E=17GPa, Femoral Head E=1.3GPa, Trochanter E=0.32GPa.

BEND LOAD CONDITION

Fracture size=0.5

	Femur	Fracture callus		Nail	Lag Screws			
Fracture Callus Elastic Modulus (GPa)	Maximum deflection of femoral head (mm)	Strain Energy (Nmm)	Strain Energy Density (Nmm^{-2})	Strain Energy (Nmm)	Strain Energy (Nmm)		Strain Energy Density (Nmm^{-2})	
					Upper (7)	Lower (9)	Upper (7)	Lower (9)
30	-1.63	115	0.62	228	28	38	0.0084	0.0066
50	-1.58	88	0.47	227	24	33	0.0071	0.0057
80	-1.54	69	0.37	225	21	29	0.0062	0.0050
100	-1.53	63	0.34	224	20	27	0.0059	0.0048
120	-1.52	58	0.31	223	19	26	0.0056	0.0046
500	-1.46	34	0.18	219	14	20	0.0042	0.0035
1000	-1.44	25	0.13	218	13	18	0.0038	0.0032
1300	-1.44	22	0.12	217	12	18	0.0036	0.0031

Neck fracture. Two lag screw Gamma nail (7-9). E = 210GPa
Cortical bone E=17GPa, Femoral Head E=1.3GPa, Trochanter E=0.32GPa.

BEND LOAD CONDITION

Fracture size=1.5

	Femur	Fracture callus		Nail	Lag Screws			
Fracture Callus Elastic Modulus (GPa)	Maximum deflection of femoral head (mm)	Strain Energy (Nmm)	Strain Energy Density (Nmm^{-2})	Strain Energy (Nmm)	Strain Energy (Nmm)		Strain Energy Density (Nmm^{-2})	
					Upper (7)	Lower (9)	Upper (7)	Lower (9)
30	-1.78	205	0.36	234	41	52	0.0121	0.0091
50	-1.69	151	0.27	232	35	45	0.0103	0.0079
80	-1.63	123	0.22	230	29	39	0.0087	0.0068
100	-1.60	111	0.20	228	27	36	0.0080	0.0063
120	-1.59	102	0.18	227	25	34	0.0075	0.0060
500	-1.49	54	0.10	220	17	24	0.0050	0.0041
1000	-1.46	40	0.07	220	15	21	0.0043	0.0036
1300	-1.45	37	0.07	218	14	20	0.0041	0.0034

Neck fracture. Two lag screw Gamma nail (7-9). E = 110GPa

Cortical bone E=17GPa, Femoral Head E=1.3GPa, Trochanter E=0.32GPa.

BEND LOAD CONDITION

Fracture size=0.5

	Femur	Fracture callus		Nail	Lag Screws			
Fracture Callus Elastic Modulus (GPa)	Maximum deflection of femoral head (mm)	Strain Energy (Nmm)	Strain Energy Density (Nmm^{-2})	Strain Energy (Nmm)	Strain Energy (Nmm)		Strain Energy Density (Nmm^{-2})	
					Upper (7)	Lower (9)	Upper (7)	Lower (9)
30	-1.97	142	0.76	231	24	40	0.0071	0.0069
50	-1.90	108	0.58	229	19	33	0.0057	0.0058
80	-1.85	82	0.44	229	16	29	0.0049	0.0050
100	-1.84	77	0.41	227	15	27	0.0045	0.0047
120	-1.82	72	0.38	226	14	25	0.0042	0.0044
500	-1.74	40	0.22	223	10	19	0.0030	0.0032
1000	-1.72	29	0.16	222	9	16	0.0026	0.0029
1300	-1.72	26	0.14	221	8	16	0.0025	0.0028

Neck fracture. Two lag screw Gamma nail (7-9). E = 110GPa

Cortical bone E=17GPa, Femoral Head E=1.3GPa, Trochanter E=0.32GPa.

BEND LOAD CONDITION

Fracture size=1.5

	Femur	Fracture callus		Nail	Lag Screws			
Fracture Callus Elastic Modulus (GPa)	Maximum deflection of femoral head (mm)	Strain Energy (Nmm)	Strain Energy Density (Nmm^{-2})	Strain Energy (Nmm)	Strain Energy (Nmm)		Strain Energy Density (Nmm^{-2})	
					Upper (7)	Lower (9)	Upper (7)	Lower (9)
30	-2.14	235	0.42	237	38	59	0.0114	0.0103
50	-2.03	186	0.33	235	31	49	0.0092	0.0086
80	-1.96	155	0.27	231	25	41	0.0074	0.0072
100	-1.93	137	0.24	231	23	38	0.0067	0.0066
120	-1.90	125	0.22	230	21	35	0.0062	0.0062
500	-1.77	65	0.12	224	13	22	0.0037	0.0039
1000	-1.74	49	0.09	223	11	19	0.0031	0.0034
1300	-1.73	45	0.08	222	10	18	0.0029	0.0032

Neck fracture. Two lag screw Gamma nail (7-9). E = 210GPa

Cortical bone E=17GPa, Femoral Head E=1.3GPa, Trochanter E=0.32GPa.

TORSION LOAD CONDITION

Fracture size=0.5

	Femur	Fracture callus		Nail	Lag Screws			
Fracture Callus Elastic Modulus (GPa)	Maximum deflection of femoral head (mm)	Strain Energy (Nmm)	Strain Energy Density (Nmm^{-2})	Strain Energy (Nmm)	Strain Energy (Nmm)		Strain Energy Density (Nmm^{-2})	
					Upper (7)	Lower (9)	Upper (7)	Lower (9)
30	-7.35	312	1.67	807	160	130	0.0475	0.0227
50	-7.21	263	1.41	798	128	110	0.0379	0.0193
80	-7.09	219	1.17	791	105	95	0.0312	0.0166
100	-7.05	199	1.07	788	97	89	0.0286	0.0155
120	-7.02	186	1.00	786	90	84	0.0268	0.0147
500	-6.81	103	0.55	774	58	57	0.0173	0.0099
1000	-6.75	70	0.38	771	50	50	0.0148	0.0088
1300	-6.73	60	0.32	770	48	48	0.0142	0.0085

Neck fracture. Two lag screw Gamma nail (7-9). E = 210GPa

Cortical bone E=17GPa, Femoral Head E=1.3GPa, Trochanter E=0.32GPa.

TORSION LOAD CONDITION

Fracture size=1.5

	Femur	Fracture callus		Nail	Lag Screws			
Fracture Callus Elastic Modulus (GPa)	Maximum deflection of femoral head (mm)	Strain Energy (Nmm)	Strain Energy Density (Nmm^{-2})	Strain Energy (Nmm)	Strain Energy (Nmm)		Strain Energy Density (Nmm^{-2})	
					Upper (7)	Lower (9)	Upper (7)	Lower (9)
30	-7.72	361	0.64	828	270	187	0.0801	0.0327
50	-7.57	367	0.65	819	217	159	0.0643	0.0278
80	-7.41	332	0.59	809	171	136	0.0507	0.0238
100	-7.34	314	0.56	805	154	126	0.0457	0.0221
120	-7.28	293	0.52	801	141	119	0.0419	0.0207
500	-6.96	171	0.30	782	79	75	0.0233	0.0131
1000	-6.85	128	0.23	776	63	61	0.0186	0.0107
1300	-6.82	113	0.20	774	58	58	0.0173	0.0101

Neck fracture. Two lag screw Gamma nail (7-9). E = 110GPa

Cortical bone E=17GPa, Femoral Head E=1.3GPa, Trochanter E=0.32GPa.

TORSION LOAD CONDITION

Fracture size=0.5

	Femur	Fracture callus		Nail	Lag Screws			
Fracture Callus Elastic Modulus (GPa)	Maximum deflection of femoral head (mm)	Strain Energy (Nmm)	Strain Energy Density (Nmm^{-2})	Strain Energy (Nmm)	Strain Energy (Nmm)		Strain Energy Density (Nmm^{-2})	
					Upper (7)	Lower (9)	Upper (7)	Lower (9)
30	-8.68	415	2.22	764	146	152	0.0432	0.0266
50	-8.47	341	1.83	756	111	123	0.0328	0.0215
80	-8.32	277	1.48	751	88	102	0.0261	0.0178
100	-8.25	253	1.35	749	79	93	0.0236	0.0163
120	-8.21	232	1.24	748	73	87	0.0218	0.0152
500	-7.93	125	0.67	738	44	53	0.0131	0.0093
1000	-7.85	84	0.45	736	37	46	0.0110	0.0080
1300	-7.82	71	0.38	735	35	44	0.0104	0.0076

Neck fracture. Two lag screw Gamma nail (7-9). E = 110GPa

Cortical bone E=17GPa, Femoral Head E=1.3GPa, Trochanter E=0.32GPa.

TORSION LOAD CONDITION

Fracture size=1.5

	Femur	Fracture callus		Nail	Lag Screws			
Fracture Callus Elastic Modulus (GPa)	Maximum deflection of femoral head (mm)	Strain Energy (Nmm)	Strain Energy Density (Nmm^{-2})	Strain Energy (Nmm)	Strain Energy (Nmm)		Strain Energy Density (Nmm^{-2})	
					Upper (7)	Lower (9)	Upper (7)	Lower (9)
30	-9.20	491	0.87	785	268	246	0.0796	0.0429
50	-8.97	489	0.87	774	207	199	0.0613	0.0347
80	-8.74	442	0.79	766	157	162	0.0466	0.0283
100	-8.64	413	0.73	762	138	147	0.0410	0.0256
120	-8.57	388	0.69	759	125	135	0.0371	0.0236
500	-8.12	214	0.38	744	63	75	0.0186	0.0131
1000	-7.98	156	0.28	740	48	59	0.0143	0.0103
1300	-7.93	137	0.24	739	44	54	0.0131	0.0095

Neck fracture. One lag screw Gamma nail (12). E = 210GPa

Cortical bone E=17GPa, Femoral Head E=1.3GPa, Trochanter E=0.32GPa.

BEND LOAD CONDITION

Fracture size=0.5

	Femur	Fracture callus		Nail	Lag Screw	
Fracture Callus Elastic Modulus (GPa)	Maximum deflection of femoral head (mm)	Strain Energy (Nmm)	Strain Energy Density (Nmm^{-2})	Strain Energy (Nmm)	Strain Energy (Nmm)	Strain Energy Density (Nmm^{-2})
30	-1.67	105	0.58	255	33	0.0031
50	-1.62	80	0.44	252	28	0.0027
80	-1.59	64	0.35	247	24	0.0023
100	-1.57	57	0.32	247	23	0.0022
120	-1.56	53	0.30	245	22	0.0021
500	-1.50	31	0.17	238	16	0.0016
1000	-1.49	23	0.13	235	15	0.0014
1300	-1.48	20	0.11	235	14	0.0013

Neck fracture. One lag screw Gamma nail (12). E = 210GPa

Cortical bone E=17GPa, Femoral Head E=1.3GPa, Trochanter E=0.32GPa.

BEND LOAD CONDITION

Fracture size=1.5

	Femur	Fracture callus		Nail	Lag Screw	
Fracture Callus Elastic Modulus (GPa)	Maximum deflection of femoral head (mm)	Strain Energy (Nmm)	Strain Energy Density (Nmm^{-2})	Strain Energy (Nmm)	Strain Energy (Nmm)	Strain Energy Density (Nmm^{-2})
30	-1.84	177	0.33	272	49	0.0047
50	-1.74	143	0.27	263	40	0.0039
80	-1.67	110	0.20	259	34	0.0032
100	-1.65	100	0.18	256	31	0.0030
120	-1.63	91	0.17	254	29	0.0028
500	-1.53	48	0.09	242	19	0.0018
1000	-1.50	37	0.07	239	17	0.0016
1300	-1.49	34	0.06	238	16	0.0015

Neck fracture. One lag screw Gamma nail (12). E = 110GPa

Cortical bone E=17GPa, Femoral Head E=1.3GPa, Trochanter E=0.32GPa.

BEND LOAD CONDITION

Fracture size=0.5

	Femur	Fracture callus		Nail	Lag Screw	
Fracture Callus Elastic Modulus (GPa)	Maximum deflection of femoral head (mm)	Strain Energy (Nmm)	Strain Energy Density (Nmm^{-2})	Strain Energy (Nmm)	Strain Energy (Nmm)	Strain Energy Density (Nmm^{-2})
30	-2.00	132	0.73	249	35	0.0034
50	-1.93	98	0.54	247	29	0.0028
80	-1.88	78	0.43	243	24	0.0023
100	-1.87	70	0.39	242	23	0.0022
120	-1.85	65	0.36	241	22	0.0021
500	-1.77	37	0.20	235	16	0.0015
1000	-1.75	27	0.15	234	14	0.0013
1300	-1.75	23	0.13	233	13	0.0013

Neck fracture. One lag screw Gamma nail (12). E = 110GPa

Cortical bone E=17GPa, Femoral Head E=1.3GPa, Trochanter E=0.32GPa.

BEND LOAD CONDITION

Fracture size=1.5

	Femur	Fracture callus		Nail	Lag Screw	
Fracture Callus Elastic Modulus (GPa)	Maximum deflection of femoral head (mm)	Strain Energy (Nmm)	Strain Energy Density (Nmm^{-2})	Strain Energy (Nmm)	Strain Energy (Nmm)	Strain Energy Density (Nmm^{-2})
30	-2.21	230	0.43	263	57	0.0054
50	-2.08	184	0.34	255	45	0.0043
80	-2.00	144	0.27	250	37	0.0035
100	-1.97	128	0.24	247	33	0.0032
120	-1.95	116	0.22	246	31	0.0029
500	-1.81	58	0.11	239	19	0.0018
1000	-1.78	44	0.08	236	16	0.0015
1300	-1.76	40	0.07	235	15	0.0015

Neck fracture. One lag screw Gamma nail (12). E = 210GPa

Cortical bone E=17GPa, Femoral Head E=1.3GPa, Trochanter E=0.32GPa.

TORSION LOAD CONDITION

Fracture size=0.5

	Femur	Fracture callus		Nail	Lag Screw	
Fracture Callus Elastic Modulus (GPa)	Maximum deflection of femoral head (mm)	Strain Energy (Nmm)	Strain Energy Density (Nmm^{-2})	Strain Energy (Nmm)	Strain Energy (Nmm)	Strain Energy Density (Nmm^{-2})
30	-7.20	337	1.87	836	146	0.0140
50	-7.03	244	1.36	826	126	0.0121
80	-6.93	192	1.07	818	111	0.0106
100	-6.89	174	0.97	815	104	0.0100
120	-6.87	161	0.90	813	99	0.0095
500	-6.71	87	0.48	798	72	0.0069
1000	-6.66	59	0.33	794	64	0.0061
1300	-6.64	50	0.28	793	62	0.0059

Neck fracture. One lag screw Gamma nail (12). E = 210GPa

Cortical bone E=17GPa, Femoral Head E=1.3GPa, Trochanter E=0.32GPa.

TORSION LOAD CONDITION

Fracture size=1.5

	Femur	Fracture callus		Nail	Lag Screw	
Fracture Callus Elastic Modulus (GPa)	Maximum deflection of femoral head (mm)	Strain Energy (Nmm)	Strain Energy Density (Nmm^{-2})	Strain Energy (Nmm)	Strain Energy (Nmm)	Strain Energy Density (Nmm^{-2})
30	-7.62	476	0.88	873	217	0.8840
50	-7.39	418	0.78	853	180	0.7760
80	-7.22	346	0.64	839	153	0.6422
100	-7.15	312	0.58	833	142	0.5802
120	-7.09	280	0.52	829	134	0.5200
500	-6.82	147	0.27	807	89	0.2739
1000	-6.74	108	0.20	800	76	0.2012
1300	-6.71	94	0.18	798	72	0.1751

Neck fracture. One lag screw Gamma nail (12). E = 110GPa

Cortical bone E=17GPa, Femoral Head E=1.3GPa, Trochanter E=0.32GPa.

TORSION LOAD CONDITION

Fracture size=0.5

	Femur	Fracture callus		Nail	Lag Screw	
Fracture Callus Elastic Modulus (GPa)	Maximum deflection of femoral head (mm)	Strain Energy (Nmm)	Strain Energy Density (Nmm^{-2})	Strain Energy (Nmm)	Strain Energy (Nmm)	Strain Energy Density (Nmm^{-2})
30	-8.44	416	2.31	788	180	0.0173
50	-8.24	301	1.67	777	152	0.0145
80	-8.11	241	1.34	769	128	0.0122
100	-8.06	217	1.20	766	119	0.0114
120	-8.03	202	1.12	764	111	0.0106
500	-7.81	106	0.59	752	74	0.0071
1000	-7.75	71	0.40	749	65	0.0062
1300	-7.73	60	0.33	748	62	0.0059

Neck fracture. One lag screw Gamma nail (12). E = 110GPa

Cortical bone E=17GPa, Femoral Head E=1.3GPa, Trochanter E=0.32GPa.

TORSION LOAD CONDITION

Fracture size=1.5

	Femur	Fracture callus		Nail	Lag Screw	
Fracture Callus Elastic Modulus (GPa)	Maximum deflection of femoral head (mm)	Strain Energy (Nmm)	Strain Energy Density (Nmm^{-2})	Strain Energy (Nmm)	Strain Energy (Nmm)	Strain Energy Density (Nmm^{-2})
30	-8.96	605	1.12	833	293	0.0281
50	-8.69	531	0.99	804	232	0.0222
80	-8.49	439	0.82	791	190	0.0182
100	-8.37	378	0.70	782	175	0.0168
120	-8.31	350	0.65	781	163	0.0156
500	-7.96	180	0.33	759	98	0.0094
1000	-7.85	130	0.24	754	81	0.0078
1300	-7.82	115	0.21	752	76	0.0072

Neck fracture. Two lag screw Gamma nail (8-8). E = 210GPa

Cortical bone E=17GPa, Femoral Head E=1.3GPa, Trochanter E=0.32GPa.

BEND LOAD CONDITION

Fracture size=1.5

	Femur	Fracture callus		Nail	Lag Screws			
Fracture Callus Elastic Modulus (GPa)	Maximum deflection of femoral head (mm)	Strain Energy (Nmm)	Strain Energy Density (Nmm^{-2})	Strain Energy (Nmm)	Strain Energy (Nmm)		Strain Energy Density (Nmm^{-2})	
					Upper (8)	Lower (8)	Upper (8)	Lower (8)
30	-1.80	193	0.34	225	58	46	0.0130	0.0104
50	-1.72	146	0.26	223	50	40	0.0112	0.0090
80	-1.65	119	0.21	219	43	35	0.0096	0.0078
100	-1.63	105	0.19	218	40	33	0.0089	0.0073
120	-1.61	96	0.17	217	38	31	0.0084	0.0069
500	-1.51	50	0.09	209	26	22	0.0058	0.0049
1000	-1.48	39	0.07	207	23	19	0.0051	0.0043
1300	-1.48	32	0.06	208	22	20	0.0050	0.0044

Neck fracture. Two lag screw Gamma nail (8-8). E = 110GPa

Cortical bone E=17GPa, Femoral Head E=1.3GPa, Trochanter E=0.32GPa.

BEND LOAD CONDITION

Fracture size=1.5

	Femur	Fracture callus		Nail	Lag Screws			
Fracture Callus Elastic Modulus (GPa)	Maximum deflection of femoral head (mm)	Strain Energy (Nmm)	Strain Energy Density (Nmm^{-2})	Strain Energy (Nmm)	Strain Energy (Nmm)		Strain Energy Density (Nmm^{-2})	
					Upper (8)	Lower (8)	Upper (8)	Lower (8)
30	-2.18	244	0.43	227	58	50	0.0130	0.0112
50	-2.07	188	0.33	224	48	42	0.0107	0.0094
80	-1.98	144	0.26	224	40	36	0.0089	0.0080
100	-1.95	134	0.24	221	36	33	0.0081	0.0073
120	-1.93	123	0.22	220	34	30	0.0075	0.0068
500	-1.80	61	0.11	214	21	20	0.0047	0.0045
1000	-1.76	46	0.08	212	18	17	0.0040	0.0039
1300	-1.75	43	0.08	210	17	16	0.0038	0.0037

Neck fracture. Two lag screw Gamma nail (8-8). E = 210GPa

Cortical bone E=17GPa, Femoral Head E=1.3GPa, Trochanter E=0.32GPa.

TORSION LOAD CONDITION

Fracture size=1.5

	Femur	Fracture callus		Nail	Lag Screws			
Fracture Callus Elastic Modulus (GPa)	Maximum deflection of femoral head (mm)	Strain Energy (Nmm)	Strain Energy Density (Nmm^{-2})	Strain Energy (Nmm)	Strain Energy (Nmm)		Strain Energy Density (Nmm^{-2})	
					Upper (8)	Lower (8)	Upper (8)	Lower (8)
30	-7.65	313	0.56	845	307	152	0.0686	0.0339
50	-7.51	320	0.57	831	255	126	0.0571	0.0282
80	-7.37	304	0.54	819	211	105	0.0472	0.0236
100	-7.30	280	0.50	813	191	97	0.0427	0.0217
120	-7.25	272	0.48	809	177	91	0.0397	0.0203
500	-6.95	165	0.29	783	104	55	0.0232	0.0122
1000	-6.85	124	0.22	775	84	44	0.0188	0.0099
1300	-6.81	110	0.19	773	79	42	0.0176	0.0093

Neck fracture. Two lag screw Gamma nail (8-8). E = 110GPa

Cortical bone E=17GPa, Femoral Head E=1.3GPa, Trochanter E=0.32GPa.

TORSION LOAD CONDITION

Fracture size=1.5

	Femur	Fracture callus		Nail	Lag Screws			
Fracture Callus Elastic Modulus (GPa)	Maximum deflection of femoral head (mm)	Strain Energy (Nmm)	Strain Energy Density (Nmm^{-2})	Strain Energy (Nmm)	Strain Energy (Nmm)		Strain Energy Density (Nmm^{-2})	
					Upper (8)	Lower (8)	Upper (8)	Lower (8)
30	-9.18	472	0.84	799	338	189	0.0757	0.0422
50	-8.95	457	0.81	785	266	149	0.0594	0.0333
80	-8.73	425	0.75	772	210	118	0.0469	0.0265
100	-8.64	398	0.71	768	186	106	0.0416	0.0238
120	-8.56	372	0.66	764	169	98	0.0378	0.0219
500	-8.12	207	0.37	745	88	53	0.0196	0.0118
1000	-7.98	153	0.27	738	68	41	0.0153	0.0091
1300	-7.94	135	0.24	736	63	38	0.0141	0.0084

Neck fracture. Two lag screw Gamma nail (9-7). E = 210GPa

Cortical bone E=17GPa, Femoral Head E=1.3GPa, Trochanter E=0.32GPa.

BEND LOAD CONDITION

Fracture size=1.5

	Femur	Fracture callus		Nail	Lag Screws			
Fracture Callus Elastic Modulus (GPa)	Maximum deflection of femoral head (mm)	Strain Energy (Nmm)	Strain Energy Density (Nmm^{-2})	Strain Energy (Nmm)	Strain Energy (Nmm)		Strain Energy Density (Nmm^{-2})	
					Upper (9)	Lower (7)	Upper (9)	Lower (7)
30	-1.80	192	0.34	244	60	33	0.0105	0.0098
50	-1.71	146	0.26	241	52	28	0.0090	0.0084
80	-1.65	114	0.20	237	45	25	0.0078	0.0073
100	-1.62	104	0.18	235	41	23	0.0072	0.0069
120	-1.60	95	0.17	233	39	22	0.0068	0.0065
500	-1.50	50	0.09	223	26	15	0.0046	0.0046
1000	-1.47	38	0.07	220	23	14	0.0040	0.0041
1300	-1.46	35	0.06	219	22	13	0.0039	0.0039

Neck fracture. Two lag screw Gamma nail (9-7). E = 110GPa

Cortical bone E=17GPa, Femoral Head E=1.3GPa, Trochanter E=0.32GPa.

BEND LOAD CONDITION

Fracture size=1.5

	Femur	Fracture callus		Nail	Lag Screws			
Fracture Callus Elastic Modulus (GPa)	Maximum deflection of femoral head (mm)	Strain Energy (Nmm)	Strain Energy Density (Nmm^{-2})	Strain Energy (Nmm)	Strain Energy (Nmm)		Strain Energy Density (Nmm^{-2})	
					Upper (9)	Lower (7)	Upper (9)	Lower (7)
30	-2.17	239	0.42	244	64	35	0.0112	0.0105
50	-2.06	183	0.32	241	53	30	0.0092	0.0088
80	-1.98	144	0.26	237	44	25	0.0076	0.0074
100	-1.94	131	0.23	236	39	23	0.0069	0.0067
120	-1.92	120	0.21	234	37	21	0.0064	0.0063
500	-1.78	60	0.11	226	23	14	0.0040	0.0041
1000	-1.74	46	0.08	223	19	12	0.0033	0.0036
1300	-1.73	42	0.07	222	18	11	0.0031	0.0034

Neck fracture. Two lag screw Gamma nail (9-7). E = 210GPa

Cortical bone E=17GPa, Femoral Head E=1.3GPa, Trochanter E=0.32GPa.

TORSION LOAD CONDITION

Fracture size=1.5

	Femur	Fracture callus		Nail	Lag Screws			
Fracture Callus Elastic Modulus (GPa)	Maximum deflection of femoral head (mm)	Strain Energy (Nmm)	Strain Energy Density (Nmm^{-2})	Strain Energy (Nmm)	Strain Energy (Nmm)		Strain Energy Density (Nmm^{-2})	
					Upper (9)	Lower (7)	Upper (9)	Lower (7)
30	-7.54	296	0.53	870	315	103	0.0550	0.0306
50	-7.41	296	0.53	856	266	83	0.0464	0.0245
80	-7.28	270	0.48	842	223	67	0.0389	0.0198
100	-7.23	257	0.46	836	205	61	0.0357	0.0180
120	-7.18	242	0.43	830	191	56	0.0334	0.0166
500	-6.91	156	0.28	801	115	33	0.0201	0.0098
1000	-6.82	119	0.21	791	94	27	0.0164	0.0080
1300	-6.79	105	0.19	788	88	25	0.0153	0.0075

Neck fracture. Two lag screw Gamma nail (9-7). E = 110GPa

Cortical bone E=17GPa, Femoral Head E=1.3GPa, Trochanter E=0.32GPa.

TORSION LOAD CONDITION

Fracture size=1.5

	Femur	Fracture callus		Nail	Lag Screws			
Fracture Callus Elastic Modulus (GPa)	Maximum deflection of femoral head (mm)	Strain Energy (Nmm)	Strain Energy Density (Nmm^{-2})	Strain Energy (Nmm)	Strain Energy (Nmm)		Strain Energy Density (Nmm^{-2})	
					Upper (9)	Lower (7)	Upper (9)	Lower (7)
30	-9.06	453	0.81	820	374	122	0.0654	0.0361
50	-8.85	438	0.78	806	299	93	0.0522	0.0276
80	-8.65	392	0.70	793	238	72	0.0416	0.0214
100	-8.56	358	0.64	788	214	64	0.0374	0.0190
120	-8.49	344	0.61	783	196	59	0.0342	0.0174
500	-8.09	200	0.36	758	105	31	0.0183	0.0093
1000	-7.96	150	0.27	750	81	25	0.0142	0.0073
1300	-7.92	132	0.23	747	75	23	0.0131	0.0067

Neck fracture. Two lag screw Gamma nail (7-9). E = 210GPa

Cortical bone E=17GPa, Femoral Head E=1.3GPa, Trochanter E=0.32GPa.

BEND LOAD CONDITION

Fracture size=0.5

	Fracture callus	Lag Screws		Nail insertion hole	
Fracture Callus Elastic Modulus (GPa)	Peak von Mises stress (MPa)	Peak von Mises stress (MPa)		Peak von Mises stress (MPa)	
		Upper (7)	Lower (9)	Upper (7)	Lower (9)
30	17	267	215	440	479
50	21	244	201	428	475
80	25	230	193	412	474
100	27	222	188	404	469
120	29	216	185	399	468
500	56	193	173	358	450
1000	71	175	162	360	451
1300	77	173	162	355	449

Neck fracture. Two lag screw Gamma nail (7-9). E = 210GPa

Cortical bone E=17GPa, Femoral Head E=1.3GPa, Trochanter E=0.32GPa.

BEND LOAD CONDITION

Fracture size=1.5

	Fracture callus	Lag Screws		Nail insertion hole	
Fracture Callus Elastic Modulus (GPa)	Peak von Mises stress (MPa)	Peak von Mises stress (MPa)		Peak von Mises stress (MPa)	
		Upper (7)	Lower (9)	Upper (7)	Lower (9)
30	10	308	245	454	485
50	13	290	229	459	494
80	16	268	213	446	486
100	18	258	208	439	482
120	19	250	204	432	477
500	38	207	182	378	454
1000	51	191	171	367	457
1300	57	185	169	360	450

Neck fracture. Two lag screw Gamma nail (7-9). E = 110GPa

Cortical bone E=17GPa, Femoral Head E=1.3GPa, Trochanter E=0.32GPa.

BEND LOAD CONDITION

Fracture size=0.5

	Fracture callus	Lag Screws		Nail insertion hole	
Fracture Callus Elastic Modulus (GPa)	Peak von Mises stress (MPa)	Peak von Mises stress (MPa)		Peak von Mises stress (MPa)	
		Upper (7)	Lower (9)	Upper (7)	Lower (9)
30	19	178	151	276	376
50	23	159	140	268	374
80	27	154	138	256	377
100	31	147	134	247	369
120	33	139	129	244	366
500	61	116	117	218	360
1000	78	106	111	209	359
1300	85	110	114	203	357

Neck fracture. Two lag screw Gamma nail (7-9). E = 110GPa

Cortical bone E=17GPa, Femoral Head E=1.3GPa, Trochanter E=0.32GPa.

BEND LOAD CONDITION

Fracture size=1.5

	Fracture callus	Lag Screws		Nail insertion hole	
Fracture Callus Elastic Modulus (GPa)	Peak von Mises stress (MPa)	Peak von Mises stress (MPa)		Peak von Mises stress (MPa)	
		Upper (7)	Lower (9)	Upper (7)	Lower (9)
30	11	211	174	303	391
50	14	194	160	293	388
80	18	181	154	276	377
100	20	170	145	276	377
120	21	164	142	272	375
500	42	130	123	231	362
1000	57	124	121	217	361
1300	64	114	116	213	357

Neck fracture. Two lag screw Gamma nail (7-9). E = 210GPa

Cortical bone E=17GPa, Femoral Head E=1.3GPa, Trochanter E=0.32GPa.

TORSION LOAD CONDITION

Fracture size=0.5

	Fracture callus	Lag Screws		Nail insertion hole	
Fracture Callus Elastic Modulus (GPa)	Peak von Mises stress (MPa)	Peak von Mises stress (MPa)		Peak von Mises stress (MPa)	
		Upper (7)	Lower (9)	Upper (7)	Lower (9)
30	31	581	490	732	562
50	40	521	440	683	575
80	49	476	398	643	584
100	54	458	379	626	589
120	59	443	364	614	591
500	106	358	264	528	604
1000	131	333	234	497	606
1300	140	323	225	491	605

Neck fracture. Two lag screw Gamma nail (7-9). E = 210GPa

Cortical bone E=17GPa, Femoral Head E=1.3GPa, Trochanter E=0.32GPa.

TORSION LOAD CONDITION

Fracture size=1.5

	Fracture callus	Lag Screws		Nail insertion hole	
Fracture Callus Elastic Modulus (GPa)	Peak von Mises stress (MPa)	Peak von Mises stress (MPa)		Peak von Mises stress (MPa)	
		Upper (7)	Lower (9)	Upper (7)	Lower (9)
30	16	739	632	869	542
50	22	666	572	805	550
80	29	597	516	741	559
100	33	568	491	719	563
120	36	546	471	697	571
500	76	414	338	584	594
1000	104	371	286	539	602
1300	115	356	269	516	525

Neck fracture. Two lag screw Gamma nail (7-9). E = 110GPa

Cortical bone E=17GPa, Femoral Head E=1.3GPa, Trochanter E=0.32GPa.

TORSION LOAD CONDITION

Fracture size=0.5

	Fracture callus	Lag Screws		Nail insertion hole	
Fracture Callus Elastic Modulus (GPa)	Peak von Mises stress (MPa)	Peak von Mises stress (MPa)		Peak von Mises stress (MPa)	
		Upper (7)	Lower (9)	Upper (7)	Lower (9)
30	35	394	397	474	423
50	45	348	347	435	431
80	54	318	307	403	441
100	60	303	290	393	443
120	64	294	277	383	449
500	117	230	194	331	455
1000	144	213	169	306	456
1300	154	206	162	455	303

Neck fracture. Two lag screw Gamma nail (7-9). E = 110GPa

Cortical bone E=17GPa, Femoral Head E=1.3GPa, Trochanter E=0.32GPa.

TORSION LOAD CONDITION

Fracture size=1.5

	Fracture callus	Lag Screws		Nail insertion hole	
Fracture Callus Elastic Modulus (GPa)	Peak von Mises stress (MPa)	Peak von Mises stress (MPa)		Peak von Mises stress (MPa)	
		Upper (7)	Lower (9)	Upper (7)	Lower (9)
30	18	521	551	578	421
50	25	461	486	526	430
80	34	406	426	479	423
100	38	384	400	461	425
120	42	366	380	448	427
500	85	271	256	367	448
1000	115	240	213	455	337
1300	127	229	200	327	455

Neck fracture. One lag screw Gamma nail (12). E = 210GPa

Cortical bone E=17GPa, Femoral Head E=1.3GPa, Trochanter E=0.32GPa.

BEND LOAD CONDITION

Fracture size=0.5

	Fracture callus	Lag Screw	Nail insertion hole
Fracture Callus Elastic Modulus (GPa)	Peak von Mises stress (MPa)	Peak von Mises stress (MPa)	Peak von Mises stress (MPa)
30	12	190	834
50	16	177	831
80	21	168	818
100	23	164	820
120	26	161	811
500	54	142	786
1000	70	137	778
1300	76	135	777

Neck fracture. One lag screw Gamma nail (12). E = 210GPa

Cortical bone E=17GPa, Femoral Head E=1.3GPa, Trochanter E=0.32GPa.

BEND LOAD CONDITION

Fracture size=1.5

	Fracture callus	Lag Screw	Nail insertion hole
Fracture Callus Elastic Modulus (GPa)	Peak von Mises stress (MPa)	Peak von Mises stress (MPa)	Peak von Mises stress (MPa)
30	9	221	877
50	11	205	851
80	14	191	853
100	15	185	842
120	17	180	837
500	37	152	800
1000	53	143	789
1300	59	141	786

Neck fracture. One lag screw Gamma nail (12). E = 110GPa

Cortical bone E=17GPa, Femoral Head E=1.3GPa, Trochanter E=0.32GPa.

BEND LOAD CONDITION

Fracture size=0.5

	Fracture callus	Lag Screw	Nail insertion hole
Fracture Callus Elastic Modulus (GPa)	Peak von Mises stress (MPa)	Peak von Mises stress (MPa)	Peak von Mises stress (MPa)
30	13	134	599
50	18	124	600
80	23	116	591
100	26	113	588
120	29	111	585
500	59	97	569
1000	77	93	565
1300	83	91	564

Neck fracture. One lag screw Gamma nail (12). E = 110GPa

Cortical bone E=17GPa, Femoral Head E=1.3GPa, Trochanter E=0.32GPa.

BEND LOAD CONDITION

Fracture size=1.5

	Fracture callus	Lag Screw	Nail insertion hole
Fracture Callus Elastic Modulus (GPa)	Peak von Mises stress (MPa)	Peak von Mises stress (MPa)	Peak von Mises stress (MPa)
30	10	162	623
50	13	148	608
80	16	135	599
100	18	130	595
120	19	126	591
500	41	105	579
1000	58	98	571
1300	65	96	569

Neck fracture. One lag screw Gamma nail (12). E = 210GPa

Cortical bone E=17GPa, Femoral Head E=1.3GPa, Trochanter E=0.32GPa.

TORSION LOAD CONDITION

Fracture size=0.5

	Fracture callus	Lag Screw	Nail insertion hole
Fracture Callus Elastic Modulus (GPa)	Peak von Mises stress (MPa)	Peak von Mises stress (MPa)	Peak von Mises stress (MPa)
30	27	257	1037
50	33	244	1048
80	42	233	1041
100	47	228	1035
120	52	224	1029
500	98	202	1005
1000	126	195	996
1300	136	193	994

Neck fracture. One lag screw Gamma nail (12). E = 210GPa

Cortical bone E=17GPa, Femoral Head E=1.3GPa, Trochanter E=0.32GPa.

TORSION LOAD CONDITION

Fracture size=1.5

	Fracture callus	Lag Screw	Nail insertion hole
Fracture Callus Elastic Modulus (GPa)	Peak von Mises stress (MPa)	Peak von Mises stress (MPa)	Peak von Mises stress (MPa)
30	17	300	1033
50	21	280	1049
80	26	263	1051
100	30	255	1044
120	33	250	1054
500	71	214	1015
1000	100	204	1006
1300	111	202	1005

Neck fracture. One lag screw Gamma nail (12). E = 110GPa

Cortical bone E=17GPa, Femoral Head E=1.3GPa, Trochanter E=0.32GPa.

TORSION LOAD CONDITION

Fracture size=0.5

	Fracture callus	Lag Screw	Nail insertion hole
Fracture Callus Elastic Modulus (GPa)	Peak von Mises stress (MPa)	Peak von Mises stress (MPa)	Peak von Mises stress (MPa)
30	30	209	744
50	37	195	753
80	47	180	738
100	53	173	734
120	58	167	727
500	109	142	712
1000	138	136	706
1300	150	134	704

Neck fracture. One lag screw Gamma nail (12). E = 110GPa

Cortical bone E=17GPa, Femoral Head E=1.3GPa, Trochanter E=0.32GPa.

TORSION LOAD CONDITION

Fracture size=1.5

	Fracture callus	Lag Screw	Nail insertion hole
Fracture Callus Elastic Modulus (GPa)	Peak von Mises stress (MPa)	Peak von Mises stress (MPa)	Peak von Mises stress (MPa)
30	18	261	763
50	24	236	751
80	30	216	750
100	34	210	755
120	37	203	755
500	79	158	722
1000	109	144	715
1300	123	141	712

Neck fracture. Two lag screw Gamma nail (8-8). E = 210GPa

Cortical bone E=17GPa, Femoral Head E=1.3GPa, Trochanter E=0.32GPa.

BEND LOAD CONDITION

Fracture size=1.5

	Fracture callus	Lag Screws		Nail insertion hole	
Fracture Callus Elastic Modulus (GPa)	Peak von Mises stress (MPa)	Peak von Mises stress (MPa)		Peak von Mises stress (MPa)	
		Upper (8)	Lower (8)	Upper (8)	Lower (8)
30	10	338	255	539	445
50	12	312	239	539	459
80	16	298	228	511	449
100	17	285	221	510	454
120	19	276	216	505	453
500	35	230	195	445	436
1000	47	215	188	428	432
1300	50	217	193	431	439

Neck fracture. Two lag screw Gamma nail (8-8). E = 110GPa

Cortical bone E=17GPa, Femoral Head E=1.3GPa, Trochanter E=0.32GPa.

BEND LOAD CONDITION

Fracture size=1.5

	Fracture callus	Lag Screws		Nail insertion hole	
Fracture Callus Elastic Modulus (GPa)	Peak von Mises stress (MPa)	Peak von Mises stress (MPa)		Peak von Mises stress (MPa)	
		Upper (8)	Lower (8)	Upper (8)	Lower (8)
30	11	243	180	353	301
50	14	223	166	349	297
80	18	201	154	346	301
100	20	196	152	331	291
120	21	191	150	323	290
500	39	153	134	284	285
1000	52	145	131	265	283
1300	57	137	125	279	261

Neck fracture. Two lag screw Gamma nail (8-8). E = 210GPa

Cortical bone E=17GPa, Femoral Head E=1.3GPa, Trochanter E=0.32GPa.

TORSION LOAD CONDITION

Fracture size=1.5

	Fracture callus	Lag Screws		Nail insertion hole	
Fracture Callus Elastic Modulus (GPa)	Peak von Mises stress (MPa)	Peak von Mises stress (MPa)		Peak von Mises stress (MPa)	
		Upper (8)	Lower (8)	Upper (8)	Lower (8)
30	14	669	717	912	484
50	20	617	642	857	469
80	27	564	572	809	459
100	30	539	539	786	458
120	34	522	514	768	455
500	71	407	356	664	462
1000	98	370	298	622	471
1300	109	357	279	610	475

Neck fracture. Two lag screw Gamma nail (8-8). E = 110GPa

Cortical bone E=17GPa, Femoral Head E=1.3GPa, Trochanter E=0.32GPa.

TORSION LOAD CONDITION

Fracture size=1.5

	Fracture callus	Lag Screws		Nail insertion hole	
Fracture Callus Elastic Modulus (GPa)	Peak von Mises stress (MPa)	Peak von Mises stress (MPa)		Peak von Mises stress (MPa)	
		Upper (8)	Lower (8)	Upper (8)	Lower (8)
30	18	496	609	632	353
50	24	443	531	578	346
80	32	397	459	541	336
100	36	375	428	523	333
120	40	360	403	508	332
500	80	274	260	422	353
1000	110	246	213	394	356
1300	121	236	199	386	357

Neck fracture. Two lag screw Gamma nail (9-7). E = 210GPa

Cortical bone E=17GPa, Femoral Head E=1.3GPa, Trochanter E=0.32GPa.

BEND LOAD CONDITION

Fracture size=1.5

	Fracture callus	Lag Screws		Nail insertion hole	
Fracture Callus Elastic Modulus (GPa)	Peak von Mises stress (MPa)	Peak von Mises stress (MPa)		Peak von Mises stress (MPa)	
		Upper (9)	Lower (7)	Upper (9)	Lower (7)
30	10	305	239	610	384
50	13	282	225	602	390
80	15	263	214	589	405
100	17	254	207	577	403
120	18	248	203	565	402
500	37	208	181	500	397
1000	51	196	178	476	392
1300	57	190	173	472	391

Neck fracture. Two lag screw Gamma nail (9-7). E = 110GPa

Cortical bone E=17GPa, Femoral Head E=1.3GPa, Trochanter E=0.32GPa.

BEND LOAD CONDITION

Fracture size=1.5

	Fracture callus	Lag Screws		Nail insertion hole	
Fracture Callus Elastic Modulus (GPa)	Peak von Mises stress (MPa)	Peak von Mises stress (MPa)		Peak von Mises stress (MPa)	
		Upper (9)	Lower (7)	Upper (9)	Lower (7)
30	12	223	188	406	295
50	14	199	167	404	287
80	17	184	149	389	281
100	19	175	143	378	276
120	20	170	137	370	273
500	42	142	126	317	258
1000	58	128	119	300	255
1300	64	122	117	297	253

Neck fracture. Two lag screw Gamma nail (9-7). E = 210GPa

Cortical bone E=17GPa, Femoral Head E=1.3GPa, Trochanter E=0.32GPa.

BEND LOAD CONDITION

Fracture size=1.5

	Fracture callus	Lag Screws		Nail insertion hole	
Fracture Callus Elastic Modulus (GPa)	Peak von Mises stress (MPa)	Peak von Mises stress (MPa)		Peak von Mises stress (MPa)	
		Upper (9)	Lower (7)	Upper (9)	Lower (7)
30	14	570	760	901	447
50	19	526	673	855	439
80	26	484	588	810	419
100	30	466	552	789	413
120	33	452	523	773	410
500	73	357	354	677	407
1000	101	327	295	643	408
1300	113	316	276	632	410

Neck fracture. Two lag screw Gamma nail (9-7). E = 110GPa

Cortical bone E=17GPa, Femoral Head E=1.3GPa, Trochanter E=0.32GPa.

BEND LOAD CONDITION

Fracture size=1.5

	Fracture callus	Lag Screws		Nail insertion hole	
Fracture Callus Elastic Modulus (GPa)	Peak von Mises stress (MPa)	Peak von Mises stress (MPa)		Peak von Mises stress (MPa)	
		Upper (9)	Lower (7)	Upper (9)	Lower (7)
30	17	437	628	636	316
50	24	393	542	587	306
80	32	354	461	544	297
100	36	339	424	526	296
120	40	325	400	512	292
500	83	246	254	436	295
1000	115	222	208	410	299
1300	127	215	195	401	301

Subtrochanteric data

Subtrochanteric fracture. One lag screw Gamma nail (12). E = 210GPa
Cortical bone E=17GPa, Femoral Head E=1.3GPa, Trochanter E=0.32GPa.

BEND LOAD CONDITION

Fracture size=0.5

	Femur	Fracture callus			Nail		Lag Screw
Fracture Callus Elastic Modulus (GPa)	Maximum deflection of femoral head (mm)	Strain Energy (Nmm)	Strain Energy Density (Nmm^{-2})	Peak von Mises stress (MPa)	Strain Energy (Nmm)	Peak von Mises stress (MPa)	Strain Energy (Nmm)
1	-2.12	15	0.06	0.5	693	1100	58
5	-2.07	48	0.20	2.0	652	1100	49
10	-2.05	68	0.28	3.3	609	1084	44
20	-2.01	83	0.35	5.1	552	1053	39
30	-1.96	88	0.37	6.4	516	1028	37
50	-1.94	85	0.35	8.2	467	998	34
80	-1.90	74	0.31	9.8	427	972	33
100	-1.88	68	0.28	10.5	411	962	32
120	-1.87	62	0.26	11.1	399	953	32
300	-1.82	35	0.14	13.7	357	926	30
500	-1.80	23	0.10	14.7	343	914	30
1000	-1.79	13	0.05	16.3	332	906	29
5000	-1.78	3	0.01	24.3	322	894	29
10000	-1.78	2	0.01	35.2	321	893	29
17000	-1.78	1	0.00	46.4	320	893	29

Subtrochanteric fracture. One lag screw Gamma nail (12). E = 210GPa

Cortical bone E=17GPa, Femoral Head E=1.3GPa, Trochanter E=0.32GPa.

BEND LOAD CONDITION

Fracture size=1.5

	Femur	Fracture callus			Nail		Lag Screw
Fracture Callus Elastic Modulus (GPa)	Maximum deflection of femoral head (mm)	Strain Energy (Nmm)	Strain Energy Density (Nmm^{-2})	Peak von Mises stress (MPa)	Strain Energy (Nmm)	Peak von Mises stress (MPa)	Strain Energy (Nmm)
1	-2.14	6	0.01	0.2	715	1111	62
5	-2.12	24	0.03	1.0	698	1119	57
10	-2.11	39	0.05	1.8	680	1118	53
20	-2.08	58	0.08	3.1	646	1107	48
30	-2.06	70	0.10	4.1	618	1094	45
50	-2.03	84	0.12	5.8	575	1071	41
80	-1.98	90	0.13	7.5	532	1042	38
100	-1.96	91	0.13	8.4	509	1027	37
120	-1.95	90	0.12	9.2	491	1015	36
300	-1.89	70	0.10	13.0	412	963	33
500	-1.85	53	0.07	14.8	381	940	31
1000	-1.82	33	0.05	16.6	353	923	30
5000	-1.78	9	0.01	21.5	326	900	29
10000	-1.77	5	0.01	24.6	322	896	29
17000	-1.78	3	0.00	28.4	320	892	29

Subtrochanteric fracture. One lag screw Gamma nail (12). E = 210GPa
Cortical bone E=17GPa, Femoral Head E=1.3GPa, Trochanter E=0.32GPa.

BEND LOAD CONDITION

Fracture size=0.5

	Femur	Fracture callus			Nail		Lag Screw
Fracture Callus Elastic Modulus (GPa)	Maximum deflection of femoral head (mm)	Strain Energy (Nmm)	Strain Energy Density (Nmm^{-2})	Peak von Mises stress (MPa)	Strain Energy (Nmm)	Peak von Mises stress (MPa)	Strain Energy (Nmm)
1	-2.82	30	0.12	0.7	979	829	65
5	-2.74	96	0.40	2.8	887	820	51
10	-2.67	135	0.56	4.6	800	806	44
20	-2.56	164	0.68	7.1	687	777	38
30	-2.49	168	0.70	8.9	616	755	35
50	-2.41	158	0.66	11.1	533	725	32
80	-2.34	135	0.56	13.2	469	700	30
100	-2.31	122	0.51	14.1	443	689	29
120	-2.28	110	0.46	14.9	425	683	29
300	-2.20	59	0.24	17.8	362	658	27
500	-2.17	39	0.16	19.0	343	650	26
1000	-2.15	21	0.09	21.0	328	642	26
5000	-2.13	5	0.02	26.1	315	635	26
10000	-2.12	3	0.01	34.1	313	634	26
17000	-2.12	2	0.01	44.2	313	634	26

Subtrochanteric fracture. One lag screw Gamma nail (12). E = 210GPa

Cortical bone E=17GPa, Femoral Head E=1.3GPa, Trochanter E=0.32GPa.

BEND LOAD CONDITION

Fracture size=1.5

	Femur	Fracture callus			Nail		Lag Screw
Fracture Callus Elastic Modulus (GPa)	Maximum deflection of femoral head (mm)	Strain Energy (Nmm)	Strain Energy Density (Nmm^{-2})	Peak von Mises stress (MPa)	Strain Energy (Nmm)	Peak von Mises stress (MPa)	Strain Energy (Nmm)
1	-2.88	12	0.02	0.3	1023	845	71
5	-2.82	47	0.07	1.4	986	845	63
10	-2.80	78	0.11	2.5	944	839	57
20	-2.74	117	0.16	4.3	872	829	49
30	-2.69	141	0.20	5.8	817	818	45
50	-2.61	165	0.23	8.0	731	796	40
80	-2.53	175	0.24	10.4	645	769	36
100	-2.49	174	0.24	11.7	605	755	34
120	-2.46	171	0.24	12.8	574	743	33
300	-2.29	126	0.17	17.6	447	691	29
500	-2.25	92	0.13	19.5	397	674	28
1000	-2.20	55	0.08	21.4	357	656	27
5000	-2.14	14	0.02	27.5	320	638	26
10000	-2.13	8	0.01	31.4	315	635	26
17000	-2.12	5	0.01	36.1	313	633	26

Subtrochanteric fracture. One lag screw Gamma nail (12). E = 210GPa

Cortical bone E=17GPa, Femoral Head E=1.3GPa, Trochanter E=0.32GPa.

TORSION LOAD CONDITION

Fracture size=0.5

	Femur	Fracture callus			Nail		Lag Screw
Fracture Callus Elastic Modulus (GPa)	Maximum deflection of femoral head (mm)	Strain Energy (Nmm)	Strain Energy Density (Nmm^{-2})	Peak von Mises stress (MPa)	Strain Energy (Nmm)	Peak von Mises stress (MPa)	Strain Energy (Nmm)
1	-8.74	48	0.20	0.9	2129	1513	224
5	-8.49	173	0.72	3.9	1954	1472	194
10	-8.26	251	1.05	6.6	1791	1430	169
20	-7.96	305	1.27	10.1	1585	1367	143
30	-7.77	311	1.30	12.4	1458	1323	128
50	-7.54	288	1.20	15.4	1311	1264	113
80	-7.36	245	1.02	18.0	1196	1210	102
100	-7.28	221	0.92	19.2	1150	1194	99
120	-7.23	201	0.84	20.1	1116	1181	96
500	-6.98	69	0.29	24.6	957	1121	88
1000	-6.93	38	0.16	25.8	928	1105	85
5000	-6.89	9	0.04	30.2	903	1092	84
17000	-6.88	3	0.01	40.4	898	1089	83

Subtrochanteric fracture. One lag screw Gamma nail (12). E = 210GPa
Cortical bone E=17GPa, Femoral Head E=1.3GPa, Trochanter E=0.32GPa.

TORSION LOAD CONDITION

Fracture size=1.5

	Femur	Fracture callus			Nail		Lag Screw
Fracture Callus Elastic Modulus (GPa)	Maximum deflection of femoral head (mm)	Strain Energy (Nmm)	Strain Energy Density (Nmm^{-2})	Peak von Mises stress (MPa)	Strain Energy (Nmm)	Peak von Mises stress (MPa)	Strain Energy (Nmm)
1	-8.79	17	0.02	0.4	2177	1537	232
5	-8.69	76	0.11	1.7	2107	1521	219
10	-8.58	133	0.18	3.2	2031	1503	205
20	-8.40	209	0.29	5.6	1901	1470	185
30	-8.26	254	0.35	7.5	1798	1442	170
50	-8.04	299	0.41	10.4	1647	1396	150
80	-7.82	316	0.44	13.5	1500	1344	132
100	-7.72	313	0.43	15.1	1430	1318	125
120	-7.63	305	0.42	16.3	1376	1296	119
500	-7.14	164	0.23	24.9	1062	1164	94
1000	-7.02	98	0.14	27.1	984	1133	89
5000	-6.90	25	0.03	30.6	914	1098	84
17000	-6.88	9	0.01	40.1	899	1089	83

Subtrochanteric fracture. One lag screw Gamma nail (12). E = 210GPa
Cortical bone E=17GPa, Femoral Head E=1.3GPa, Trochanter E=0.32GPa.

TORSION LOAD CONDITION

Fracture size=0.5

	Femur	Fracture callus			Nail		Lag Screw
Fracture Callus Elastic Modulus (GPa)	Maximum deflection of femoral head (mm)	Strain Energy (Nmm)	Strain Energy Density (Nmm^{-2})	Peak von Mises stress (MPa)	Strain Energy (Nmm)	Peak von Mises stress (MPa)	Strain Energy (Nmm)
1	-11.43	108	0.45	1.4	2883	1195	294
5	-10.85	366	1.53	5.6	2498	1139	235
10	-10.37	504	2.10	9.2	2195	1088	194
20	-9.79	580	2.42	13.8	1846	1018	152
30	-9.45	572	2.39	16.7	1646	971	132
50	-9.05	510	2.13	20.3	1421	916	112
80	-8.75	417	1.74	23.4	1244	873	99
100	-8.63	370	1.55	24.8	1176	855	95
120	-8.55	333	1.39	25.8	1128	843	93
500	-8.16	109	0.46	31.1	920	789	84
1000	-8.08	59	0.25	32.5	883	778	82
5000	-8.02	13	0.06	38.5	852	766	80
17000	-8.01	5	0.02	51.0	846	765	80

Subtrochanteric fracture. One lag screw Gamma nail (12). E = 210GPa
Cortical bone E=17GPa, Femoral Head E=1.3GPa, Trochanter E=0.32GPa.

TORSION LOAD CONDITION

Fracture size=1.5

	Femur	Fracture callus			Nail		Lag Screw
Fracture Callus Elastic Modulus (GPa)	Maximum deflection of femoral head (mm)	Strain Energy (Nmm)	Strain Energy Density (Nmm^{-2})	Peak von Mises stress (MPa)	Strain Energy (Nmm)	Peak von Mises stress (MPa)	Strain Energy (Nmm)
1	-11.56	40	0.05	0.5	2993	1221	309
5	-11.32	170	0.24	2.5	2827	1200	281
10	-11.07	287	0.40	4.6	2656	1175	255
20	-10.67	432	0.60	7.9	2396	1134	218
30	-10.37	510	0.71	10.5	2207	1100	194
50	-9.95	576	0.80	14.4	1947	1047	162
80	-9.55	585	0.81	18.4	1709	993	137
100	-9.36	572	0.79	20.4	1604	967	127
120	-9.22	551	0.76	22.0	1522	945	119
500	-8.41	271	0.38	32.5	1056	827	89
1000	-8.22	156	0.22	34.6	955	800	85
5000	-8.05	39	0.05	39.4	865	766	81
17000	-8.01	14	0.02	50.7	847	765	80

ANSYS code used for the creation of a Gamma nail inserted into a femur with a subtrochanteric fracture.

```
fini
/cle

/prep7

!Define parameters

!!!!!!!!DISTAL

DistDia=14
DistConDia=8
LCone=15
DistLen=91
DistTop=30
DistBot=0
Distfunc=46
DistScrewLen1=10
DistScrewLen2=30
DistScrewLen=40
DistElemThk=1.5
DistCut=(DistDia/2)-1

*afunc,deg
DistOpp=(DistDia/2)-(DistConDia/2)
DistConeAlpha=aTan(DistOpp/LCone)

HDistScrwBlck=1.2
WDistScrwBlck=3

*afunc,deg
teta=atan(HDistScrwBlck/WDistScrwBlck)

HolScrewDia=6.02
HolScrewDiaB=6
DistalInnDia=4.5
SlotLen=8
slotx=SlotLen/2
sloty=HolScrewDia/2
sloty2=sloty+DistElemThk
slotz=DistScrewLen

!!!!!!!DISTAL SCREW

DistScrewDia=6.0

!!!!!!!!Bone
```

```
GapBone=0.05
BoneThk=1.0
BoneRad=15
BoneExt=30

!!!!!!!!PROXIMAL

!!!!!!!!LAG SCREW

LLScone=10
LLSconeB=10

LLScrw=20
LLScrwB=20

LSCDia=10
LSCDiaB=5

LagDia=12
LagDiaB=7

LagLenBod=70
LagLenBodB=70

LagScrewPro=70
LagScrewProB=55

ProxElemThk=1.0

HProxScrwBlck=4
WProxScrwBlck=8

*afunc,deg
lagteta=atan(HProxScrwBlck/WProxScrwBlck)

HProxScrwBlckB=4
WProxScrwBlckB=6

*afunc,deg
lagtetaB=atan(HProxScrwBlckB/WProxScrwBlckB)

!!!!!!Proximal Nail

ProxDia=17
LProxCone=30
ProxLen=70

ProxOpp=(ProxDia/2)-(DistDia/2)
*afun,deg
ProxConeAlpha=atan(ProxOpp/LProxCone)
```

```
TotNailLen=220
ProxAngle=4
Lagelemthk=1.5
LagHolDia=12.02
LagHolDiaB=8.02
ProxGap=0.05

ProxLen1=47
ProxLen2=32
PAngle=130
ProxLagAng=180-PAngle

!Create Distal End of nail

numstr,kp,
numstr,line,
numstr,area,
numstr,volu,

wprot,,-90
cswpla,99

wpoff,,,LCone
cswpla,98

!create top distal cylinder
wpoff,,,Distfunc
cylind,,DistDia/2,DistTop,,0,360

!create inner annulus
wpcsys,-1,99
cylind,,DistalInnDia/2,,DistLen+LCone,0,360
allsel,all
vsbv,all,2

wprot,,90
cswpla,97
vsbw,all

wpoff,,,DistCut
cswpla,96
vsbw,all

wpoff,,,-2*DistCut
cswpla,95
vsbw,all

wprot,,,-90
cswpla,94
```

```
vsbw,all

!Create distal cone

wpcsys,-1,98

cone,DistConDia/2,DistDia/2,,-LCone,0,360
cylind,,DistalInnDia/2,,-LCone,0,360
vsbv,2,3

vsel,s,,,4,,,1

wpcsys,-1,94
vsbw,all
wpcsys,-1,97
vsbw,all

wpcsys,-1,96
wpoff,,LCone,
wprot,,DistConeAlpha
vsbw,all

wprot,,-DistConeAlpha
wpoff,,,-2*DistCut
wprot,,-DistConeAlpha
vsbw,all

!!!!!!!!Distal function volume Created

!Create distal screw insertion holes

numstr,kp,200
numstr,line,200
numstr,area,200
numstr,volu,200

wpcsys,-1,98
wpoff,,,DistBot
cylind,,DistDia/2,Distfunc,,0,360

vsel,s,,,200,300,1,1

wpcsys,-1,99
wpoff,DistScrewLen/2,,LCone+DistBot+DistSCrewLen1
wprot,,,-90
cswpla,11

wpcsys,-1,99
wpoff,DistScrewLen/2,,LCone+DistBot+DistScrewLen2
wprot,,,-90
```

```
cswpla,12

wpcsys,-1,12
cylind,,HolScrewDia/2,,DistScrewLen,0,360

vsbv,200,201

cylind,HolScrewDia/2,HolScrewDia/2+DistElemThk,,DistScrewLen,0,360

vovlap,all

csys,12
asel,r,loc,z
asel,a,loc,z,DistScrewLen
lsla
vsla
allsel,below,volu
vplo
vdele,all,,,1

vsel,s,,,200,300,1,1

wpcsys,-1,99
cylind,,DistalInnDia/2,,DistLen+LCone,0,360

vsbv,all,200

vsel,s,,,200,300,1,1

wpcsys,-1,97
vsbw,all

wpcsys,-1,96
vsbw,all
wpcsys,-1,95
vsbw,all
wpcsys,-1,94
vsbw,all

wpcsys,-1,12
wprot,,90
wprot,,,90-teta

cswpla,13
vsbw,all

wprot,,,-(90-teta)
wprot,,,-(90-teta)
cswpla,14
vsbw,all
```

```
wpcsys,-1,12
wprot,,,-90
wpoff,,,9
vsbw,all

wpcsys,-1,12
wprot,,,-90
cswpla,20
vsbw,all

allsel
vsel,s,,,1,899,1,1

allsel,all
wpcsys,-1,99
wpoff,,,DistLen
cswpla,88
*afun,deg
k,999,-10/sin(4)
k,998,-10/sin(4),1

asel,s,loc,z
vrotat,all,,,,,,998,999,4

allsel,all
nummrg,kp

!Create distal locking screws

numstr,kp,900
numstr,line,900
numstr,area,900
numstr,volu,900

wpcsys,-1,12
cylind,,DistScrewDia/2,,DistScrewLen,0,360

block,HDistScrwBlck/2,-HDistScrwBlck/2,WDistScrwBlck/2,-
WDistScrwBlck/2,,DistScrewLen

vsel,s,,,900,1000,1,1
vovlap,all

wprot,,90
wprot,,,90-teta
vsbw,902

wprot,,,-(90-teta)
wprot,,,-(90-teta)
```

```
vsbw,900
vsbw,903

wpcsys,-1,12
wprot,,90
vsbw,all

wpcsys,-1,12
wprot,,,-90
vsbw,all

vsel,s,,,900,1200,1,1
nummrg,kp

!Disect distal locking screws for conforming surfaces

numstr,kp,20001
numstr,line,20001
numstr,area,20001
numstr,volu,20001

wpcsys,-1,98
cylind,,DistDia/2+GapBone+BoneThk,DistLen,,0,360

numstr,kp,900
numstr,line,900
numstr,area,900
numstr,volu,900

vsel,s,,,900,1000,1,1
asel,a,,,20004
vsba,all,20004,,,keep

asel,a,,,20003
vsba,all,20003,,,keep

numstr,kp,30001
numstr,line,30001
numstr,area,30001
numstr,volu,30001

wpcsys,-1,98
cylind,,DistDia/2,DistLen,,0,360

numstr,kp,900
numstr,line,900
numstr,area,900
numstr,volu,900
```

```
vsel,s,,,900,1000,1,1
asel,a,,,30004
vsba,all,30004,,,keep

asel,a,,,30003
vsba,all,30003,,,keep

vsel,s,,,10000,50000,1,1
vdele,all,,,1

vsel,s,,,900,2500,1,1
nummrg,kp

!Create bone layer surrounding distal end

numstr,kp,8000
numstr,line,8000
numstr,area,8000
numstr,volu,8000

wpcsys,-1,99

cylind,GapBone+DistDia/2,GapBone+BoneThk+DistDia/2,DistLen,,0,360

vsel,s,,,8000,8500,1,1
wpcsys,-1,97
vsbw,all

wpcsys,-1,12
cylind,,HolScrewDiaB/2,,DistScrewLen,0,360

vsbv,all,8000

!Create volumes for brick meshing
cylind,HolScrewDiaB/2,HolScrewDiaB/2+DistElemThk,,DistScrewLen,0,360

vovlap,all

wpcsys,-1,12
wpoff,,,DistScrewLen/2
cswpla,56
wpcsys,-1,56
csys,56
vsel,r,loc,x
vsel,r,loc,z
vplo
vdele,all,,,1

vsel,s,,,8000,9000,1,1
```

```
vsel,r,loc,x
allsel,below,volu
vplo

wpcsys,-1,12
wprot,,,90
vsbw,all
wprot,,,,-90
vsbw,all

vsel,s,,,8000,9000,1,1
wpcsys,-1,98
wpoff,,,DistBot
vsbw,all

wpoff,,,Distfunc
vsbw,all

wpcsys,-1,12
wprot,,,,-90
wpoff,,,9
vsbw,all

wpcsys,-1,13
vsbw,all

wpcsys,-1,14
vsbw,all

wpcsys,-1,88
csys,88
vsel,r,loc,x
allsel,below,volu
vplo

wpcsys,-1,94
vsbw,all

wpcsys,-1,20
vsbw,all

wpcsys,-1,95
vsbw,all

wpcsys,-1,96
vsbw,all

wpcsys,-1,88
csys,88
```

```
*afun,deg
k,30001,-10/sin(4)
k,30000,-10/sin(4),1

vsel,s,,,8000,9000,1,1
ksel,a,,,30000,30001,1
asel,r,loc,z
vrotat,all,,,,,,30000,30001,4

vsel,s,,,8000,9000,1,1
vplo
nummrg,kp

numstr,kp,20000
numstr,line,20000
numstr,area,20000
numstr,volu,20000

allsel,all
wpcsys,-1,99
wpoff,,,DistLen
cswpla,88
*afun,deg
k,20001,-10/sin(4)
k,20000,-10/sin(4),1

asel,s,loc,z
vrotat,all,,,,,,20000,20001,4

vsel,s,,,20000,21000,1,1
wpcsys,-1,99
lwplan,-1,20012,1
wpoff,,-DistDia/2
cswpla,44

vdele,all,,,1

!Create proximal end of nail

!Create Proximal cone

numstr,kp,600
numstr,line,600
numstr,area,600
numstr,volu,600

vsel,s,,,1,899,1,1
vplo

cone,DistDia/2,ProxDia/2,,LProxCone,0,360
```

```
cylind,,DistalInnDia/2,,LProxCone,0,360
vsbv,600,601

vsel,s,,,600,700,1,1

wprot,,,-90
vsbw,all
cswpla,25
wpcsys,-1,97
vsbw,all

wpcsys,-1,44
wprot,,90
wpoff,,,DistCut
wprot,,ProxConeAlpha
cswpla,93
vsbw,all

wprot,,-ProxConeAlpha
wpoff,,,-2*DistCut
wprot,,-ProxConeAlpha
cswpla,92
vsbw,all

wpcsys,-1,44
wpoff,,,LProxCone
cswpla,49
csys,49
asel,r,loc,z,
vext,all,,,,,ProxLen,

!Define working planes for lag screw position

wpcsys,-1,49

wpoff,,,ProxLen
cswpla,53
wpoff,-ProxDia/2
wpoff,,,-ProxLen1
wprot,,,-ProxAngle
wprot,,,-ProxLagAng
cswpla,50

wpcsys,-1,49

wpoff,,,ProxLen
wpoff,-ProxDia/2
wpoff,,,-ProxLen2
wprot,,,-ProxAngle
wprot,,,-ProxLagAng
```

```
cswpla,51

!Create lag screw insertion hole

wpcsys,-1,50
wpoff,,,LagScrewPro
wpoff,,,-LLScrw-LLScone
wpoff,6
cswpla,52
cylind,,LagHolDia/2,,-LagLenBod,0,360

vsel,s,,,600,700,1,1
vsbv,all,616

cylind,LagHolDia/2,LagHolDia/2+ProxElemThk,,-LagLenBod,0,360
vovlap,all

ksel,s,loc,z
ksel,a,loc,z,-LagLenBod
lslk,
asll,
vsla
vplo

vdele,all,,,1

vsel,s,,,615,616,1,1
vdele,all,,,1

vsel,s,,,600,700,1,1
wpcsys,-1,52
wprot,,90
wprot,,,90-lagteta

cswpla,22
vsbw,all
wpcsys,-1,52
wprot,,90
wprot,,,-90+lagteta
cswpla,23
vsbw,all

wpcsys,-1,52
vsel,s,,,600,700,1,1
wprot,,-90
wprot,,,-90
cswpla,24
vsbw,all
```

```
!Split lag end for hexahedral meshing

vsel,s,,,600,700,1,1
vplo
wpcsys,-1,49
wpoff,,,55
vsbw,all

vsel,s,,,1,899,1,1
vplo
nummrg,kp

!Create Lag screw

numstr,kp,4000
numstr,line,4000
numstr,area,4000
numstr,volu,4000

wpcsys,-1,52
wpoff,,,-12
cswpla,54
cylind,,LagDia/2,,-LagLenBod,0,360

vsel,s,,,4000,5000,1,1

block,HProxScrwBlck/2,-HProxScrwBlck/2,WProxScrwBlck/2,-
WProxScrwBlck/2,,-LagLenBod
vovlap,all
wpcsys,-1,22
vsbw,4002
wpcsys,-1,23
vsbw,4000
vsbw,4003

wpcsys,-1,54
wprot,,,90
vsbw,all
wprot,,90
vsbw,all

!Create lag screw thread portion

vsel,s,,,4000,5000,1,1
vplo
wpcsys,-1,54
csys,54
asel,r,loc,z,
allsel,below,area
aplo
```

```
vext,all,,,,,LLSCone,(LSCDia/2)/(LagDia/2),(LSCDia/2)/(LagDia/2),

wpoff,,,LLSCone
cswpla,55
csys,55

asel,r,loc,z,
allsel,below,area
aplo
vext,all,,,,,LLScrw

vsel,s,,,4000,4999,1,1
vplo
nummrg,kp

!Split lag screw relative to bone

numstr,kp,20001
numstr,line,20001
numstr,area,20001
numstr,volu,20001

wpcsys,-1,49
cylind,,ProxDia/2+GapBone+BoneThk,ProxLen,,0,360

numstr,kp,4000
numstr,line,4000
numstr,area,4000
numstr,volu,4000

vsel,s,,,4000,5000,1,1
asel,a,,,20004
vsba,all,20004,,,keep

asel,a,,,20003
vsba,all,20003,,,keep

numstr,kp,30001
numstr,line,30001
numstr,area,30001
numstr,volu,30001

wpcsys,-1,49
cylind,,ProxDia/2,ProxLen,,0,360

numstr,kp,4000
numstr,line,4000
numstr,area,4000
numstr,volu,4000
```

```
vsel,s,,,4000,5000,1,1
asel,a,,,30004
vsba,all,30004,,,keep

asel,a,,,30003
vsba,all,30003,,,keep

vsel,s,,,10000,50000,1,1
vdele,all,,,1

vsel,s,,,4000,5000,1,1
vplo
nummrg,kp

!Create Proximal bone layer

numstr,kp,3000
numstr,line,3000
numstr,area,3000
numstr,volu,3000

!Create Bone Cone

vsel,s,,,8000,9000,1,1

wpcsys,-1,44
cone,DistDia/2+GapBone+BoneThk,ProxDia/2+GapBone+BoneThk,,LProxCon
e,0,360
cone,DistDia/2+GapBone,ProxDia/2+GapBone,,LProxCone,0,360
vsbv,3000,3001

vsel,s,,,3000,3999,1,1

wpcsys,-1,25
vsbw,all
wpcsys,-1,97
vsbw,all

wpcsys,-1,93
vsbw,all

wpcsys,-1,92
vsbw,all

vsel,s,,,3000,3999,1,1

wpcsys,-1,49
csys,49
asel,r,loc,z,
```

```
allsel,below,area

vext,all,,,,,ProxLen,

wpcsys,-1,54
cylind,LagDia/2+ProxGap,,,-LagLenBod,0,360
vsbv,all,3016

cylind,LagDia/2+ProxGap,LagDia/2+ProxGap+ProxElemThk,,-
LagLenBod,0,360
vovlap,all

vsel,s,,,3023,,,1

vdele,all,,,1

vsel,s,,,3000,3999,1,1
wpcsys,-1,54
csys,54
ksel,r,loc,x,LagDia/2+ProxGap
kplo
lslk
asll
vsla
allsel,below,volu
vplo
wprot,,,-90
vsbw,all
wprot,,-90
vsbw,all

wpcsys,-1,54
asel,r,loc,z,
allsel,below,area
aplo

vext,all,,,,,LLScone,(LSCDia)/(LagDia+ProxGap+ProxGap),(LSCDia)/(LagDia+
ProxGap+ProxGap)

wpcsys,-1,55
csys,55
asel,r,loc,z,
allsel,below,area
aplo

vext,all,,,,,LLScrw

vsel,s,,,3000,3999,1,1
wpcsys,-1,22
vsbw,all
```

```
wpcsys,-1,23
vsbw,all

wpcsys,-1,24
vsbw,all

vsel,s,,,3000,9000,1,1
vsel,u,,,4000,5000,1
allsel,below,volu
vplo
nummrg,kp

!Input femur geometry

*SET,Dinn200,12.38
*SET,Dout200,27.05
*SET,Dinn150,12.49
*SET,Dout150,28.21
*SET,Dinn100,15.14
*SET,Dout100,29.93
*SET,LenB7,70.29
*SET,LenA7,36.72`   !44.72
*SET,Len56,103.82   !93.82
*SET,AngCB7,175.61
*SET,Ang1OB,120.86          !126.86

!Create femur

/prep7

numstr,kp,40001
numstr,line,40001
numstr,area,40001
numstr,volu,40001

wpcsys,-1,0
wprot,,-90

!wpoff,,,5

CSWPLA,40001,0,1,1
k,40001                     !Point L200
k,40002,,,50            !Point L150
k,40003,,,100           !Point L100
k,40004,,,200-(LenB7*cos((180-AngCB7)*acos(-1)/180))  !Point B
k,50000,,,200           !auxiliar kp, axe of the circles
KWPAVE,40004
wprot,,,-(180-AngCB7)
CSWPLA,40002,0,1,1,
k,40005,,,LenB7             !Point 7
```

```
k,40006,,,LenB7-LenA7       !Point A
KWPAVE,40006
wprot,,,-(Ang1OB-(180-AngCB7))
CSWPLA,40003,0,1,1,
k,40007,,,.28*Len56  !Point 5
k,40008,,,-.72*Len56 !Point 6
WPCSYS,-1,0
wprot,,-90
CSWPLA,50000,1,1,1
k,50001,10,20          !auxiliar kp, beginning of large circles
k,50002,10,-20              !auxiliar kp, beginning of small circles
LSTR,50000,40001            !auxiliar line 1001

!to obtain the kp 1009
KWPAVE,40007
CSYS,4
K,50003,50,,,
LSTR,40007,50003            !auxiliar line 1002
LSBL,40001,40002,,,keep     !output kp 1009, and lines 1003 and 1004
ldele,40002

!to obtain the kp 1010
KWPAVE,40004
CSYS,4
k,40010,,,distkp(40004,40009)/2

numstr,kp,40101
numstr,line,40101
circle,40001,Dinn200/2,50000,50001,320,4  !circle L200
circle,40001,Dinn200/2,50000,50002,40,2
circle,40001,Dout200/2,50000,50001,320,4
circle,40001,Dout200/2,50000,50002,40,2
ksel,s,,,40101,40200
nummrg,kp
ksel,all

numstr,kp,40201
numstr,line,40201
circle,40002,Dinn150/2,50000,50001,320,4  !circle L150
circle,40002,Dinn150/2,50000,50002,40,2
circle,40002,Dout150/2,50000,50001,320,4
circle,40002,Dout150/2,50000,50002,40,2
ksel,s,,,40201,40300
nummrg,kp
ksel,all

numstr,kp,40301
numstr,line,40301
circle,40003,Dinn100/2,50000,50001,320,4  !circle L100
circle,40003,Dinn100/2,50000,50002,40,2
```

```
circle,40003,Dout100/2,50000,50001,320,4
circle,40003,Dout100/2,50000,50002,40,2
ksel,s,,,40301,40400
nummrg,kp
ksel,all

numstr,kp,40401
numstr,line,40401
circle,40004,(Dinn100+5)/2,50000,50001,320,4      !circle B      !!!!!!!
circle,40004,(Dinn100+5)/2,50000,50002,40,2       !!!!!!!!!
circle,40004,(Dout100+5)/2,50000,50001,320,4      !!!!!
circle,40004,(Dout100+5)/2,50000,50002,40,2       !!!!!!!!!
ksel,s,,,40401,40500
nummrg,kp
ksel,all

numstr,kp,40501
numstr,line,40501
circle,40010,((Dinn100+5)/2+(distkp(40007,40009)-5))/2,50000,50001,320,4
        !circle lesser trochanter !!!!!!!
circle,40010,((Dinn100+5)/2+(distkp(40007,40009)-5))/2,50000,50002,40,2
        !!!!!!!!!!
circle,40010,((Dout100+5)/2+distkp(40007,40009))/2,50000,50001,320,4
        !!!!!!!!!
circle,40010,((Dout100+5)/2+distkp(40007,40009))/2,50000,50002,40,2
        !!!!!!!!!
KWPAVE,40010
CSYS,4
kmodif,40515,distkp(40007,40009)
bsplin,40513,40515,40509
ldele,40511,40512
wpro,,90.000000,
LSBW,40513

!!!!!!!!!!!!!!!!!!!!!!!!!!!!!!!!!!!!

wpro,,-90.000000,
ksel,s,,,40501,40600
nummrg,kp
ksel,all

numstr,kp,40601
numstr,line,40601
circle,40009,((Dinn100+5)/2+(distkp(40007,40009)-5))/2,50000,50001,320,4
!circle 5       !!!!!!!!!!!!!
circle,40009,((Dinn100+5)/2+(distkp(40007,40009)-5))/2,50000,50002,40,2
        !!!!!!!!!!!!!
circle,40009,((Dout100+5)/2+distkp(40007,40009))/2,50000,50001,320,4
        !!!!!!!!!!!!!
```

```
circle,40009,((Dout100+5)/2+distkp(40007,40009))/2,50000,50002,40,2
        !!!!!!!!!!
kwpave,40009
csys,4
kmodif,40611,-distkp(40007,40009)
kmodif,40603,-distkp(40007,40009)+5        !!!!!!!!
ldele,40602,40603
bsplin,40602,40603,40604
ldele,40608,40609
bsplin,40610,40611,40612
wpro,,90.000000,
LSBW,40602
LSBW,40603
wpro,,-90.000000,
ksel,s,,,40601,40700
nummrg,kp
ksel,all

s=2.88/2
s1=2*s
*afun,deg
numstr,kp,60001
numstr,line,60001
numstr,area,60001
numstr,volu,60001
KWPAVE,40008
wprot,,,-(Ang1OB-90)

wprot,,,-90
wprot,-90
k,60001,0,0,0
k,60002,0,0,2*s1
k,60003,0,0,2*2*s1
k,60004,0,0,2*3*s1
k,60005,0,0,2*4*s1
k,60006,0,0,2*5*s1
k,60007,0,0,2*6*s1
k,60008,0,0,2*7*s1
k,60009,0,0,2*8*s1
k,60010,0,0,2*9*s1
k,60011,0,0,2*9.5*s1
k,60012,0,0,2*10.5*s1
k,60013,0,0,2*13*s1

CSWPLA,40100,1,1,1,
k,60098,10,-70
k,60099,10,-110
CSYS,4
```

```
numstr,kp,60101
numstr,line,60101
circle,60001,3*s,40007,60098,320,4
circle,60001,3*s,40007,60099,40,2
ksel,s,,,60101,60200
nummrg,kp
ksel,all
!!!!!!!!!!!!!!!!!!!!!!!!!!!!!!!!!!!!
numstr,kp,60201
numstr,line,60201
circle,60002,11*s,40007,60098,320,4
circle,60002,11*s,40007,60099,40,2
ksel,s,,,60201,60300
nummrg,kp
ksel,all

numstr,kp,60301
numstr,line,60301
circle,60003,14.5*s,40007,60098,320,4
circle,60003,14.5*s,40007,60099,40,2
ksel,s,,,60301,60400
nummrg,kp
ksel,all

numstr,kp,60401
numstr,line,60401
circle,60004,16*s,40007,60098,320,4
circle,60004,16*s,40007,60099,40,2
ksel,s,,,60401,60500
nummrg,kp
ksel,all

numstr,kp,60501
numstr,line,60501
circle,60005,16*s,40007,60098,320,4
circle,60005,16*s,40007,60099,40,2
ksel,s,,,60501,60600
nummrg,kp
ksel,all

numstr,kp,60601
numstr,line,60601
circle,60006,14*s,40007,60098,320,4
circle,60006,14*s,40007,60099,40,2
ksel,s,,,60601,60700
nummrg,kp
ksel,all

numstr,kp,60701
```

```
numstr,line,60701
circle,60007,11*s,40007,60098,320,4
circle,60007,11*s,40007,60099,40,2
kmodif,60703,,9*s
bsplin,60702,60703,60704
ldele,60702,60703
wpro,,,90
LSBW,60707
wpro,,,-90
ksel,s,,,60701,60800
nummrg,kp
ksel,all
!!!!!!!!!!!!!!!!!!!!!!!
numstr,kp,60801
numstr,line,60801
circle,60008,9*s,40007,60098,320,4
circle,60008,9*s,40007,60099,40,2
kmodif,60803,,8*s
bsplin,60802,60803,60804
ldele,60802,60803
wpro,,,90
LSBW,60807
wpro,,,-90
ksel,s,,,60801,60900
nummrg,kp
ksel,all

numstr,kp,60901
numstr,line,60901
circle,60009,9*s,40007,60098,320,4
circle,60009,9*s,40007,60099,40,2
kmodif,60903,,8*s
bsplin,60902,60903,60904
ldele,60902,60903
wpro,,,90
LSBW,60907
wpro,,,-90
ksel,s,,,60901,70000
nummrg,kp
ksel,all

numstr,kp,70001
numstr,line,70001
circle,60010,11*s,40007,60098,320,4
circle,60010,11*s,40007,60099,40,2
kmodif,70003,,11.5*s
bsplin,70002,70003,70004
ldele,70002,70003
wpro,,,90
LSBW,70007
```

```
wpro,,,-90
ksel,s,,,70001,70100
nummrg,kp
ksel,all

numstr,kp,70101
numstr,line,70101
circle,60011,12.5*s,40007,60098,320,4
circle,60011,12.5*s,40007,60099,40,2
kmodif,70103,,21*s
bsplin,70102,70103,70104
ldele,70102,70103
wpro,,,90
LSBW,70107
wpro,,,-90
ksel,s,,,70101,70200
nummrg,kp
ksel,all

!!! Geometric model of the cross sections (circles)

numstr,kp,70201
numstr,line,70201
KWPAVE,60012
wprot,,10
k,60097,,,100
CSWPLA,40200,1,1,1,
k,60095,10,-70
k,60096,10,-110
CSYS,4
circle,60012,14*s,60097,60095,320,4
circle,60012,14*s,60097,60096,40,2
kmodif,70203,,25*s
bsplin,70202,70203,70204
ldele,70202,70203
wpro,,,90
LSBW,70207
wpro,,,-90
ksel,s,,,70201,70300
nummrg,kp
ksel,all

numstr,kp,70301
numstr,line,70301
KWPAVE,60013
wprot,,25
k,60094,,,100
CSWPLA,40300,1,1,1,
k,60092,10,-70
k,60093,10,-110
```

```
CSYS,4
circle,60013,19*s,60094,60092,320,4
circle,60013,19*s,60094,60093,40,2
ksel,s,,,70301,70400
nummrg,kp
ksel,all


numstr,kp,60001
numstr,line,60001
numstr,area,60001
numstr,volu,60001

!Create femur areas

askin,60101,60201,60301,60401,60501,60601,60701,60801,60901,70001
askin,70001,70101,70201,70301


askin,60102,60202,60302,60402,60502,60602,60702,60802,60902,70002
askin,70002,70102,70202,70302


askin,60103,60203,60303,60403,60503,60603,60703,60803,60903,70003
askin,70003,70103,70203,70303


askin,60104,60204,60304,60404,60504,60604,60704,60804,60904,70004
askin,70004,70104,70204,70304


askin,60105,60205,60305,60405,60505,60605,60705,60805,60905,70005
askin,70005,70105,70205,70305


askin,60106,60206,60306,60406,60506,60606,60706,60806,60906,70006
askin,70006,70106,70206,70306


askin,40107,40207,40307,
askin,40307,40407,40507,40607,70304

askin,40108,40208,40308,
askin,40308,40408,40508,40602,70303

askin,40109,40209,40309,
askin,40309,40409,40509,40613,70302

askin,40110,40210,40310,
askin,40310,40410,40510,40610,70301
```

```
askin,40111,40211,40311,
askin,40311,40411,40512,40611,70306

askin,40112,40212,40312,
askin,40312,40412,40511,40612,70305


al,40107,40108,40109,40110,40111,40112
al,60101,60102,60103,60104,60105,60106
al,70304,70303,70302,70301,70306,70305
al,70001,70002,70003,70004,70005,70006
al,40307,40308,40309,40310,40311,40312

asel,s,,,40000,90000,1,1
aplo

!Create femur volumes

va,60001,60003,60005,60007,60009,60011,60026,60028
va,60002,60004,60006,60008,60010,60012,60027,60028
va,60014,60016,60018,60020,60022,60024,60027,60029
va,60013,60015,60017,60019,60021,60023,60025,60029

!extend bone to base of skin

vsel,s,,,40000,90000,1,1
wpcsys,-1,99
csys,99
asel,r,loc,z
aplo
vext,all,,,,,-30

!extend bone skin

numstr,kp,8000
numstr,line,8000
numstr,area,8000
numstr,volu,8000

vsel,s,,,8000,9000,1,1
wpcsys,-1,99
csys,99
asel,r,loc,z
aplo
vext,all,,,,,-30

!Split volumes for conforming surfaces

!split distal bone
```

```
vsel,s,,,8000,9000,1,1
wpcsys,-1,11
csys,11
ksel,r,loc,z,DistScrewLen
lslk
asll
vsla

asel,a,,,60017
vsba,all,60017,,,keep
asel,a,,,60015
vsba,all,60015,,,keep

numstr,kp,8000
numstr,line,8000
numstr,area,8000
numstr,volu,8000

vsel,s,,,8000,9000,1,1
wpcsys,-1,11
csys,11
ksel,r,loc,z,
lslk
asll
vsla

asel,a,,,60021
vsba,all,60021,,,keep
asel,a,,,60023
vsba,all,60023,,,keep

!Split distal screws with femur

numstr,kp,900
numstr,line,900
numstr,area,900
numstr,volu,900

vsel,s,,,900,2000,1,1
wpcsys,-1,11
csys,11
ksel,r,loc,z,DistScrewLen
lslk
asll
vsla

asel,a,,,60017
vsba,all,60017,,,keep
asel,a,,,60015
```

```
vsba,all,60015,,,keep

vsel,s,,,900,2000,1,1
wpcsys,-1,11
csys,11
ksel,r,loc,z,
lslk
asll
vsla

asel,a,,,60021
vsba,all,60021,,,keep
asel,a,,,60023
vsba,all,60023,,,keep

vsel,s,,,8000,9000,1,1
wpcsys,-1,11
csys,11
ksel,r,loc,z,DistScrewLen
lslk
asll
vsla
vdele,all,,,1

vsel,s,,,8000,9000,1,1
wpcsys,-1,11
csys,11
ksel,r,loc,z,
lslk
asll
vsla
vdele,all,,,1

!Split Lag Bone layer

numstr,kp,3000
numstr,line,3000
numstr,area,3000
numstr,volu,3000

vsel,s,,,3000,3900,1,1
csys,54
wpcsys,-1,54
wpoff,,,-LagLenBod
cswpla,77
csys,77
ksel,r,loc,z
lslk
asll
vsla
```

```
asel,a,,,60016
vsba,all,60016,,,keep
asel,a,,,60018
vsba,all,60018,,,keep

csys,77
ksel,r,loc,z
lslk
asll
vsla
vdele,all,,,1

!SPLIT lAG screw

numstr,kp,4000
numstr,line,4000
numstr,area,4000
numstr,volu,4000

vsel,s,,,4000,4900,1,1
wpcsys,-1,77
csys,77
ksel,r,loc,z
lslk
asll
vsla

asel,a,,,60016
vsba,all,60016,,,keep
asel,a,,,60018
vsba,all,60018,,,keep

!Split Proximal Top bone layer

numstr,kp,3000
numstr,line,3000
numstr,area,3000
numstr,volu,3000

vsel,s,,,3000,3900,1,1
wpcsys,-1,53
csys,53
ksel,r,loc,z
lslk
asll
vsla
vplo

asel,a,,,60004
```

```
vsba,all,60004,,,keep
asel,a,,,60006
vsba,all,60006,,,keep

wpcsys,-1,53
csys,53
ksel,r,loc,z
lslk
asll
vsla
vplo
vdele,all,,,1

!Split proximal nail

numstr,kp,600
numstr,line,600
numstr,area,600
numstr,volu,600

vsel,s,,,600,800,1,1

asel,a,,,60004
vsba,all,60004,,,keep
asel,a,,,60006
vsba,all,60006,,,keep

!Split femoral head for subtraction

numstr,kp,60000
numstr,line,60000
numstr,area,60000
numstr,volu,60000

vsel,s,,,60000,70000,1,1
wpcsys,-1,54
wpoff,,,LLScrw+LLSCone
cswpla,79
vsbw,all

!Split end femoral head volume by lag bone areas

vsel,s,,,60000,
vsel,a,,,3000,3999,1
allsel,below,volu
vplo

wpcsys,-1,79
csys,79
asel,r,loc,z,
```

```
aplo

vsba,all,all,,,keep

!Introduce capsular volume

vsel,s,,,60000,70000,1,1
wpcsys,-1,54
wpoff,,,2

vsbw,all,

numstr,kp,3000
numstr,line,3000
numstr,area,3000
numstr,volu,3000
vsel,s,,,3000,3999,1,1
vplo
vsbw,all

!Split bone for cortical layer

numstr,kp,3000
numstr,line,3000
numstr,area,3000
numstr,volu,3000

proxshell=36

wpcsys,-1,99
wpoff,,,DistLen+proxshell
vsel,s,,,3000,3999,1,1
vsbw,all

numstr,kp,60000
numstr,line,60000
numstr,area,60000
numstr,volu,60000

vsel,s,,,60000,70000,1
allsel,below,volu
vplo
vsbw,all

!Add certain bone volumes for subtraction process

vadd,60000,60002,60006
vadd,60008,60004,60005

!Begin subtraction process
```

```
!!!!!!!!!

vsel,s,,,60007
vsel,a,,,3000,3999,1
allsel,below,volu
vplo

vsbv,60007,all,,,keep

!!!!!!!!!

vsel,s,,,60003
vsel,a,,,3000,3999,1
allsel,below,volu
vplo

vsbv,60003,all,,,keep

!!!!!!!!

vsel,s,,,60000
vsel,a,,,3000,3999,1
vsel,a,,,8000,9000,1
allsel,below,volu
vplo

vsbv,60000,all,,,keep

!!!!!!!

!!Split bone into two halves

vsel,s,,,40000,90000,1,1
allsel,below,volu
vplo
wpcsys,-1,98
wprot,,90
vsbw,all

!!!!!!!delete inner volumes

vsel,s,,,60000,90000,1,1
FLST,5,6,6,ORDE,6
FITEM,5,60000
FITEM,5,60008
FITEM,5,60015
FITEM,5,-60016
FITEM,5,60019
FITEM,5,-60020
```

```
VSEL,R, , ,P51X
ALLSEL,BELOW,VOLU

vdele,all,,,1

!!!!Merge lag screw thread with bone

numstr,kp,4000
numstr,line,4000
numstr,area,4000
numstr,volu,4000

vsel,s,,,3000,5000,1,1
vplo
FLST,5,20,6,ORDE,6
FITEM,5,3068
FITEM,5,-3071
FITEM,5,3084
FITEM,5,-3087
FITEM,5,4024
FITEM,5,-4035
VSEL,R, , ,P51X
ALLSEL,BELOW,VOLU
VPLOT
nummrg,kp

!Create subtrochanteric fracture zone

numstr,kp,3000
numstr,line,3000
numstr,area,3000
numstr,volu,3000

vsel,s,,,3000,3999,1,1
wpcsys,-1,99
wpoff,,,115
vsbw,all,sepo

numstr,kp,60000
numstr,line,60000
numstr,area,60000
numstr,volu,60000

vsel,s,,,60000,90000,1,1
vsbw,all,sepo

numstr,kp,60000
numstr,line,60000
numstr,area,60000
numstr,volu,60000
```

```
vsel,s,,,60000,90000,1,1

wpcsys,-1,99
wpoff,,,DistLen
cswpla,88

wpcsys,-1,88
vsbw,all,
```

Finite Element Modelling for Intramedullary Devices

C.J.Brown[a†], D.J.Simpson[a], A.L.Yettram[a], P.Procter[ab], G.J.Andrew[c]

a School of Engineering and Design, Brunel University, Uxbridge, UB8 3PH, UK

b Stryker Trauma S.A., Ch. du Pont-du-Centenaire 110, CH-1228 Plan-les-Ouates, Geneva, Switzerland

c Dept. of Orthopaedics, Ysbyty Gwynedd, Bangor, LL57 2PW, UK

† Author to receive correspondence

Abstract:

The analysis of intramedullary devices using finite element models requires considerable modelling effort, and it is difficult to build generic models that account for small changes associated with individual constructs and patient geometry. In addition, modelling the contacts between the various elements of such a construct requires care. This paper outlines a modelling approach that standardises structural elements to be used in a subsequent analysis that may include patient-specific data. Development times for models can be reduced and some of the problems associated with modelling the contact elements can be eliminated.

Results from the FE model are compared to available data from experiments carried out on constructs of bone and device that use intramedullary femoral nails. An acceptable level of agreement is obtained.

We conclude that this technique can be developed to deal not only with femoral nails but any form of intramedullary device for which contact at the bone/implant interface is important.

Keywords: Intramedullary nail, femur, finite element method, contact mechanics, strain gauge.

1. Introduction

The design of trauma treatment devices has, historically, been dominated by surgical innovation and clinical trial. However, engineering analysis - and in particular the use of finite element (FE) models –is now well established, Huiskes and Chao [1] and is a necessary and integral part of the implant design process, EU Directive 93/42/EEC [2]. This paper deals with a modelling process using the FE method applied to one such device - an intramedullary nail for the treatment of proximal femoral fractures.

The use of intramedullary nails is now a well-established surgical technique for treating certain fractures of the proximal femur, e.g. McRae, [3], Gahr *et al*, [4]. Reported failures of intramedullary nails include cut-out of the lag screw, Dubbeld and Den Outer, [5], and failure of the nail at the lag screw insertion hole due to the large stress concentration in this region, Randle *et al*, [6].

The behaviour of a nail/screw/bone construct can be obtained relatively quickly using FE and there is the possibility of varying parameters and geometries used, leading to a large data set at relatively low cost. Patient or case-specific studies, Sitthiseripratip *et al*, [7], Seral *et al*, [8], Cheung *et al*, [9], are popular. However, these models often contain simplifying assumptions about the intramedullary nailing system, for instance by fixing or merging of certain "disconnected" components (e.g. screw and nail) to have connectivity at selected nodes, or pre-assumed contact points. Solution accuracy can be an issue, Viceconti *et al*, [10], Bernakiewicz and Viceconti, [11]. Wang *et al*, [12], and Brown *et al* 13], have assessed the interaction between implant and bone by using a generic model case

that is not patient specific; the results then give the relative benefits of any particular construct configuration.

This paper presents a modelling procedure that can be used to describe the interaction between implant and bone without having to pre-assume contact points. It is a three-dimensional technique that has more general application to implant design. Results from the model are compared to those obtained from laboratory experiments *in vitro*.

2. Method

Modelling the complex geometry associated with fitting one structural element inside another provides a significant challenge for FE. In the case of intramedullary nails this happens up to four times if two distal screws and two lag screws are used.

Our modelling strategy begins by generating a solid model of the required nail and screw construct. This construct is then covered with a layer of bone (cancellous or cortical as appropriate). The solid volume of this composite construction can then be removed from a model of the actual bone using mathematical operations (available in much FE software) leaving a solid with a known void inside. This void is then "filled" with the nail/screw/bone solid for which meshing and contact elements have been completed and the whole joined at the interface to form a model of the complete construct.

The major advantages of such a technique are that:

- it does not require any contacts to be pre-assumed
- it can be readily used to model complex fractures

- it can be located within the bone to reflect the actual position after surgery, and
- the process is highly repeatable, enabling an envelope of plausible cases to be analysed, and the effects of parametric change to be identified.

In the work described below, the strategy has been implemented using a commercially available package, ANSYS, [14], but this choice is somewhat arbitrary as other packages have the same capability. This enables software specially written for the generation of complex geometries using Boolean operations, e.g. Moaveni, [15]. Our experience, Wang, [16] and Simpson *et al*, [17], suggests best results are obtained using surface-to-surface contact elements whose contacting faces are quadrilateral and are initially meshed identically at the potentially corresponding contacting elements.

Figure 1a shows a modelled lag screw and nail combination. Under vertical loading the key stresses generated in the nail/screw interface are at the lower contact medially and the upper contact laterally, and with such loading it might be possible to pre-assume these contacts adequately. However, given that the problem is treated in a fully three-dimensional manner, and that one of the key load conditions is combined vertical and posterior-anterior loading, it is necessary to allow contact to be determined as an outcome of the loading regime. Furthermore, contacts may not always occur at the extreme edges of contacting components, Allison, [18], [19], Wang, [16].

The ultimate objective of our work is to use patient-specific geometric data to estimate the effects of different nail/bone configurations rapidly in a clinical situation. To achieve this we have adopted the following finite element modelling procedure described below:

- We model each component of the implanted construct (e.g. nail, lag screw etc.) using hexahedral elements so that the external faces of each component are quadrilateral, (Figure 1a).
- We construct a thin layer of bone to surround the nail/lag screw elements of the implant. This layer is made of thin brick elements that have the same mesh as the outside of the implant. There are two bone materials – the proximal nail and lag screw(s) are enclosed by cancellous bone, while the distal end of the nail is surrounded by cortical bone. (Figure 1b, 1c). At this stage the mesh on potentially contacting surfaces is identical. A solid is then generated whose surface is formed by the outer skin described above.
- We construct the femoral bone using geometry and material properties from anatomical data – shown in the outline in Figure 2a. The single volume outline of the implant, including the bone layer, is subtracted from the femur. The implant and bone layer are re-introduced into the femur volume and the two components are connected at their interface (Figure 2b).
- The remaining unmeshed bone volume is meshed using tetrahedral elements, taking the mesh on the outer surface of the bone "skin" as a starting point for the mesh of these elements. A regular annulus of hexahedral elements is used at the proximal end of the diaphysis to make introduction of any osteotomy contacts more precise. The meshing is the last part of the procedure, and the nail is meshed first, then the layer, and finally the remainder of the bone.

The advantages of this strategy are clear. The challenging task of modelling the implant and its associated contacts is completed once for each construct. While there is a range of different diameters and proximal/distal lengths, these can be defined in parametric terms, and so it is relatively straightforward to examine the effects of making changes. The combined "implant and layer" volume can be inserted into any bone volume, and so individual patient geometries can be readily analysed (techniques for the generation of geometric models that relate to x-rays and CT scans are widely reported elsewhere, e.g. Viceconti *et al*, [20]). The layer of bone around the implant has the properties of the surrounding bone. While no contact is pre-assumed, any initial lack of fit is also omitted at this stage. This may be relevant in the clinical situation, as it is well known that the curvature of nails and femora do not always match well, Leung *et al*, [21]. Fracture planes can be readily introduced to the model of the femur, and from contact elements on these planes, the stresses on the fracture plane can be assessed.

The location and nature of contacts is important. In practice, intramedullary nails are fitted into reamed canals that are usually approximately 1mm greater than the nail diameter. Any stresses resulting from geometric discontinuity or initial lack of fit are not considered here. Thus the effect of live loads is reported. There is everywhere initially a small radial gap between the nail and the bone of 0.05mm. Smaller gaps make no change to stresses while larger gaps require longer solution times. The choice of this gap is based on experience, Wang, [16].

3. Assessment of the FE Model

To assess the quality of the model a series of experiments on femora containing instrumented nails was devised. The experiments used dry human femora. The measured quantities were then used to test the modelling procedure.

3.1 Specimens

Two dried cadaver femora used were supplied by Sawbones Europe AB (Limhamm, Sweden) and are numbered femur 1, and femur 2. Figure 3 shows both instrumented femora. The condyles and distal part of the diaphysis of each femur have been removed, so that each has an overall length of 300mm, taken from the most distal to the most proximal parts of the femora on a line parallel to the axis of the femoral shaft. The distal ends of the bone were placed in a mould and fixed using Cerrobend (Hoyt-Darchem, UK) potting compound to align the bone in the cup.

To assess the elastic modulus of the dry cortical bone a small sample is taken from the unused distal diaphysis of the femora and loaded in compression. The moduli for femur 1 and 2 respectively are 5.3GPa and 5.4GPa, approximately one third of the value for cortical bone often quoted in literature - typically around 17GPa , Reilly and Burstein, [22], Currey, [23] and Taylor *et al*, [24]. Precise heat treatment methods for the femora in this study are not known, but as expected the dried bone has significantly lower moduli than live bone. The properties of cancellous bone in the femoral head were not measured directly.

Cortical shell thickness was obtained from measuring the specimens and by noting carefully the penetration of a 0.5mm diameter drill, Simpson, [25].

A modulus value is required for the cancellous bone in the femoral head and trochanter. Taylor *et al* [26] divided the cancellous bone into five groups, varying the modulus of elasticity from 250MPa to 1250MPa, but a study by Seral *et al*

[8] split the femur into only two sections - cortical and cancellous, with the cancellous bone having a modulus of 100MPa, while the work by Sitthiseripratip *et al* [7], divided the femur into four sections – one cortical and three cancellous, with the femoral head having a modulus of 900MPa, the neck 620MPa, and the trochanteric region a modulus of 260MPa. In our model the trochanter is assumed to have a modulus of 320MPa and the femoral head 720MPa. These are the material property divisions used by Wang *et al*, [27].

3.2 Construct

A practising consultant orthopaedic surgeon at Manchester Hope Hospital (see authors) implanted the instrumented nails into the specimens. The devices chosen were standard Gamma Locking Nails. The recommended procedure for implanting the device was followed where possible. Drilling and reaming for the nail and lag screw were carried out using the appropriate guide tools from a standard set. Subtrochanteric fractures or osteotomies were then created in the femora by a simple transverse saw cut. The instrumented device was then fitted to stabilise the fractures.

Standard stainless steel Gamma locking nails with one distal locking screw and one lag screw were used. The key dimensions for the gamma nails used are 17mm diameter proximal, 12mm diameter distal, with a 135° angle between nail and lag screw.

3.3 Instrumentation and Testing

Each femur is mounted in an Instron universal testing machine using a special jig (Figure 4). The material used for each component of the support rig is mild steel.

The shaft axis is inclined at 21° to the vertical in the coronal plane and 10° to the vertical in the sagittal plane. This orientation represents the first maximum resultant peak load during a walking phase, and replicates a load condition used by Haynes *et al* , [28], who investigated lag screw cut-out with a gamma nail in cadaveric specimens.

Six linear strain gauges were bonded to the exterior surface of the femur, two each on the femoral neck, the trochanter and the femoral shaft - positioned proximally and distally to the distal locking screw.

The load and deflection data from the Instron machine were recorded. Additionally a dial gauge was positioned under the femoral head, in line with the point and direction of load application from the test machine. This is used to determine the localised deformation of the femoral head at the point where the load is applied. The load rate in each test was 1kN per minute. Each test was repeated three times.

Femur 1 was of good quality with no visible cracking and little signs of general wear, but femur 2 was considerably degraded. Cracking was visible in the cortical shaft and also at the lateral edge of the trochanter. Therefore it was tested at a lower maximum load. Femur 1 was subjected to a maximum compressive load of 2.8kN, while femur 2 was subjected to a maximum load of 1.3kN.

3.4 Results from experiment

The key results obtained are the displacements at the femoral head, and the strains on the outer surface of the cortical layer. Typical are those shown in Figures 5 and 6. Figure 5 shows the load-displacement results for each femur. It can be seen that there are two distinct stages to the deflection pattern – especially

evident for femur 2 - but that after "settling in" the load/deflection relation is quite linear. This could be due to closure of the small gap at the osteotomy and small differences in that gap initially, or simply a different fit of the nail in the intramedullary canal. For the load/displacement data for femur 1, once the gaps have closed a very good linear relation is displayed (r^2>0.99) with a slope of 2.1 kN/mm. For femur 2, the gradient of the relationship is 1.06, 0.95, and 1.07kN/mm for the three tests respectively; the best fit to the data for all three tests together is 0.96kN/mm. The mechanisms for gap closure might be slightly different even for femur 1, affecting the stiffness of each load cycle.

Figure 6 shows typical strain data for the strain gauge locations for both femurs. There is an initial part of the loading range (up to about 0.6 kN) where the contacts have not completely closed at the artificially introduced osteotomy. In this phase, some load is transferred in regions where the strain gauges are located, but some gauges may not yet be loaded as they are in zones where the closure of the osteotomy is essential for load transfer. However, once this same settling in load has been exceeded, the load/strain relation is virtually linear.

4. The finite element model

The experiment was simulated using the finite element model. The geometric data for each femur was obtained from orthogonal radiographs. The lateral free surface of the distal locking screw is restrained in all directions, as is the base of the femur. This accounts for the locking action of the distal screw in the bone, and the restraint on the base of the femur.

4.1 Results from FE model

The FE predicted stiffness is plotted in Figure 5, and is very close to the measured stiffness after any initial "settling in" has been completed. Contours of deformations are shown in Figure 7. They indicate that the femur is deflecting downwards under the action of the load, but is constrained from moving sideways as also were the experimental specimens. Further inspection of Figure 7 reveals that there is a region under the loaded point that undergoes significant local deformation. Closer inspection of the physical models revealed that there was a corresponding local (recoverable) bending in the shell of the experimental femoral heads. The mean deformation measured by the Instron for femur 1 was 0.60 mm greater than that measured on the underside of the femoral head. For femur 2 the value is 0.96 mm. From the FE model the corresponding values are 0.79mm and 1.25mm respectively, so that in each case the FE is predicting a slightly higher local deformation.

5 Comparison between experimental and theoretical behaviour

Comparison between the stiffness of the experiment and the simulation is given in Table 1. The values of stiffness are close to one another, although in both cases the FE model slightly underestimates. Comparison of strains with the linear gauges that were used is obtained by transformation of the FE results. In some regions strains are underestimated by the FE, while in others they are overestimated. Nevertheless, in the two cases there was some measure of agreement between the experiment and FE prediction (Table 2).

Perhaps surprisingly there are very large differences between the results for gauges 4 and 5 on both femora in both magnitude and sign. While the gauges

appear to be in approximately the same position on both specimens, and while there would not seem to be such marked differences in the geometry of the specimens, the strains are markedly different between femur 1 and femur 2. However these results are supported by the FE, and closer inspection reveals that this region on the side of the neck is one of high strain gradient, and small changes of position or of femur geometry have a major impact. The characteristics that determine global stiffness can be measured readily, but there will be some local deviations due to variation in, for example, shell thickness that will affect comparisons to local measured strains. Given this, the trends from the experiment and FE are similar.

6 Conclusions

The development of a finite element modelling technique to enable rapid analysis of medical devices, and in particular intramedullary devices, has been outlined. The process has been assessed against experimental data.

The technique allows standard constructs to be developed, with a solid pre-determined external geometry that can then be "extracted" from the particular geometry of any patient's bone – in the case described here a femur. The advantages to parametric studies are evident, but it also enables practitioners to analyse the potential consequences of surgical decisions.

With increasing facility of data import from such sources as CT scans, this FE modelling technique has significant potential to enable rapid prototyping to be developed for intramedullary devices.

Acknowledgement

The authors would like to acknowledge the contribution of Dr P J Hillard for his original work on the design and construction of the experimental setup. Additionally, we would acknowledge the assistance of Stryker Trauma in the provision of devices and the specialised equipment with which to fit them.

Tables

		Stiffness (kN/mm)
Femur 1	Finite element	2.10
	Experimental	2.31
Femur 2	Finite element	0.80
	Experimental	0.96

Table 1 – Comparison of stiffness based on maximum deflection

	Strain Gauge No.	1	2	3	4	5	6
Femur 1	Finite element	-971	n/a	-937	-236	382	742
	Experimental	-1350	n/a	-875	-305	850	800
	Strain Gauge No.	1	2	3	4	5	
Femur 2	Finite element	n/a	-593	-342	-1408	-174	112
	Experimental	n/a	-360	-380	-1260	-100	100

Table 2 – Maximum Strains (με) for both femora from FE and Experiment

References

1. **Huiskes, R. and Chao, E.Y.S.** A survey of finite element analysis in orthopaedic biomechanics; the first decade. *Journal of Biomechanics*, 1983, 16, 385-409.

2. **Medical Devices, EU Directive 93/42/EEC, 1993.**

3. **McRae, R.** Practical Fracture Treatment, *Churchill Livingstone* London, 1996.

4. **Gahr, R.H., Leung, K.S. and Rosenwasser, M. P. (Eds).** The Gamma Locking Nail, ten years results and surgical experience. *Einhorn-Presse Verlag Gmbh.*, 1999.

5. **Dubbeld, J. and Den Outer, A.J.** Proximal femoral nail – first experience with a new technique in a teaching hospital. Poster in *Hip Fractures – state of the art* meeting, Amsterdam, 2000.

6. **Randle, J.A. Meisami-Fard, B. and McKee, M.D.** Mechanical failure of a Gamma Nail in a patient with an impending pathologic subtrochanteric fracture *Canadian Journal of Surgery*, 1999, 384-386.

7. **Sitthiseripratip, K., Van Oosterwyck, H. , Vander Sloten, J., Mahaisavariya, B., Bohez, E.L.J., Suwanprateeb, J., Van Audekercke, R., and Oris, P.** Finite element study of trochanteric Gamma Nail for trochanteric fracture. *Medical Engineering and Physics*, 2003, **25**, 99-106.

8. **Seral, B., Garcia, J.M., Cegonino, M., and Doblare, F.** Finite element study of intramedullary osteosynthesis in the treatment of trochanteric fractures of the hip: Gamma and PFN, *Injury*, 2003, **35**, 130-135.

9. **Cheung, G., Zalzal, P., Bhandari, M., Spelt, J.K. and Papini, M.** Finite element analysis of a femoral retrograde intramedullary nail subject to gait loading. *Medical Engineering and Physics*, 2004, **26**, 93-108.

10. **Viceconti, M., Muccini, R., Bernakiewicz, M., Baleani, M. and Cristofolini, L.** Large sliding contact elements accurately predict levels of bone-implant micro-motion relevant to osseointegration. *Journal of Biomechanics*, 2000, **33**, 1611-1618.

11. **Bernakiewicz, M. and Viceconti, M.** The role of parameter identification in finite element contact analyses with reference to orthopaedic biomechanics applications. *Journal of Biomechanics*, 2002, **35**, 61 – 67.

12. **Wang, C.J., Brown, C.J., Yettram, A.L. and Procter, P.** Intramedullary nails: some design features of the distal end. *Medical Engineering and Physics*, 2003, **25**, 789 – 794.

13. **Brown, C.J., Wang, C.J., Yettram, A.L. and Procter, P.** Intramedullary nails with two lag screws. Clinical Biomechanics, 2004, **19**, 519 – 525.

14. **ANSYS (v 6.0)**, Swanson Analysis Systems, Inc.

15. **Moaveni, S.**, Finite Element Analysis, *Prentice-Hall*, New Jersey, 2003.

16. **Wang, C.J.** Structural Behaviour of Femoral Intramedullary Fracture Stabilising Devices, Thesis submitted as partial requirement for the degree of PhD, *Brunel University*, Uxbridge, U.K., 1999.

17. **Simpson, D.J., Yettram, A.L., Brown, C.J. and Procter, P.** Modelling Aspects of Contact in Intramedullary Nailing, in Proceedings of MAFELAP03, *Brunel University*, Uxbridge, U.K., 2003.

18. **Allison, I.M.** Stress Concentrations in Tube Intersections. Proceedings of SEM Spring Conference on Experimental Mechanics, *Society for Experimental Mechanics*, Albuquerque, New Mexico, USA, 1990.

19. **Allison, I.M.** Load Transmission between Cylinders made from Different Materials. Experimental Mechanics. Technology Transfer between High Tech Engineering and Biomechanics, *E.G.Little*, Ed., 1992.

20. **Viceconti, M.,Davinelli, M., Taddei, F. and Capello, A.** Automatic generation of accurate subject-specific bone finite element models to be used in clinical studies. *Journal of Biomechanics*, 2004, **37**, 1597-1605.

21. **Leung, K.S., Procter, P., Robioneck, B. and Behrens, K.** Geometric mismatch of the Gamma Nail to the Chinese femur. *Clinical Orthopaedics and Related Research*, 1996, 323, 42-48.

22. **Reilly, D. T. and Burstein, A.H.** The mechanical properties of cortical bone, *Journal of Bone and Joint Surgery*, 1974, 56A, 1001 – 1022.

23. **Currey, J.D**. Bones: structure and mechanics, 2002, *Princeton University Press*.

24. **Taylor, W.R., Roland, E., Ploeg, H. and Hertig, D.** Determination of orthotropic bone elastic constants using FEA and modal analysis. *Journal of Biomechanics*, 2002, **35**, 767 – 773.

25. **Simpson, D.J.** A finite element modelling strategy for the analysis of trauma treatment devices – application to fractures of the proximal femur. Thesis submitted as partial requirement for PhD, *Brunel University, Uxbridge, U.K.* 2005.

26. **Taylor, M.E., Tanner, K.E., Freeman, M.A.R. and Yettram, A.L.** Stress and strain distribution within the intact femur: compression or bending. *Medical Engineering and Physics*, 1996, **18**, 122 - 131.

27. **Wang, C., Brown, C.J. Yettram, A.L. and Procter, P.**, Intramedullary femoral nails: one or two lag screws? a preliminary study. *Medical Engineering and Physics*, 2000, **22**, 613 – 624.

28. **Haynes, R.C., Poll, R.G., Miles, A.W. and Weston, R.B**. An experimental study of the failure modes of the Gamma locking nail and AO dynamic hip screw under loading: a cadaveric study. *Medical Engineering and Physics*, 1997, 19, 446 – 453.

List of Figures

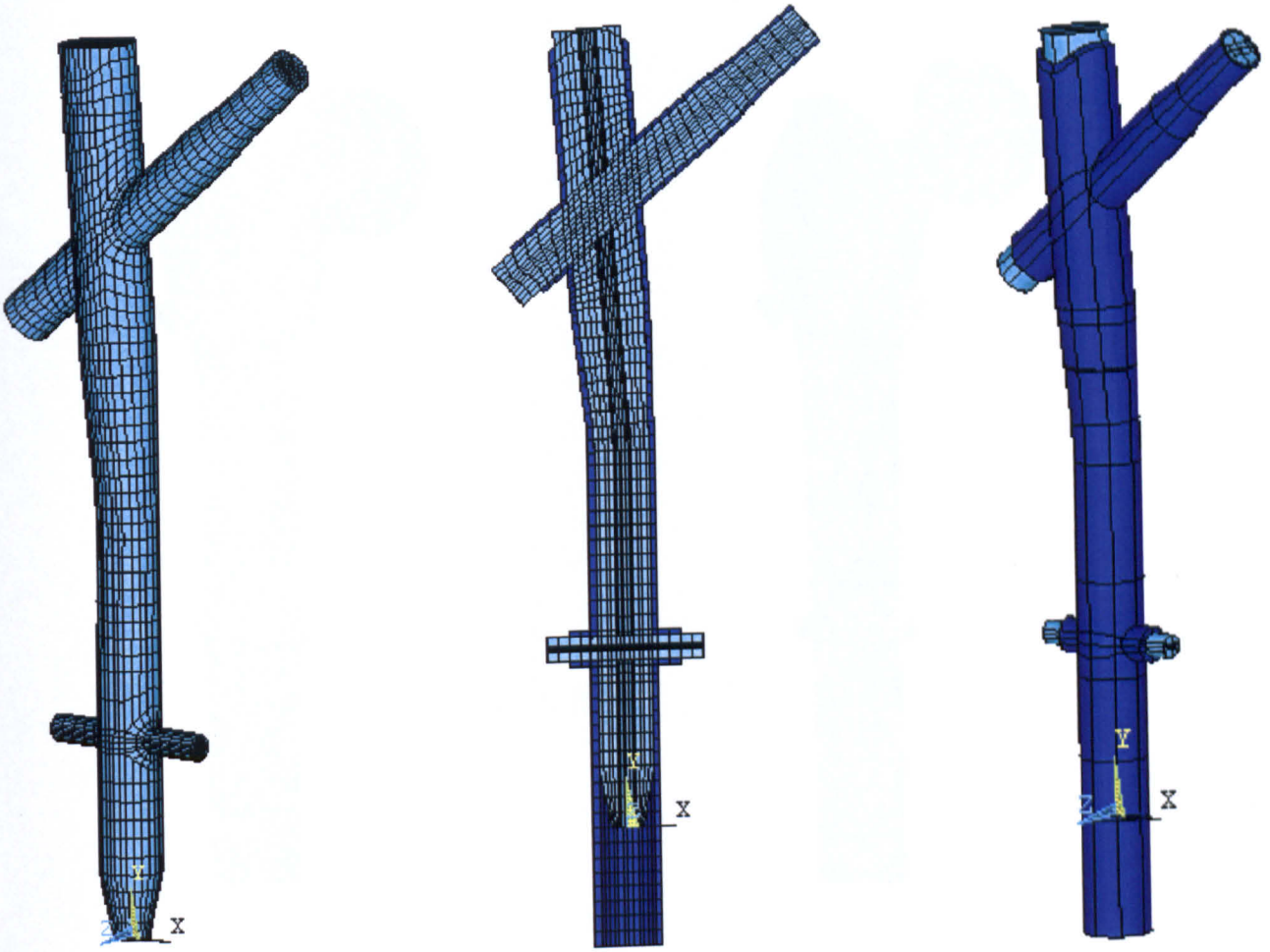

a) b) c)

Figure 1

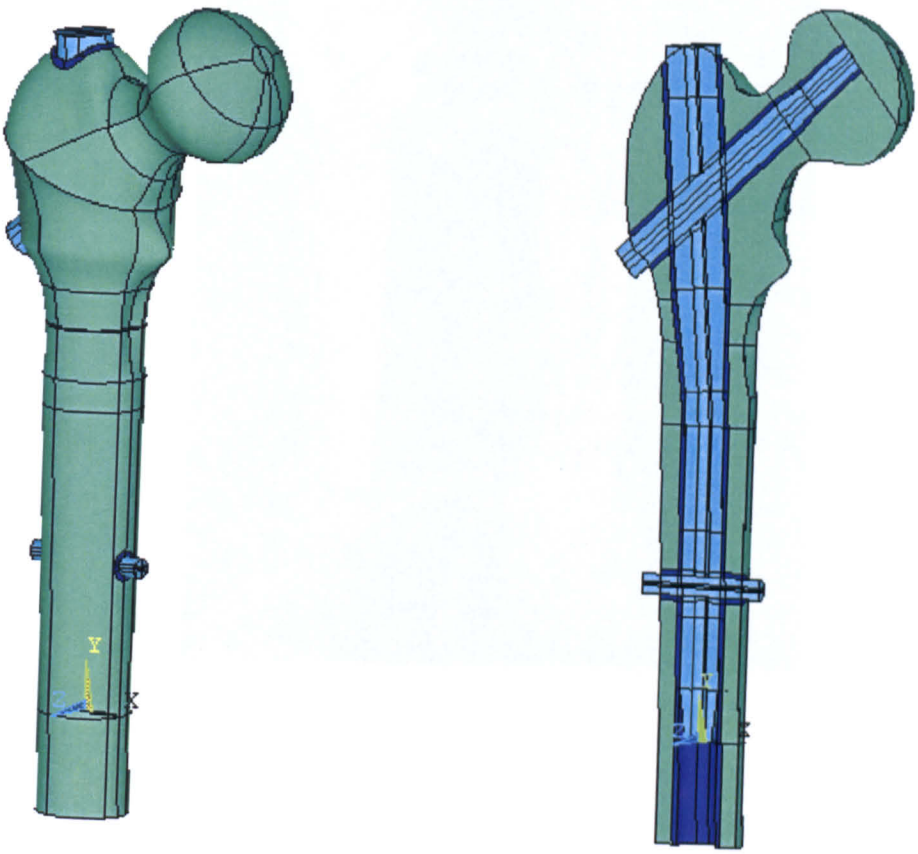

a) b)

Figure 2

Figure 3

Figure 4

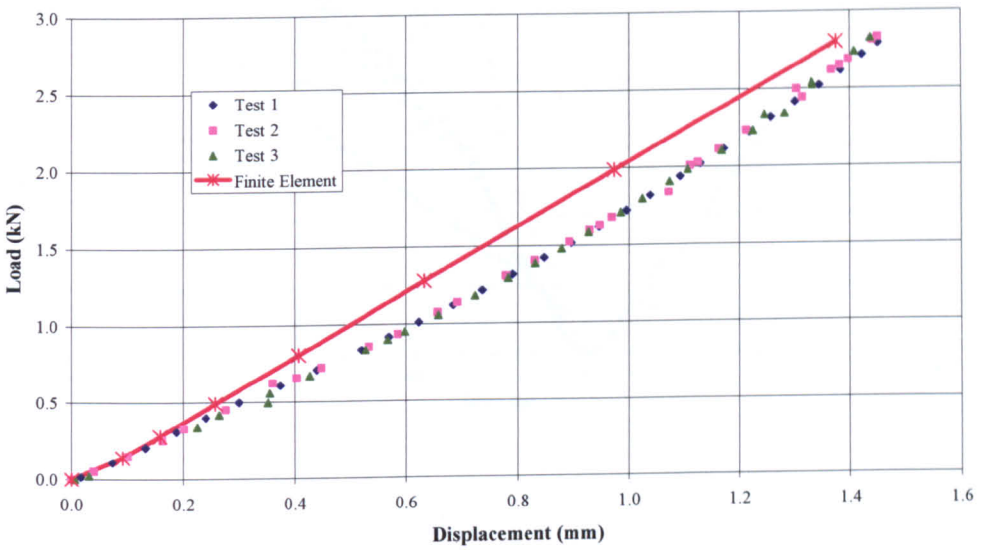

Figure 5a

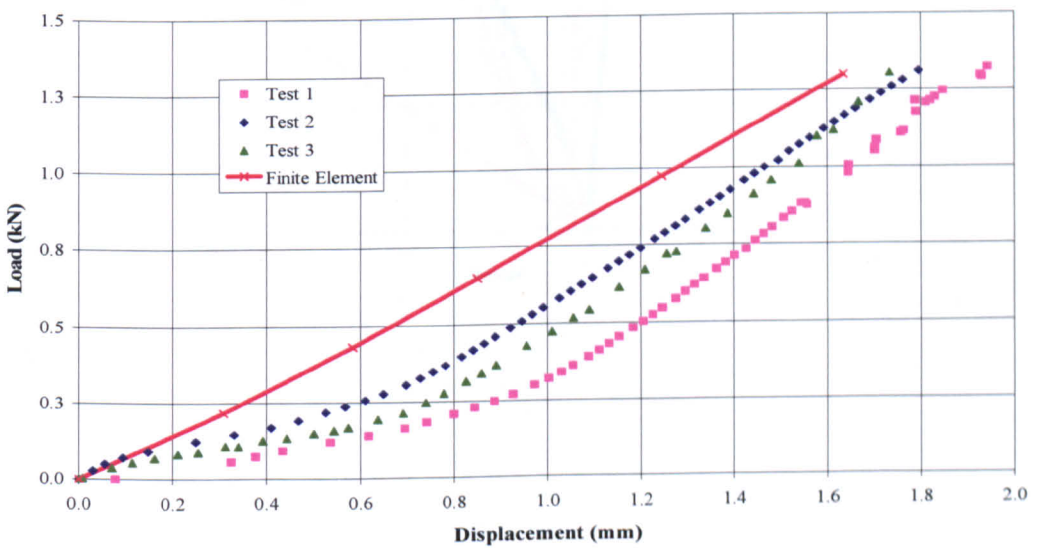

Figure 5b

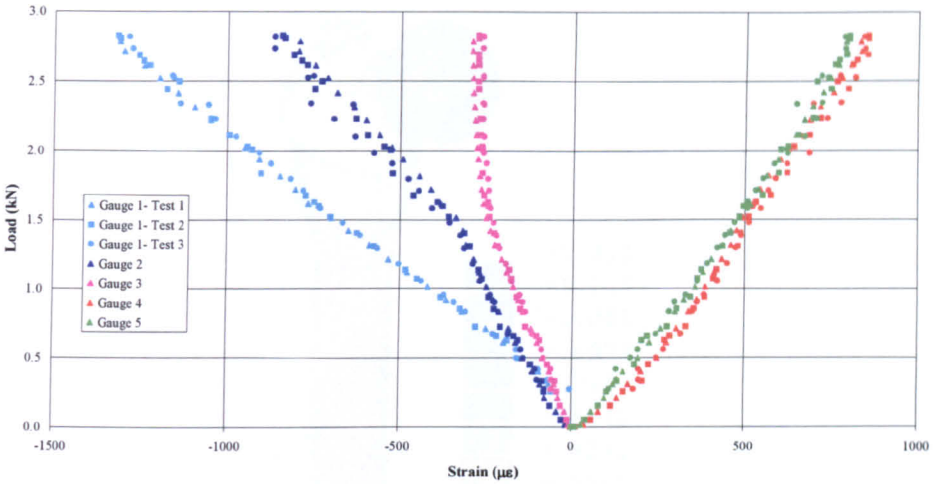

Figure 6a

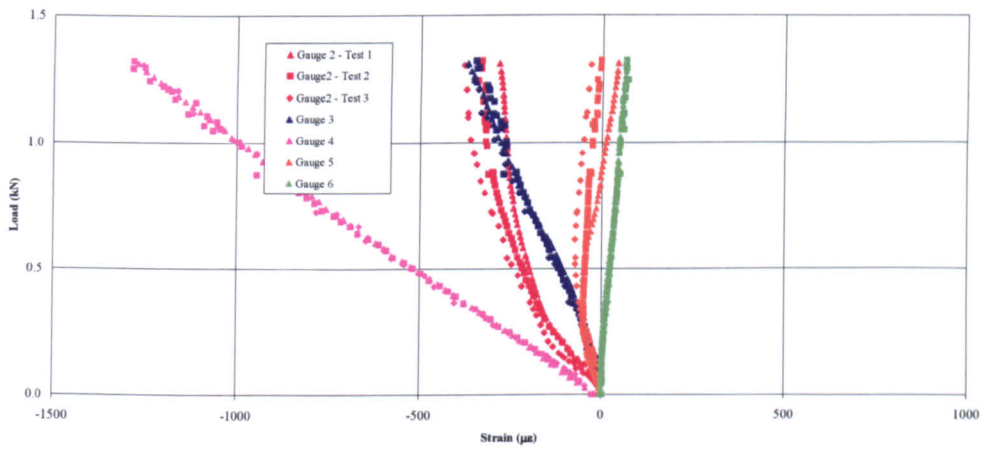

Figure 6b

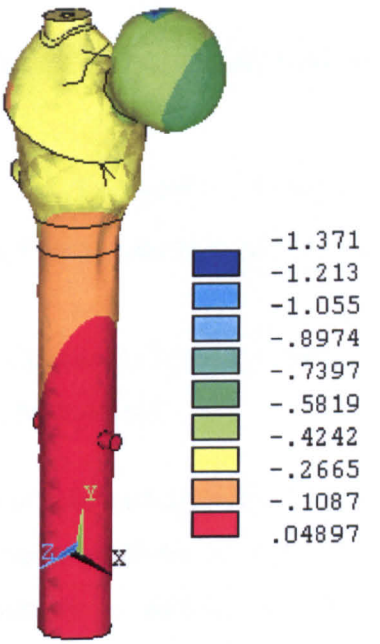

Figure 7

Modelling Aspects of Contact in Intramedullary Nailing

D. J. Simpson[a1], A.L.Yettram[a], C. J. Brown[a], and P. Procter[b]

a Brunel University, Dept. of Mechanical Engineering, Uxbridge, UB8 3PH, UK.

b Stryker Trauma S.A., Chemin du Pont du Centenaire 110, CH11111-228, Plan-les-Ouates, Geneva, Switzerland

Abstract: The analysis of intramedullary devices poses particular problems for finite element analysis. Some problems are familiar - the materials involved are non-linear, and the geometry is difficult to define because of anatomical differences. However, one of the other major problems is the definition of contact. Some researchers have allowed the pre-determination of areas of contact, but our preliminary studies have shown this can be both difficult to predict and misleading.

This paper describes a strategy adopted to enable different geometries to be rapidly generated. The models incorporate a method for allowing contact to occur anywhere on the interface between the device and bone, and to retain conformity of surface and element face. The use of such a strategy in considering two tubes in contact is also presented.

Most importantly we are able to determine the load sharing in screws used to fix intramedullary nails against different load cases.

[a1] Author to receive correspondence.

Presented to 'Conference on the Mathematics of Finite Elements and Applications', 21-24th June 2003.